

Advanced Reliability Analysis of Polymer Electrolyte Membrane Fuel Cells In Automotive Applications

by

Michael Whiteley

A doctoral thesis

Submitted in partial fulfilment of the requirements for the award of Degree of
Doctor of Philosophy of Loughborough University

©by Michael Whiteley, 2016

Abstract

Hydrogen fuel cells have the potential to dramatically reduce emissions from the energy sector, particularly when integrated into an automotive application. However, there are three main hurdles to the commercialisation of this promising technology; one of which is reliability. Current standards require an automotive fuel cell to last around 5000 h of operation (equivalent to around 150,000 miles), which has proven difficult to achieve to date. This hurdle can be overcome through in-depth reliability analysis including techniques such as Failure Mode and Effect Analysis (FMEA), Fault Tree Analysis (FTA) and Petri-net simulation. This research has found that the reliability field regarding hydrogen fuel cells is still in its infancy, and needs development, if the current standards are to be achieved. In this research, a detailed reliability study of a Polymer Electrolyte Membrane Fuel Cell (PEMFC) is undertaken. The results of which are a qualitative and quantitative analysis of a PEMFC. The FMEA and FTA are the most up to date assessments of failure in fuel cells developed using a comprehensive literature review and expert opinion.

Advanced modelling of fuel cell degradation logic was developed using Petri-net modelling techniques. 20 failure modes were identified that represented the interactions of all failure modes and operational parameters in a PEMFC. Petri-net simulation was used to overcome key pitfalls observed in FTA to provide a verified degradation model of a PEMFC in an automotive application, undergoing a specific drive cycle, however any drive cycle can be input to this model. Overall results show that the modelled fuel cell's lifetime would reach 34 hours before falling below the industry standard degradation rate of more than 5%. The degradation model has the capability to simulate fuel cell degradation under any drive cycle and with any operating parameters.

A fuel cell test rig was also developed that was used to verify the simulated degradation. The rig is capable of testing single cells or stacks from 0-470W power. The results from the verification experimentation agreed strongly with the degradation model, giving confidence in the accuracy of the developed Petri-net degradation model.

This research contributes greatly to the field of reliability of PEMFCs through the most up-to-date and comprehensive FMEA and FTA presented. Additionally, a degradation model based upon Petri-nets is the first degradation model to encompass a 1D performance model to predict fuel cell life time under specific drive cycles.

Acknowledgements

Firstly I would like to thank my supervisors, Dr Lisa Jackson and Dr Sarah Dunnett. Without your patient guidance and support, this work would not have come to fruition. I am forever grateful for the opportunity to undertake this work, and the supportive working environment I was provided during the work.

Secondly I would like to thank my best man and friend, Dr Ashley Fly. Thank you for making my time at the university enjoyable and making up the second half of the Loughborough University international conference karaoke sensation. “No Raybans”.

Also to Johanna Leigh, you proved to me that posh people can be all right, and I thank you for all of the fun that we had.

To my dad, Philip; One of the main motivations for this work was to make you proud, and I hope that I achieved that. You did a great job of raising me on your own, even if I didn't make it easy for you.

I couldn't have coped during this project without my two little cats, Alfie and Blossom. After stressful days of broken test rigs and non-running simulations, you were there to make me smile. You are sorely missed Alf.

Finally and most importantly, to my dear wife Jo. There is no scenario where this PhD would have been possible without your tireless support and selfless help. You sacrificed a great deal for me to undertake this work and I will never forget it. You are my world.

Contents

1	Introduction	2
1.1	Types of FC	4
1.2	Polymer Electrolyte Membrane Fuel Cell	6
1.3	Polarisation Curve	8
1.4	Current Uses and Applications of PEMFC	9
1.5	FC degradation and reliability	9
1.6	FC Modelling	10
1.6.1	Model Classification	10
1.6.2	0D Models	10
1.6.3	Further dimensional models	12
1.7	Thesis Aims & Objectives	13
1.8	Layout of Remaining Thesis	13
2	Durability & Reliability - Literature Review	15
2.1	Understanding FC Failures	15
2.1.1	Failure Mode and Effect Analysis (FMEA)	15
2.1.2	FMEA used in the literature	17
2.1.3	Fault Tree Analysis	19
2.1.4	FT Method used in the Literature	21
2.1.5	Petri-net Modelling	27
2.1.6	Qualitative Analysis	28
2.1.7	Quantitative Analysis	29
2.1.8	Petri-nets in the literature.	29
2.1.9	Markov Modelling	30
2.2	Modelling Conclusion	32
2.2.1	Next Steps	32
3	Failure Mode and Effect Analysis (FMEA)	33
3.1	PEMFC Construction	33
3.1.1	PTFE Membrane	33
3.1.2	Carbon GDL	35
3.1.3	Pt/C Catalyst	35
3.1.4	Stainless-Steel BIP	35
3.2	Operating Conditions	35
3.3	Performance Loss Mechanisms	37
3.3.1	Membrane	37
3.3.2	Catalyst Layer	38
3.3.3	BIP	39
3.3.4	Differences from the literature	39
3.4	FMEA Table	40
3.4.1	Membrane Section	40
3.4.2	Catalyst Layer	47

3.4.3	Gas Diffusion Layer (GDL)	50
3.4.4	Bipolar Plate (BIP)	52
3.5	Conclusions	54
4	Existing Reliability Modelling	55
4.1	Analysis Review - Limitations Determined	55
4.1.1	Top Event	55
4.1.2	Bipolar Plate Omission	56
4.1.3	Ambiguity of Intermediate Events	57
4.1.4	Lack of Standardised Data	57
4.2	Conclusions	57
4.3	Advancing the FT	58
4.3.1	Top event & intermediate top level structure	58
4.3.2	Proposed FT	60
4.3.3	FT Summary	66
4.4	Qualitative and Quantitative Analysis	66
4.4.1	Qualitative	66
4.4.2	Quantitative	66
4.5	Results	70
4.5.1	Relationship Concerns	71
4.5.2	Dependencies Summary	76
4.6	Conclusions	76
5	Proposed Petri-Net Analysis	78
5.1	Petri-Net Graphs	78
5.1.1	Operating State - Place	78
5.1.2	Degradation - Transition	84
5.1.3	Failure - Transition & Failed state - Place	84
5.2	Petri-Net Module Overview	84
5.2.1	Example net: H ₂ O ₂ Degradation	88
5.3	Simulation of the Petri-Net	89
5.3.1	Petri-Net Firing	89
5.3.2	Petri-Net Simulation Logic	90
5.3.3	Token movement	92
5.4	Derived Rates	94
5.4.1	Platinum Agglomeration	95
5.4.2	Membrane Flooding	98
5.4.3	Relative Humidity Variation	100
5.4.4	Hydrogen Peroxide	100
5.5	Quantification Data	101
5.6	Integration into Petri-Net Model	105
5.6.1	Informed data generation	106
5.7	Petri-Net Conclusions	106
6	Experimental Rig & 1D Model Validation	109
6.1	Introduction	109
6.2	Fuel Cell Experimental Rig Development	109
6.3	Characterisation of MEA	116
6.4	Validation of the model	123
6.4.1	Experimental Data	124
6.5	Conclusions	129

7	Degradation Simulation Results	130
7.1	Stop/Start Cycling	130
7.1.1	Data extrapolation from literature	130
7.2	Degradation Validation Test	137
7.2.1	Analysis	141
7.2.2	EIS data	141
7.3	Weibull Degradation	144
7.4	Conclusions	146
8	Conclusions and Future Work	148
8.1	Introduction	148
8.2	Major contributions in the area of reliability	149
8.3	Experimentation	149
8.4	Future Work	149
A	FMEA	157
B	Placca & Kouta FTA [30]	170
C	Rama FMEA & FTA [30]	174
D	Petri-Net Degradation Modules	181
E	International Journal of Hydrogen Energy Paper	197
F	International Journal of Hydrogen Energy Paper (2)	207
G	Publications	224

List of Figures

1.1	US oil production figures [6].	2
1.2	Range Comparison of BEV & Fuel Cell Vehicles [11].	3
1.3	PEMFC Drawing.	7
1.4	Standard Polarisation Curve [14].	8
1.5	Polarisation curve for typical, low temperature, air pressure, FC.	11
1.6	Integration of Objectives.	14
2.1	Criticality Matrix	17
2.2	Sample from full table in [28]	18
2.3	Example of common Fault Tree gates and events	20
2.4	Example of common Fault Tree gate use	20
2.5	Top level interaction in work presented by Placca & Kouta [30]	22
2.6	Drying out of the Membrane FT [14]	23
2.7	Flooding of the Membrane FT [14]	26
2.8	Catalyst Degradation Example [34]	27
2.9	Detail of Branch from Drying out Tree [14]	27
2.10	Example of a simple Petri-Net	28
2.11	Example Petri-net for PEMFC system [35]	29
2.12	State Space Model Presented by Tamrioven & Alam[36]	31
3.1	Functional Block Diagram of PEMFC automotive system	34
3.2	Components of a PEMFC [37]	35
3.3	ECE 15 Drive Cycle [39]	36
3.4	Extra-Urban Drive Cycle [39]	36
3.5	New European Drive Cycle [39]	37
3.6	Polymer resistivity as a function of applied stress on membrane [41]	44
3.7	Difference between standard polarisation curve, and polarisation curve with 1 ohm/cm ² increase	44
3.8	Pt Agglomeration observed by Transmission Electron Microscopy (TEM) [47]	49
3.9	Pt Agglomeration observed by X-Ray Diffraction (XRD) [48]	50
4.1	Metal Ion Intermediate Event from [30]	57
4.2	Proposed Change to 'Global' Tree	58
4.3	Proposed 'Membrane' Top level	60
4.4	Proposed mechanical section of the 'Membrane' FT	61
4.5	Proposed chemical section of 'Membrane' FT	62
4.6	Proposed Thermal section of 'Membrane' FT	63
4.7	Proposed 'GDL' FT	64
4.8	Proposed 'Catalyst' FT	65
4.9	PEMFC Membrane flooding degradation test [56]	67
4.10	Unavailability of cell over Time	70
4.11	Unavailability	71
4.12	Relationship Analysis of Basic Events	72

4.13	Pt Catalyst Degradation FT Logic	73
4.14	SEM image of Pinhole damage to a membrane. ([62])	75
4.15	Pinholes logic within chemical and mechanical branches	75
4.16	Pinhole cycle	76
5.1	Global Petri-Net for Polymer Electrolyte Membrane Fuel Cell (PEMFC)	78
5.2	Cell voltage polarisation curve [65].	79
5.3	Modified simulink model of 1D FC model [65]	82
5.4	Interactions between Petri-Net Modules	85
5.5	Example Petri-Net for H ₂ O ₂ Degradation	88
5.6	Petri-Net Logic Flow Chart	91
5.7	Petri-Net module for Ice formation	92
5.8	Petri-Net module for Swelling	93
5.9	Petri-Net module for GDL Degradation	94
5.10	Platinum Agglomeration [47]	95
5.11	Petri-net modules for immature and mature platinum agglomeration	96
5.12	Threshold for Pt Agglomeration degradation in relation to RH	97
5.13	Simulink model of Platinum Agglomeration	97
5.14	Voltage drop data by [60]	98
5.15	PEMFC Membrane flooding degradation test [56]	99
5.16	Modelled performance drop due to RH drop from 120% to 20%	100
5.17	Observed voltage drop at OCV due to H ₂ O ₂	101
5.18	Example of Petri-Net in Simulink	104
5.19	Example of Weibull calculation block	104
5.20	Simulink model block of membrane resistance increase due to swelling of the membrane	106
5.21	Images showing mechanical failure of BIP material blocking feed gas	107
6.1	Complete test rig schematic	110
6.2	Pragma 7 cell, 470W research development stack	111
6.3	MEA assembly	112
6.4	Coolant channels in between each cell	112
6.5	Gas channels in between each cell	113
6.6	TDI Power load bank	113
6.7	Humidity sensor T-piece detail	114
6.8	Complete test rig	114
6.9	Stack cooling system	115
6.10	Front end of the software developed for the fuel cell test rig	116
6.11	EIS Nyquist plot interpretation [71]	117
6.12	Gas feed pressures	118
6.13	Cell and gas feed temperatures	119
6.14	Feed gas flow rates	119
6.15	Feed gas relative humidities	120
6.16	Current and Voltage profile throughout test	121
6.17	Polarisation curve averages for each set of tests	122
6.18	Comparison of modelled system performance, and experimental data	123
6.19	Look-up table of endplate bolt torques against MEA pressure [72]	124
6.20	Polarisation curves for different endplate torques before conditioning	125
6.21	Polarisation curves for different endplate torques after conditioning	126
6.22	Electrochemical Impedance Spectroscopy of different endplate bolt torques at different current densities	127
6.23	RH and resistance equation derivation	128
7.1	Experimental results of SSC during (a)0% (b)50% and (c)100% RH [74]	131

7.2	SSC module in SimuLink model	132
7.3	SSC logic flow diagram	133
7.4	SSC logic flow diagram continued	134
7.5	Modelled SSC degradation for (a)0% (b)50% and (c)100% RH	136
7.6	Current profile of the FC vehicle for 5 NEDCs	137
7.7	Experimental polarisation curves	138
7.8	Fitted experimental polarisation curves	139
7.9	Comparison of raw data vs fitted for cycle one	139
7.10	Modelled degradation vs experimental degradation	140
7.11	Modelled degradation vs experimental degradation zoomed	141
7.12	EIS plots for each current density after each cycle	143
7.13	Flat rate degradation vs Weibull distribution degradation	144
7.14	Flow diagram of overall degradation model running	145
7.15	Cumulative average lifetime of the cell over 151 simulations	146
B.1	Membrane Layer	171
B.2	Catalyst Layer	172
B.3	Gas Diffusion Layer	173
C.1	FMEA Part 1	175
C.2	FMEA Part 2	176
C.3	FTA for Activation losses	177
C.4	FTA for Mass Transport Losses	178
C.5	FTA for Ohmic losses	179
C.6	FTA for Gas Crossover and Catastrophic losses	180
D.1	Pinholes	182
D.2	Reactant MAI-Distribution	183
D.3	Excess Heat	183
D.4	Bipolar Plate Degradation	183
D.5	Increased Pressure	184
D.6	Gas Diffusion Layer Degradation	185
D.7	Catalyst Carbon Degradation	186
D.8	Polymer Membrane Creep	187
D.9	Swelling of the Membrane	188
D.10	Micro-Crack Fracture to Membrane	189
D.11	Mature Pt Agglomeration	190
D.12	Immature Pt Agglomeration	191
D.13	Ice Formation	192
D.14	Gas Crossover	193
D.15	H ₂ O ₂ degradation	194
D.16	Radical attack	195
D.17	Reactant Mal-Distribution	196

List of Tables

1.1	FC Classification [13].	5
2.1	Example FMEA Worksheet from [27]	16
2.2	Basic Events from Placca et al. [30]	24
2.3	Intermediate events for Membrane FT [30]	25
2.4	Intermediate events for Catalyst FT [30]	25
2.5	Intermediate events for Diffusion Layer FT [30]	25
3.1	Failure Mode and Effect Analysis - Incorrect BIP Torque	42
3.2	Failure Mode and Effect Analysis - Radical and Hydrogen Peroxide Attack	46
3.3	Failure Mode and Effect Analysis - Pt Agglomeration & Particle Growth	48
3.4	Failure Mode and Effect Analysis - Gas Diffusion Layer OH radical attack to PTFE	51
3.5	Failure Mode and Effect Analysis - BIP section, Oxide film formation	53
4.1	List of Basic Events	59
4.2	List of Degradation Parameters Used	68
4.3	Table of Weibull distribution data used	69
5.1	Simulation parameters	83
5.2	List of Places and Transition in all Modules	87
5.3	List of Degradation Parameters Used	102
5.4	Table of Weibull distribution data used	103
6.1	Table of parameters logged	117
6.2	Table of fuel cell operational parameters	122
7.1	Table of vehicle parameters	137
7.2	Table of FC operational parameters	138
A.1	Failure Mode and Effect Analysis	169

Nomenclature

A	Area (m ²)
a, b	Empirical constants
C_d	Drag coefficient
E_n	Reversible cell voltage (V)
F	Faraday constant (C/mol)
G	Mass transfer coefficient (kg/m ² s)
gf	Gibbs free energy
H	Enthalpy (J/kg)
I	Current (A)
i	Current density (A/cm ²)
i_{oc}	Exchange current density (A/cm ²)
i_n	Internal current density (A/cm ²)
J	Mass flux across the membrane (mol/cm ² s)
k	intrinsic rate constant
M	Molar mass (kg/mol)
m	Mass (kg)
n_{drag}	Electro osmotic drag coefficient
P	Pressure (Pa)
Q	Energy (J)
q	Heat transfer (W/m ²)
R	Universal gas constant (J/molK)
RH	Relative humidity
S	Entropy
T	Temperature (K)
t	Time (s) / Thickness (m)
V	Voltage
z	Thickness (m)

Subscript

0	Value at STP
a	Ambient
act	Activation
an	Anode
ca	Cathode
cd	Condensation
$cell$	Single cell
$concentration$	Concentration
$drag$	Electro osmotic drag

<i>ec</i>	Standard rate free energy of activation
<i>elec</i>	Electrical power
<i>eqth</i>	Theoretical reversivle
<i>f</i>	Failed
<i>fc</i>	Fuel crossover
<i>loss</i>	Loss from stack to environment
<i>nernst</i>	Nernst
<i>ohmic</i>	Ohmic
<i>reac</i>	Electrochemical reaction
<i>ref</i>	Reference
<i>trans</i>	Transport (membrane or losses)
<i>v</i>	vapour
<i>w</i>	Working

Greek

α	Charge transfer coefficient
β	Shape parameter
$\Delta\hat{h}$	Enthalpy change (J/molK)
$\Delta\hat{s}$	Entropy change (J/mol)
η	Scale parameter
γ	location parameter
λ	Membrane water content / failure rate
μ	Degradation rate
Ω	Membrane resistance (Ω/cm^2)

Acronyms

<i>AFC</i>	Alkaline Fuel Cell
<i>BEV</i>	Battery Electric Vehicle
<i>BIP</i>	Bipolar Plate
<i>CHP</i>	Combined Heat and Power
<i>DECC</i>	Department of Energy and Climate Change
<i>DoE</i>	Department of Energy
<i>EASA</i>	Electrochemically Active Surface Area
<i>ECE</i>	Economic Commission for Europe
<i>EIS</i>	Electrochemical Impedance Spectroscopy
<i>EU</i>	European Union
<i>FC</i>	Fuel Cell
<i>FCEV</i>	Fuel Cell Electric Vehicle
<i>FMEA</i>	Failure Mode and Effect Analysis
<i>FTA</i>	Fault Tree Analysis
<i>GDL</i>	Gas Diffusion Layer
<i>HFC</i>	Hydrogen Fuel Cell
<i>HFP</i>	Hydrogen and Fuel Cell Technologies Platform
<i>HOR</i>	Hydrogen Oxidation Reaction
<i>ICE</i>	Internal Combustion Engine
<i>IP</i>	Implementation Panel
<i>MCFC</i>	Molten Carbonate Fuel Cell
<i>MCS</i>	Minimal Cut Sets
<i>MEA</i>	Membrane Electrode Assembly
<i>MM</i>	Markov Model
<i>MtCO_{2e}</i>	Million tonnes of Carbon Dioxide equivalent
<i>MTTF</i>	Mean Time To Failure
<i>NEDC</i>	New European Drive Cycle
<i>NEDO</i>	New Energy and Industrial Technology Development Organisation
<i>OCV</i>	Open Circuit Voltage
<i>ORR</i>	Oxygen Reduction Reaction
<i>PAFC</i>	Phosphoric Acid Fuel Cell
<i>PEMFC</i>	Polymer Electrolyte Membrane Fuel Cell
<i>PTFE</i>	Polytetrafluoroethylene
<i>RH</i>	Relative Humidity
<i>SOFC</i>	Solid Oxide Fuel Cell
<i>SSC</i>	Start-up/Shut-down Cycle
<i>STP</i>	Standard Temperature and Pressure
<i>TEM</i>	Transmission Electron Microscopy

UK United Kingdom
US United States
XRD X-Ray Diffraction

Chapter 1

Introduction

Climate change issues and sustainability concerns have increased in interest and awareness in recent years, since anthropogenic activities have been found to impact considerably upon the environment [1]. The way in which manmade activities contribute to climate change is mainly due to Greenhouse Gas (GHG) emissions. These include, among others, carbon dioxide (CO_2), methane (CH_4) and nitrous oxide (N_2O) that contribute to the greenhouse effect. Additionally, energy prices are set to continue to rise by alarming rates [2] which will disrupt the UK's energy system due to a rise in oil prices. As a consequence of that, there will be an increase in the volatility in the politics of security of energy. Currently Europe has an 80% dependence on oil that is from outside the EU [3], which could increase tensions with oil producing countries in the future.

A report by the Department of Energy and Climate Change (DECC) showed an increase in the price of oil over the next 15 years [4]. The estimated increase in oil prices is directly linked to the fact that it is now estimated that the world's oil reserves are running out at a rapid rate;

oil reserves are projected to only last 40-50 years with current technology and usage. Transport is already responsible for almost 70% of the European Unions (EUs) oil use and this share continues to increase [5].

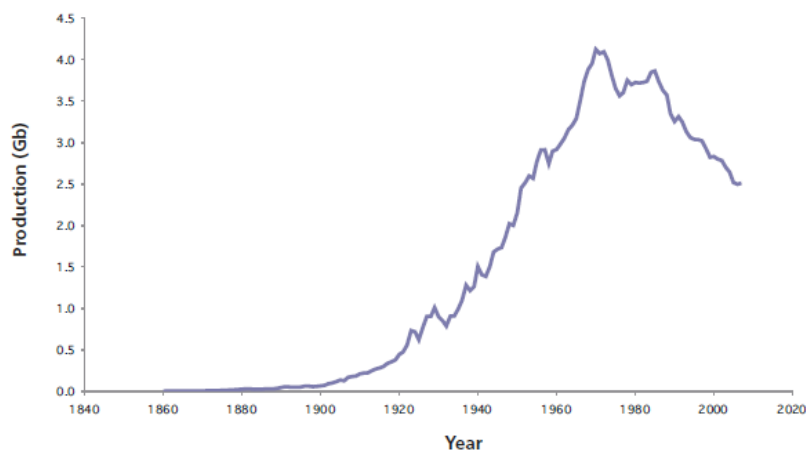


Figure 1.1: US oil production figures [6].

This can be alluded to when observing the total US output of oil; Figure 1.1 shows the total United States (US) production of oil in Giga-barrels, and shows a clear peak in the production, and thus a decline in output over the past few decades. This can be considered to be an indication of the lack of abundance of this fossil fuel.

The United Kingdom (UK) emitted 549.3 Million tonnes of Carbon Dioxide equivalent (MtCO₂e) in 2011 [7] and 122.2 MtCO₂e was due to the transport industry, with 74% of this figure due to cars, taxis and busses [8]. Due to the aforementioned negative environmental impacts of emissions from fossil fuel energy sources, this figure needs to be dramatically reduced not only to meet government targets, but for the health of the biosphere.

The UK government set out targets to reduce GHG emissions in the Climate Change Act of 2008. The act presents the targets of an 80% reduction of greenhouse gas levels by 2050, with a closer target of a 34% reduction by 2020. These two targets are based upon the level of GHG emissions in 1990 [9]. The targets are legally bound and therefore need to be met, thus many initiatives and research have emerged to aid the UK in reaching these targets.

There are some technologies that can be used as alternatives to the fossil fuel dependent transport industry and alleviate our negative impact upon the environment. Battery Electric Vehicles (BEVs) have increased in popularity in recent times due to their potential to be zero emission vehicles at the point of use, and if charged with a renewable energy source could reduce transport emissions drastically. However, their popularity is somewhat limited due to their small ranges when compared to Internal Combustion Engine (ICE) vehicles, and long recharging time requirements[10]. These negative attributes have affected their uptake with the general public customer base, and stunted their growth and commercialization.

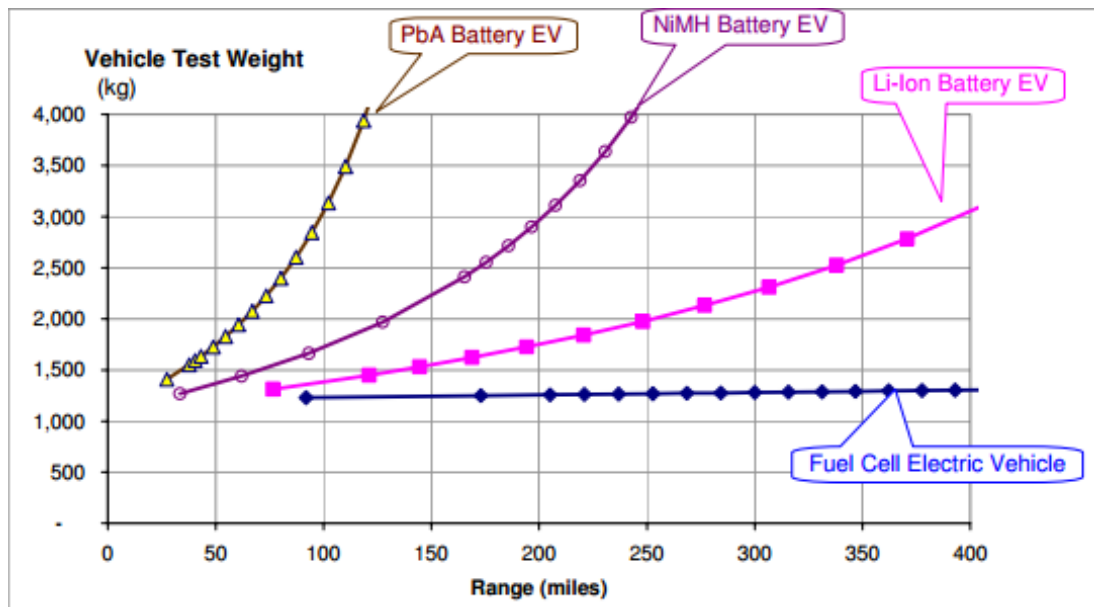


Figure 1.2: Range Comparison of BEV & Fuel Cell Vehicles [11].

Charge times for BEVs are notoriously timely and it is common for current commercial BEVs to take up to 8 hours to fully charge from a zero state of charge. This issue is not present for the current ICE owner, who can fully restock the vehicles energy reserves in a couple of minutes. The charge and range issues combined are one of the major hurdles to the uptake of BEVs. If one has a BEV that has a range of 150 miles from a full charge, but a journey is 300 miles, it would require an 8 hour charge at the halfway point. Therefore it is apparent that a low-zero emissions vehicle is required that has the same range as the ICE, but without the emissions and oil dependency.

Figure 1.2 shows a comparison of total range for vehicles propelled by different types of batteries, and a Fuel Cell (FC). The FC range is only limited by the amount of hydrogen (H₂) the vehicle can store.

FCs negate the above issues as they are an electro-chemical, zero-emission energy conversion and power generation device. Their only exhaust emission is water that is so pure, it was used

by the Apollo astronauts as drinking water on their lunar missions [12]. They can be re-fuelled in a similar time to conventional ICE vehicles, and can operate to a similar range. These positive attributes have put FCs in the limelight as an attractive alternative to the fossil fuel dependant ICE.

Fuel Cell Electric Vehicles (FCEVs) could mitigate the negative attributes of the BEV, as they have comparable ranges to ICE vehicles, and are re-fuelled in a similar time too. Figure 1.2 shows how BEVs suffer from range issues when compared to a FCEV system. If a BEV system was required to meet the range of a standard FCEV system, it would have many banks of Li-ion batteries which are massive, and as such, would vastly increase the weight of the vehicle. So much so that it would not be feasible to create a vehicle of that size and mass. With every additional kg of weight added by the extra battery capacity would require larger brakes, body structure and electric power to handle the mass of the vehicle.

1.1 Types of FC

There are five main types of FC that have been developed over the years, these are; Polymer Electrolyte Membrane Fuel Cell (PEMFC), Alkaline Fuel Cell (AFC), Phosphoric Acid Fuel Cell (PAFC), Molten Carbonate Fuel Cell (MCFC) and the Solid Oxide Fuel Cell (SOFC). The main way in which they are segregated is by their constituent materials for the electrolyte based upon the operating temperature. PEMFC, AFC and PAFC have relatively low operating temperatures ($<200^{\circ}\text{C}$), and can thus utilise aqueous or thin polymer electrolytes, whereas MCFC and SOFC operate at temperatures from 600°C and 1000°C respectively, and thus cannot use aqueous electrolytes due to vapour pressure [13]. Table 1.1 taken from [13] shows the different types of FC, listing their component materials and operating temperature.

Table 1.1: FC Classification [13].

	PEMFC	AFC	PAFC	MCFC	SOFC
Electrolyte	Hydrated Polymeric Ion Exchange Membranes	Mobilized or Immobilized Potassium Hydroxide in asbestos matrix	Immobilized Liquid Phosphoric Acid in SiC	Immobilized Liquid Molten Carbonate in LiAlO ₂	Perovskites
Electrodes	Carbon	Transition metals	Carbon	Nickel and Nickel Oxide	Perovskite and perovskite / metal cermet
Catalyst	Platinum	Platinum	Platinum	Electrode material	Electrode material
Interconnect	Carbon or metal	Metal	Graphite	Stainless steel or Nickel	Nickel, ceramic, or steel
Operating Temperature	40-80°C	65-220°C	205°C	650°C	600-1000°C
Charge Carrier	H ⁺	OH ⁻	H ⁺	CO ₃ =	O=
External Reformer for Hydrocarbon Fuels	Yes	Yes	Yes	No, for some fuels	No, for some fuels and cell designs
External Shift Conversion of CO to Hydrogen	Yes, plus purification to remove trace CO	Yes, plus purification to remove CO and CO ₂	Yes	No	No
Prime Cell Components	Carbon-based	Carbon-based	Graphite-based	Stainless-based	Ceramic
Product Water Management	Evaporative	Evaporative	Evaporative	Gaseous Product	Gaseous Product
Product Heat Management	Process Gas + Liquid Cooling Medium	Process Gas + Electrolyte Circulation	Process Gas + Liquid Cooling	Internal Reforming + Process Gas	Internal Reforming and Process Gas

The charge carriers from left to right are: hydrogen protons, hydroxides, hydrogen protons, carbonates, and oxygen.

MCFC and SOFC are more generally used for static power supply and Combined Heat and Power (CHP) stations for buildings. This is mainly due to their high operating temperatures ability to be harnessed for the heating of the building, increasing overall efficiency. They have the ability to use natural gas as the fuel with on-board reformers to create a hydrogen feed. They do this using their high operating temperatures to steam reform natural gas into hydrogen. PAFC are mainly used in medium scale CHP applications as they have a relatively high operating temperature that can produce enough warm water for medium scale applications. AFC have become less popular in recent years, and PEMFC have taken over in popularity for small scale and transport applications. Mainly due to the PEMFC having a higher power density, operating

at lower temperatures, and having a solid electrolyte rather than a liquid.

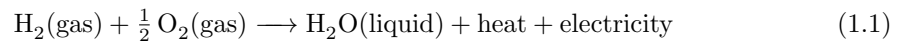
Out of the many classifications of FC, the PEMFC is commonly singled out as the most appropriate to be implemented into an automotive application. This is due to its relatively low operating temperature of around 50-80°C, its ability to use air as the cathode reactant and its rapid start-up time. Due to this, the PEMFC will be the main focus of this thesis.

1.2 Polymer Electrolyte Membrane Fuel Cell

The first practical demonstration of a hydrogen FC was by lawyer and amateur scientist Sir William Grove in 1839. He understood that through electrolysis, an electrical current can be passed through water (H₂O) to break it down into its constituent H₂ and oxygen (O₂) molecules. From this he believed that the reverse of the electrolysis should be possible, and set up an experiment with platinum (Pt) electrodes in two separate bottles containing H₂ and O₂. When he submersed the bottles into dilute sulphuric acid, he observed that the gases were consumed and an electrical current was produced when the gasses recombined to form H₂O.

A FC is an electro-chemical energy generation device that directly uses H₂ and O₂ to create electrical and heat energy. The only by-product of the reaction is water.

The overall reaction that takes place in a PEMFC is shown in Equation 1.1.



At the anode side (the negative electrode), H₂ is passed over the catalyst layer of Platinum (Pt) nanoparticles which breaks the H₂ molecule down into protons 2H⁺ and electrons 2e⁻, establishing an oxidation reaction. The electrons travel through the anode and to an external circuit to create the electrical current that can be used for work, such as to spin a motor, as given by Equation 1.2.

At the cathode side (the positive electrode), O₂ is passed over the Pt catalyst layer which breaks the O₂ down into two oxygen atoms with negative charge, establishing a reduction reaction. The negative charge pulls the hydrogen protons through the electrolyte membrane to meet the electrons and oxygen atoms at the cathode side to form water, and completing the reaction shown in Equation 1.3.

The two half-cell reactions together complete the overall redox reaction of the FC (Equations 1.2 & 1.3).

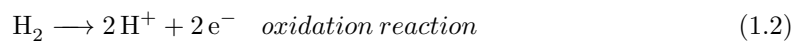


Figure 1.3 graphically depicts the main components and passage of protons in a basic PEMFC.

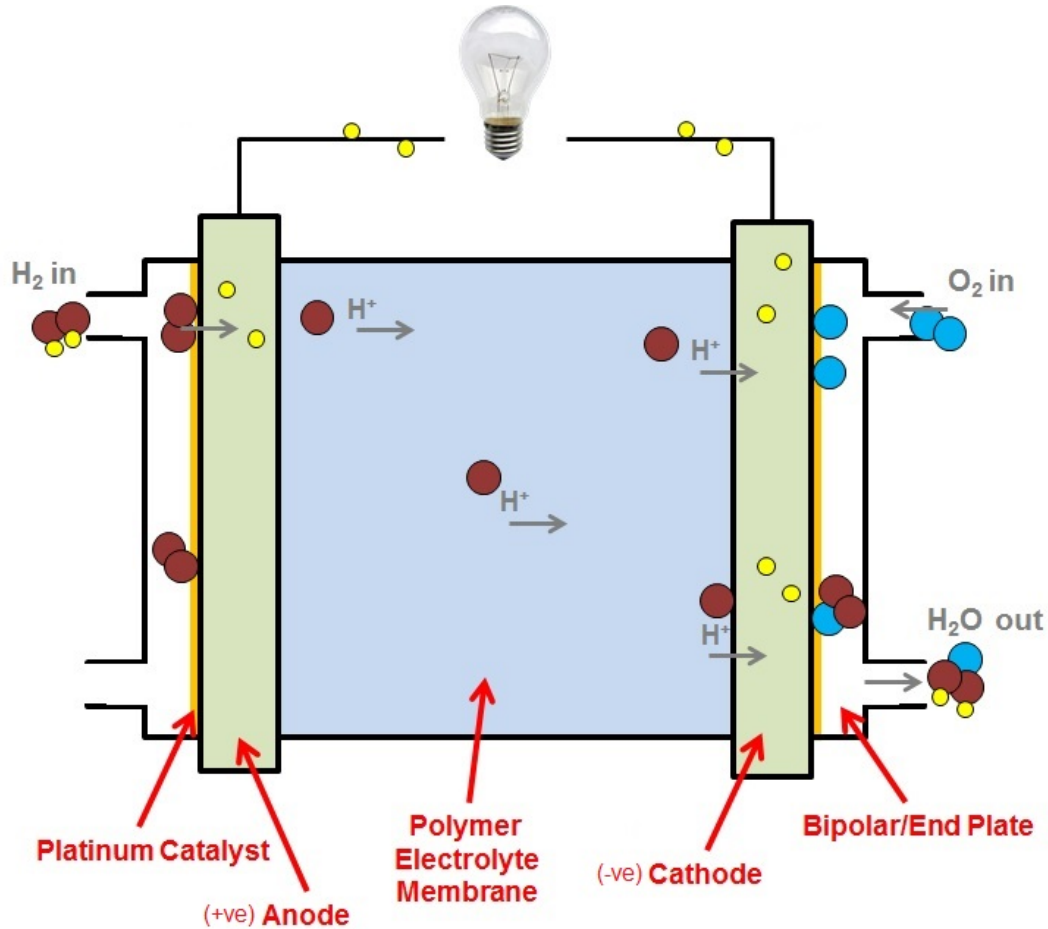


Figure 1.3: PEMFC Drawing.

The membrane at the core of a Hydrogen Fuel Cell (HFC) is made of Polytetrafluoroethylene (PTFE) commonly known as Teflon®), which can be found as a non-stick coating applied to frying pans. The PTFE core is hydrophobic which means that it repels water, and this aids with the removal of excess water during the reaction. The core material is modified to have side chains ending with sulphonic acid (HSO_3) which is hydrophilic, meaning that it attracts water. The combination of a hydrophobic and hydrophilic material means that the material can remain hydrated but expel excess water. The ability to do this is fundamental to the transport of the H^+ protons through the electrolyte membrane. The protons achieve this by bonding to a H_2O molecule in the hydrated membrane forming a hydronium ion H_3O^+ , this way they can piggyback across the membrane to meet the electron at the other end (shown in Equation 1.4).



The resulting voltage created by the redox reaction, at Standard Temperature and Pressure (STP) ($25^\circ\text{C} / 1 \text{ bar}$) is 1.23 volts. The voltage produced during the reaction is often displayed in the form of a polarisation curve, or I-V curve. To create a usable amount of energy, cells are arranged in large stacks separated by Bipolar Plates (BIPs) that feed gas to each cell and conduct the electricity in series along the stack to the end plates. This modular design allows the possible power output to be as high as practicably desired.

1.3 Polarisation Curve

Figure 1.4 presents the standard polarisation curve which is used throughout FC science. It indicates the evolution of the PEMFC voltage in relation to the applied current, and the losses associated with certain FC phenomenon. It is used throughout FC research as a tool to ascertain FC performance and health over the range of operating current. Any reduction in the gradient of the curve will signify a phenomena that is causing performance losses to either of the three loss regions in the system.

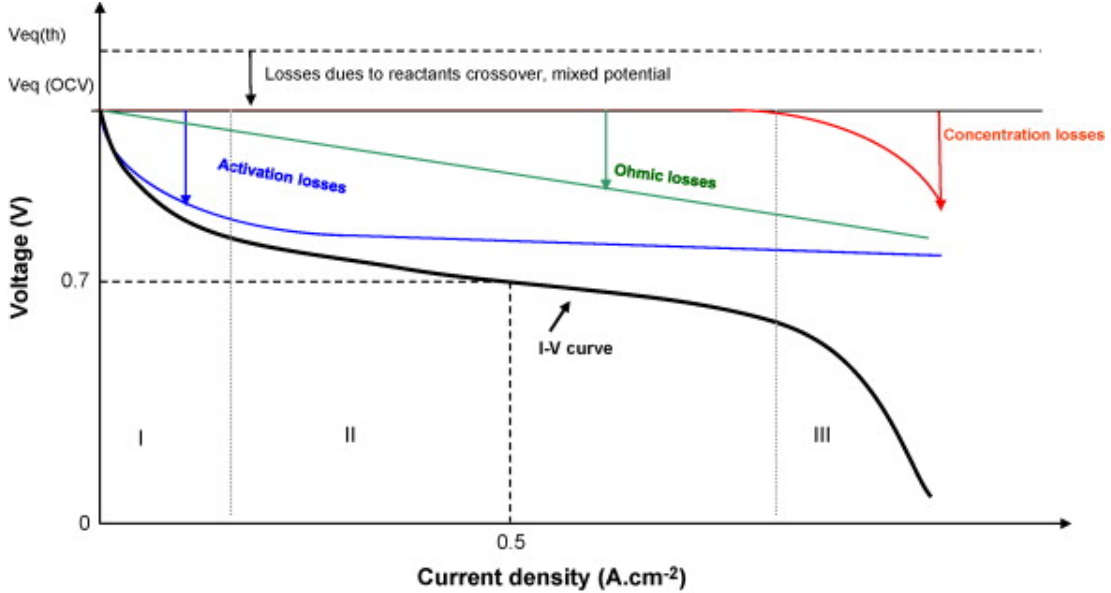


Figure 1.4: Standard Polarisation Curve [14].

$V_{eq(th)}$ shown by the dotted line at the top of the graph is the FC's theoretical maximum potential, this is commonly known as 1.23V. The theoretical maximum potential can be calculated using Equation, 1.5.

$$V_{eq(th)} = \frac{-\Delta g\bar{f}}{2F} \quad (1.5)$$

Where $V_{eq(th)}$ is the reversible voltage of the cell at standard temperature and pressure, $-\Delta g\bar{f}$ is the change in Gibbs free energy of formation per mole, and F is Faradays constant of $96485 \cdot 3 \text{ Cmol}^{-1}$. Therefore when using H_2 and O_2 at standard temperature and pressure, the equation yields 1.23 V.

$V_{eq(OCV)}$ (from Figure 1.4) is the measured Open Circuit Voltage (OCV) and is lower than the theoretical maximum potential due to reactants crossover through the membrane (thus not being reacted in the cell) and mixed potential losses. These are inevitable losses, and are expected when manufacturing and operating hydrogen FCs. Therefore, in practice, one would expect to see an OCV of around 1V.

The x axis shows the current density for the cell, and often reaches up to around 2 A/cm^2 in commercial FCs.

The initial dip in the I-V curve that can be observed in section I of Figure 1.4 shows the activation losses in a FC system. These are attributable to the overall slowness of the reactions taking part at the electrodes, more specifically the cathode O_2 reduction reaction. The O_2 reduction reaction at the cathode is in orders of magnitude slower than the H_2 oxidation reaction at the anode, thus the disparity of rate of reaction culminates in an initial decay in the polarisation curve at low current densities [15].

The linear drop in cell voltage that can be seen in the centre portion of the graph is attributable to ohmic losses in the cell. Ohmic losses are resistive losses in the system and can be either from the external electrical circuit, or the PEM itself. Therefore the total ohmic losses can be calculated from the resistance of the entire system to the flow of protons and electrons.

The exponential decay observable at higher current densities is due to the concentration losses. This is where the gas supply from the inlet feed is not fast enough to diffuse through the gas supply channels to the active reaction sites, and can also be termed mass transport losses.

1.4 Current Uses and Applications of PEMFC

PEMFCs initial breakthrough came by the hands of General Electric in the 60s, when they developed PEMFCs for the US Navy and Army. Fascinated by the results of the FCs, NASA obtained a number of PEMFCs for the Gemini space project, and successfully used pairs of 1kW PEMFCs to power the Gemini 6-12 expeditions [12].

Since their breakthrough, they have been adapted to be used in many applications from small mobile energy generators, to large-scale CHP stations. In between the two extremes, PEMFCs have been known to power cars, buses and even light aircraft.

The automotive industry is starting to see the potential with this technology, and as such, PEMFCs are used exclusively in the latest commercially available FCEVs such as the Toyota Mirai and Hyundai ix35. Manufacturers such as Audi, Mercedes-Benz and Honda have also alluded towards the introduction of production FCEVs in the near future. However, there are issues with this promising technology in the form of: **cost**, **infrastructure** and **reliability**.

Cost - The majority of PEMFC vehicles are limited run research projects and as such, the economy of scale cannot reduce the price. Additionally PEMFCs use Pt nanoparticles as the reaction catalyst, which is an inherently expensive material.

Infrastructure - There are currently limited H₂ fuelling stations to cater for this technology, with the majority being within university campuses or company grounds.

Reliability - PEMFCs are required to meet specific lifetime goals, and currently they struggle to reach these goals due to unforeseen degradation of the membrane, Catalyst Layer (CL), Gas Diffusion Layer (GDL) and BIP components, all of which contribute towards a reduction of FC performance.

1.5 FC degradation and reliability

There are a range of targets for different FC applications, with the main two being set for stationary and automotive applications respectively.

The US Department of Energy (DoE), Japanese New Energy and Industrial Technology Development Organisation (NEDO) and European Hydrogen and Fuel Cell Technology Platform (HFP) Implementation Panel (IP) have all set reliability targets for PEMFCs in automotive application of a lifetime of more than 5000 hours of operation (equivalent to around 150,000 miles operation) [16]. The current state of FC development struggles to meet these targets, and as such, an in-depth reliability analysis of PEMFCs is invaluable to help manufacturers and developers. Such an analysis requires obtaining a detailed understanding of the failure modes of all the different parts of the cell, and the effects the failures have on the cell as a whole. The target set for stationary applications is set at a minimum lifetime of 40,000 hours of operation.

Currently, the understanding of the reliability of PEMFCs is still in its infancy, and requires further development to help with the commercialisation of this promising technology.

1.6 FC Modelling

Due to the high costs involved in purchasing PEMFCs, it is wise to model the behaviour of the cells to elucidate key performance characteristics. The majority of PEMFC modelling in the literature is empirical in nature, that is to say that the models utilise experimental parameters that were observed, rather than relying on theory [17].

The modelling of HFCs has progressed rapidly in the past decade, from relatively simple one dimensional models, to highly complex three dimensional models. One of the initial and better known one dimension models comes from Springer et. al [18]. The authors initiated the HFC model movement with more and more complex models being developed to try to replicate observable polarization curves based upon input parameters.

1.6.1 Model Classification

Mathematical modelling of PEMFCs can broadly be classified into two main types; Empirical Performance models and Mechanistic models[19]. Empirical models are sometimes further broken down into two sub-types; Analytical models, and semi-empirical models[20].

Analytical models are very simple and are often only used for quick calculations regarding analytical voltage versus current density curves. They classify the operation of a FC utilising short equations to represent the reversible voltage and any losses in the system. They are limited due to their inherent simplicity, therefore more complex calculations require more intricate models.

Semi-Empirical models combine equations derived from theory with empirical relationships.

Mechanistic modelling uses terms derived from theory and not from experimental results as with empirical modelling.

1.6.2 0D Models

0D models are the most basic method of computing the voltage output of a cell. It is usually computed using Equation 1.6 and is seldom used in modern FC research as there is little to learn from the results, however it is a good way to reduce computational loads when using simulation methods such as Monte-Carlo simulations with many iterations.

The Nernst equation can be calculated from the following.

$$E_{nernst} = \frac{\Delta G}{2F} + \frac{\Delta S}{2F}(T - T_{ref}) + \frac{RT}{2F}[\ln(P_{H_2}) + 1/2\ln(P_{O_2})] \quad (1.6)$$

Where ΔG is the change in Gibbs free energy; F is Farady's constant; ΔS is the change in entropy; R is the universal gas constant; and P_{H_2} and P_{O_2} are partial pressures for H_2 and O_2 respectively. T is the temperature of the cell, whereas T_{ref} is the reference temperature for the cell. Solving this equation using STP values, the following is found.

$$E_{nernst} = 1.229 - 0.85x10^{-3}(T - 298.15) + 4.31x10^{-5}T[\ln(P_{H_2}) + 1/2\ln(P_{O_2})] \quad (1.7)$$

A simple plot of a polarisation curve can be obtained using the Nernst potential calculation in Equations 1.6 and 1.7 and the five main loss pathways in a FC, as in Equation 1.8.

$$V_{cell} = E_{nernst} + \eta_{act,a} + \eta_{act,c} + \eta_{fc} + \eta_{ohmic} + \eta_{concentration} \quad (1.8)$$

Where E_{nernst} is the Nernst equation, $\eta_{act,a}$ and $\eta_{act,c}$ are the activation losses at respective electrodes, η_{fc} is the overvoltage due to fuel crossover, η_{ohmic} is the loss due to electrode, connections and polymer proton resistance, and $\eta_{concentration}$ relates to the losses due to concentration of fuel.

A simple polarisation curve can be easily replicated through a simplified 0D model as in Equation 1.9, also known as the Tafel equation.

$$E = E_{nernst} - i r - A \ln(i) + m \exp(ni) \quad (1.9)$$

Where E is equal to the cell voltage, E_{nernst} is the Nernst voltage, A represents the Tafel slope, i shows the current density, r is the area specific resistance, and m & n are constants regarding the mass-transfer overvoltage. Plotting this simple relationship gives us the familiar polarisation curve used in FC science (See Figure 1.5).

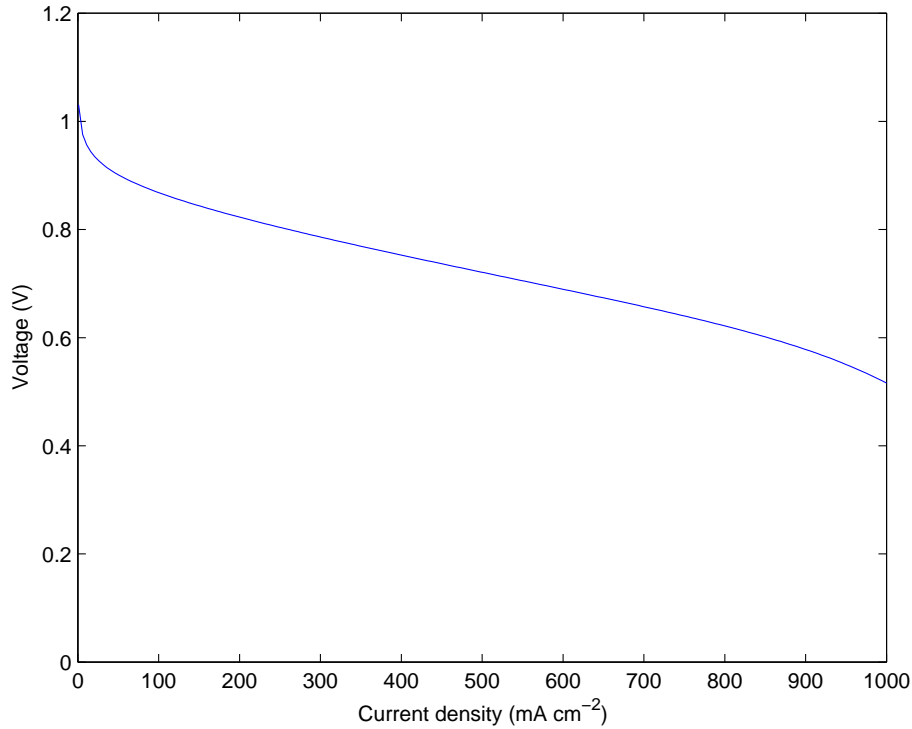


Figure 1.5: Polarisation curve for typical, low temperature, air pressure, FC.

The x axis here is represented in mA/cm² rather than A/cm² in Figure 1.4 as the current density itself doesn't reach more than 1 A/cm², therefore it was rescaled to show the detail of the polarisation curve.

The loss mechanisms are noted in the literature, Mann et al.[21] present the the activation, ohmic and concentration losses expressed as shown in Equation 1.10, Equation 1.11 and Equation 1.12.

$$\eta_{act,a} = -\frac{\Delta G_{ec}}{2F} + \frac{RT}{2F} \ln(4FAk_0c_{H_2}^*) - \frac{RT}{2F} \ln i \quad (1.10)$$

Where ΔG_{ec} is the standard-state free energy of activation for chemisorption (J/mol), F is Faradays constant, A is the active cell area (cm²), $c_{H_2}^*$ is the liquid-phase concentration of

hydrogen (mol/cm³), k_a is the intrinsic rate constant for anode reaction (cm/s), R is the gas constant (J/mol K), and i is the current (amps).

$$\eta_{act,c} = \frac{RT}{\alpha_c F n} \left(\ln \left[n F A k_c \exp \left(- \frac{\Delta G_e}{RT} \right) \times (c_{O_2}^*)^{(1-\alpha_c)} (c_{H^+}^*)^{(1-\alpha_c)} (c_{H_2O}^*)^\alpha \right] - \ln i \right) \quad (1.11)$$

$$\eta_{ohmic} = \eta_{ohmic}^{electronic} + \eta_{ohmic}^{proton} + -i(R^{electronic} + R^{proton}) = -iR^{internal} \quad (1.12)$$

Where R^{proton} corresponds to;

$$R^{proton} = \frac{r_M l}{A} \quad (1.13)$$

Where r_M is the membranes specific resistivity to the flow of hydrated protons (ohm.cm), and l is the thickness of the membrane in (cm), which has the function of the cell electrolyte.

Adequate hydration of the membrane in a PEMFC is of paramount importance. As discussed in section 1.2, the H₂ protons travel through the membrane due to a piggy back method with H₂O molecules, creating H₃O⁺ ions. If the water levels in the membrane decrease, the resistance to proton migration increases.

The voltage losses due to mass transportation/concentration loss are taken from Larminie and Dicks[22]; shown in Equation 1.14.

$$\Delta V_{concentration} = -B \ln \left(1 - \frac{i}{i_1} \right) \quad (1.14)$$

Where B is a constant that depends on the cell and the operating conditions, i_1 is a limiting current density (mA cm⁻²) where the fuel is used up equal to its supply rate, and i is the operating current density. As the PEMFC system is designed to be operated in the mid-range of the polarisation curve, it is seldom the case where concentration losses are observed in a healthily operating PEMFC system.

1.6.3 Further dimensional models

Other than the basic 0D models, more in-depth and complex modelling can be undertaken to ascertain FC performance.

1D models

1D models are a description of the phenomena taking place on a 1D plane, through the membrane from anode to cathode. This latitudinally dimensional model approach is based upon flux balance, and models the exact amount of species moving in and out of the FC.

2D models

2D models go a step further and look at the phenomena taking place on two planes through the cell, both latitudinally and longitudinally. They also often include more detailed equations relating to heat transfer and the mass of reactants, amongst others.

Modelling Verification

The modelling of FC performance can help with reliability and degradation analysis of FCs, however experimentation can further solidify any results obtained through modelling. The modelling of the FC's performance is valuable to reliability as it can map changes in performance of the FC through the modification of key variables that the model uses to plot performance.

Verification of the FC model should be undertaken to show how the theoretical performance of a specified cell compares to the real world example. Once a verified FC model has been created, modifying this model with degradation due to failure modes can be done.

Verification is done by undertaking experimentation at certain operating conditions, taking into account temperatures of ambient atmosphere and gas feeds etc. Completing a polarisation curve to ascertain the performance of the cell. Then comparing the data from the experimentation to the same conditions used in the FC model. For instance, if a gas feed temperature was at STP, then the model would use the same STP rates for its inputs. The comparison of the modelled FC performance and the experimental data should agree, which would show a model that emulates what is seen in the real world and therefore accurate.

1.7 Thesis Aims & Objectives

Currently there are three main hurdles to the commercialisation of PEMFCs and their competition with the ICE, these are; infrastructure, cost and durability[23]. The aim of this work is to research into the reliability issues concerning PEMFC for transport applications, culminating in an affective model to predict the lifetime and degradation of a FC in an automotive environment.

The main aim of the thesis will be satisfied using the following objectives:

1. Understand current PEMFC degradation phenomena and modelling methods.
2. Gain a greater understanding of PEMFC reliability studies currently in the literature.
3. Based upon the literature review;
 - i Assemble a Failure Mode and Effect Analysis (FMEA)/Failure Mode, Effect and Criticality Analysis (FMECA) regarding a single cell PEMFC system.
 - ii Create a Fault Tree (FT) for a single cell PEMFC system .
4. Analyse the FT to understand the interactions of the various failure modes in a PEMFC system.
5. Use advanced techniques, such as Petri-Net analysis, to generate a quantitative model for PEMFC degradation.
6. Validate the model with experimental results where appropriate.

The integration of these objectives is shown in Figure 1.6.

1.8 Layout of Remaining Thesis

The remaining chapters of the thesis are listed below.

Chapter 2 - Durability & Reliability - Literature Review

A review of the current literature regarding the durability and reliability of PEMFCs is presented. Different techniques that have been used by numerous authors are discussed.

Chapter 3 - Failure Mode and Effect Analysis (FMEA)

This chapter details the work undertaken in construction an FMEA that represents all of the failure modes that an automotive FC system could experience.

Chapter 4 - Enhancing the Existing Reliability Modelling

An in-depth analysis of the most recent, and most advanced reliability analysis found in the literature is presented. Key errors found in the work from the literature are scrutinised and a

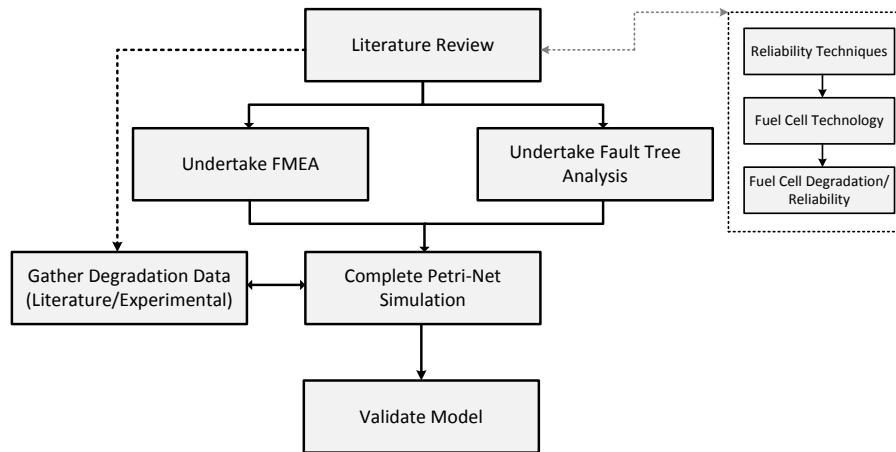


Figure 1.6: Integration of Objectives.

re-evaluation is presented to improve the work.

Chapter 5 - Proposed Petri-Net Analysis

The model of choice is then presented given the determined model complexities. Showing the way in which Petri-Net modelling techniques can be used to model FC degradation.

Chapter 6 - FC Model Integration and Validation

The use of a zero dimensional fuel model is explained, alongside some experimental validation of the model. The use of degradation observation techniques such as polarisation curve and Electrochemical Impedance Spectroscopy (EIS) techniques are also explained.

Chapter 7 - Results

The resulting data from the degradation modelling is presented in this chapter. Different aspects of the models' outputs are discussed and analysed.

Chapter 8 - Conclusions and Future Work

The final chapter looks at what can be ascertained from the work, and where the work could go in the future.

Chapter 2

Durability & Reliability - Literature Review

PEMFCs in an automotive application are required to perform under dynamic loads, freeze thaw conditions and around 30,000 start-up/shutdown cycles for 5,000 hours to be competitive with current ICEs [24]. State of the art PEMFC system lifetimes are not satisfactory to date due to decay in performance and ultimately catastrophic failure of the FC [25]. Thus it is paramount that the reliability issues are understood and mitigated against to aid in the commercialisation of this promising technology. PEMFC degradation can be measured by the drop in output power over time and is noted as μVh^{-1} .

2.1 Understanding FC Failures

A premature failure for this case would entail degradation of more than 5% or a lifetime of less than 5000 hours of operation as per the previously identified standards. To try to mitigate premature failures in a PEMFC system, one must first fully understand the contributing factors that might lead to the failure. Two techniques to aid in the achievement of this are FMEA and Fault Tree Analysis (FTA). These techniques can be used to broaden the knowledge of possible failures that can occur in a HFC system, with the view to predict and reduce the occurrence of the issues.

2.1.1 Failure Mode and Effect Analysis (FMEA)

FMEA is a systematic procedure to evaluate the potential failures that can occur in a system. FMEA works in a bottom up fashion where all potential failure modes that could cause the system to fail are listed to give a better idea of the systems potential failures. FMEA also analyses the effect that the failure modes might have on the system (effect analysis). FMEA of systems are common ground and required in many industries, and government agencies such as the Air Force and Navy [26]. FMEA is often undertaken at the earliest stage possible, as to pre-empt potential difficulties in the system once in operation. However, they are also used to gain a greater understanding of a system that is yet to be built and still in its design stage.

FMEA techniques can be approached with two main methods of analysis of a system; Functional, and Hardware. Functional FMEAs are coarse system breakdowns, where sub-systems are chosen to be analysed that provide some function to the overall system in question. This method is the more basic option, and gives the analyst an idea of how certain sub-systems interact in the main system. Hardware FMEAs are slightly more complex, and delve deeper into the component failure modes in a system, and how they interact with the system.

Table 2.1 shows an example of an FMEA table used to analyse a system. Each column is filled out for each component or sub-system to yield a complete picture of the overall system's

Table 2.1: Example FMEA Worksheet from [27]

IDENTIFICATION	FUNCTION	FAILURE MODE	FAILURE EFFECT		FAILURE DETECTION METHOD	COMPENSATING PROVISIONS	SYSTEM OUTCOME	REMARKS
			LOCAL EFFECT	SYSTEM				

potential failure modes. Each column is filled in with its respective data as per;

- Identification –Usually containing the component name and possible reference code. i.e. 1.1 Actuator ACT11.
- Function –The intended function of the component. i.e. open/close flap.
- Failure Mode –How the component has failed. i.e. stuck failed closed/failed open.
- Failure Effect
 1. Local Effect –The localised effect of the failure.
 2. System –The global effect of the failure on the whole system.
- Failure Detection Method –Are there any methods to observe if a failure has occurred? i.e. alarms.
- Compensating Provisions –Are there any failsafes in place to mitigate against the failure mode? i.e. redirect fluid via alternate route.
- System Outcome –The overall conclusive effect the failure mode has on a system. Sometimes not included due to correlation with Failure Effect - System.

FMEAs can be further evolved into FMECA where each failure mode is given a ranking based upon its probability of occurrence and severity to the system. The rank given to each failure mode is the product of severity classification and the probability of the failure modes occurrence/frequency. Thus two more columns are added to the FMEA Table 2.1; Probability/frequency of occurrence, and severity.

The severity classifications are defined at four levels;

1. Minor –No effect on system performance, no damage or injury.
2. Marginal –Degradation of item functional output, minor damage, delay to mission or minor injury.
3. Critical –Severe reduction of functional output affecting system performance, perhaps loss of mission, major damage or severe injury.
4. Catastrophic –Complete loss of system, system function or fatalities.

The severity classification number (1-4) is plotted with the frequency/probability data (also broken into sections from 1-4/5), if available. This yields a criticality matrix as per Figure 2.1. The frequency data is a numerical value that can be determined based upon either the frequency of occurrence or the probability of occurrence:

The shaded region in Figure 2.1 is therefore the unacceptable region and would require further analysis or a design change to make that failure mode fall into an acceptable region of the criticality matrix.

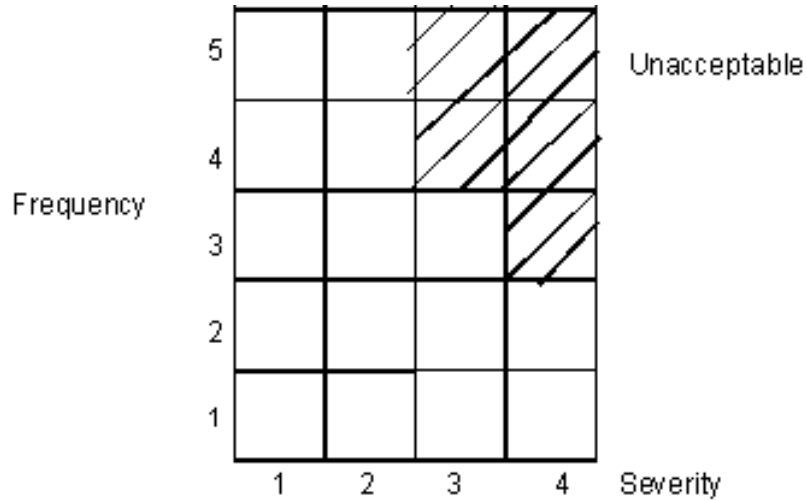


Figure 2.1: Criticality Matrix

2.1.2 FMEA used in the literature

There are no full FMEA tables available in the literature; however Rama, et al. [28] compiled a table for a single cell PEMFC listing the component, failure mode and the cause of the failure (see Figure 2.2). The full table is presented in Appendix A. The authors used five main degradation/failure modes, relating to; activation losses, mass transport losses, ohmic losses, efficiency loss and catastrophic cell failure.

Degradation / Failure Mode	Fuel Cell Component	Fault	Cause	References
D1. Increase of Activation Losses	Platinum catalyst	(1) Platinum agglomeration causing loss of EASA	(1) Repetitive on/off load cycling (2) High voltage induce at cathode equivalent to OCV due to residual hydrogen (3) Loss of carbon support	[7] [7] [8]
		(2) Platinum migration causing loss of catalyst material	(4) Solubility of platinum when cell is operated through hydrogen-air open circuit to air-air open circuit	[9]

Figure 2.2: Sample from full table in [28]

Arguably, the first three degradation/failure modes mentioned are the only ones necessary in that column, efficiency loss and catastrophic FC failure are effects that can pertain from the aforementioned failure modes. To this end, there appears to be no mention of the effects of each failure mode in the table. The authors list the main areas of degradation relating to the polarisation curve (see Section 1.6) and the FC component where the failure mode occurs. After this the authors list faults such as Platinum agglomeration causing loss of electrochemically active surface area (EASA), and what may cause this fault. There is no mention of how this failure mode would affect the overall operation of the PEMFC system. This is a limitation to the table proposed by the authors, as one of the main objectives of compiling an FMEA is to understand the failure modes within a defined system, and to understand how each failure can affect the system. This knowledge can help the designers and engineers mitigate against premature failure of the overall system, however without all the qualitative data regarding the FMEA, it is difficult to do so. With the increasing speed of data release, and only the one aforementioned table for failure mode analysis, it is required to compile a full FMEA of a PEMFC using the most up-to-date data.

2.1.3 Fault Tree Analysis

FTA is an analytical technique where the ‘top event’ or undesired event is specified, and the contributing factors are evaluated in the context of the system environment. This produces a graphical model which depicts a failure structure by highlighting the potential basic events that lead to it. This is a top-down approach as opposed to a bottom-up approach that can be used to analyse the causal relationship between component failure events and system failures [27]. It is a qualitative model that can be, and often is, evaluated quantitatively [29].

In order to compile a FT, several steps must be taken:

1. Clearly define the overall undesired event or ‘Top Event’
2. Based upon an in-depth literature review, expert knowledge and/or experimentation; determine the possible failure modes that can occur in the system that would contribute towards the top event
3. Once the tree has been drawn, analyse the logic of the tree to check its integrity
4. Qualitatively analyse the FT and determine the MCS
5. If failure probability is available, quantitatively analyse the tree with the most up-to-date and relevant data for each failure mode

Intermediate events are indicated by boxes, and contain a description, whereas basic events are denoted by circles, often containing codes. The relationship between the events are represented by gates. Gates can take many forms, and the gates can either allow passage or inhibit the flow of logic through the tree, and the way in which the decision is made is dependent upon the type of gate, with the most basic types listed in Figure 2.3. The gates also indicate the relationship between different events in the fault tree depiction. The circles represent the basic events of the tree, which is to say that the event cannot be further broken down into other relationships. Basic events feed into gates as per the example in Figure 2.4.

FT models can be evaluated either qualitatively or quantitatively to ascertain required data. The FT model is itself a qualitative model as it is constructed, but it can be further evaluated to delve deeper into the failure possibilities in a system. The way in which FT are further qualitatively evaluated is by ascertaining the Minimal Cut Sets (MCSs) of the top event. These MCSs are the lowest combination of basic events that can cause the undesired top event. These MCS are a valuable tool for reliability engineers to focus on the most likely failure roots and components that could cause the system to fail. Through this type of analysis of the FT model, one can identify weak links in the system, where one basic event may cause the top event failure.

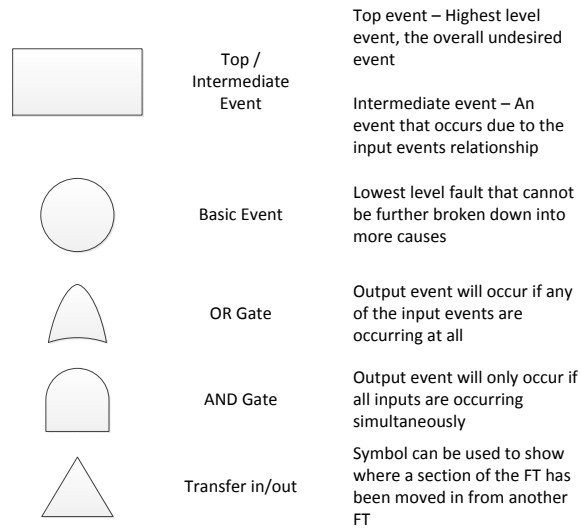


Figure 2.3: Example of common Fault Tree gates and events

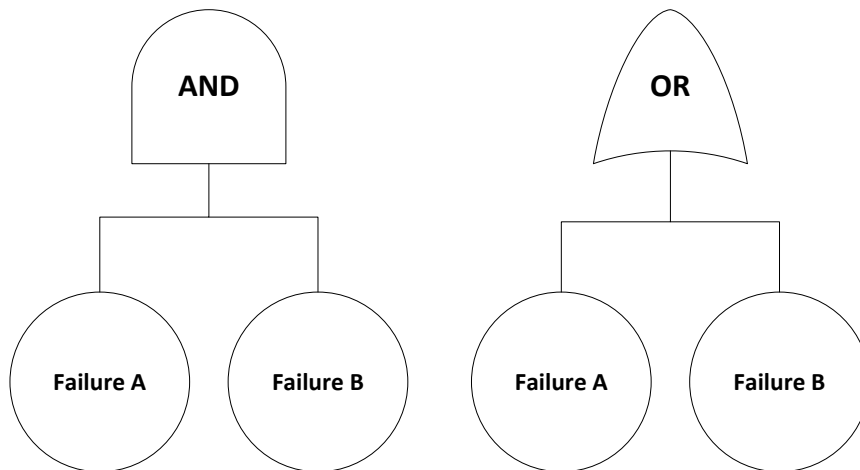


Figure 2.4: Example of common Fault Tree gate use

These areas can be mitigated against after identification through MCS analysis of the FT. The qualitative aspect is due to the graphical representation of the subject system, and this can be quantitatively evaluated by obtaining the probabilistic reliability data for each component and importing said data into the model. One can find the failure combinations from the graphical representation of a FT in the form of MCSs. FTs can be evolved to yield numerical data through quantitative evaluation in addition to the aforementioned MCS qualitative assessment technique. Boolean logic is used to quantify MCS information, where a ‘•’ denotes ‘AND’ and a ‘+’ represents ‘OR’ logic.

Dominant cut sets can be determined from this method of analysis, which are the MCSs that have the most influence upon the top event probability of occurrence, and where most effort should be concentrated initially.

There are many ways in which to calculate the top event probability, with the inclusion-exclusion method, rare event method, lower bound, and MCS upper bound methods listed below.

The inclusion-exclusion method is shown in Equation 2.1.

$$\begin{aligned}
P(TOP) = & \sum_{i=1}^{N_c} P(C_i) - \sum_{i=2}^{N_c} \sum_{j=1}^{i-1} P(C_i \cap C_j) \\
& + \sum_{i=3}^{N_c} \sum_{j=2}^{i-1} \sum_{k=1}^{j-1} P(C_i \cap C_j \cap C_k) - \dots \\
& \dots + (-1)^{N_c+1} P(C_1 \cap C_2 \cap \dots \cap C_{N_c}) \quad (2.1)
\end{aligned}$$

In Equation 2.1, the combinations of MCSs in pairs, threes, fours and so on, are listed to determine the overall probability.

The rare event approximation is shown in Equation 2.2.

$$P(TOP) = \sum_{i=1}^{N_c} P(C_i) \quad (2.2)$$

The lower bound method is shown in Equation 2.3.

$$P(TOP) = \sum_{i=1}^{N_c} P(C_i) - \sum_{i=2}^{N_c} \sum_{j=1}^{i-1} P(C_i \cap C_j) \quad (2.3)$$

The MCS upper bound method is shown in Equation 2.4.

$$P(TOP) = 1 - \prod_{i=1}^{N_c} (1 - P(C_i)) \quad (2.4)$$

Depending upon the accuracy needed, and the computing resources available in relation to the complexity of the FT to analyse, any of the above methods can be used to determine the top event probability.

2.1.4 FT Method used in the Literature

Placca and Kouta [30] recently used FT analysis to investigate PEMFC degradation. They constructed a FT of a single cell PEMFC with the overall concerning factor being the top event

of ‘reduction in voltage output’ to an extent that was detrimental to the functioning of the PEMFC system.

Placca et al. constructed a physical fault tree of a single cell PEMFC by splitting the top-event of the ‘Degradation of the Cell’ down into three sub-events: Membrane Degradation, Catalyst Layer Degradation and GDL Layer Degradation (See Figure 2.5). The entire FT can be found in Appendix B.

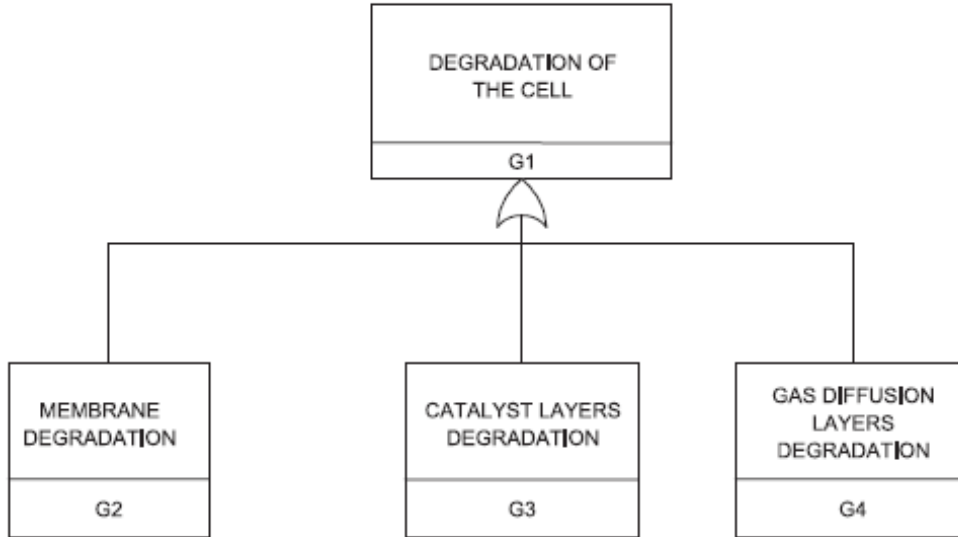


Figure 2.5: Top level interaction in work presented by Placca & Kouta [30]

These are three of the four main physical components of a PEMFC with only the bipolar plate being omitted. The omission of the bipolar plate component of a PEMFC is another issue that needs to be addressed with this work. There are many studies in the literature that document and analyse the degradation and failures of bipolar plate materials in PEMFC. Corrosion and mechanical failure are common occurrences in many studies [31][32]. It is recommended that for a more reliable FT, one would need to include ‘G5 Bipolar plate failure’. Failure modes affecting the bipolar plates include, but are not limited to; corrosion of the metal bipolar plate when in contact with the aqueous and acidic environment of the PEMFC, mechanical fatigue caused by repeated thermal cycles and silicone sealant used as a gasket on the bipolar plate can degrade and enter the membrane. According to the authors, the bipolar plate issue was omitted due to the degradation rates shown in the literature were considered negligible.

All of the failure modes used in the French work were translated from French to English and checked with the original authors and are presented in Tables 2.2 - 2.5.

The majority of the basic events are too equivocal and are not necessarily binary in nature. E002 ‘long-term functioning’ is too ambiguous in description, not informing the reader whether it means that the cell is completely failed or is degraded to a lower output state due to long-term operation. There is no explanation of what this pertains to, such as a time frame, or what the failure mode is. During long term operation, many components can fail by any number of failure modes. As such this basic event is misleading and should be further explained or changed for specific failure modes. The reference is from a review paper of multiple lifetime studies by J. Wu et al.[23]. The authors list 12 studies of lifetime analysis of PEMFC experiments. Placca et al. chose to take the first result by Ralph [33] where it would have been more scientific to take an average of all the studies to more adequately represent the scope of all works in this area, and get a more reliable value of ‘long term operation’ degradation.

The intermediate events are shown in separate tables as some of the numbered events have

different text labels in different trees. They used reliability data compiled from many sources within the literature, and extrapolated the data to acquire a formatted degradation measure. Difficulties arise with this work as the data accumulated is from different tests that use differences in variables such as; pressure, temperature, cycling, and even different membranes. This makes the data heterogeneous in nature and can therefore skew the accuracy of the output data pertaining to reliability values. Some data that could not be found in the literature was proposed by the authors based on ‘previous experience’. From the above two examples, the data could be seen as fundamentally unreliable, and this is acknowledged to some extent by the authors in their concluding remarks regarding weaknesses in the work. The lack of homogenised data for a PEMFC is a pitfall that can only be overcome by an increase in experimental analysis of certain failure modes in a FC. An ideal scenario would incorporate sets of standardised experiments to homogenate degradation data, aiding with the validity of failure analysis.

Yousfi-Steiner, et al.[14] looked into using FT analysis to help understand contributing factors towards water management issues in a PEMFC.

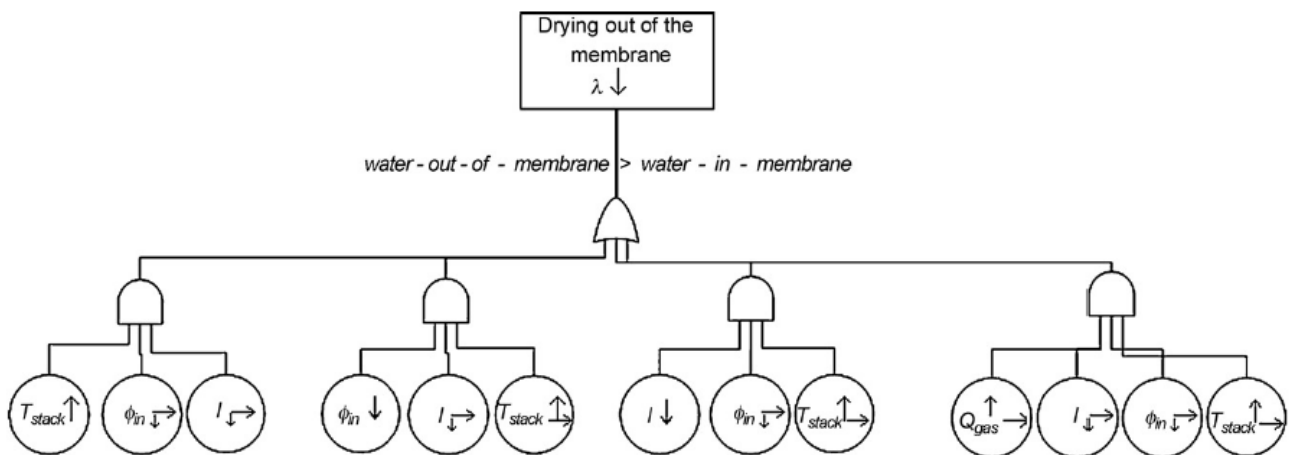


Figure 2.6: Drying out of the Membrane FT [14]

The example shown in Figure 2.6 indicates the basic use of OR and AND gates to determine whether a mixture of certain phenomena can cause the top event of Drying out of the membrane. For example the leftmost branch looks at how a combination of stack temperature increase ($T_{stack} \uparrow$), relative humidity decrease ($\phi_{in} \downarrow \rightarrow$) and current density reduction ($I \downarrow \rightarrow$), will result in the drying of the membrane.

Table 2.2: Basic Events from Placca et al. [30]

Numer	French (as per paper)	Translation (Google&manual)
E001	Radicaux OH	OH Radicals
E002	Fonctionnement à long terme	Long-term functioning
E005	Noyage	Flooding
E006	Potentiel d'oxidation	Oxidation potential
E007	Faible stoichiometrie	Low stoichiometry
E008	Difficultés d'accès des gaz aux couches actives	Difficult access to the active layers of gas
E009	Cyclages	Cycling
E010	Longues périodes d'OCV	Long periods of OCV
E011	Stratégie de contrôle	Control strategy
E012	Transitoires	Transient
E013	"Crossover" de réactifs	Crossover of reactants
E014	Existence d'impuretés lessivées	Existence of impurities leached
E015	Contamination	Contamination
E016	Anomalie de fabrication	Manufacturing abnormality
E017	Eau ou glace	Water or Ice
E018	Défauts congénitaux de la membrane	Congenital defects of the membrane
E019	Processus de fabrication impropres de l'assemblage membrane electrodes (AME)	Improper manufacturing process of membrane electrodes assembly (MEA)
E020	Augmentation du crossover des gaz	Increase in gas crossover
E021	Formation de trous (dégradation mécanique)	Forming holes (mechanical damage)
E022	Mauvaise répartition des contraintes mécaniques	Poor distribution of mechanical stresses
E023	Perte importante de la conductivité ionique	Significant loss of ionic conductivity
E024	Perte importante de l'imperméabilité aux gaz	Significant loss of impermeability to gases
E025	Température de transition vitreuse des polymères APFS	Glass transition temperature of the polymers APFS
E027	Production de dioxyde sulfurique, et de radicaux OH	Sulfuric dioxide production, and radical OH
E028	Baisse de la conductivité protonique	Decrease in proton conductivity
E030	Accélération de l'amincissement de la membrane	Acceleration of the thinning of the membrane
E031	Formation de trous	Formation of holes
E037	Trous (combustion exo-thermale entre H2 et O2)	Holes (exo-thermal combustion between H2 and O2)
E038	Destruction de l'AME	Destruction of the AME
E039	Présence d'ions cationiques étrangers	Presence of foreign ions cationic
E040	Formation de H2O2	Formation of H2O2
E041	Formation des radicaux OH et OOH	Formation of OH and OOH radicals
E042	Formation des radicaux COOH	Formation of COOH radicals
E043	Formation de la structure d'acide amide	Structure formation of acid amide
E044	Formation des groupes amines et de diacides terminaux	Formation of amino groups and terminal diacids
E047	Faible HR des réactifs	Low HR reactants

Table 2.3: Intermediate events for Membrane FT [30]

Numer	French (as per paper)	Translation (Google&manual)
G1	Dégradation Membrane	Membrane degradation
G2	Dégradation Mécanique	Mechanical degradation
G3	Degradation Thermique	Thermal degradation
G4	Dégradation Chimique/Electrochimique	Degradation Chemical / Electrochemical
G5	Dégradation en début de vie	Degradation in early life
G6	Dégradation en fonctionnement	Deterioration in functioning
G7	Dégradation à températures très basses	Degradation at very low temperatures
G8	Dégradations à hautes températures	Degradation at high temperatures
G9	Combustion exothermique entre H2 et O2	Exothermic combustion between H2 and O2
G10	Contamination (par des traces d'ion métallique)	Contamination (by traces of metal ion)
G12	Flux d'eau modifié à l'intérieur de la membrane	Feed water modified within the membrane
G14	Dégradation Peroxide/Radical	Peroxide degradation / Radical
G15	Dégradation hydrolytique	hydrolytic degradation

Table 2.4: Intermediate events for Catalyst FT [30]

Numer	French (as per paper)	Translation (Google&manual)
G2	Dégradation des couches actives	Degradation of active layers
G5	Dissolution de platine	Dissolution of platinum
G7	Dégradation de carbone	Degradation of carbon
G16	Réversibilité de la cellule	Reversibility of the cell
G17	Mauvaise distribution des réactifs	Poor distribution of reagents
G18	Réactifs insuffisants	insufficient reactive
G30	Dégradation à l'anode	Degradation at the anode
G32	Dissolution de platine	Dissolution of platinum
G33	Dégradation de carbone	Degradation of carbon
G34	Fonctionnement global/local à forts potentiels à la cathode	Functioning global / local strong potential at the cathode
G35	Hétérogénéités de la distribution de courant	Heterogeneities of the current distribution
G38	Réactifs insuffisants	insufficient reactive
G39	Dégradation à la cathode	Degradation at the cathode

Table 2.5: Intermediate events for Diffusion Layer FT [30]

Numer	French (as per paper)	Translation (Google&manual)
G4	Dégradation des couches de diffusion	Degradation of the diffusion layers
G11	Dégradation du carbone	Degradation of carbon
G12	Dégradation de PTFE	Degradation of PTFE
G33	Dégradations à la cathode	Degradation at the cathode
G34	Dégradations à l'anode	Degradation at the anode
G35	Dégradation de PTFE	Degradation of PTFE
G36	Dégradation du carbone	Degradation of carbon

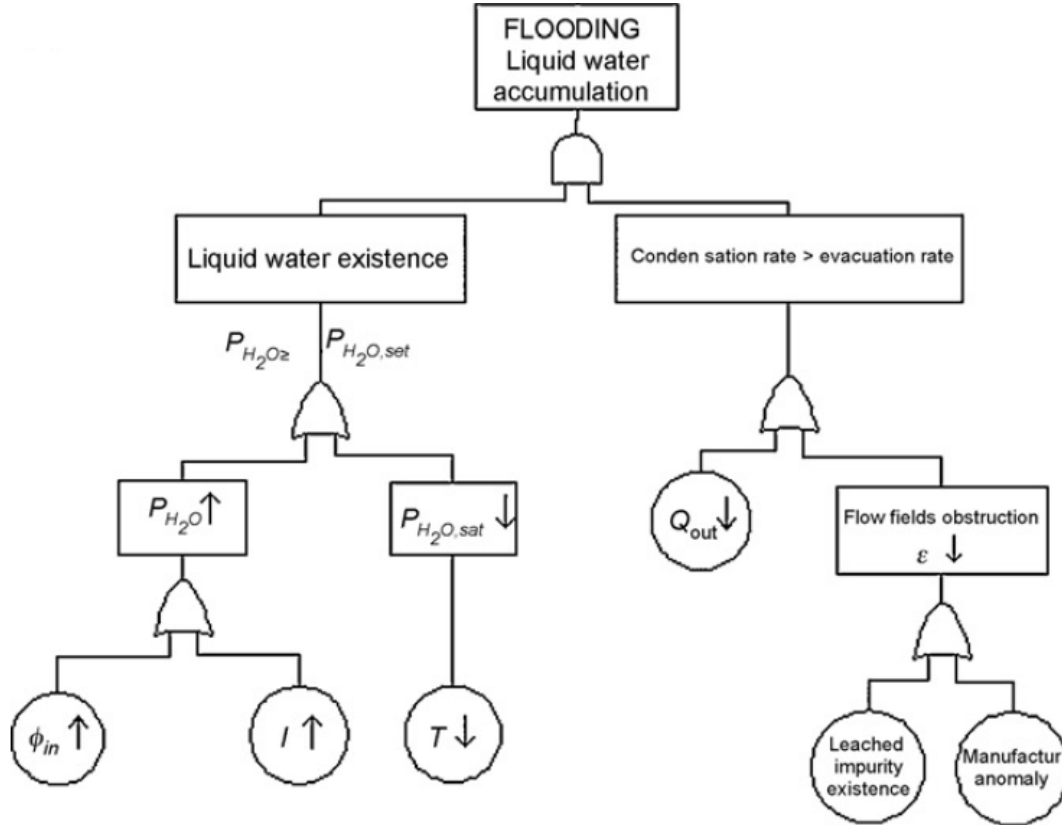


Figure 2.7: Flooding of the Membrane FT [14]

Figure 2.7 presents a more detailed overview of failure logic for a different top event. Membrane flooding is detailed with less ambiguity in the failure events. However the logic could be developed further, such as the intermediate event Flow Fields Obstruction.

There are more failure modes that could cause flow field obstruction, such as BIP corrosion, pressure increase due to swelling/corrosion and ice formation due to subfreezing temperatures. For a comprehensive analysis of the factors that could lead to flow field obstruction, these should be factored into the FT. Alternatively, Figure 2.7 shows the relationships required for the flooding of a membrane to occur, taking into account the relationship between liquid water existence and the condensation rate overpowering the evacuation rate.

The same authors also used FT analysis in another publication regarding Pt catalyst degradation mechanisms [34]. Figure 2.8 shows how the authors chose to not only include the basic events (presented in circles) however they also chose to list some operating conditions that can also lead to the top event. For example; Low stoichiometry and long periods at OCV from the left branch of the tree.

The trees presented in Figures 2.6-2.8 are a good way of indicating logic of failure modes and operating parameters that might influence the top event. However, as with the work from Placca & Kouta, there are some anomalies. Figure 2.6 shows some instances that might lead to the drying out of the cell, however the right most branch needs to be improved upon. In Figure 2.9, Q_{gas} refers to the volumetric flow rate of the gas, I is in reference to the current density, ϕ_{in} is the relative humidity and T_{stack} is the temperature of the stack. The upward arrows indicate an increase in the parameter; a horizontal arrow indicates no change and the downward arrows show a decrease in the value of the given parameter. Therefore, according to the authors, if all four variables remain constant, the membrane will dry out. This is not the case, as a constant flow of gas to maintain a constant current density, in the environment of constant Relative Humidity (RH) and stack temperature, are ideal scenarios for the operation

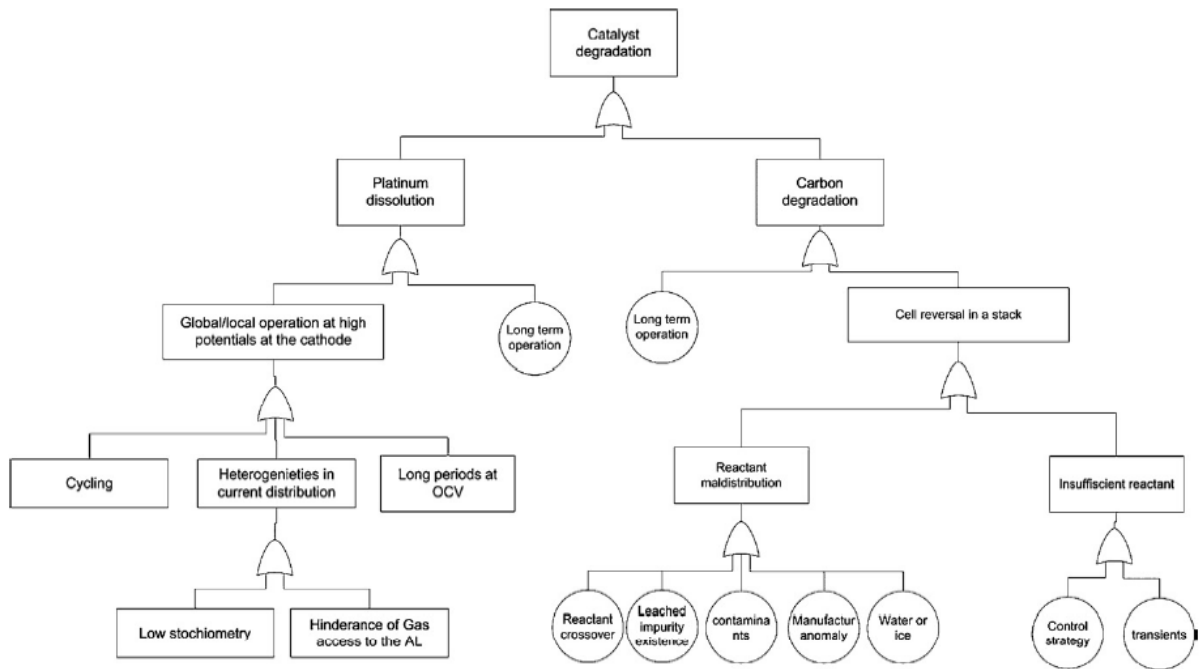


Figure 2.8: Catalyst Degradation Example [34]

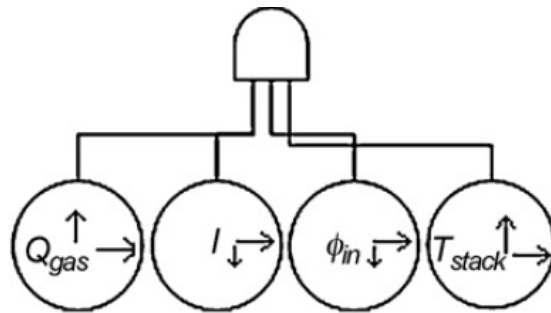


Figure 2.9: Detail of Branch from Drying out Tree [14]

of a PEMFC. This may be due to oversimplification of the basic events; it is difficult to state that a basic event can be either constant/decreasing, or constant/increasing. These should have been further split down into one basic event for increasing and one for constant rate (with the same done for decreasing rate respectively).

2.1.5 Petri-net Modelling

Petri-nets were first conceived by Carl Adam Petri and have a solid mathematical modelling language foundation. Petri-nets consist of two types of nodes; Places and Transitions. Places can be understood as representing an event in the system, and the transitions can be understood to represent the conditions. A simple Petri-net structure [35] can be based upon (P,T,F,B) where:

- A finite set of places $P = \{p_1, \dots, p_{|P|}\}$
- A finite set of transitions $T = \{t_1, \dots, t_{|T|}\}$ with $P \cap T = \{\}$
- A $|P| \times |T|$ matrix F with elements out of $\{0,1\}$, and
- A $|P| \times |T|$ matrix B with elements out of $\{0,1\}$

The F & B matrices are the Forward and Backward transitional states of the places. These are the sets of arcs that connect places and transitions in the graphical model.

Figure 2.10 shows a simple two place, one transition Petri-Net. ‘P1’ is the first place, and represents the system’s working state. However, if a set of predetermined criteria are met, ‘T1’ transition can fire, and represents the transition of the system going from a working state, to a failed state ‘P2’. The arrows connecting the places and transitions are the arcs, and indicate direction of flow of the logic.

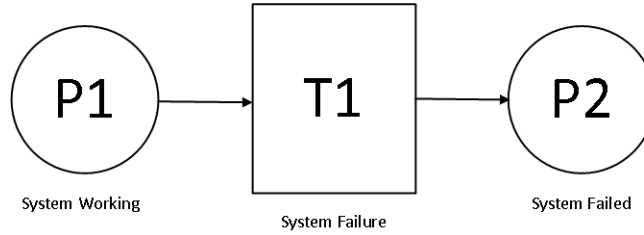


Figure 2.10: Example of a simple Petri-Net

Coloured Petri-nets are similar in fashion to the standard Petri-net, however the tokens that fire from place-to-place can contain information about the system. Whereas the standard Petri-net is used to determine the system state from the position of the tokens, coloured Petri-nets can hold pertinent data about the system in the same token. This aspect of coloured Petri-nets makes them an ideal candidate for use in PEMFC systems, as certain levels of degradation can be stored in the token, rather than having multiple places to represent multiple levels of degradation. The data contained within the tokens can be analysed or modified depending upon the transitions it passes through or the system state information. Using coloured Petri-nets allows the combination of multiple sub-modules of Petri-nets to combine into an overall Petr-net model.

Petri-net graphs can be analysed in a number of ways, from the duration of a token’s placement in a place or frequency of occupation of a place.

2.1.6 Qualitative Analysis

As shown, Petri-Nets have a graphical representation which can be qualitatively analysed. They show the different states of a system and what transitions exist between them. One can place tokens in places to easier understand the current state of the system. Following the token marks through the running of the Petri-Net model is a useful qualitative tool to see how certain interactions in a system can lead to other effects. Evaluating the matrices for Figure 2.10 is a method to do this. The starting matrix can be shown as Equation 2.5.

$$P = \begin{pmatrix} 1 \\ 0 \end{pmatrix} \quad (2.5)$$

This shows that there is a token in P1, and no token placed into P2.

A transition matrix can be used to determine the token movement when a transition fires as in Equation 2.6.

$$\begin{matrix} T1 \\ P1 \\ P2 \end{matrix} \begin{pmatrix} -1 \\ 1 \end{pmatrix} \quad (2.6)$$

This shows how a token is removed from P1 (-1) and is placed into P2 (1) upon firing of T1. This would result in a new marking matrix denoted by Equation 2.7.

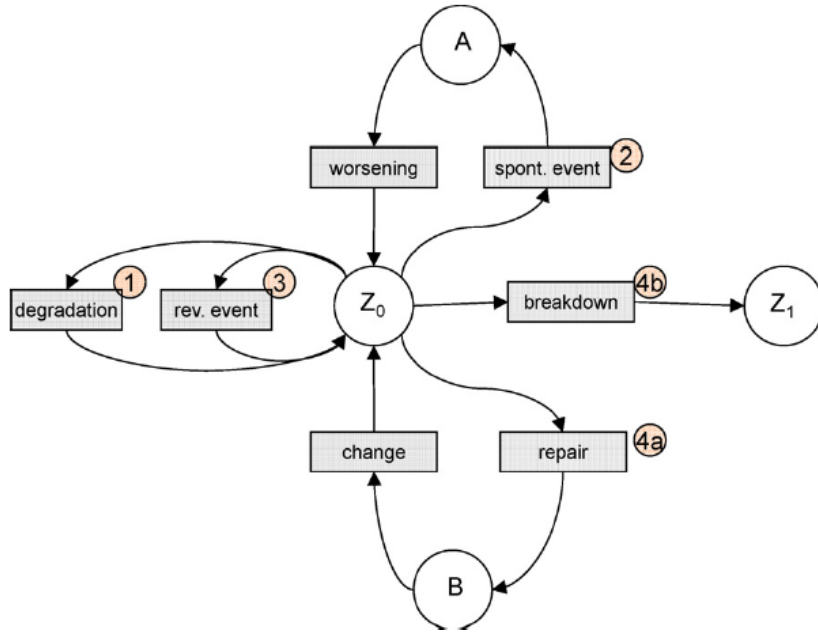


Figure 2.11: Example Petri-net for PEMFC system [35]

$$P = \begin{pmatrix} 0 \\ 1 \end{pmatrix} \quad (2.7)$$

2.1.7 Quantitative Analysis

The quantification of Petri-Net structures is often undertaken using a probability distribution functions such as the Weibull distribution, modelling values such as lifetime of components/systems. The token placement in a place/state would initiate a calculation of event probability based upon data such as the Mean Time To Failure (MTTF). The quantification can take the form of a cumulative average lifetime of a system, or a percentage of times that places are marked with a token.

Coloured Petri-nets can assign a value to a token that moves through the net. This could be in the form of a counter or level of degradation in a system.

2.1.8 Petri-nets in the literature.

Petri-net modelling is presented by Wieland, et al [35]. The model presented is flexible as it can accommodate expansion and adaptation, where it can represent a single cell, a stack, or even fleet of cars.

Figure 2.11 shows the graphical representation of the Petri-net model presented. Z_0 indicates the initial starting place for the modelling and that the cell is operational. Z_1 refers to the cell being out of order, resulting in the stack being out of order. Place A is indicative of the states of spontaneous nature, whereas place B is the state of repair. From here, transitions 1-4b can fire, dependent upon the random numbers designated to the transitions.

Transition 1 'Degradation' fires in any case and is representative of stack aging. It also takes into account the worsening of each of the five characteristics the model takes into account; MEA Voltage, internal leakage, external leakage, voltage loss from BIP and coolant gas leakage. The model takes a mean and standard deviation for each and this is used against the age value to generate a random number for computing the worsening of the characteristic.

Transition 2 ‘Spontaneous event’ is housed in place ‘A’ and does not operate in the same manner as transition 1. This does not fire at each step, however it fires through the following logic process [35];

1. Firstly, it is determined if a spontaneous event j is happening at time t . Every spontaneous event j occurs with a certain probability $p(j, a_{stack})$. Here a_{stack} is the stack age, which is defined by the age of the oldest component. The spontaneous event takes place if a uniformly distributed random variable $U(0,1)$ is less than or equal to the given probability $p(j, a_{stack})$.
2. After deciding whether the spontaneous event j is occurring, the number of effected cells next to a randomly chosen start cell z_s is determined. Some mechanisms affect weak cells in favour. In such cases the start cell z_s is the cell with the lowest voltage or the cell with the greatest leakage. The number of cells that are affected by the event j is generated by the normal distribution. For every event $a_{meanj, num}$ and standard deviation j, num is saved. The number num_j of affected cells is specified by Eq. (3):

$$num_j = N(j, num, 2j, num). (3)$$

Transition 3 ‘Reversible Event’ is operated in the same way as transition 2, however there is no lasting effect on the system, the failure is noted but the system returns to the place Z_0 .

Transitions 4a and 4b represent repair or breakdown respectively. Thresholds are set for each characteristic, that when exceeded, either repair or breakdown of the system is initiated.

The output of the model is a percentage contribution to cell degradation based upon the input failure modes. For example; ‘Natural Ageing’ is quoted to be the most significant contributor to cell degradation. There is no mention of an estimated lifetime of the cell/stack.

A potential weakness to this research is again that data used is aggregated from numerous sources in different formats. This cherry-picking of data does not give an accurate representation of an individual cell with its own environmental and operational parameters. It is highlighted by the authors as a weakness in the fact that the models degradation state is steady and not associated with environmental factors, such as time of year. It could be argued that freeze thaw related degradation will not be as significant in summer as it is in winter. Petri-net modelling is known for its ability to be adaptable to situations that contain dependencies and features that can include numerous degraded states.

2.1.9 Markov Modelling

The underlying principle of Markov Modelling (MM), is that they make use of the Markov Property in that the model uses stochastic variables for its calculations that only depend on the current state of the system, and has no memory of previous events. MM is potentially well suited to PEMFC reliability analysis as the state transitions in a MM occur continuously instead of at discrete time intervals. This is beneficial as PEMFC components can suffer deterioration as a consequence of age and spontaneous negative events.

The structure of MM involved the listing of all the possible states of the system to be analysed. These take the form of circles in a diagram that indicate what state the system is in. Arrows joining these possible states indicate the logic flow between states, or transitions. Once all states of the system that is being analysed have been determined and joined by transition arrows, the graph can be converted into equations that model the system. The state equations will contain the probabilities of failure or repair for each transition. MM is often used when FTA has been exhausted due to dependencies in the system that is being analysed. MM suffer slightly in terms of adaptability, any MM that is adapted with a new state or transition structure is deemed to be a new MM with an increased complexity. MMs work by having transitions entering and leaving a state, with the total probability equal to the sum of all transitions leaving the state, multiplied by the probability of the actual state. For large and complex models, single

determining equations are replaced with matrices that show the state of the system, and larger equations dealing with these matrices determine the modelling of the system state.

For a MM to be applicable, the system being analysed has to be stationary, it must use the memoryless property and all possible states of the system must be identifiable. It must also be noted that the models themselves can grow very large when considering a system with many components with many states for each component.

Work in this area is very sparse and still under development, however a recent work was published by an American research group, looking at MM of a standalone power supply unit [36]. This work looked at a power plant system level analysis (See Figure 2.12), including; cooling system, humidification system, fuelling & humidification system, air circulating system, energy storage system, and the FC itself.

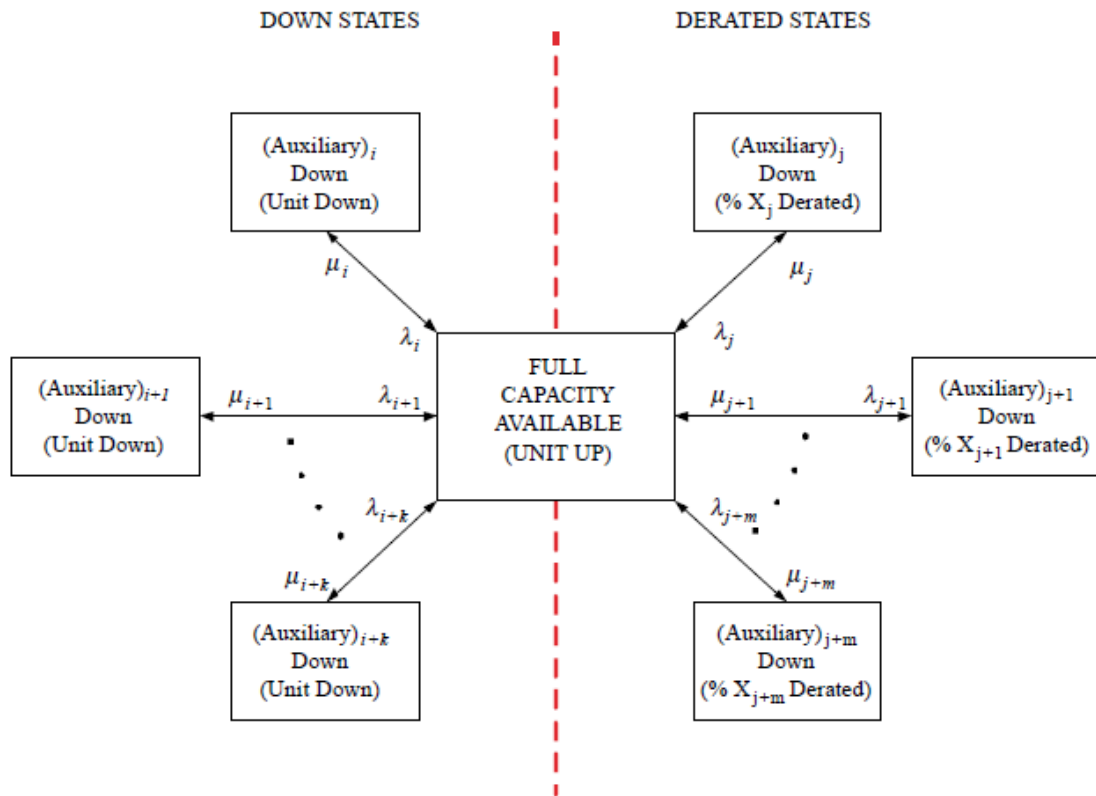


Figure 2.12: State Space Model Presented by Tanrioven & Alam[36]

A fundamental issue with the presented work, is the fact that degradation is only considered after 5000 hours of operation, and that stack degradation is assumed to be a flat rate drop of 0.0001% per hour. Additionally, for a fully comprehensive MM of a PEMFC system, one would need an endless amount of states to represent every level of degradation for every component. Therefore a true appraisal of a PEMFC system would have an infeasibly large state transition diagram.

Additionally, MMs offer no versatility in regards to expansion. With the infancy of the area of PEMFC reliability analysis it is assumed that any model will need to be easily adaptable when new data is acquired by the research field.

The overall MM presented is a good first step into looking at MM of PEMFC systems on the whole. However it fails to consider differing degradation rates based upon component level failures in the PEMFC itself.

2.2 Modelling Conclusion

Within the FC area, reliability modelling is still in its infancy and current analysis undertaken in the literature has been highlighted to show potential weaknesses with the current methods. Petri-nets have proven to be a useful method to analyse failures, however they are more involved than a simple FT model, and if verification of a simple, quantitatively analysed FT model can be achieved, it would highlight what areas PEMFC designers and engineers need to focus on to make PEMFCs last longer than ICE. The focus of this work is to improve the methods currently used in PEMFC reliability analysis, and ascertain a functional reliability model to accurately predict degradation phenomenon and lifetimes of PEMFC.

Additionally it was found that no research to date has modelled a PEMFC and verified the outputs against real-world drive cycles. The data review thus far has seen that verification is usually done under full load and partial loads for certain timescales. In the real world, it is highly unlikely that a PEMFC car user will drive at full load for extensive periods of time. They are more likely to vary greatly dependent upon routes, traffic and other factors.

The analysed methods in this chapter have all displayed weaknesses due to a lack of complexity of the FC system, which is an area that will be developed in future chapters.

2.2.1 Next Steps

Due to the previously highlighted limitations and modelling review, the next steps would be to start with a fully comprehensive FMEA of a PEMFC. The FT previously presented by Placca & Kouta [30] will be analysed in depth, as to acquire its applicability and accuracy for PEMFC reliability research. This will inevitably lead on to an optimised FT based upon the results of the FMEA.

Chapter 3

FMEA

As previously highlighted in Chapter 2, there are no previous examples of a full FMEA for a PEMFC in the literature. Therefore a full FMEA was constructed through an in depth literature search, to agglomerate the known failure modes that can occur in a PEMFC, alongside their effects and any important remarks.

An overall PEMFC system in an automotive application has numerous interacting systems and support mechanisms to get power from the gas, to the wheels. Therefore the system boundaries for this work are set at only the PEMFC itself as in Figure 3.1. The black-dashed, boxed out area is the main focus of this work, excluding any failure phenomenon experienced in the ancillary components of the automotive system.

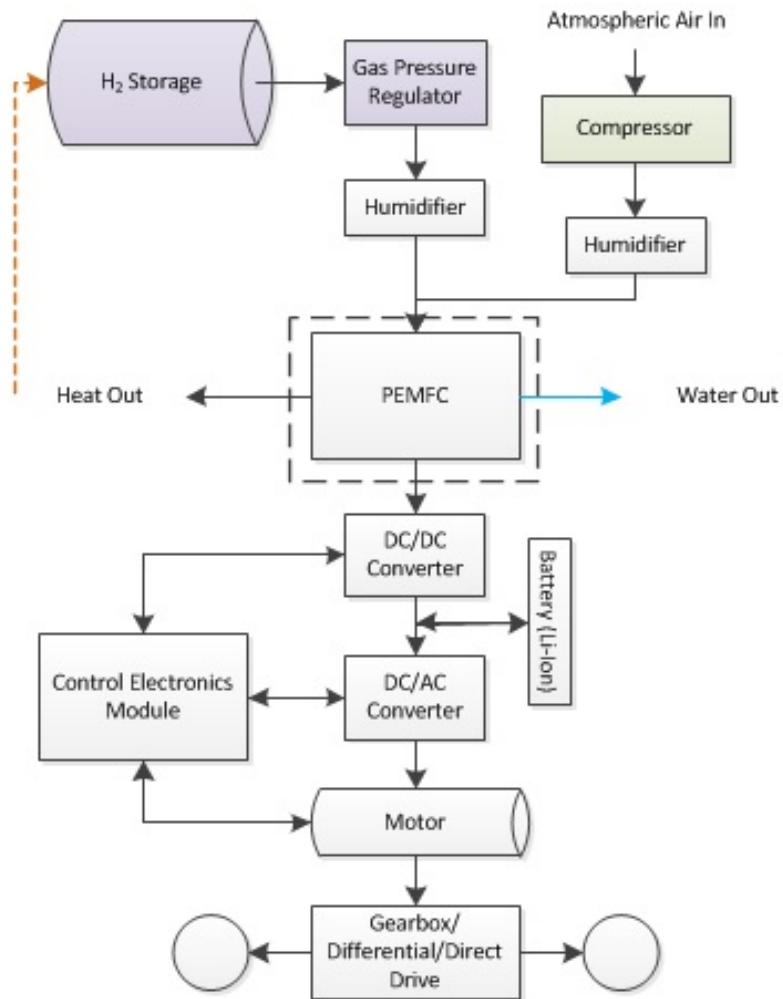
3.1 PEMFC Construction

Due to the range of materials and components that can be used to create a PEMFC, the following analysis is based upon the key assumptions of material and construction (Figure 3.2);

- Standard PEMFC construction.
 - PTFE membrane.
 - Carbon GDL.
 - Pt/C catalyst layer.
 - Stainless-Steel BIP.
- Using H_2 fuel feed with a purity of 99.97% as required by the ISO standard 14687-2:2012 [38].

3.1.1 PTFE Membrane

PTFE membranes are perfluorinated polymers, with the most commonly available being Nafion. Perfluorinated polymer membranes are also available from Tokuyama (Neosepta-F®), W. L. Gore and Associates, Inc. (Gore-Select®), Asahi Glass Company (Flemion®), Asahi Chemical Industry (Asiplex®) and Dow. Nafion has a backbone chemical structure very similar to PTFE (Teflon®) however, where it differs is that Nafion includes sulfonic acid (SO_3-H^+) functional groups. The PTFE backbone forms the strength of the membrane, and the SO_3-H^+ terminal groups provide charge sites for protonic transport. This study considers the Nafion brand PTFE membrane.



- = Anode side (H₂)
- = Cathode side (O₂)
- ➔ = Heat can be used to released H₂ from storage (metal hydride)

Figure 3.1: Functional Block Diagram of PEMFC automotive system

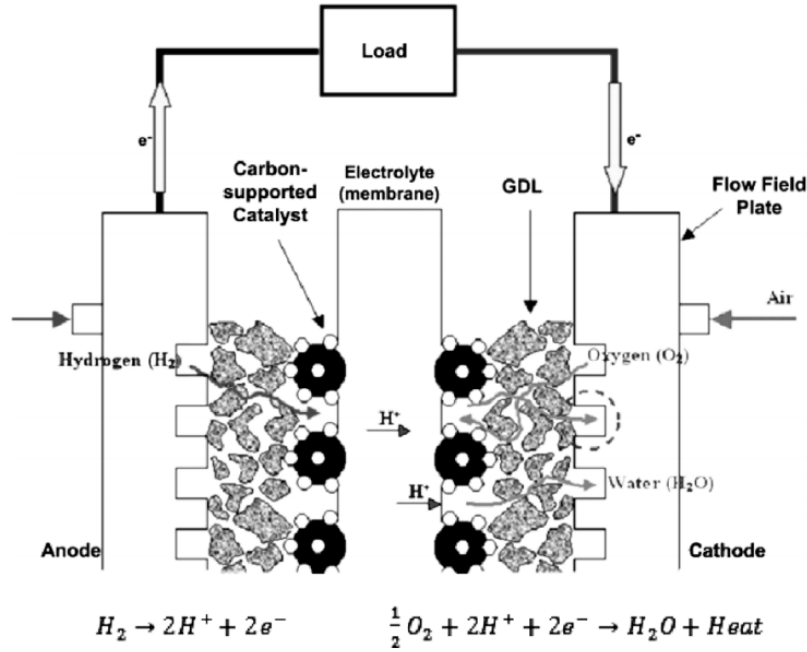


Figure 3.2: Components of a PEMFC [37]

3.1.2 Carbon GDL

The GDL is made from a carbon-fibre based material that is either formed into a paper or woven cloth type. Carbon-fibre is used due to its high electrical conductivity and high porosity values. Due to the materials for each method of constructing the GDL being identical, the failure mechanisms that can be experienced by either construction method are the same, therefore each construction method can be considered, as only the construction style differs and the material is the same. This study uses the carbon paper type GDL.

3.1.3 Pt/C Catalyst

Pt and C are mixed in an ionomer and usually ball milled to mix into an ink. This is then either screen printed or directly printed onto the membrane or GDL surfaces.

3.1.4 Stainless-Steel BIP

The endplates, or BIP are usually made from steel, and are routed to form serpentine channels for the gas to be delivered to the GDL component.

3.2 Operating Conditions

The operating conditions for the system are considered to be reflective of the power requirements of the New European Drive Cycle (NEDC), used to assess the emissions of car engines and fuel economy in passenger cars. The NEDC is representative of the typical usage of a car in Europe, consisting of an Economic Commission for Europe (ECE)-15 urban drive cycle (Figure 3.3) repeated four times, followed by an extra-urban driving cycle (Figure 3.4). The product of which is shown in Figure 3.5. It is assumed that due to the power demand from the vehicle during this cycle, the failure modes identified can occur.

During operation in the above context, the FC can experience the following:

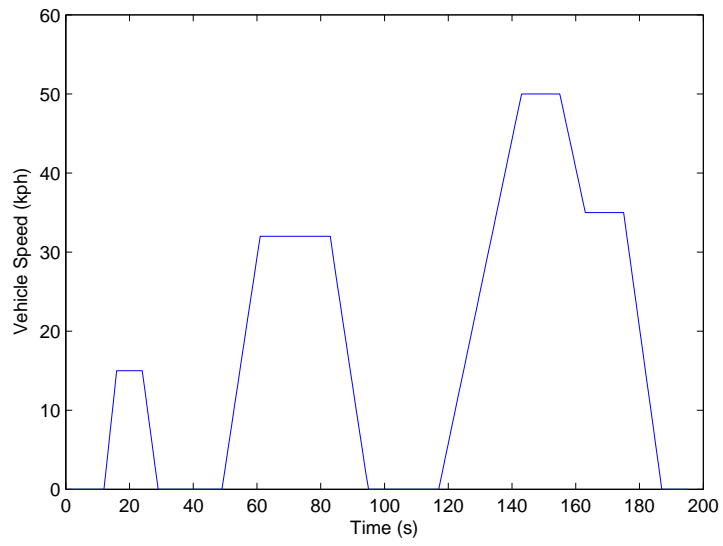


Figure 3.3: ECE 15 Drive Cycle [39]

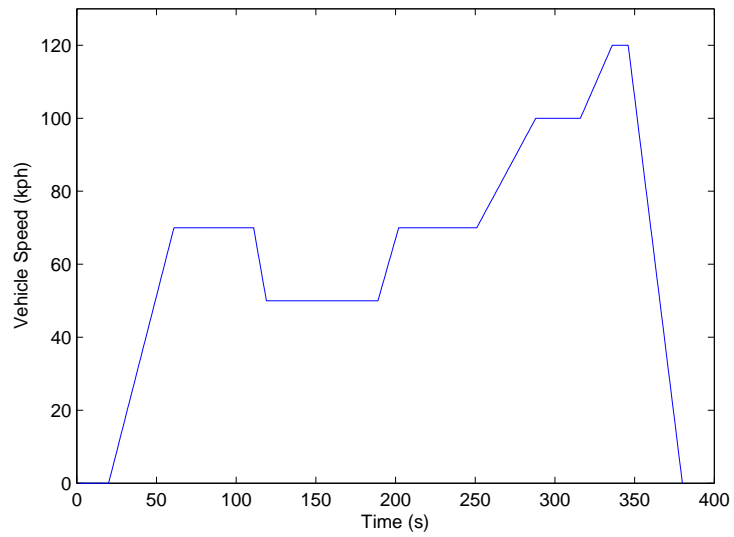


Figure 3.4: Extra-Urban Drive Cycle [39]

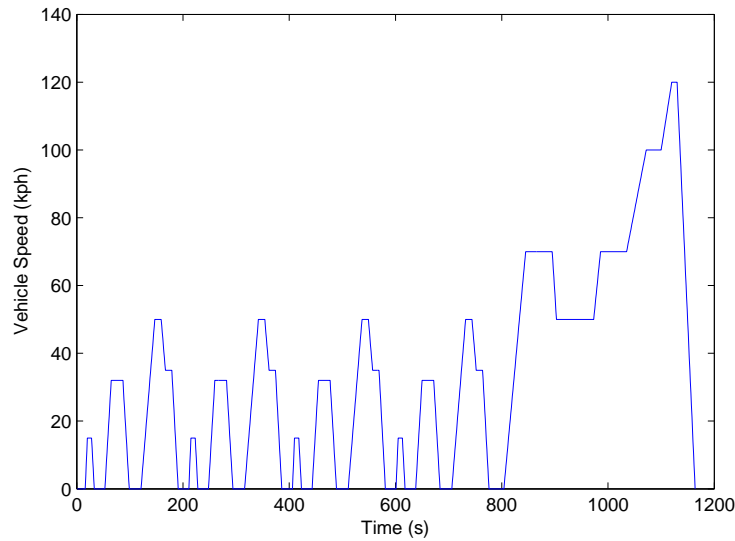


Figure 3.5: New European Drive Cycle [39]

- OCV
- Steady state voltage (constant load output of around 0.6-0.7 V)
- Load following state (FC demand from 0-1.2 V dependent upon drive cycle phase)
- Cold temperatures ($<80^{\circ}C$)
- Ideal temperatures ($80^{\circ}C$)
- Hot temperatures ($>80^{\circ}C$)

It is also noted that modern day PEMFCs systems purge the hydrogen gas feed at regular intervals, therefore this should be taken into consideration with any failure mode evaluation. Experimentation with a 100W PEMFC stack showed that the manufacturers' recommended 0.5 second purge every 30 seconds was not optimal for the unit. Changing the purge interval to 0.5 seconds every 20 seconds increased the performance of the stack, by decreasing the build-up of excess water in the stack.

3.3 Performance Loss Mechanisms

The performance loss mechanisms are split into the four main components of a PEMFC; Membrane, Catalyst Layer, GDL, and BIP of which they effect. This is to help to understand which failure modes occur in which of the main sub-layers of a PEMFC single cell.

3.3.1 Membrane

The membrane forms the heart of the PEMFC stack and is the electrolyte that blocks the flow of electrons, however it allows the passage of H^{+} protons through from anode to cathode side. It can suffer from 8 separate basic failure modes, that can lead on to localised and system effects.

- **Incorrect BIP torque** can increase the membrane's resistance consistent with the viscoelastic compression of the membrane.

- Polymer '**creep**' causes membrane thinning and can lead to mechanical damage of the membrane.
- **OH and OOH radicals & H₂O₂** can contaminate the PTFE material of the membrane through end group unzipping.
- The **presence of foreign cationic ions** can adsorb onto the membrane, and they have a stronger affinity with H⁺ ions in the membrane. This can lead to extensive drying of the membrane and attenuated water flux/protonic conductivity.
- **Ice formation** can seriously impair the mechanical strength of the membrane by rearranging ionomer at a molecular level through freeze cycling. Additionally, frozen water reduces the conductivity of the membrane and the impermeability of the membrane.
- **Fatigue from relative humidity and temperature cycling** can cause a weakness and eventual mechanical breach of the membrane.
- **Excessive heat** in a PEMFC can cause Sulphur Dioxide OH radical formation, and the glass transition state of Per-FluoroSulfonic Acid (PSFA) polymers. Additionally, excessive heat can dry out the membrane, causing a drop in protonic conductivity.
- **Flooding** swells the membrane which increases pressure build-up, and actively blocks pores, reducing protonic conductivity, and risks freezing if operating temperatures are low.

3.3.2 Catalyst Layer

The Catalyst Layer is sandwiched between the membrane and GDL, and it facilitates the electrochemical reaction kinetics of the Hydrogen Oxidation Reaction (HOR) and the Oxygen Reduction Reaction (ORR). This component can suffer from 6 main failure modes, leading to a reduction in cell performance.

- **Pt agglomeration and particle growth** is the electrochemical phenomenon often referred to as 'Ostwald Ripening'. This is where small nano-particles of Pt tend to group together, and form larger particles. This reduces the surface area of the Pt catalyst, slowing the reaction kinetics.
- **Pt elemental loss** is where Pt particles can separate from the catalyst layers binding, and moving out of the cell without predisposition, reducing the speed of the reaction.
- **Pt migration** is where the Pt particles move from their original position to other areas of the cell, such as the membrane.
- **Pt can be contaminated by impurities in the gas feed, air feed or system born contaminants, such as silicone from gaskets or metals from BIP.** These poison the catalyst layer.
- **Flooding** blocks the porous pathways, leading to reactant mal-distribution which can further lead to either; delamination of the membrane, cut-off of electron pathway and Pt agglomeration/dissolution.
- **Ice Formation** as with flooding.

GDL

The GDL provides electrical conductivity from the reaction sites to the external circuit. It also diffuses the gas feeds to the reaction sites on the catalyst layer. This component can experience 3 main failure modes, however the first listed can effect two main areas of the GDL.

- **OH radicals** can degrade the PTFE material used to make the GDL hydrophobic as with the membrane failure mode.
- The **OH radicals** can also contaminate the Carbon material decreasing GDL conductivity and hydrophobicity.
- Water can **flood** the GDL which blocks the passage of gasses to the reaction sites through the GDL pore.
- Water can also **freeze** in the GDL, which also blocks gas flow through the pores of the GDL.

3.3.3 BIP

The BIP encapsulates a single cell of the PEMFC. It separates fuel, oxidant gas and coolant. It also homogeneously distributes reactant gasses to the GDL, whilst collecting current from the FC reaction. This component suffers from 2 failure modes.

- An **oxide film** can develop that slowly builds up in thickness. This increases the resistance of the BIP and reduces the current collected by the BIP.
- The **BIP can corrode** leading to the release of Fe, Ni (Nickel) and Cr (Chromium) atoms into the PEMFC.

3.3.4 Differences from the literature

The previous work in [30] identified 22 failure modes attributable to reduction in performance or catastrophic cell failure. Certain failure modes identified in [30] were omitted from this work. Namely:

- ‘Membrane short circuit’ - This is not necessary as this failure would be noticed during the pre-commissioning checks by the manufacturer, rather than a developing fault.
- ‘Gas leak from seals’ - This is not considered as part of this work as seal degradation has been singled out as a negligible failure mode when PEMFC construction is quality controlled.

“Only in a couple of long-term experiments was seal degradation observed, and this might have been the consequence of an inappropriate materials selection.” pp.18 [40]

Additionally, gasket seals that do suffer from degradation are the liquid applied sealant types used in the past. Modern systems use a solid type gasket that doesn’t suffer the same degradation.

- ‘BPP warping of polymer matrix’ - As the boundaries for this work state a steel BIP, a polymer BIP failure is not necessary.
- ‘BPP cracking’ - This has been omitted as the steel plates do not suffer from cracking, only the polymer and graphite BIPs suffer from this.
- ‘Injection-moulded BPP low electrical conductivity’ - Polymer material BIPs are not considered in this work.

- ‘Coated stainless-steel BPP loss of surface electrical conductivity’ - As above, only plain stainless steel BIPs are considered in this work.

The work in [30] considered multiple construction materials for the BIP, however for the sake of an accurate end result pertaining to a single construction type PEMFC that would be manufactured with only one type of BIP, this work only considers one construction type BIP (stainless-steel). Hence the four failure modes related to the BIP are all omitted due to the material considerations. Six failure modes were removed when compared to other works, however five new failure modes were identified and added to advance this area of work. This work is therefore more specific and detailed in comparison to the existing works.

Aside from the above omissions from previous work, this work shares some similarities with previous examples, however developments to logic and basic event definitions have been made.

3.4 FMEA Table

A comprehensive FMEA has been developed which consists of the identification of the physical component of the PEMFC being analysed, followed by a brief description of its function. The failure modes that can be experienced in this area are then listed, detailing the effects that this failure mode has. The local effect is the contained effect of the failure mode, whereas the system effect is how the failure mode will affect the overall operation of the entire system. Failure detection methods are listed for more details on how to distinguish these failures, whether it be in-situ or ex-situ. Mitigation strategies are listed where previous work has identified a way to reduce or mitigate against these failure modes. Any poignant remarks are listed that may help further the understanding of any of the previously highlighted points, followed by any key relationships between the listed failure mode, and any other failure mode in the system that is being analysed. Finally the source of the failure mode information is listed for integrity.

3.4.1 Membrane Section

From a full literature review of membrane degradation and failure experimentation, an FMEA can be constructed containing all known basic events that affect the membrane component of a PEMFC with the construction previously mentioned.

The first failure mode ‘1.0/1.1 Incorrect BIP torque’ is taken from work in [41] which shows how increasing the pressure experienced by the membrane directly influences the resistivity of the membrane (Table 3.1).

Table 3.1 can be explained further by considering each individual column:

Column:

1. Identifies the component of the PEMFC where the given failure mode is experienced. In this instance, ‘Incorrect BIP torque’ affects the membrane, and as such the Polymer Electrolyte Membrane component is listed.
2. Gives a brief description of the component and its function within the PEMFC. The Polymer Electrolyte Membrane component of a PEMFC is the central part of the cell which forms the electrolyte, and serves to block the passage of reactant gasses and electrons released during the reaction, however allows the passage of hydrogen protons from the anode side, to cathode.
3. Contains the identification number and description of the failure mode to affect the PEMFC. The number 1.0 identifies the failure mode is in relation to the Polymer Electrolyte Membrane, listed in column one. The number /1.1 identifies the first failure mode listed of that section, in it’s own sub-section. Therefore failure modes 1.0/1.1 and 1.0/1.2 are both primarily related to mechanical degradation.

4. Contains information pertaining to the local effect of the failure mode, taken from the literature. For this instance, the local effect of increased BIP torque involves increased pressure on the membrane, which in turn increases the membrane resistance. Membranes are increasingly being made thinner and thinner to reduce membrane resistance, and therefore improve system voltage output. Therefore increasing the membrane resistance is considered to be an undesirable effect.

Identification	Function	Failure Mode	Local Effect	System Effect	Failure detection method	Mitigation Strategy	Remarks	Relationship	Source
1.0 Polymer Electrolyte Membrane	The 'heart' of the PEMFC. Forms the electrolyte at the centre of the cell. Blocks passage of gasses and electrons, but facilitates passage of hydrogen protons from anode to cathode side.	1.0/1.1 Incorrect BIP torque	Local mechanical stress due to increased pressure. Increase of membrane resistance, consistent with the viscoelastic compression of the membrane.	Reduced passage of H+ protons. Reduction in voltage output	Polarisation Curve, Linear sweep Voltammetry	Check bipolar plate compression torque is suitable for the application		Oxide Film Formation (BIP), Flooding, Ice Formation, Creep.	Satterfield, et al. (2006) Mechanical properties of Nafion and titania/Nafion composite membranes for polymer electrolyte membrane FCs. & Wang, H, et al. (2012) PEM FC failure mode analysis. New York, CRC Press. (pp87) & Borup, R, et al. (2007) Scientific aspects of polymer electrolyte fuel

Table 3.1: Failure Mode and Effect Analysis - Incorrect BIP Torque

5. Lists how this local effect affects the system overall. For this example the incorrect BIP torque reduces the passage of protons which reduces the output voltage of the system through an increase in ohmic resistance. This can be observed in a polarisation curve from a linear drop in the centre section of the curve.
6. Lists the potential methods to detect this failure mode's affect on the system. For this example, a polarisation curve would show a drop in the middle linear section of the curve, as the failure mode is regarding ohmic losses in the system. Linear sweep voltammetry could potentially identify this failure mode as it is most commonly used to identify gas crossover. The rate of gas crossover would change with mechanical compression of the membrane through incorrect BIP torque.
7. Lists any potential mitigation strategies to reduce the likelihood of occurrence, or the severity of the effect. For this example, a simple quality control measure of checking the BIP torque would identify this failure mode at an early stage. It is recommended that due to creep, this torque should be checked after assembly, and after the commissioning phase.
8. Contains any pertinent remarks that would either help the reader to understand the entire row, or any factors to consider regarding the failure mode.
9. Lists any relationships that this failure mode may have with other aspects of the FMEA. For this example, oxide film formation on the surface of the BIP can also increase the mechanical compression of the membrane, as does flooding and ice formation. These will worsen the effect of incorrect BIP torque by taking up more room inside the cell, increasing pressure on the membrane.
10. Finally, the source of the data is noted for ease of referencing the experimentation that tested the failure mode. The references for this example are from a review paper [16], a review book [42], and specific membrane compression experimentation [41]. Figure 3.6 shows how an increase of pressure from 0-7.25 MPa increases the resistivity of the membrane by $1\text{ohm}/\text{cm}^2$. The effect of this resistance increase can be observed through a polarisation curve change. Figure 3.7 shows how the increase in mechanical stress on the membrane, vastly degrades the performance of the cell after the activation region of the PEMFC operation. At higher current densities, the performance drops of significantly quicker than with standard compression as opposed to a 7.25 KPa.

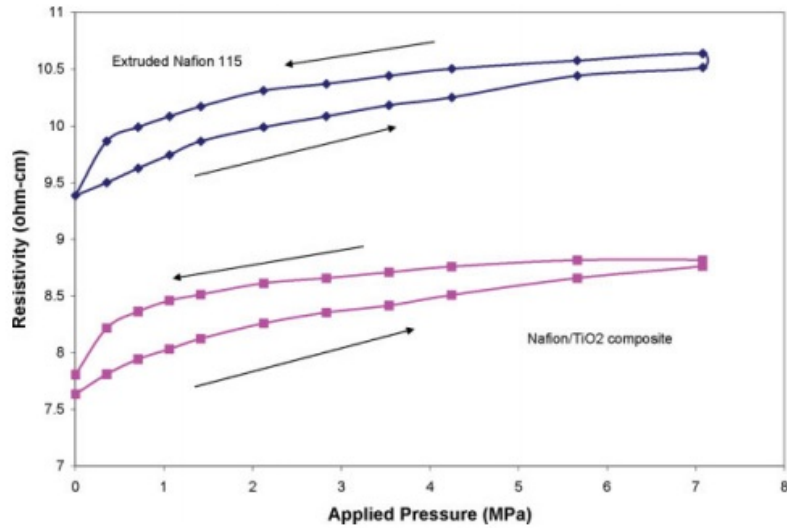


Figure 3.6: Polymer resistivity as a function of applied stress on membrane [41]

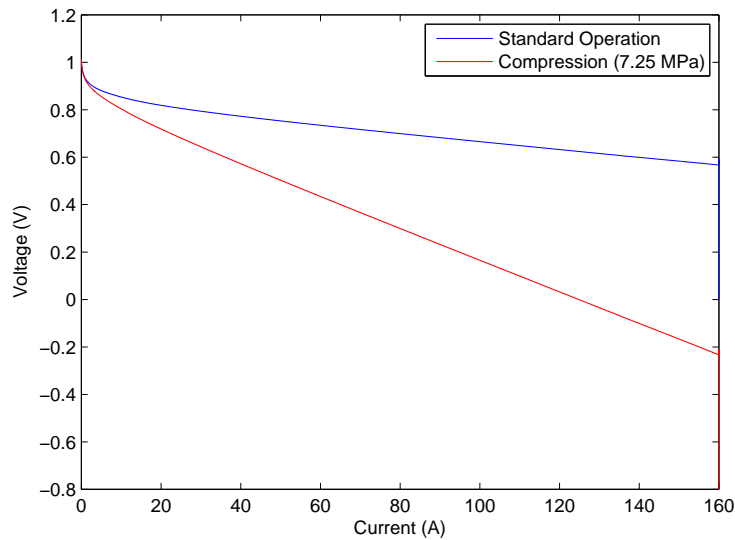


Figure 3.7: Difference between standard polarisation curve, and polarisation curve with 1 ohm/cm² increase

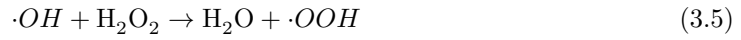
Another failure mode analysed in the membrane section is ‘1.0/2.1 OH and OOH radicals & H₂O₂ contamination to PTFE’. This failure mode has been presented in different ways in previous reliability work, and the numerous different observations can make this failure mode difficult to fully understand. To clarify this area, a review of radical attack and hydrogen peroxide degradation was undertaken.

Radical and Hydrogen Peroxide attack in the membrane has a complicated relationship with other components and failure modes within a PEMFC system. The ways in which this failure mode was analysed is through results from chemical degradation studies [16] [43] [44]. It has been discovered that radicals can be formed from oxygen molecules permeating through from the cathode side of the FC, to the anode side of the FC. This O₂ can reduce at the anode Pt catalyst, forming ·OOH radicals, and then lead on to H₂O₂ formation, and more radical

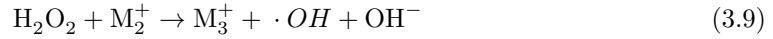
formation (Equations 3.1 - 3.3).



If there are foreign ions present such as Fe_2^+ and Cu_2^+ released from BIP degradation, the H_2O_2 formed can further develop into $\cdot\text{OH}$ and $\cdot\text{OOH}$ radicals, and at a higher rate. Therefore the metal ions from the BIP catalyse, can severely increased the radical and peroxide degradation to the membrane, as presented in [16] (Equations 3.4 & 3.5).



Another mechanism for radical and peroxide attack is presented in [45] proposed a method of production of radicals, which occurs due to the diffusion of gasses through the membrane, and formation of H_2O_2 .



Equations 3.6-3.10 show the stages of how radicals are a product of H_2O_2 production which occurs under normal operating conditions and membrane health. It is suggested in [46] that peroxide can form, by Equation 3.11, by a 2 electron reduction of O_2 pathway;



Due to the above, OH and OOH radical attack, and H_2O_2 attack were grouped into one basic events; ‘OH and OOH radicals & H_2O_2 contamination to PTFE’, which represents the formation under normal conditions, and H_2O_2 created from 2 electron reduction of O_2 on Pt.

The way in which radicals and peroxide degrade the membrane is through end-group unzipping, as stated in the local effect column of the FMEA entry (Table 3.2). The PTFE backbone of the membrane is modified with end-groups or side chains of perfluorosulfonic acid ionomers which help facilitate the FC reaction. These are attacked and ‘unzip’ from the PTFE core, releasing fluorine into the exhaust water.

Identification	Function	Failure Mode	Local Effect	System Effect	Failure detection method	Mitigation Strategy	Remarks	Relationship	Source
1.0 Polymer Electrolyte Membrane	The 'heart' of the PEMFC. Forms the electrolyte at the centre of the cell. Blocks passage of gasses and electrons, but facilitates passage of hydrogen protons from anode to cathode side	1.0/2.1 OH and OOH radicals & H ₂ O ₂ contamination to PTFE	End group unzipping. The Polytetrafluoroethylene (PTFE) core material is modified with side chains of Perfluorosulfonic acid Ionomers. These can be lost through OH and OOH radical attack. (PFSI) membrane	Weaker membrane, and therefore increase in risk of mechanical damage. Reduction in voltage output	Electron Spin Resonance (ESR) spectroscopy, Polarisation Curve, Linear Sweep Voltammetry	Modifying polytetrafluoroethylene with in situ sol-gel polymerization of titanium isopropoxide to generate titania quasiretworks in the polar domains of a polymer electrolyte membrane FC, can mitigate against the risk of H ₂ and O ₂ gas crossover.	Low humidity and OCV can exacerbate the attack and degradation	Protonic resistance of membrane, H ₂ O ₂ formation, Mechanical Damage	Wang, H, et al. (2012) PEM FC failure mode analysis. New York, CRC Press. (pp87)

Table 3.2: Failure Mode and Effect Analysis - Radical and Hydrogen Peroxide Attack

3.4.2 Catalyst Layer

The first failure mode ‘2.0/1 Pt agglomeration and particle growth’ is taken from review papers [16] and [42] which shows the effect of Ostwald Ripening and Pt Agglomeration on the loss of Electrochemically Active Surface Area (ECSA) (Table 3.3).

The section of FMEA can be explored through considering each column:

Column:

1. ‘Pt agglomeration and particle growth’ affects the catalyst layer of the PEMFC, and as such the Catalyst Layer component is listed with its numerical identifier ‘2.0’.
2. The catalyst layer component of a PEMFC is the layer immediately adjacent to the membrane on either side. It sandwiches the membrane and facilitates the electrochemical reaction kinetics of the HOR and ORR.
3. The number 2.0 identifies the failure mode relates to the Catalyst Layer, listed in column one. The number /1 identifies the first failure mode listed of that section.
4. Contains information pertaining to the local effect of the failure mode, taken from the literature. For this instance, the local effect of the nanoparticles of Pt clumping together and reducing their surface energy, reduces the active surface area for reaction. This slows down the reaction kinetics by actively reducing the amount of sites for the HOR & ORR. Therefore reducing the ECSA is considered to be an undesirable effect.
5. For this example the reduction of ECSA reduces the output voltage of the system through a decrease in reaction kinetics. This can be observed in a polarisation curve from a drop in the beginning section of the curve pertaining to an increase in activation losses.

Identification	Function	Failure Mode	Local Effect	System Effect	Failure detection method	Mitigation Strategy	Remarks	Relationship	Source
2.0 Catalyst Layer	Layer sandwiched between PEM and GDL. Facilitates electrochemical reaction kinetics of the HOR and ORR.	2.0/1 Pt agglomeration and particle growth	Pt nanoparticles have inherent tendency to combine to reduce their high surface energy. This agglomeration reduces the electrochemically active surface area. Reducing voltage output	Reduction in voltage output	Ex situ transmission electron microscopy (TEM), X-ray diffraction (XRD) using Averbach Fourier transform method for determination of weighted crystallite sizes. Polarisation Curve. Cyclic Voltammetry		Borup et al (2006) showed that Pt particle growth increases with temperature. Critically when increasing temp from 60 - 80oC. Ref (p12 in Wang book)		Wang, H, et al. (2012) PEM fuel cell failure mode analysis. New York, CRC Press. (pp87) \& Borup, R, et al. (2007) Scientific aspects of polymer electrolyte fuel cell durability and degradation. Chemical Review, vol. 107, pp3927.

Table 3.3: Failure Mode and Effect Analysis - Pt Agglomeration & Particle Growth

6. Some methods to detect the failure are listed in this column. Ex-situ Transmission Electron Microscopy (TEM) is a method where a beam of electrons are transmitted through a specimen and the beams then interact with the sample. An image can be formed from this interaction for analysis of the material constitution (Figure 3.8).

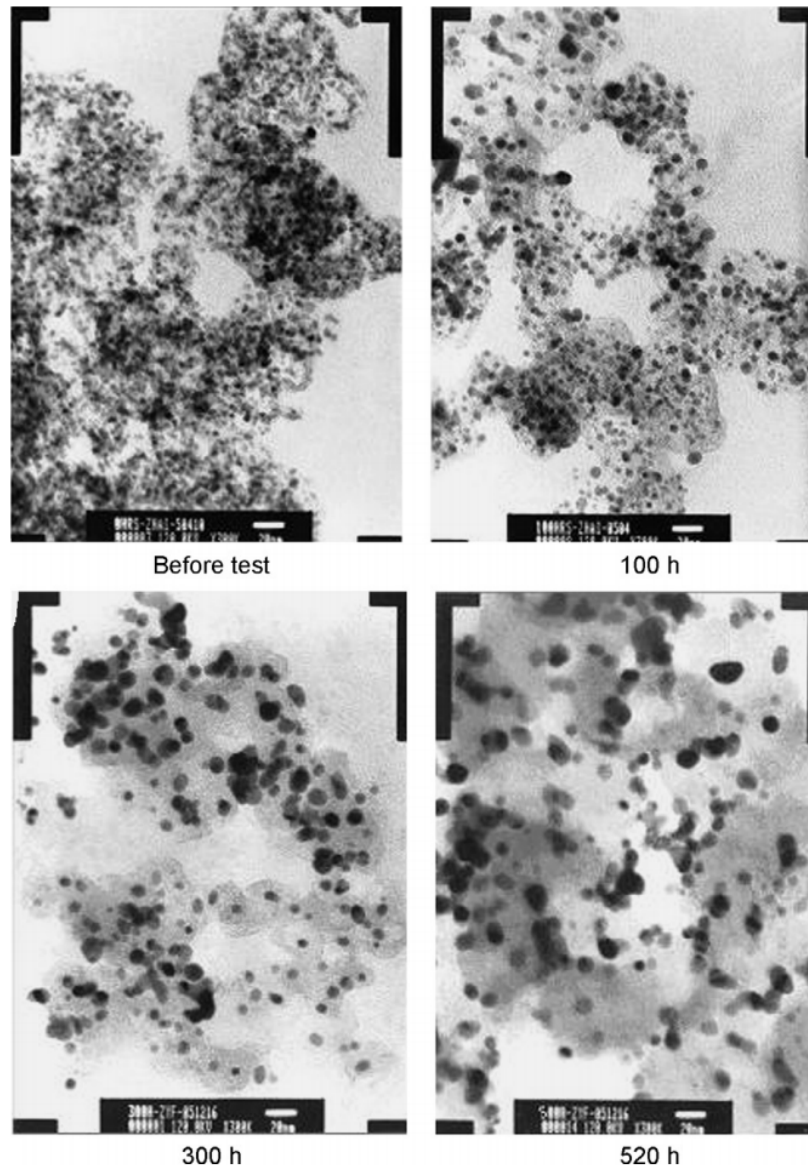


Figure 3.8: Pt Agglomeration observed by TEM [47]

X-Ray Diffraction (XRD) experimentation uses an incident beam of x-rays created by accelerating electrons between two electrodes. On impact, the x-rays fly off in all directions, most of this is lost as heat, however a small percentage transformed into x-rays consist a mixture of wavelengths. These wavelengths can be plotted to see what materials and what size are present. Using the Averbach Fourier transform method, one can determine the weighted crystallite sizes. An example of this is shown in Figure 3.9.

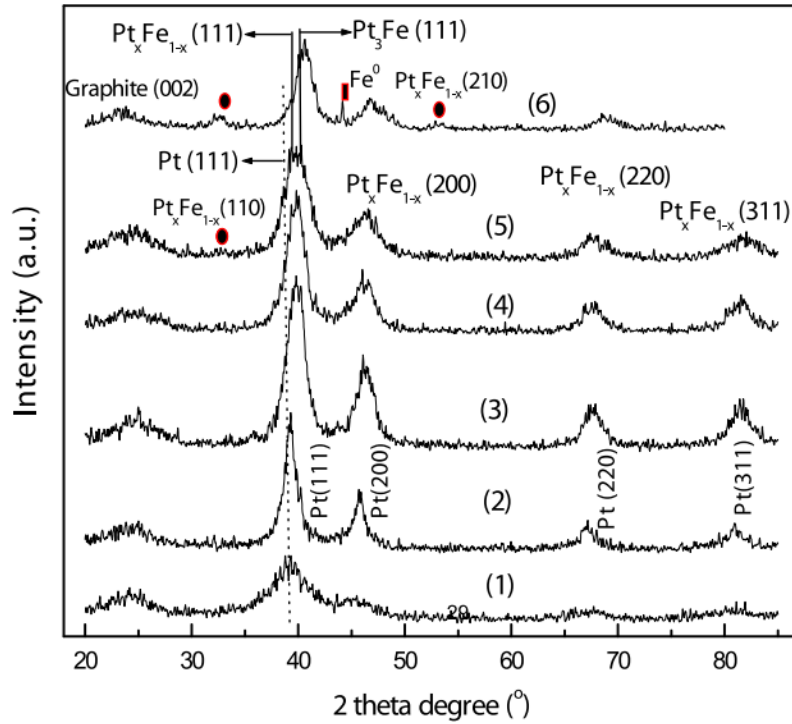


Figure 3.9: Pt Agglomeration observed by XRD [48]

As for in-situ methods; A polarisation curve would show a drop in the curve at the beginning due to an increase in activation losses. Cyclic Voltammetry can be used to analyse the ECSA of the cell.

7. There are no mitigation strategies for Pt agglomeration.
8. The remark for this failure mode is regarding temperature increase effects on Pt agglomeration. It was found in [16] and [42] that an increase in temperature of the cell, increases the degradation rate due to Pt agglomeration and particle growth.
9. There are no relationships for Pt agglomeration and particle growth.
10. The source of the data is noted for ease of referencing the experimentation that tested the failure mode. The references for this example are from a review paper [16], and a review book [42].

3.4.3 GDL

The first failure mode ‘3.0/1 OH Radicals contamination to PTFE’ is taken from a review paper [23] and is presented in Table 3.4.

Identification	Function	Failure Mode	Local Effect	System Effect	Failure detection method	Mitigation Strategy	Remarks	Relationship	Source
3.0 Gas Diffusion Layer	Provides electrical conductivity from reaction site to external circuit. Also known as 'electrode'. GDL is porous carbon with PTFE coatings, the porosity diffuses the reaction gasses and disperses them to the reaction sites on the catalyst layer.	3.0/1.0 OH Radicals contamination to PTFE	OH radicals attack the carbon material in the PTFE and Carbon support, decreasing GDL conductivity and hydrophobicity	Reduction in voltage output	Polarisation Curve	Using graphitized fibers during GDL preparation to improve GDL oxidative and electrooxidative stability.		Flooding	J. Wu et al, (2008) 'A review of PEM fuel cell durability: Degradation mechanisms and mitigation strategies' pp110-111

Table 3.4: Failure Mode and Effect Analysis - Gas Diffusion Layer OH radical attack to PTFE

A further explanation of the above table is detailed below:

Column:

1. 'OH Radicals contamination to PTFE' affects the GDL of the PEMFC, and as such the GDL component is listed with its numerical identifier '3.0'.
2. The GDL has two main functions; it disperses the feed gases from the BIP gas channels to the reactive sites on the Catalyst Layer. It also serves to provide an electrically conductive bridge from the reaction site to the BIP where the electrical 'work' energy can be utilised.
3. The number 3.0 identifies the failure mode is in relation to the GDL, listed in column one. The number /1.0 identifies the first failure mode listed of that section.
4. The radical contamination can attack the PTFE material used in GDL construction, and this directly affects the GDL's electrical conductivity and its hydrophobicity. This means that the removal of excess water is limited, and less electrical 'work' energy can be harvested by the system.
5. For this example, the overall system effect is a reduction in the output voltage.
6. A polarisation curve can be used to identify this failure mode occurrence. The reduced electrical conductivity is related to ohmic resistance of the polarisation curve, and as such, the center section relative to ohmic resistance would show a linear drop.
7. One can increase the GDL's resistance to this type of degradation by using graphitised fibers during the GDL construction process. This would improve the oxidative and electro-oxidative stability of the GDL.
8. There are no remarks for this failure mode.
9. Due to the loss of GDL hydrophobicity, this failure mode will have an affect on flooding phenomena in the PEMFC.
10. The source information for this failure mode is from a review paper [23].

3.4.4 BIP

The first failure mode '4.0/1 Oxide film formation' is taken from a review paper [23] and is analysed in Table 3.5.

Identification	Function	Failure Mode	Local Effect	System Effect	Failure detection method	Mitigation Strategy	Remarks	Relationship	Source
4.0 Bipolar Plate	The BIP is a multifunctional component of a PEMFC. It separates fuel, oxidant gas and coolant; homogeneously distributing reactant gases to the GDL. It also collects the current from the FC reaction, delivering it to the external circuit.	4.0/1 Oxide film formation	An oxide film layer can form at the junction between GDL and BIP. This can increase in size and increase internal resistance to current flow.	Drop in output voltage due to resistance increase	Polarisation Curve			Swelling	J. Wu et al, (2008) 'A review of PEM fuel cell durability: Degradation mechanisms and mitigation strategies' pp110-111

Table 3.5: Failure Mode and Effect Analysis - BIP section, Oxide film formation

The table entries contents are further explained below:
Column:

1. 'Oxide film formation' affects the BIP of the PEMFC, and as such the BIP component is listed with its numerical identifier '4.0'.
2. The BIP has two main functions; it delivers the feed gases from the hydrogen storage and air compressor to the GDL whilst separating the coolant flow from the PEMFC inners, and collects the current to pass on to the next cell in the stack.
3. The number 4.0 identifies the failure mode is in relation to the BIP, listed in column one. The number /1.0 identifies the first failure mode listed of that section.
4. During operation, the BIP can start to build up an oxide film layer on the boundary of the BIP and the GDL. This increases internal resistance and increases pressure in the cell.
5. For this example, the overall system effect is a reduction in the output voltage.
6. A polarisation curve can be used to identify this failure mode occurrence. The reduced electrical conductivity is related to ohmic resistance of the polarisation curve, and as such, the centre section relative to ohmic resistance would show a linear drop.
7. There are no mitigation strategies in relation to this failure mode.
8. There are no remarks for this failure mode.
9. Oxide film formation increases the thickness of the BIP, and as the torque levels are set from commissioning, this will increase the mechanical pressure in the cell. As such, this failure mode can be related to membrane swelling.
10. The source information for this failure mode is from a review paper [23].

3.5 Conclusions

In total, the complete FMEA has 21 failure modes identified; 8 membrane layer failure modes, 7 catalyst layer, 4 GDL and 2 BIP failure modes. The full FMEA covering all the component failure modes listed in this section is given in Appendix A.

Due to the complicated nature of the relationships between failure modes, a most significant failure mode is not easily singled out. To ascertain a greater understanding of the logic pertaining to failure modes in PEMFCs, alternative methods of reliability analysis need to be considered. The fact that the membrane has the most failure modes identified, would suggest that this component is one of the most susceptible to degradation and failures in the system.

The most common system effect is the overall drop in voltage, with the most common and easily undertaken failure detection method is considered to be the polarisation curve. An overview of the main findings are presented by Whiteley, et al. in [49].

The full FMEA is a detailed analysis of the degradation phenomena that can be observed in a PEMFC environment. The failure modes are taken from the literature based upon the key assumptions previously mentioned.

This work has extended the previous work in [30] by developing their list of operating failures into a full FMEA. Details are provided in this work that were previously unavailable, giving a greater insight into failure modes in a PEMFC and how they interact. This FMEA table is invaluable in the FT production process, as it take a very detailed view of all of the possible failure modes and their possible interactions in a specified system. The data from the above forms the basis of the following FT section. Due to the full FMEA, it was discovered that there are numerous relationships between failure modes that need be further analysed. A FT can graphically identify the logic of failure modes in a system to greater understand the implications of this work.

Chapter 4

Existing Reliability Modelling

As previously mentioned in Chapter 2, FT analysis was recently used in [30] to try to model the reliability of a single cell PEMFC. From various literary sources, they came to the conclusion that there are 37 individual basic events to be considered when analysing the degradation of a PEMFC. The FT presented is a ‘physical analysis of a single cell PEMFC’, splitting the top-event of the ‘Degradation of the Cell’ down through an OR gate into three physical components of a PEMFC; Membrane (G2), Gas Diffusion Layer (G4) and Catalyst Layer (G3) as in Figure 2.5. These are three of the four main physical components of a PEMFC with only the bipolar plate being omitted.

G2, G3 and G4 each had 12, 12 and 6 intermediate events respectively, which further branched down through OR gates to the basic events. As all of the gates in the presented FT were of the OR variety, the minimum cut sets are simply all order ones, representing the basic events of the tree.

This chapter presents an intensive review of the existing work and will enhance the present work with the followings reported for consideration.

4.1 Analysis Review - Limitations Determined

4.1.1 Top Event

The top event for the tree developed in [30] can be interpreted as equivocal; ‘Degradation of the cell’ does not directly inform the reader of what ‘degradation’ is classed as, and what drop in voltage output is considered to be degraded. A failure of a sub-system or process is an ideal scenario for using FT analysis, however the top event of ‘Degradation of a cell’ does not fit these criteria. A more prudent way of defining the top event would be to suggest a rate of degradation over a time period that is unacceptable. Partial failures can be used in a FT, however the terms must be clearly defined as to not cause ambiguity.

The commonly agreed criteria for the PEMFC is to have a reduction in output voltage of no more than 5% over the 5000 hours period [23]. Therefore for a failure at the top level of the FT, unacceptable conditions would entail a performance drop of >5% before 5000 hours, or failure to meet 5000 hours of operation. A top event reflecting this standard would alleviate the uncertainty with the current top event. It is suggested that a new top event is used to emulate the commonly accepted lifetime requirements of a PEMFC for automotive applications to have a top event of; ‘<5000h cell lifetime or >5% drop of output voltage’. This proposed top event represents a reduction of more than 5% of the performance of the fuel cell over the operating time of 5000 hours. A drop in performance of 6% in the first 1000 hours would therefore trigger this top event, however a total drop in performance of 4% over 6000 hours would not trigger the top event. This target is used due to the fuel cell community accepting this as their standards, however in reality it is a very stern target. Fuel cells operate in very

harsh conditions, experiencing oxidising, acidic, temperature variation and potential/current variations. They therefore inherently degrade during normal operating conditions. PEMFCs in automotive applications are exclusively hybridised with conventional batteries, both to allow for regenerative braking, and to level the load out from the electric motor. It is therefore completely feasible that a PEMFC vehicle could still perform well even after 10-15% voltage degradation. However, the finer details of international target setting is not the subject of this work, and therefore this work is bound by the current regulations set out in [23].

4.1.2 Bipolar Plate Omission

The omission of the bipolar plate component of a PEMFC is an issue that needs to be addressed. There are many studies in the literature that document and analyse the degradation and failures of bipolar plate materials in PEMFC. Failure modes affecting the bipolar plates are; corrosion of the metal bipolar plate when in contact with the aqueous and acidic environment of the PEMFC, releasing metal ions, and oxide film formation.

Corrosion related failures have documented occurrences in a number of studies [50][32][51]. A 2012 study showed that cell performance can be dramatically reduced through bipolar plate corrosion and the formation of passive oxides creating an oxide film [52]. The corrosion of the plate material and the formation of the oxide film reduce the electrical conductivity of the plate. They showed that the film gradually increases in thickness with age, and as such the resistance increases with the thickness of the film. This phenomenon is only present on the cathode side where O_2 is the fuel and hence having the opportunity to form the oxide layer. At the anode side, H_2 is the fuel, and thus this issue is not apparent.

The bipolar plate can also affect other parts of the PEMFC, for example steel bipolar plates can release Iron (Fe^+) and Copper (Cu^+) ions that can have a detrimental affect elsewhere. For example in an intermediate event in the membrane branch named 'Contamination by trace metal ion - G10'. As can be seen in Figure 4.1, G10 is split into the presence of foreign cations and altered water flux.

The FT presented puts accelerated membrane thinning and pinholes as the cause of altered water flux, whereas review papers [40][23] suggest that the presence of the foreign cations displace the H^+ ions in the membrane, and would lead to membrane thinning and possibly pinhole formation. As can be seen in Figure 4.1, 'Contamination by trace metal ion - G10' is shown as an intermediate event that can be caused by either the undeveloped event of 'Presence of foreign cationic ions - E039' or 'Altered water flux inside the membrane - G12'. 'Altered water flux inside the membrane - G12' is further split into two basic events; 'Formation of pinholes - E031' and 'Acceleration of membrane thinning - E030'. The logic here requires further development, as the presence of trace metal ions could be considered to be a basic event leading towards pinholes/accelerated thinning of the membrane. Additionally 'Presence of foreign cationic ions - E039' which is an undeveloped event in the tree, is arguably identical to 'Contamination by trace metal ion - G10', and is therefore redundant.

As mentioned earlier, foreign cations can stem from the bipolar plate material as well as inlet piping or humidifier materials. This fact, alongside the other bipolar plate corrosion issues mentioned previously, would indicate that the overall structure of the tree would need further evaluation.

Trace metal ions such as Fe_2^+ from the bipolar plate can have adverse effects throughout the cell. It is known that these metal ions can contaminate the membrane and poison the electrode catalyst. The current logic regarding the trace metal ions in the membrane degradation section needs re-evaluating. The presence of foreign metal ions leads to accelerated membrane thinning and possibly pinhole generation, therefore the tree should reflect this. This would require the replication of the above basic event 'E050 Metal Ion Release' in the newly proposed G2 and G3 intermediate events.

It has been stated that oxide film formation can increase the contact resistance of the bipolar plate by 'many orders of magnitude' [32]. This basic event would need to be included in the

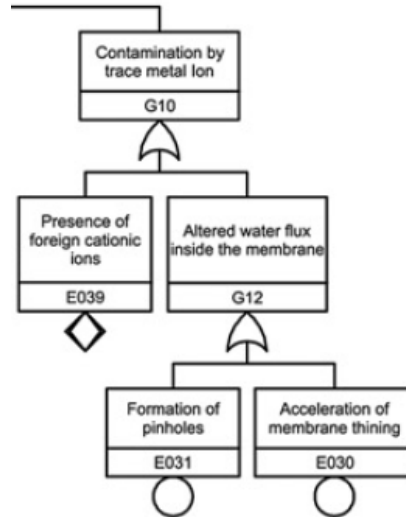


Figure 4.1: Metal Ion Intermediate Event from [30]

overall model due to its effect on the reduction of output voltage, which is the quantifier for degradation, leading to the top event failure.

4.1.3 Ambiguity of Intermediate Events

As with the previous issues found with the top event and first intermediate events, the majority of the basic events are also equivocal and are not necessarily binary in nature. E002 ‘long-term functioning’ (see Appendix B) is ambiguous in description, not informing the reader whether it means that the cell is completely failed or is degraded to a lower output state due to long-term operation. There is no explanation of what this pertains to, such as a time frame, or what the failure mode is. During long term operation, many components can degrade by any number of failure modes.

The membrane branch contains three basic events that need to be further considered. ‘Pinholes’, ‘Pinhole Production’ and ‘Formation of Pinholes’ are all listed as basic events, and are explained as follows; ‘Pinholes’ are stated as occurring ‘due to exothermal combustion between H_2 and O_2 ’. ‘Pinhole Production’ is listed as not due to, but related to ‘mechanical degradation’. Finally ‘Formation of Pinholes’ is considered to be ‘due to contamination by trace metal ion’. This would suggest that the three ‘basic’ events could be further broken down to fundamental basic events.

4.1.4 Lack of Standardised Data

The lack of homogenised data for a PEMFC is a pitfall that can only be overcome by an increase in experimental analysis of certain failure modes in a FC. An ideal scenario would incorporate sets of standardised experiments to homogenate degradation data, aiding with the validity of failure analysis. These would use the same cell materials, size and construction to make sure that degradation data is as reliable as possible.

4.2 Conclusions

A recently presented quantitative FT has proven to be a good first step in degradation analysis and failure forecasting. Some areas that need to be addressed have been identified in [53][54], in

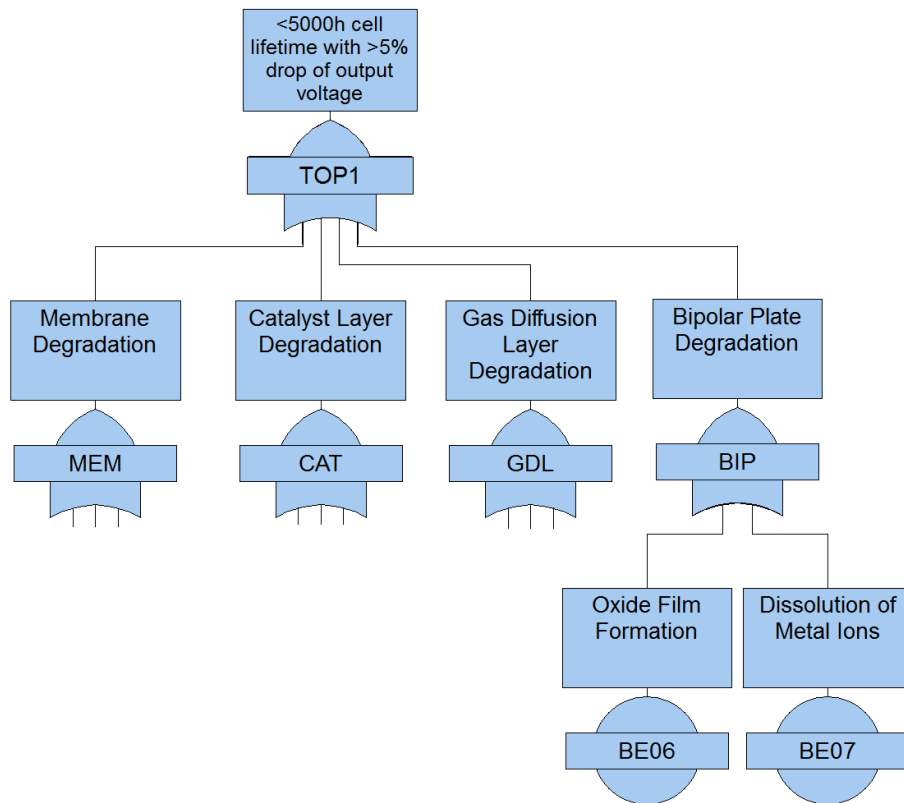


Figure 4.2: Proposed Change to 'Global' Tree

particular critical component omission, basic event logic & structure, ambiguity of events and lack of standardised data sets. It is envisaged that if these issues can be addressed, the overall degradation analysis of PEMFCs will become increasingly more accurate.

Building upon the information ascertained from the previous FMEA, and from the analysis of the presented FT, a new FT is developed to advance this field of PEMFC degradation and reliability concerns.

4.3 Advancing the FT

4.3.1 Top event & intermediate top level structure

Following investigation into the operation of the PEMFC and a FMEA analysis carried out to understand the effect of the component failure modes, 21 basic events were found relating to the top event '<5000h cell lifetime or >5% drop of output voltage', and for which data is available for a quantitative analysis.

The basic events for the overall FT are shown in Table 4.1.

Some of the basic events listed in this table were not previously considered in existing work with FTA, the existing failure modes that have remained unchanged are listed in bold text. Some of the basic events listed in Table 4.1 were omitted in previous works, however they have been introduced as the literature shows that these failure modes have been observed in PEMFC operation.

The overall intermediate events are also presented in Figure 4.2, containing Catalyst Layer Degradation, Membrane Degradation, Gas Diffusion Layer Degradation and Bipolar Plate Degradation. These represent the grouping and classification of the types of intermediate or

Table 4.1: List of Basic Events

Basic Events - Membrane
Flooding
Ice Formation
Incorrect BIP torque
Creep
Fatigue from Relative Humidity and Temperature cycling
Oxide Film Formation
Dissolution of Metal Ions
Contamination from Humidifier/air pipe/gas impurity
OH or OOH Radical Attack
Previously Formed Pinholes
Excess Heat
Exothermal Combustion due to previously formed pinholes
Basic Events - Catalyst
Pt Loss and Distribution
Pt Migration
Dissolution of Metal Ions
Contamination from Humidifier/air pipe/gas impurity
Pt Agglomeration/Dissolution
Ice Formation
Flooding
Creep
Exothermal Combustion due to previously formed pinholes
Basic Events - Gas Diffusion Layer
OH or OOH Radical Attack
Flooding
Ice Formation
Basic Events - Bipolar plate
Oxide Film Formation
Corrosion leading to release of multivalent cations

basic events that feed into that branch. All of the intermediate events from this level contribute towards the specific top event degradation levels.

4.3.2 Proposed FT

A new FT has been developed that goes further than the work in [30]. The Bipolar plate omission has been addressed with the addition of a fourth level 2 intermediate event; ‘Bipolar Plate Degradation’. The basic events feeding this intermediate event include; ‘Oxide film Formation’ and ‘Dissolution of metal ions’.

Cho, et al. [55] showed that the corrosion of the metal bipolar plates for stainless steel releases metallic elements such as Fe, Nickel (Ni), Chromium (Cr) and Titanium (Ti). The dissolution of these metals into the Membrane Electrode Assembly (MEA) can increase the ohmic resistance and the charge transfer resistance by taking up space on the active sites of the catalyst.

Wu, et al. [23] discuss the degradation mechanisms of bipolar plate materials in a PEMFC, paying attention to the formation of an oxide film on the plate. A large concern with bipolar plates, is the contact resistance between the BIP and the GDL, attributed to the resistance caused by the formation of the oxide film.

Due to the aforementioned factors observed in [55] and [23], these two factors are included in the presented FT under gate ‘BIP’ in Figure 4.2.

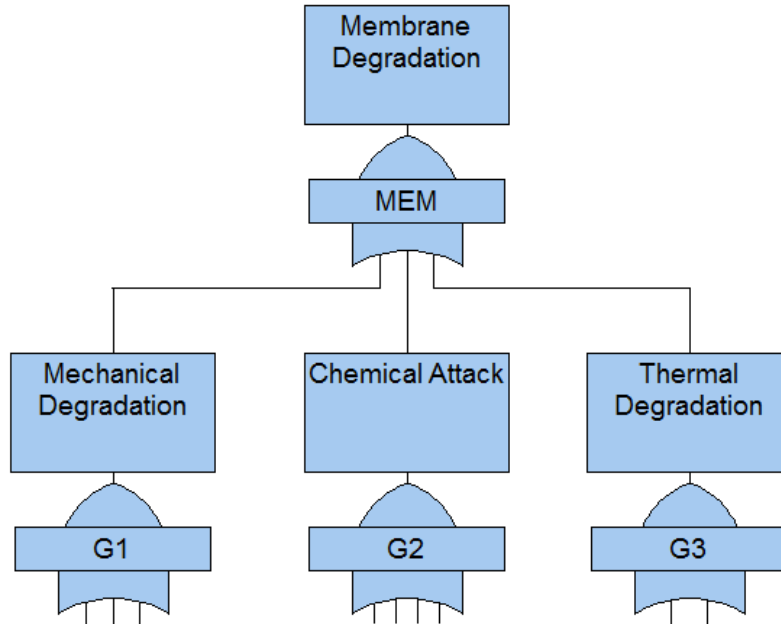


Figure 4.3: Proposed ‘Membrane’ Top level

The membrane degradation branch of the global FT is further split down into the three main pathways of degradation in the membrane; ‘Mechanical Degradation’, ‘Chemical Attack’ and ‘Thermal Degradation’ as per Figure 4.3.

The mechanical degradation branch of the membrane branch of the global FT is presented in Figure 4.4 and shows the failure modes that contribute towards membrane degradation contributing towards the top event voltage drop. Level 1 intermediate events of this sub-branch include; ‘Local mechanical stress due to increased pressure’, ‘Microcrack Fracture’ and ‘Pinholes’. Any localised mechanical stress is caused by swelling inside the cell, and as such the swelling relationships are repeated from the basic events under the ‘Non-Uniform Contact Pressure’ intermediate event under the ‘Microcrack Fracture’ intermediate event. Microcrack fractures

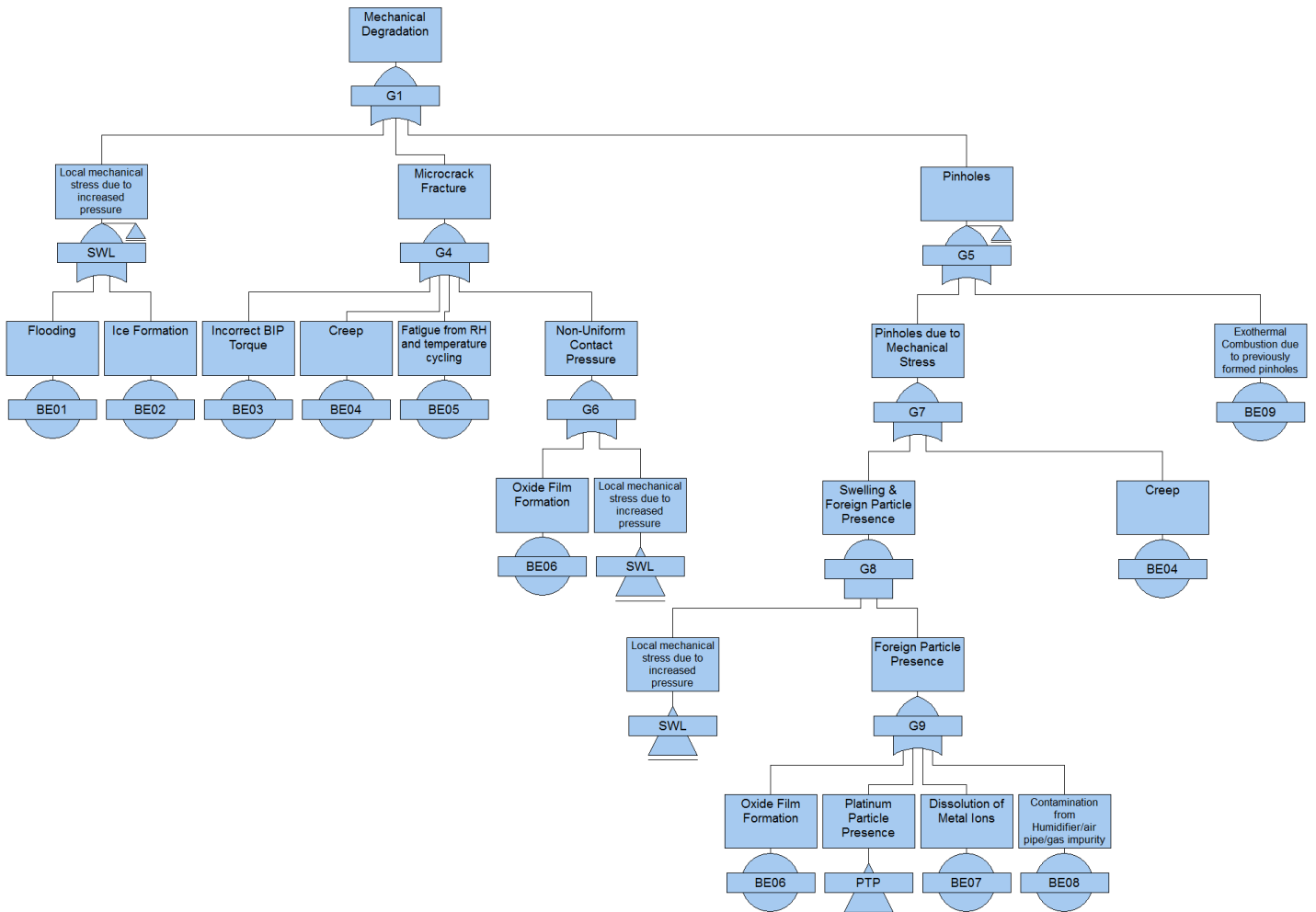


Figure 4.4: Proposed mechanical section of the ‘Membrane’ FT

can be considered to be anything that results in a physical breach of the membrane, and is segregated from pinholes due to geometry. Microcracks can be considered to be tears, whereas pinholes are circular holes. These are not grouped under one mechanical breach intermediate event due to the varying conditions and events leading to each phenomena. The Pinholes section describes the basic events and combinations of said events leading to the formation of pinholes on the membrane material. The two main pathways described are from either mechanical stress (such as punctures from foreign bodies) and a chemical measure from the chemical degradation segment of the membrane FT that is transferred in.

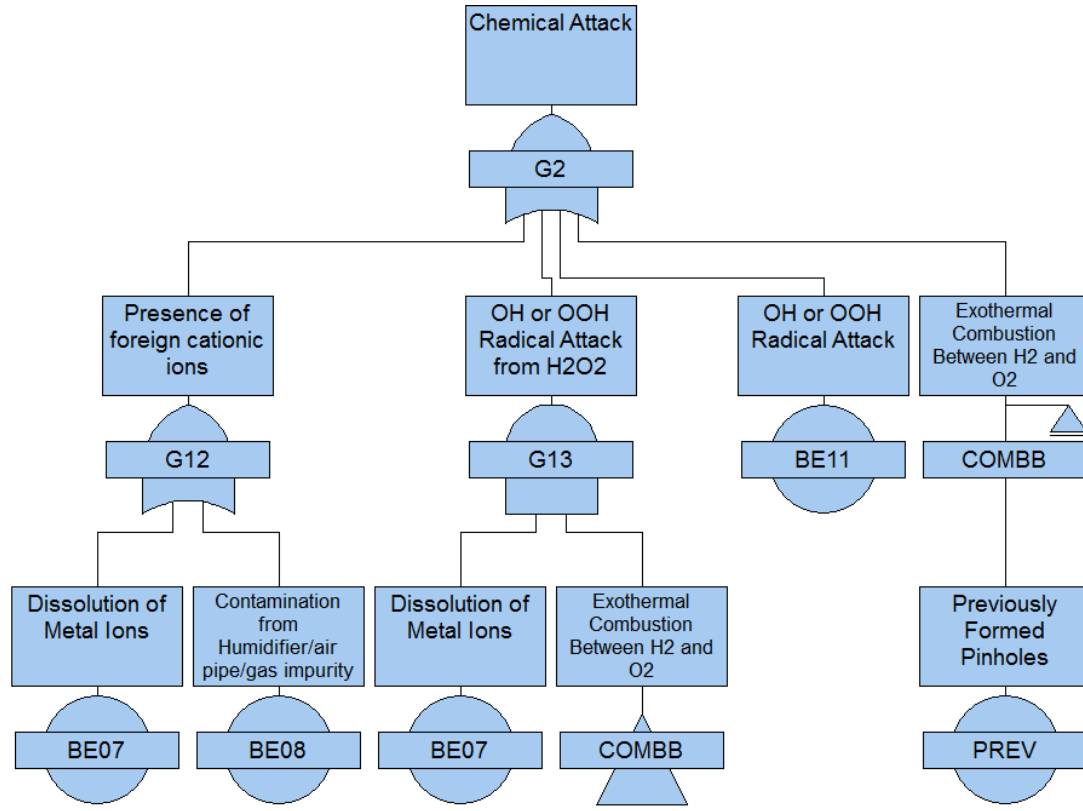


Figure 4.5: Proposed chemical section of 'Membrane' FT

The chemical attack branch is further divided into three intermediate events and one basic event in level 1, shown in Figure 4.5. 'Exothermal Combustion Between H₂ and O₂' is caused by any previously formed pinholes, and thus the feed gasses meeting and reacting. The 'Presence of foreign cationic ions' can be caused by either the 'Dissolution of metal ions' and any 'Contamination from Humidifier/air pipe/gas impurity'. The radical attack level 1 event needs to have any dissolution of metal ions from the bipolar plate and hydrogen peroxide formation to be fulfilled. However radical attack can fulfil the criteria for overall chemical degradation on its own, and as such is listed as a basic event.

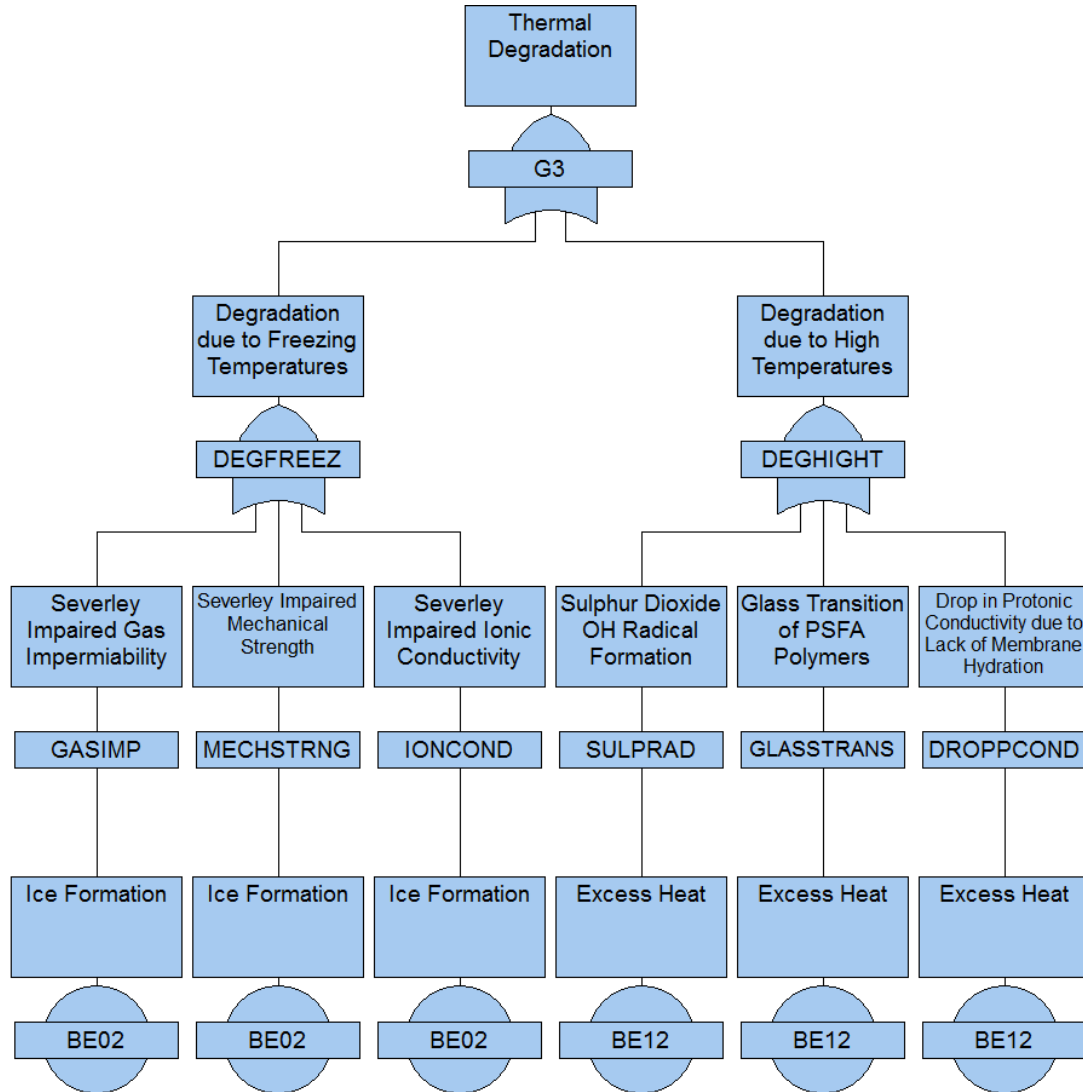


Figure 4.6: Proposed Thermal section of ‘Membrane’ FT

Thermal degradation is then listed with two intermediate events of ‘Degradation due to freezing temperatures’ and ‘Degradation due to high Temperatures’. The two main basic events that feed these are; ‘Ice Formation’ and ‘Excess Heat’ as can be seen in Figure 4.6. Under a normal temperature range for a PEMFC (around 60-80°C), there is no degradation in relation to only temperature. Only when the cell is operated below freezing, or above the designated operating temperature is degradation observed. Each basic event feeds into an intermediate event which further explains the degradation caused by either too much heat or too little heat, however the only available data is attributable to the basic event itself, therefore the additional intermediate events are there for strictly qualitative purposes.

The FT for the GDL presented in Figure 4.7 is split from overall ‘Gas Diffusion Layer Degradation’ into the level 1 intermediate events; ‘Anode Side’, ‘Mechanical Compression’ and ‘Cathode Side’. This is primarily a physical representation of the failure modes that can be experienced at either side of the cell. ‘Mechanical Compression’ is an undeveloped event due to the lack of literature regarding the degradation of GDL material due to mechanical compression and the related degradation data. This area has been identified as an area for potential further development through experimentation and in-depth research.

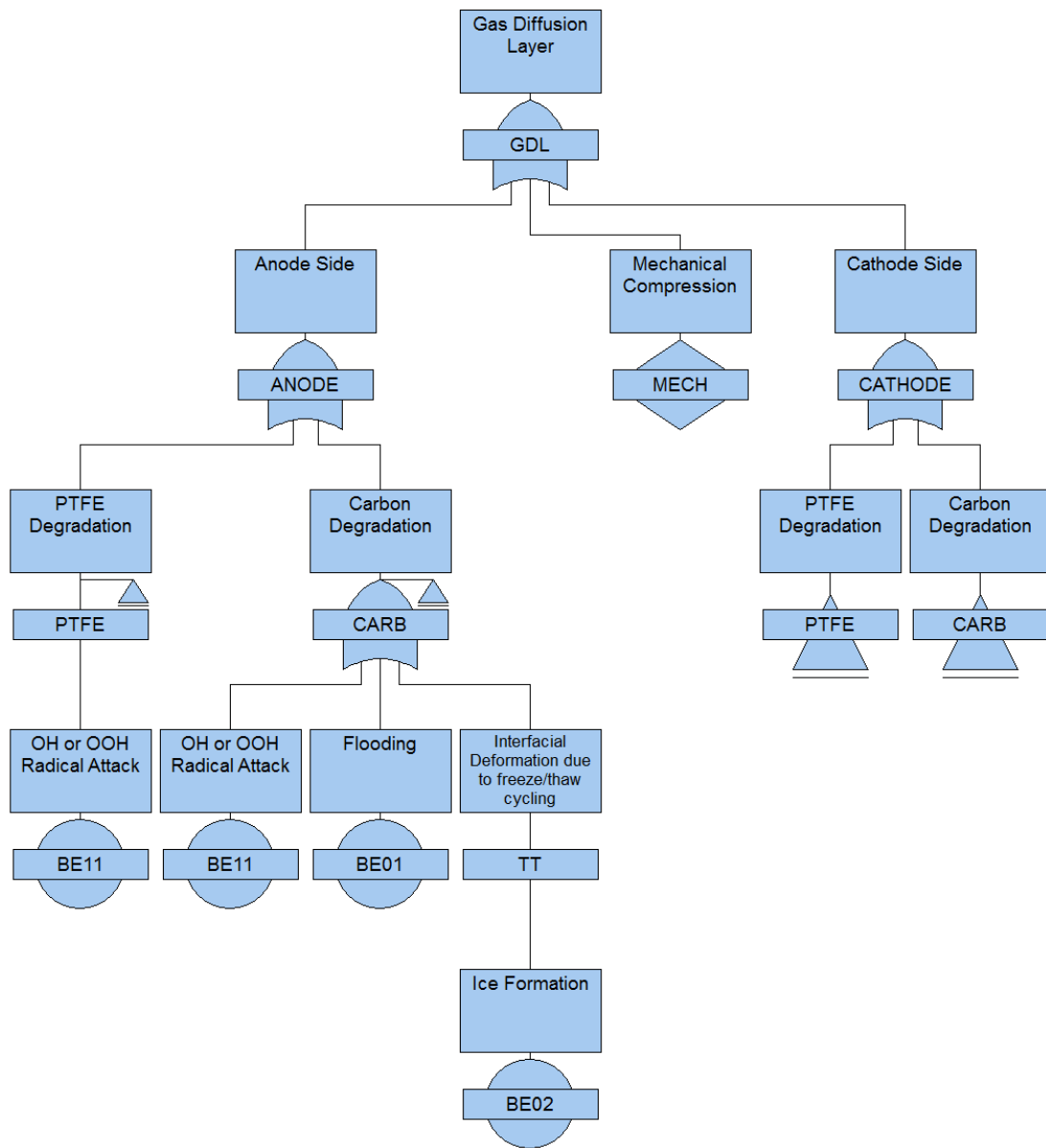
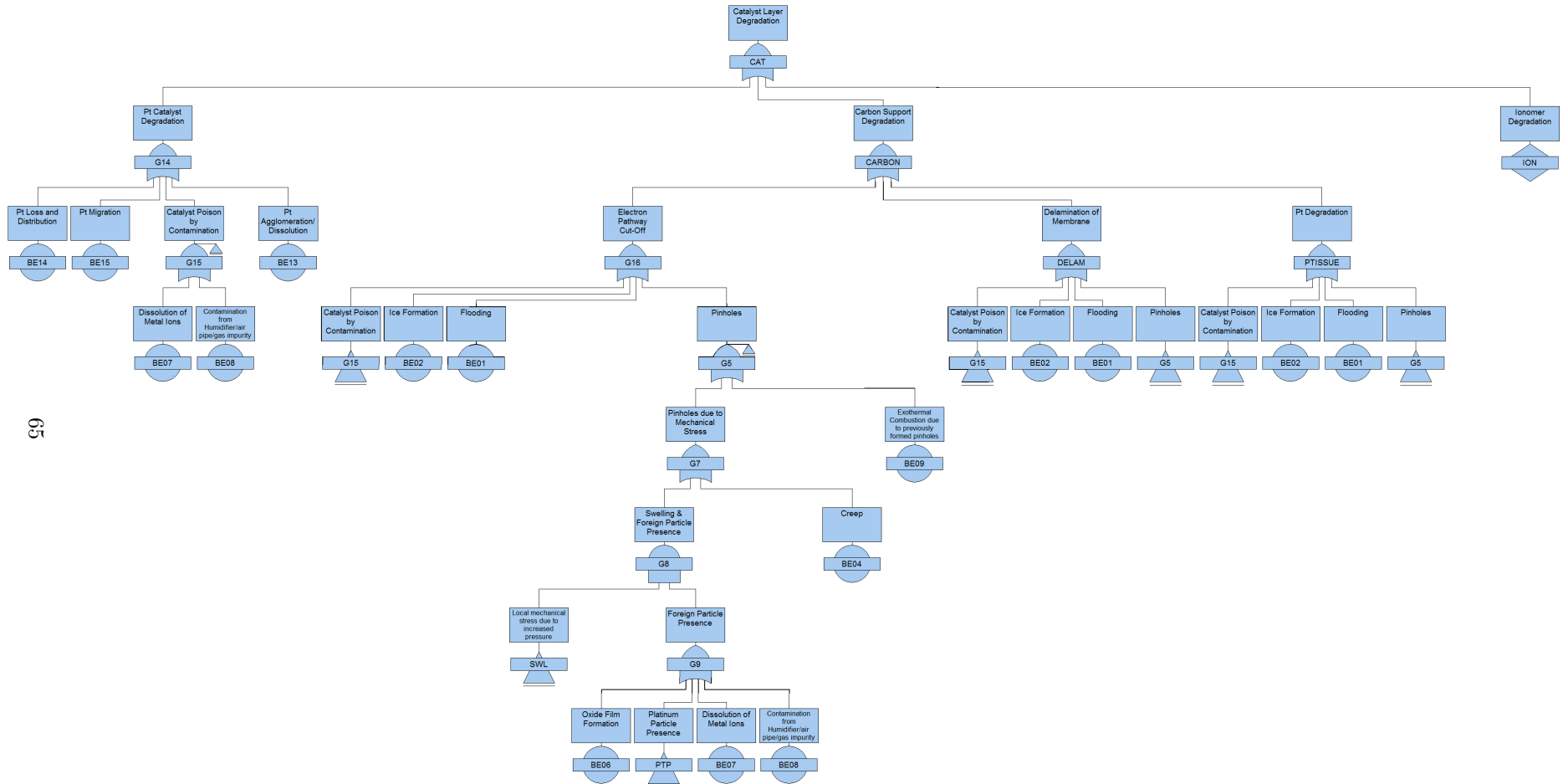


Figure 4.7: Proposed 'GDL' FT



G5

Figure 4.8: Proposed 'Catalyst' FT

‘Catalyst Layer Degradation’ was split into its three main constituent materials. When constructing the catalyst ink, carbon support material is mixed with the Pt nanoparticles, an ionomer (usually PTFE based), and finally a solvent as a mixer. After ball milling for a while the solvent is lost during curing, leaving the mixed carbon/Pt/ionomer ink. Degradation regarding these component materials is therefore proposed in Figure 4.8. Failure phenomena such as Pt agglomeration locally affect the dispersion of Pt nanoparticles on the carbon support, and as such are listed in the ‘Pt Catalyst Degradation’ section of the tree. Any failure modes that affect the Carbon support material are listed in the corresponding branch of the FT.

4.3.3 FT Summary

The FT was split into branches representing the physical components of a PEMFC; membrane, gas diffusion layer, catalyst layer and bipolar plate as shown in Figure 4.2. These were further broken down depending upon the categorisation of the failure phenomena. The FT was drawn based upon the information gleaned from the FMEA completed previously.

The FT was created based upon the same initial assumptions regarding the construction and operation of the cell, highlighted in chapter 2.

The membrane is a single component which can experience failures from mechanical, thermal or chemical degradation mechanisms. Therefore this section was split into the three degradation mechanisms shown in Figure 4.3. The GDL has a single component construction, however there are two GDL layers in a PEMFC and as such, this segment was split into anode side and cathode side degradation mechanisms. As can be seen in Figure 4.7, mechanical compression was also included which would affect both sides of the GDL. The BIP is a very simple segment with only few failure mechanisms that they need not be further split down into sub-categories.

In terms of the full tree, there are 70 overall events, stemming from 37 overall intermediate events. The majority of basic events are all stemmed from OR gates as each basic event can lead to the overall top event individually, leaving only two AND gates in the membrane section. Due to the absorption law the MCS for the overall FT are all of the basic events individually.

This section has re-evaluated the previous FT logic including the addition of previously omitted failure modes. The new FT layout is a more logical progression of the failure modes in a PEMFC, and as such is a step forward towards to reliability analysis of PEMFC. Not only this, but this section has shown an up to date validity of the causes of degradation in a PEMFC, by systematically analysing all the potential failure modes in a specific type of FC. This enhances the understanding of reliability issues in PEMFCs.

4.4 Qualitative and Quantitative Analysis

Because of their graphical representation and ability to assign data to basic events, FTs can be evaluated both qualitatively and quantitatively. The MCS are a list of cut sets that are the minimal and necessary conditions for the top event to be realised. These can inform the reader of what are the most severe basic events in a system, and where the most attention needs to be applied.

4.4.1 Qualitative

Qualitative analysis is in the form of analysing the combination of gates through either algebraic representations or listing cut sets. A cut set is a list of events where all of which will lead to the occurrence of the top event.

4.4.2 Quantitative

Quantification of the FT was undertaken to gain an understanding of the expected failure occurrence during operating life. Degradation rates were sought from the literature where available, with any gaps in the data filled by expert evaluation as in Table 4.2. For example, where

available, previously published experimental studies were analysed and the degradation rate presented due to an adverse operating condition was used in this work as the rate associated with the same basic event occurring. For example J.M.L Canut. et, al. [56] found that when flooding occurred, a degradation in voltage equal to 0.39 Vh^{-1} was observed. Therefore this rate was used to correspond to the failure mode of ‘flooding’.

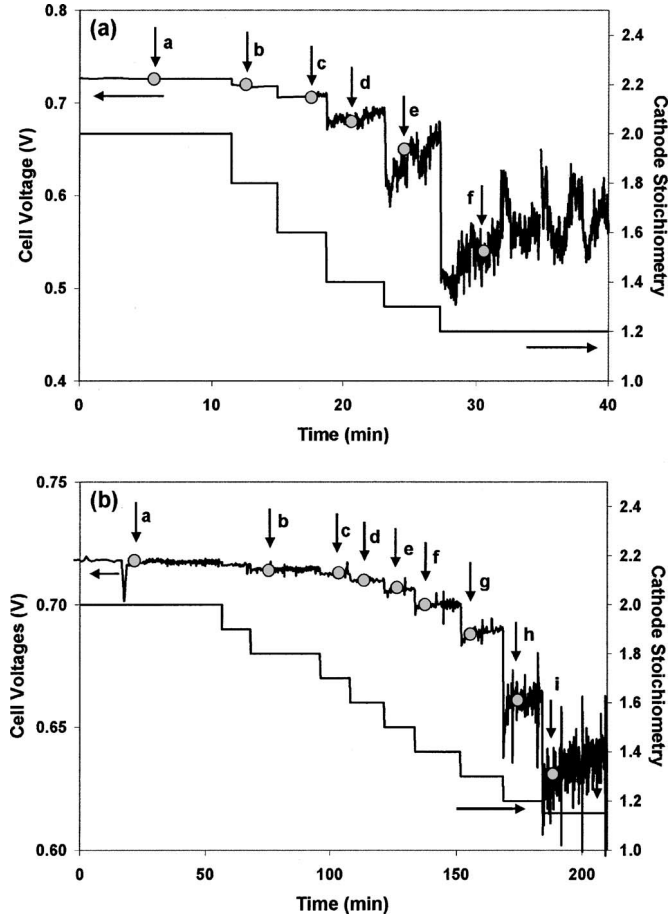


Figure 4.9: PEMFC Membrane flooding degradation test [56]

In their experimentation, the flow rate of cathode supply feed was decreased to induce flooding effects in the cell, and produced the results presented in Figure 4.9. Two testes were conducted, and for integrity of results, both test were considered and averaged for the overall voltage drop due to cell flooding of 0.39 Vh^{-1} .

Table 4.2 shows the basic event codes for each corresponding basic event description. This code will be used in later tables for brevity and formatting limitations.

As in [30], for each basic event listed in Table 4.2, $\mu(t)$ is assumed to follow a Weibull distribution, where $\mu(t) = 1/\lambda(t)$ and $\lambda(t)$ is the degradation rate. The probability density function $F(t)$ is given by Equation 4.1. The Weibull distribution was used as it adds a level of randomness to the flat degradation rates used. It can be assumed that a real world system would not always behave in the exact way that the flat degradation rate would suggest, therefore the Weibull distribution varies the outcome based upon the integration of a random number.

$$F(t) = \frac{\beta}{\eta_d} \left(\frac{t - \gamma}{\eta_d} \right)^{\beta-1} e^{-\left(\frac{t - \gamma}{\eta_d} \right)^\beta} \quad (4.1)$$

Where β is the shape parameter or Weibull slope, η_d is the scale parameter or characteristic

Table 4.2: List of Degradation Parameters Used

ID	Failure Mode Parameter	Value (Vh ⁻¹)	Ref
BE01	Flooding	0.39	[56]
BE02	Ice Formation	0.5	Proposed
BE03	Incorrect BIP torque	10 ⁻³	Proposed
BE04	Creep	10 ⁻⁵	Proposed
BE05	Fatigue from Relative Humidity Cycling	1.2 x 10 ⁻⁴	[57]
BE06	Oxide film formation	3.125 x 10 ⁻⁵	[58]
BE07	Dissolution of metal ions	3.125 x 10 ⁻⁵	[58]
BE08	Contamination from Humidifier..	4.37 x 10 ⁻³	[25]
BE09	Exothermal Combustion due to..	1.3 x 10 ⁻²	[59]
BE10	Previously Formed Pinholes	1.3 x 10 ⁻³	[59]
BE11	OH or OOH Radical Attack	1.3 x 10 ⁻³	[59]
BE12	Excess Heat	0.25	[56]
BE13	Pt Agglomeration/Dissolution	2.5 x 10 ⁻²	[60]
BE14	Pt Loss & Distribution	2.5 x 10 ⁻²	[60]
BE15	Pt Migration	2.5 x 10 ⁻²	[60]

lifetime, and γ is the location parameter. The shape parameter is equal to the slope of the line in a probability plot. This equation was used by the software FaultTree+ to determine the failure behaviour for the assembeled FT by applying the Weibull rates to each individual basic event in the tree, and analysing the failure logic to determine the top event unavailability.

The scale parameter can be determined from:

$$\eta_d = \frac{\mu(t)}{\Gamma(1 + \frac{1}{\beta})} \quad (4.2)$$

Where:

$$\Gamma(\eta) = \int_0^{\infty} x^{\eta-1} e^{-x} dx \quad (4.3)$$

The location parameter, γ , is left at 0 for this study, as it is assumed that all degradation starts at the beginning of life for the cell.

It was shown in [61] that if $\mu(t)$ follows a Weibull distribution with parameters β & η_d then times to failure (T) will also follow a Weibull distribution with parameters β and $\eta = D_f \eta_d$. Where D_f is the degradation level at which failure occurs. In the analysis performed for this work, failure is assumed to occur when there is a 5% drop in voltage. Therefore $D_f = 0.05V_{in}$ where V_{in} is the initial voltage of the cell. V_{in} is assumed to be 1 V for this work, as discussed in chapter 1 where it was suggested that a real world FC would expect an OCV of around 1V due to losses.

Using the parameters η and β for T in the FT enables the probability of the top event to be determined.

Each parameter calculated for each basic event is listed in Table 4.3, and shows the degradation rate, multiplicative inverse, scale parameter for $\mu(t)$, scale parameter for T , gamma function, and the shape parameter.

Table 4.3: Table of Weibull distribution data used

ID	Deg. Rate	Mu (t)	Scale Parameter for $\mu(t)$ [Eq. 4.2]	Scale Parameter for T [$0.005 \times \mu(t)$]	Gamma Function	Shape Charac- teristic
	$\lambda(t)$	$\mu(t)$	η_d	η	$\Gamma(\alpha)$	β
BE01	0.39	2.56	2.56	0.13	1	1
BE02	0.5	2	2	0.1	1	1
BE03	10^{-3}	100	88.26	4.41	1.13	0.8
BE04	10^{-5}	10000	11283.79	564.19	0.89	2
BE05	1.2×10^{-4}	8333.33	9403.16	470.16	0.89	2
BE06	3.125×10^{-5}	32000	36108.13	1805.41	0.89	2
BE07	3.125×10^{-5}	32000	36108.13	1805.41	0.89	2
BE08	4.37×10^{-3}	228.83	258.21	12.91	0.89	2
BE09	1.3×10^{-2}	76.92	86.80	4.34	0.89	2
BE10	1.3×10^{-2}	76.92	86.80	4.34	0.89	2
BE11	1.3×10^{-2}	76.92	86.80	4.34	0.89	2
BE12	0.25	4	4	0.2	1	1
BE13	2.5×10^{-2}	40	35.30	1.77	1.13	0.8
BE14	2.5×10^{-2}	40	35.30	1.77	1.13	0.8
BE15	2.5×10^{-2}	40	35.30	1.77	1.13	0.8

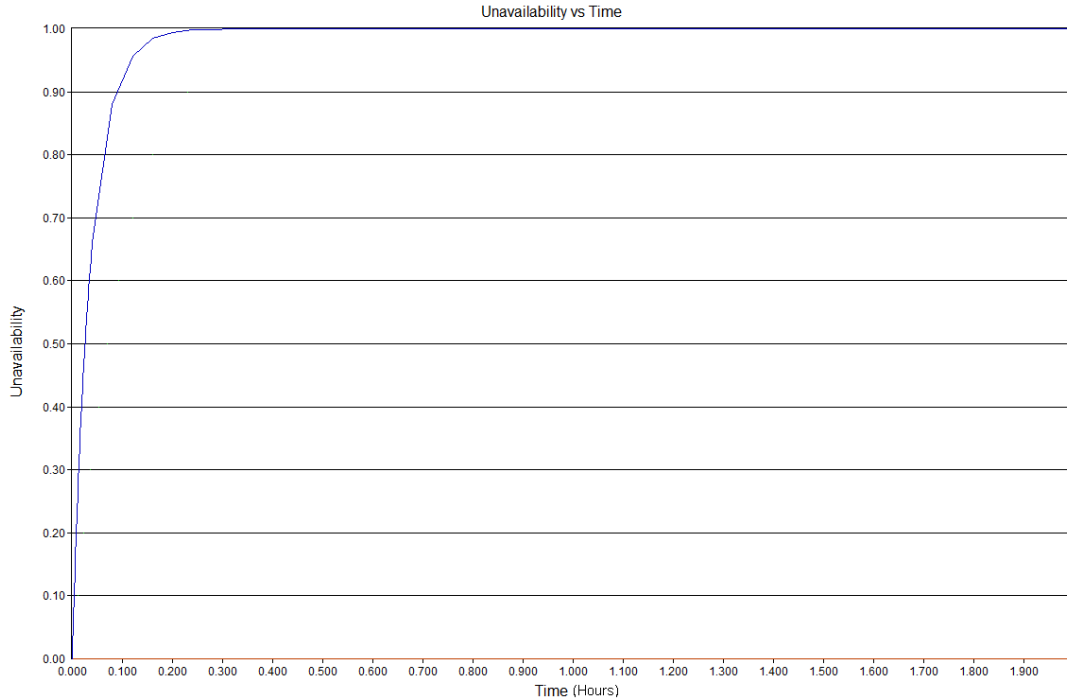


Figure 4.10: Unavailability of cell over Time

4.5 Results

The minimal cut sets for the FT developed are in fact the basic events themselves due to the fact that the vast majority of the logic gates are of ‘OR’ gates. This means that the basic event with the highest likelihood of failure will trigger the top event first under every iteration of the model. A plot of the unavailability of the cell over time is shown in Figure 4.10.

As can be seen, the unavailability of the FC - when the cell is considered failed - is after around 30 minutes. This is a very low lifetime for a FC, and is solely due to the highest degradation rate interacting with the logic of the FT. BE02 - Ice Formation, has a degradation rate of $0.5Vh^{-1}$ as operating a FC in sub-zero temperatures has severe effects on the materials of the FC and even the blockage of feed gasses to the reactant sites, however the probability of this occurring depends on operating conditions.

If high degradation failure modes such as BE12, BE02 and BE01 are removed, we see the unavailability increase to around 3 hours of operation (Figure 4.11), which is consistent with a failure due to the next highest degradation rate. This shows that the failure mode with the lowest η and corresponding β will be the failure mode to trigger the top event soonest.

BE01, BE02 and BE12 are failure modes that shouldn’t occur under normal operating conditions, however they can be triggered by the occurrence of alternative failure modes. If pinholes occur during normal operation, they can trigger the exothermal combustion of the feed gasses, which leads to excess heat. The FTA approach does not consider these knock on failure occurrences, and is an additional pitfall to using this technique for a highly accurate degradation model.

Also, in order to understand the degradation experienced under all possible operating conditions, a FT would need to be analysed for each condition, which can be considered to be infeasible. To do so would require a FT for every type of operating mode, from differing pressures to differing temperatures, and therefore would be very large and complex. Alternative methods to understand degradation in FCs is needed to overcome this shortfall.

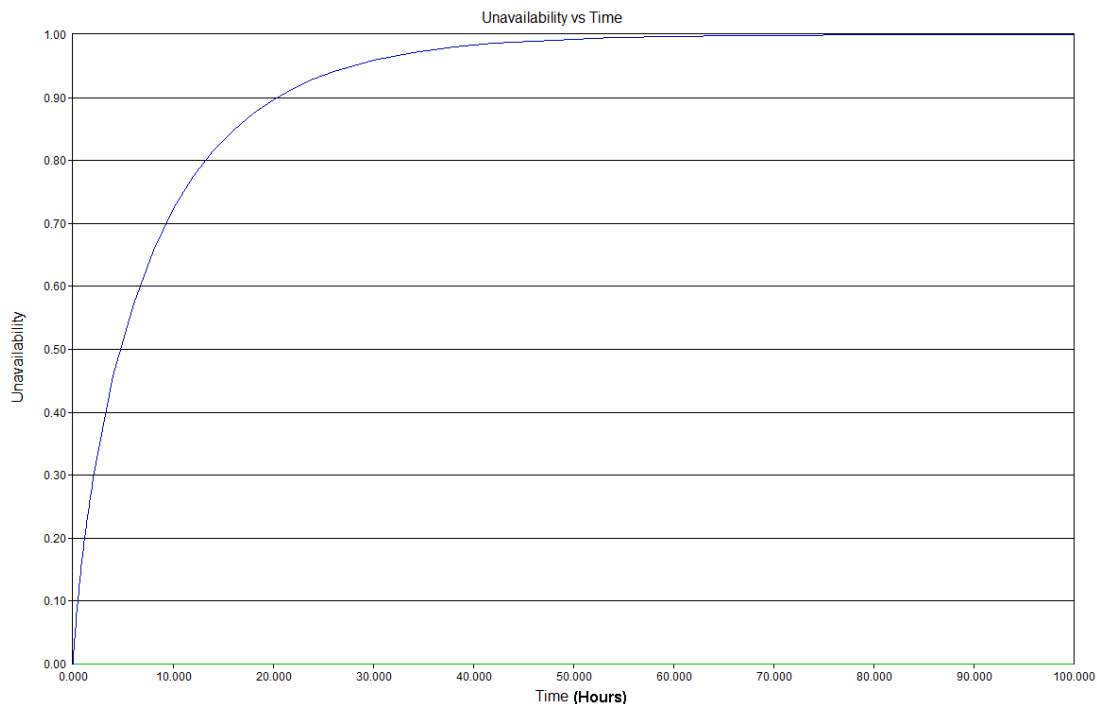


Figure 4.11: Unavailability

4.5.1 Relationship Concerns

The basic events in the membrane branch of a PEMFC FT are intrinsically linked. Some events can lead on to other events occurring, additionally some events can exacerbate other issues. To discuss this further, under the membrane degradation branch of the tree, G2, gas crossover has been listed as a basic event ('Increasing gas crossover' E020). H_2O_2 formation is listed as a basic event under the peroxide/radical degradation and is placed under the chemical degradation branch. In the 'Electrocatalysts and catalyst layers degradation' branch, a basic event of 'Platinum dissolution' highlights the issue of Pt nanoparticles separating from the CL and migrating to other areas of the cell. F.A.D. Bruijn, et, al. [40] suggest that radicals are formed at either; the cathode through H_2O_2 which is formed as part of the oxygen reduction reaction, or through the decomposition of H_2O_2 at the anode through the crossover of O_2 from the cathode to anode. Additionally, they state that recent work shows how radicals can be formed through a more direct pathway as opposed to the H_2O_2 intermediary pathway, in the presence of Pt. This is where favourable conditions for degradation can be provided by a reaction between molecular H_2 and O_2 in the presence of Pt particles that have separated from the CL through electrode degradation. This shows that gas crossover, H_2O_2 formation and Pt dissolution are interlinked and therefore should not be listed as segregated basic events. Gas crossover creates H_2O_2 , which causes radical introduction, and Pt nanoparticles from dissolution create radicals that attack the membrane. The radical attack causes thinning of membrane which can create pinholes and increased gas crossover. Operating conditions have been proven to exacerbate the above relationships, namely; high temperature, low humidification and high gas pressure.

In order to understand the links between the different basic events in the current FT, the entirety of the basic events contained in the intermediate events branches were plotted out with any potential links and relationships highlighted, the relationships are shown in Figure 4.12.

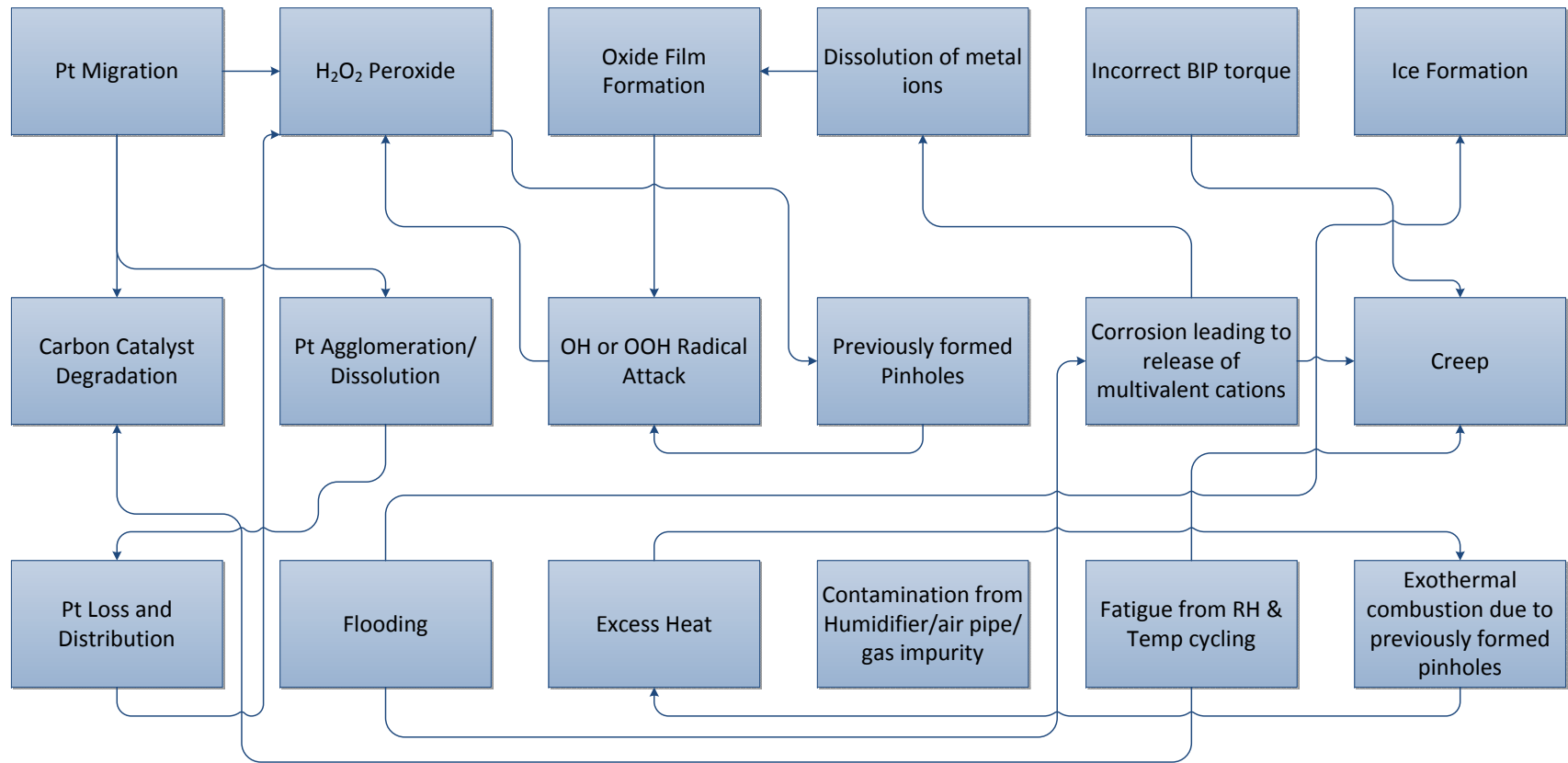


Figure 4.12: Relationship Analysis of Basic Events

In Figure 4.12, arrows link basic events that can have an affect upon the other. The Figure highlights the complex nature of the basic events experienced in such a system.

Pt Catalyst Degradation

One of the main overarching pitfalls regarding relationships between basic events occurs within Pt catalyst degradation. The catalyst layer is comprised of a fine distribution of Pt nanoparticles, dispersed over carbon black support. The catalyst layer is subject to research attention as it feeds into one of the three main hurdles to commercialisation of FCs; cost. Pt is a fundamentally expensive metal and the most effective way to utilise this commodity is to reduce the Pt loadings and increase their durability in a cell. The mechanisms for Pt catalyst degradation are; (i) Agglomeration and Particle Growth; (ii) Loss; (iii) Migration and (iv) Poisoning due to Contamination (shown in Figure 4.13).

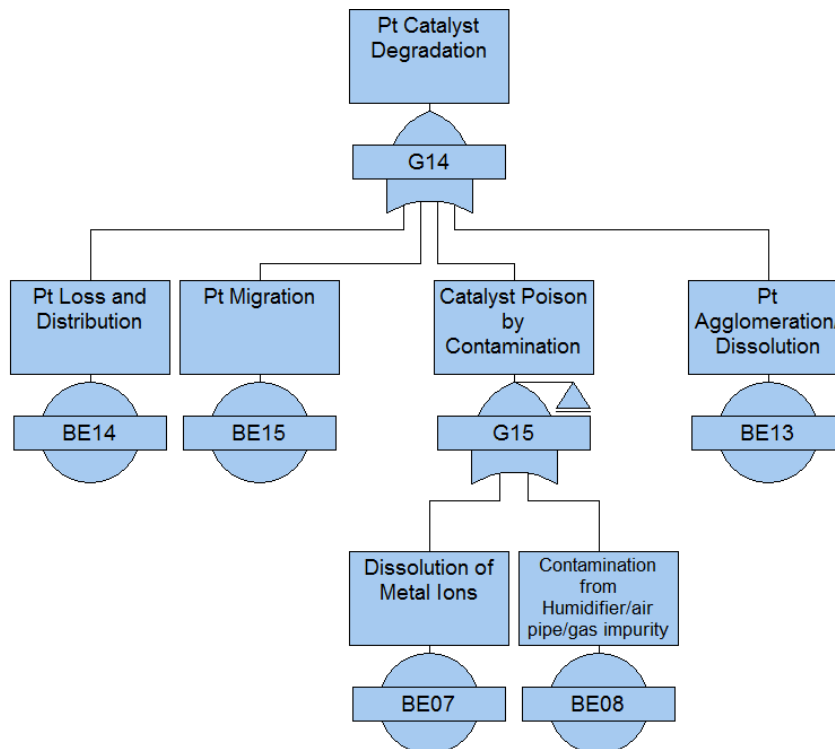


Figure 4.13: Pt Catalyst Degradation FT Logic

Agglomeration and Particle Growth refers to the tendency for small nanoparticles of Pt to want to group together and cluster to form larger particles. The thermodynamically driven development is apparent due to larger particles of Pt being more energetically preferential than smaller ones. This mechanism is often referred to as ‘Ostwald Ripening’.

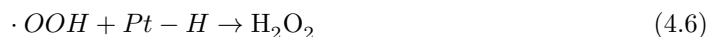
Pt Loss is a process where nanoparticles of Pt can be detached from their carbon support and flow through the FC to be removed by the product water.

Migration is a similar process to Loss, however the detached particles can be redistributed to other areas of the FC, causing adverse effects with other components.

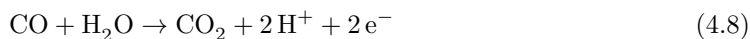
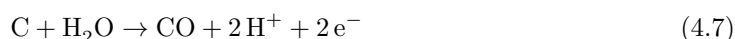
Poisoning due to Contamination can be categorised by the degradation of the catalyst due to foreign contaminants from either fuel supply or system-derived contaminants.

The above mechanisms of degradation will reduce the overall surface area of catalyst and reduce the ECSA of the cell. Not only does the loss of ECSA due to the previous degradation mechanisms cause an overall reduction in output voltage, but Pt particles present in other areas

of the FC can cause concerns. In these other area Pt contamination will cause exacerbations in other failure modes. Pt can facilitate the creation of OOH radicals in the membrane, also leading to H₂O₂ formation, by the process denoted in Equations 4.4,4.5 & 4.6.



Pt can also act as a catalyst for carbon oxidation which can affect the catalyst support and the GDL. Carbon can be oxidised to form CO₂ at relatively low potentials. However the kinetics of this process is so slow, that carbon is fine to use in FC applications. However when Pt is present, it can speed up this reaction to cause cell degradation as per Equations 4.7 & 4.8.



Equation 4.8 uses Pt to catalyse the reaction forming CO₂ from the Carbon material in the FC. The presence of Pt particles reduces the potential region from 1.1 V vs reversible Hydrogen Electrode (RHE) for carbon corrosion, to 0.55 V vs RHE. The FC is far more likely to be operating at the lower voltage and as such poses a significant risk of performance loss.

Pinhole Relationships

It has been highlighted that the basic events presented by Placca and Kouta have certain relationships that make it difficult to make equivocal statements regarding the FT logic.

Pinholes were found to be three events listed as basic, but were all caused by certain conditions or phenomena. Therefore they need to be broken down further to the basic events that cause the pinholes.

Pinholes are a mechanical deformation of the membrane (as shown in Figure 4.14). Pinholes, from previous research, were cited as three separate basic events explained as; (i) Pinholes Production (mechanical degradation); (ii) Pinholes (due to exothermal combustion between H₂ and O₂); (iii) Formation of Pinholes (due to contamination by trace metal ion). These failure modes were adapted to fit logically into the new tree, however further analysis has identified a potential issue with this failure mode.

This mechanical deformation of the membrane leads on to mechanical degradation of the FC. The descriptions given for previous basic events indicate the inherent further causal links between lower level events and pinholes. This is to say that if an event is due to something else, then it can be disseminated down to the said cause.

Pinholes were adapted into the presented tree as three basic events(as shown in Figure 4.15).

The membrane can indeed suffer pinholes from the exothermal combustion of H₂ and O₂, however that is not the only chemical attack phenomenon that can lead to pinholes. Chemical attack of any kind causes membrane thinning, which increases the risk of pinholes. Therefore it would be prudent to try to group all the pinholes basic events into one group.

Pinholes Issue Pinholes pose a drawback when utilising FTA for PEMFC degradation modelling, through its ‘vicious cycle’ tendency. Pinholes can be created through the exothermal combustion of H₂ and O₂ which comes around from reactant gas crossover. Once a pinhole has propagated through this process, more gas is allowed to cross over, resulting in more combustion of gases, causing hot spots and consequently more pinholes. This vicious cycle starts an exponential decay or PEMFC performance.

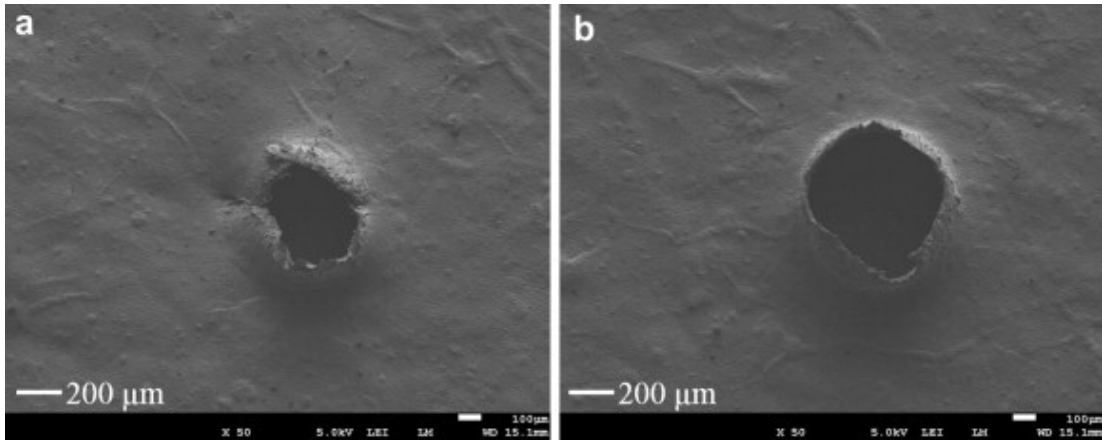


Figure 4.14: SEM image of Pinhole damage to a membrane. ([62])

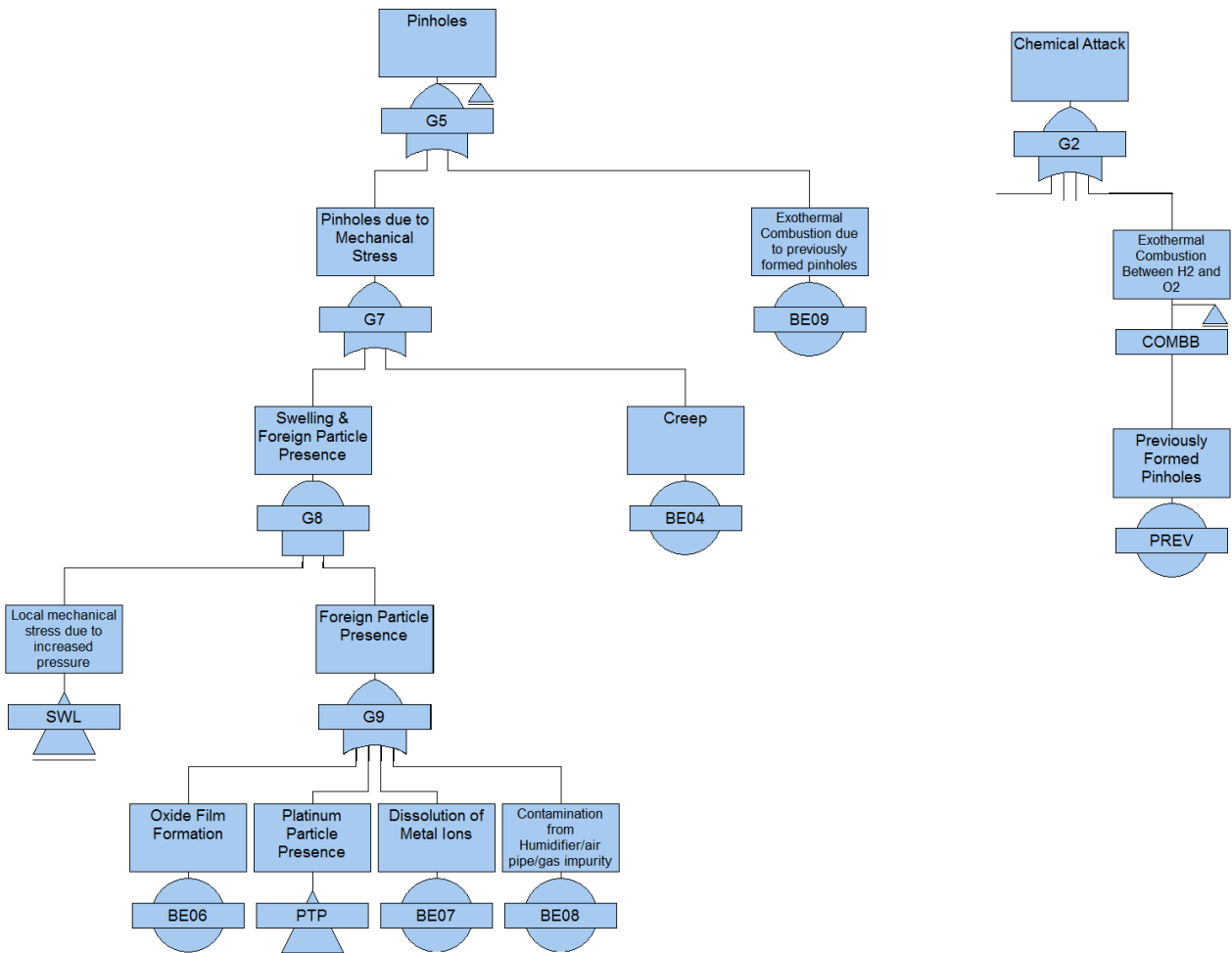


Figure 4.15: Pinholes logic within chemical and mechanical branches

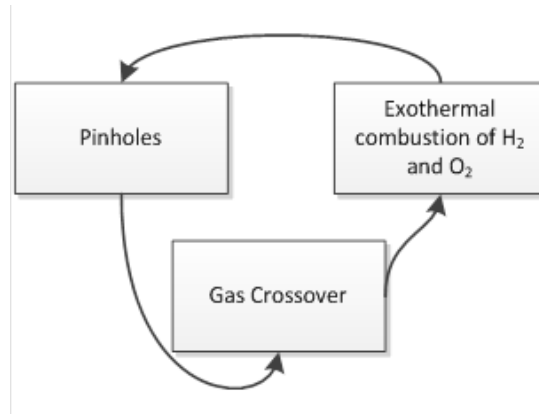


Figure 4.16: Pinhole cycle

Not only is the above true, but the knock on effects of Pt degradation also leads on to other degradation phenomenon additionally.

This unearths difficulties in using a standard FT layout to model PEMFC degradation.

Increased Pressure in Cell

There are four basic events that can contribute towards an increase in the pressure of a PEMFC; ‘Incorrect BIP torque’, ‘Flooding’, ‘Ice Formation’ and ‘Oxide film formation’. **‘Incorrect BIP torque’** during assembly can actively compress the internal component materials of the FC. **‘Flooding’** takes up room inside the cell and can push from the inside against the BIP walls. **‘Ice Formation’** acts in a similar fashion to flooding, however any frozen water will expand further, and place more stress on the PEMFC. **‘Oxide film formation’** acts to increase the internal pressure by building up a layer on the surface of the BIP, reducing the internal space for the interior component materials of the cell. All of these individual components can cause an increase in pressure in the cell, however combinations of the above will have increased affects on FC performance.

Ice Formation

A hydrated membrane is essential to the operation of the cell, and this hydration is achieved through a chemical bond of water to the membrane. Bound water cannot freeze to form ice until -120°C [16], and therefore ice formation in the cell is dependant upon water flooding in the cell. Any unbound water behaves as expected and will freeze at 0°C causing an issue.

4.5.2 Dependencies Summary

There are numerous circumstances in FC degradation where failure modes have dependencies highlighted above. A key pitfall to using FTA is the fact that FTA cannot take this into account, and therefore would require alternative methods either integrated into the FTA or a different method used altogether.

4.6 Conclusions

This work has re-evaluated FT logic determined in the earlier work, including the addition of previously omitted failure modes. The new FT layout developed here is a more logical progression of the failure modes in a PEMFC than shown previously, and as such is a step forward in

the reliability analysis of PEMFC. Up to date validity of the causes of degradation in a PEMFC have also been shown, enhancing the understanding of reliability issues in PEMFCs.

Figure 4.12 showed how certain basic events can lead on to others, and how they can also make other events worse. In particular, this instance of making others worse, questions the assumptions of the FTA techniques and its suitability for modelling these relationships with the PEMFC. It is therefore suggested that further research should look at re-evaluating the logic and structure of the presented FT. This would identify if FTA can be used for PEMFC degradation analysis, and failure forecasting.

By examining the events in the FT it is felt that further advancements can be made with regards to better portrayal of the event interactions. The main concern with the FT approach used to evaluate a PEMFC, is the pitfall of intricate relationships. It is seldom the case that one failure mode will be isolated from other failure modes influences. This flags a problem where alternative reliability techniques may need to be exploited.

One of the main limitations with current FT analysis of PEMFCs is the lack of forged links between different failure modes, where upon there exists key relationships between certain failure modes in a PEMFC system.

The presented FTA goes on from the FMEA to graphically show the logical interactions between failure mode areas. The FTA has highlighted where each failure mode stems from, with reference to each physical component of a PEMFC. Although the FTA presented is a step forward in the qualitative reliability understanding of PEMFCs, the work has uncovered the fact that relationships and dependencies between failure modes exist that make a quantifiable reliability analysis not totally accurate when using FTA methods. Dependencies have been found to exist between failure modes which would discount FTA for a quantitative analysis of a PEMFC. Specifically, any failure due to pinholes was highlighted as an area where loops occur, and basic events are intrinsically linked through dependent relationships. As pinholes can be caused by the crossover of gas, which increases the rate of gas crossover, which in turn increases pinhole production. Additionally, due to the minimal cut sets being each individual failure mode, the failure mode with the shortest η is the failure mode that will inevitably cause the occurrence of the top event first.

Hence, although FTA can be seen as a tool to gain a greater understanding of how failure occurs in a PEMFC, and what basic events lead on to in a cell, it has limited use in reliability assessment as no useful quantification can be made. Hence, if a true understanding of the probability or frequency of failure is required, a different approach must be adopted.

Markov modelling and Petri-Net simulation can take into account dependencies between failure modes and could therefore be exploited in a PEMFC study. However, Markov Modelling is not suitable for detailed component failure modelling due to the sheer amount of states that would be required for each of the many components in the system. As such, future work will entail development of a Petri-Net model that can take into account dependencies between failure modes and deal with the inherent issues with using FTA for quantitative analysis of PEMFCs.

Chapter 5

Proposed Petri-Net Analysis

5.1 Petri-Net Graphs

Based upon the previous FMEA and FTA, a Petri-Net has been developed to consider the interactions between failure modes and operating conditions in a PEMFC. The overall ‘global’ Petri-Net is presented in Figure 5.1. The global net is a coloured type Petri-net as the system state is determined by the data contained within the token that passes through each transition.

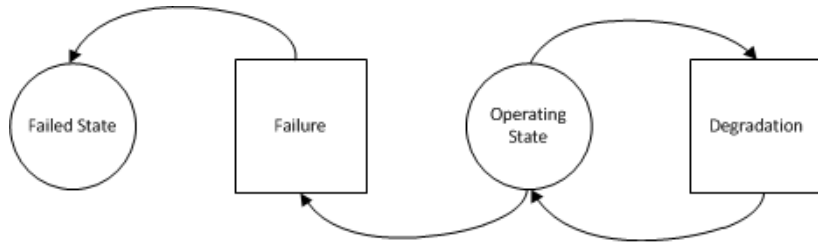


Figure 5.1: Global Petri-Net for PEMFC

The Petri-Net consists of an **Operating State** place, which can either transfer through the **Degradation** transition, or through the **Failure** transition into the **Failed State** place.

5.1.1 Operating State - Place

The operating state will contain the performance data from a FC model by Fly, et al [63]. It uses a model based upon Equation 1.8, using; E_{nernst} , $\eta_{act,a}$, $\eta_{act,c}$, η_{fc} , η_{ohmic} and $\eta_{concentration}$. E_{nernst} is found for a PEMFC with liquid product, considering temperature and pressure differences. The Tafel equation (Equation 1.9) is used for $\eta_{act,a}$, $\eta_{act,c}$ and η_{fc} overpotentials. $\eta_{concentration}$ values are determined from an empirical exponential relationship, and the remaining η_{ohmic} value is determined from a membrane hydration model.

A PEMFC performance model was integrated into the Petri-Net degradation model, which increases the accuracy of the predictions made by the degradation model over using simple FC equations. A 1D dimensional FC model developed by Fly & Thring [64] is used to predict FC behaviour based upon key operational parameters. Sub-systems of the FC are modelled in separate blocks using Simulink including voltage, hydration, mass and energy balances, and are discussed in more detail below.

The key output from the 1D model is that of the voltage for the cell. This is what is modified by the degradation model to show a drop in performance.

Cell Voltage

The cell voltage is calculated using Equation 1.8 in section 1.6 using the OCV, and subtracting the losses due to activation, ohmic, mass transport and fuel crossover losses. OCV is found using Equation 1.5, whereas the activation and fuel crossover losses are found using the Tafel equation (Equation 1.9). The mass transport losses are determined by empirical exponential relationships, whereas ohmics losses come from the membrane hydration model block. The resulting voltage profile and potential loss mechanisms are shown in Figure 5.2.

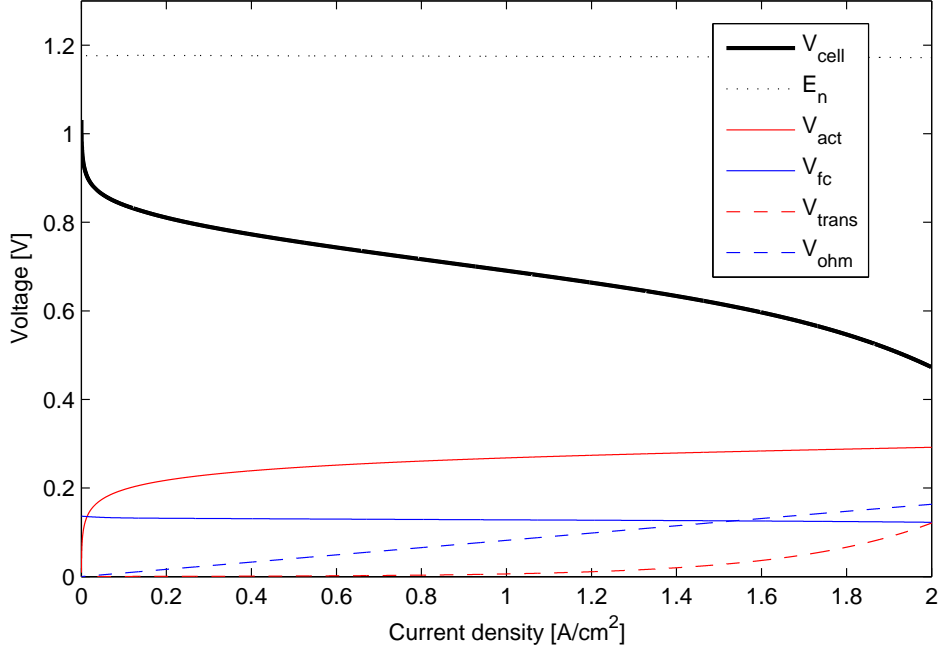


Figure 5.2: Cell voltage polarisation curve [65].

Hydration

The hydration of the membrane, which is paramount to the performance of the cell/stack, is calculated from the empirical model of Springer, et al. [18]. This includes the effects of electro-osmotic drag and back diffusion across the membrane.

Mass Balance

The anode and cathode are modelled separately as lumped volumes, and the mass of each gas is calculated from the first order differential mass balances in equations 5.1 - 5.5.

Cathode

$$\frac{dm_{N_2}}{dt} = \dot{m}_{N_2in} - \dot{m}_{N_2out} \quad (5.1)$$

$$\frac{dm_{O_2}}{dt} = \dot{m}_{O_2in} - \dot{m}_{O_2out} - \dot{m}_{O_2reac} \quad (5.2)$$

$$\frac{dm_{H_2O}}{dt} = \dot{m}_{H_2Oin} + \dot{m}_{H_2Oreac} - \dot{m}_{H_2Oout} - \dot{m}_{H_2Otrans} \quad (5.3)$$

Anode

$$\frac{dm_{H_2}}{dt} = \dot{m}_{H_2in} - \dot{m}_{H_2out} - \dot{m}_{H_2reac} \quad (5.4)$$

$$\frac{dm_{H_2O}}{dt} = \dot{m}_{H_2Oin} - \dot{m}_{H_2Oout} + \dot{m}_{H_2Otrans} \quad (5.5)$$

Where m is the mass of the gas species, in shows the species in, out shows the species out, $reac$ is the electrochemical reaction energy, and $trans$ is the transport loss.

Energy Balance

The temperature of the FC is calculated using a single thermal capacitance model as shown in equations 5.6 & 5.7.

$$m_s C_{ps} \frac{dT_s}{dt} = \dot{Q}_{reac} - \dot{Q}_{elec} + \dot{Q}_{in} - \dot{Q}_{out} - \dot{Q}_{loss} \quad (5.6)$$

$$\dot{Q} = \dot{m}_{H_2Ov} \Delta H_v + \sum_{j=1}^n \dot{m}_j C_{pj} (T - T^0) \quad (5.7)$$

Where m_s is the mass of the stack, C_{ps} is the specific heat, \dot{Q}_{reac} is the heat released during the reaction, \dot{Q}_{elec} is the electrical power generated by the cell/stack, \dot{Q}_{in} and \dot{Q}_{out} represent the heat flows into and out of the cell/stack, \dot{Q}_{loss} is a term to represent the small amount of energy lost from the cell/stack surface due to natural convection, and H_v is the enthalpy of water vapour.

1D model overview

Figure 5.3 shows how these separate blocks interlink to give the FC voltage based upon an input current. Cell voltage is determined in the ‘stack voltage’ block, hydration is determined in the ‘membrane hydration’ block, the anode and cathode mass balance equations are calculated in the ‘cathode model’ and ‘anode model’ blocks, and the energy balance is determined in the ‘thermal module’ block. The current is fed into the model and is the determining factor for the calculations. The cathode and anode blocks take the current, and determining variables from Equations 5.1 - 5.5. The membrane hydration block uses the product of the mass balance equations to calculate the resistance of the MEA, and feeds back data into the anode and cathode mass balance blocks. The resistance values feed directly into the stack voltage calculation block, with its product being the stack power. The thermal block takes outputs from all of the other blocks for its calculations.

The 1D model used is a highly complex model that is computationally intensive. As to reduce the computational time required to solve the model, certain aspects that were not required for the purposes of degradation were removed from the model. A significant area of improvement in the reduction of calculation time was achieved by removing the hybrid battery model. Automotive PEMFCs are always hybridised with conventional battery systems as to help with regenerative braking and load smoothing. However, for this work, precise control over the PEMFC current and voltage was required and therefore the battery system model was deemed redundant. Removal of this sub-system increased calculation time significantly.

A large section of the anode model was removed that calculated the mass flow of water in to the anode. This section was replaced with a more simple calculation of this value that doesn’t effect the outcome of the performance model. The more complex calculations were used by the creators of the 1D model to calculate heat transfer, and is not required for this work.

Additionally, simplifications were made to the RH calculations that gave a greater amount of control over the values if required. Simplifications were also made to the cathode model sub-blocks to reduce the computational time required while still retaining accuracy.

The 1D model runs in Simulink software which means that the calculations vary per real world second which could skew degradation results. Therefore the time-step was smoothed out to only offer values for the degradation model to handle at one second time-steps.

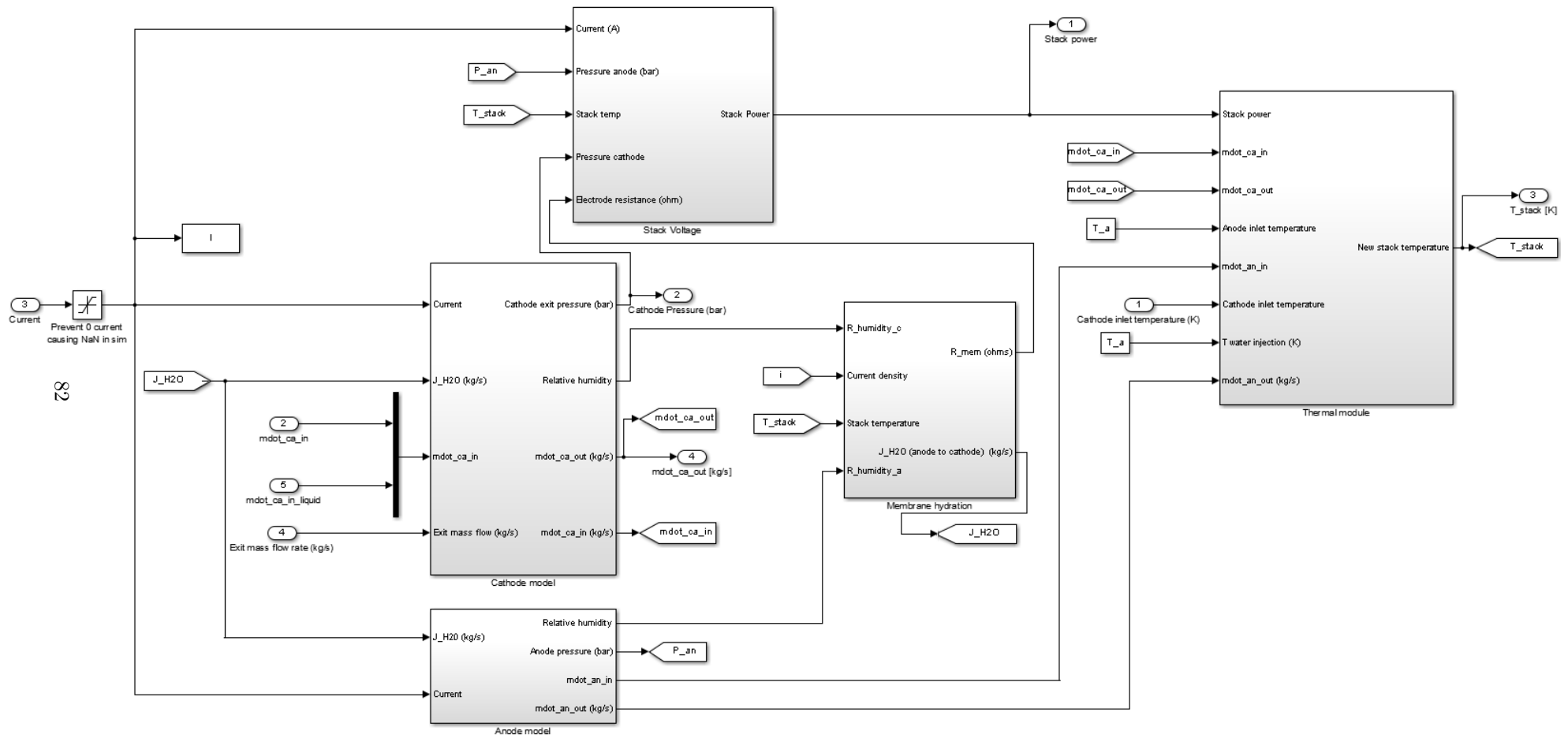


Figure 5.3: Modified simulink model of 1D FC model [65]

Model Parameters

The FC performance model is run based upon initialisation data that sets key variables as listed in Table 5.1. These data are the input data that are required before the running of the cell, and are representative of the type of FC being modelled, and are used in the equations that determine the FC performance during operation. The model can be run either in a steady state load or dynamic load mode, indicative of a drive cycle to match what would be required in an automotive environment.

The values presented in Table 5.1 are either representative of the test rig materials or common operational conditions used in the industry. ‘Test cell’ denotes that the value is inherent from the MEA used, ‘Standard’ denotes that it is common practise, ‘Test rig’ means that the value is set due to the rig itself, ‘FC model’ shows that the value is taken from the FC model by Fly & Thring [65], and ‘Calculated’ means that the value was derived from an equation for the specific MEA.

Table 5.1: Simulation parameters

Parameter	Value	Justification
<i>Fuel cell</i>		
Fuel cell rated power	67W	Test cell
Number of cells	1	Test rig
Cell active area	200cm ²	Test rig
Cathode stoichiometry	2.5	Standard
Anode stoichiometry	1.5	Standard
Ambient humidity	55%	Test rig
Membrane thickness (z)	27.5 μ m	Test cell
Internal current density (i_n)	1.5 $\times 10^{-4}$ A/cm ²	FC model
Mass transport coefficient (a_{trans})	3 $\times 10^{-4}$	FC model
Mass transport coefficient (b_{trans})	3.0	FC Model
Exchange current density at STP ($i_{oc,0}$)	3.2 $\times 10^{-8}$ A/cm ²	FC Model
Water entrainment constant (δ)	2.0	FC model
Molar mass membrane (M_{mem})	1.1 kg/mol	FC Model
Dry density membrane (ρ_{dry})	1.98g/cm ³	FC Model
Cathode activation energy (E_c)	66kJ/mol	Standard
Resistance Correction Factor	1.62	Calculated

The resistance correction factor is used to modify the membrane resistance to accurately represent the membrane and GDL used for comparison. The model uses the resistance value of 68.68mS/cm for the Nafion 117 membrane and no GDL resistance. The correction factor is based upon the Nafion XL membranes conductivity of 50mS/cm which is used in the experimentation, and the GDL resistance due to compression of an additional 0.018/cm² [66] calculated based upon the resistivity of the GDL material and the clamping force applied to the end-plates of the test rig.

This modification of the 1D model is paramount to increasing the accuracy of this work. The output of the 1D model is heavily influenced by the thickness of the membrane, and thus, the resistance of said membrane. One of the main ways in which to increase the performance of a PEMFC is to reduce the thickness of the membrane, and therefore reduce the resistance value. However, a balance needs to be struck when thinning the membrane excessively, as too much thinning will weaken its structure and therefore become more susceptible to damage during use. It was therefore of paramount importance to make sure that the 1D model was modified in the aforementioned manor as to be certain that the output of the model was indicative of the exact materials being tested in the experimental rig.

5.1.2 Degradation - Transition

For every time step, the degradation transition fires, which links a variety of more detailed Petri-net modules related to failure modes from the FMEA & FTA work. Whether or not the individual degradation Petri-Nets are enabled, depends on the relationships for said Petri-net. These can include operating conditions and previous interactions of failure modes. Each failure mode previously identified in the FMEA and FTA has a Petri-Net attributed to it, which shows the logic contributing towards its activation. A total of 20 Petri-Net modules have been identified and a selection are described, with the entirety available in Appendix D.

5.1.3 Failure - Transition & Failed state - Place

The failure transition will be fired based on a simple relationship between expected FC performance, and actual FC performance. As per the previously identified PEMFC degradation and lifetime requirements, if the actual FC performance drops below 5% of expected FC performance, the transition will fire.

The 'Failed' place, is a state of FC failure as identified above.

5.2 Petri-Net Module Overview

The degradation modules that are contained within the 'degradation' transition of the global Petri-net are standard Petri-nets with the tokens containing no data, and only being used to determine degradation occurrence due to their positions. The full list of the 21 Petri-Net modules used for this study, and what they are composed of are listed in Table 5.2. Their interactions, are displayed in Figure 5.4.

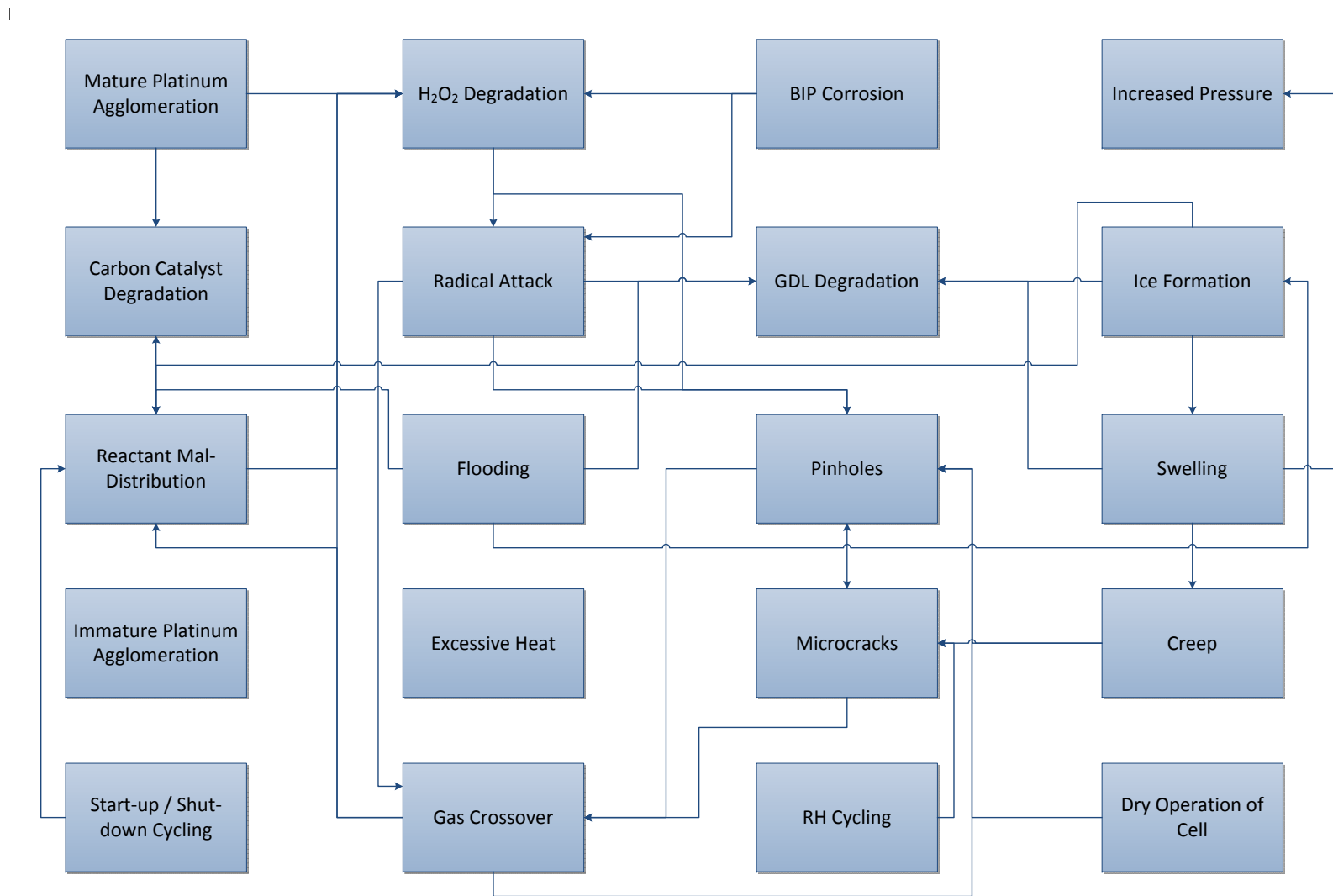


Figure 5.4: Interactions between Petri-Net Modules

Module	Place ID	State Name
BIP Corrosion	P1	No BIP Corrosion
	P2	BIP Corrosion
Carbon Catalyst Degradation	P3	No Carbon Catalyst Degradation
	P4	Reactant Mal-Distribution
	P5	Potential <0.55V & Loss of Platinum
	P6	Loss of Platinum
	P7	Potential <0.55V
	P8	Potential <1.1V
	P9	Catalyst Carbon Degradation
Creep	P10	No Creep
	P11	Initial Creep
	P12	Dry Operation of cell
	P13	Hot Operation of cell
	P14	Wet Operation of cell
	P15	Time <100min
	P16	Time >100min
	P17	Early Creep
	P18	Late Creep
Excessive Heat	P19	Normal Creep
	P20	Normal Heat
Gas Crossover	P21	Excessive Heat
	P22	No Gas Crossover
GDL Degradation	P23	Low rate of GCO
	P24	Pinholes
	P25	Microcrack
	P26	High rate of GCO
H ₂ O ₂ Degradation	P27	No GDL Degradation
	P28	PTFE & Carbon Deg.
	P29	Swelling
	P30	Flooding
	P31	Radical Attack
	P32	Freezing
	P33	GDL Degradation
Ice Formation	P34	No H ₂ O ₂ Degradation
	P35	H ₂ O ₂ Degradation below 30%
	P36	Pt dissolution
	P23	Low rate of GCO
	P2	BIP Corrosion
	P26	High rate of GCO
	P37	Potential >0.695V
	P38	H ₂ O ₂ Degradation
Increased Pressure	P39	No Ice Formation
	P30	Flooding
	P32	Ice Formation
	P40	Temperature >0C
Increased Pressure	P41	Normal Pressure
	P29	Swelling
	P3	Incorrect BIP Torque
	P43	Increased Pressure

Pinholes		P44	No Pinholes
		P19	Creep
		P38	H ₂ O ₂ Degradation
		P45	Radical Attack
		P26	High rate of GCO
		P12	Dry operation of cell
		P46	Intermediate Pinhole
Immature Platinum Agglomeration		P24	Pinholes
		P47	No Im. Pt. Agg.
		P48	Operating time <40 hours
		P49	25% RH or less
Mature Platinum Agglomeration		P50	Potnetial >1.0V
		P51	Im. Pt. Agg.
		P52	No Mat. Pt. Agg.
		P53	Operating time >40 hours
Radical attack		P49	25% RH or less
		P50	Potnetial >1.0V
		P54	Pt. Agg.
		P55	No Radical attack
		P2	BIP Corrosion
Reactant Distribution	Mal-	P38	H ₂ O ₂ Degradation
		P56	Inhibitor
		P57	Radical attack
		P58	Normal Reactant Distribution
		P62	Reactant flow obstruction
		P63	Catalyst poison by contaminant
Flooding		P32	Ice formation
		P64	Flooding
Microcracks		P65	Startup/Shutdown Cycling
		P26	High rate of Gas Crossover
		P4	Reactant Mal-Distribution
		P66	No Flooding
		P67	Flooding
Start-up/Shut-down Cycling		P44	No Microcrack
		P45	Pinhole effects
RH Cycling		P46	RH cycling
		P19	Creep
Dry Operation of the Cell		P47	Microcrack effects
		P48	Microcrack
Swelling		P68	No Start-up/Shut-down Cycling
		P65	Start-up/Shut-down Cycling
Swelling		P69	No RH Cycling
		P70	RH Cycling
Swelling		P69	No Dry Operation of the Cell
		P70	Dry Operation of the Cell
Swelling		P69	No Swelling
		P70	Swelling

Table 5.2: List of Places and Transition in all Modules

Summary of the Petri-Net Model

The Petri-Net degradation model developed in this work is a comprehensive model of the interactions between the previously identified failure modes in a PEMFC of standard construction (PTFE based membrane, Carbon/Pt catalyst, steel BIP, carbon GDL). The individual modules range from relatively simple relationships with 2-3 places and a low number of transitions, to larger modules with 8 places and 8 transitions. It contains 21 separate modules that interact to both; deliver a voltage degradation value, and further interact with other failure modes. However, if further interactions or modules are discovered that need to be added, the Petri-Net model can easily facilitate this occurrence, with a simple addition to the script files.

5.2.1 Example net: H₂O₂ Degradation

Figure 5.5 shows an example of a Petri-Net module for a given failure mode: ‘H₂O₂ Degradation’.

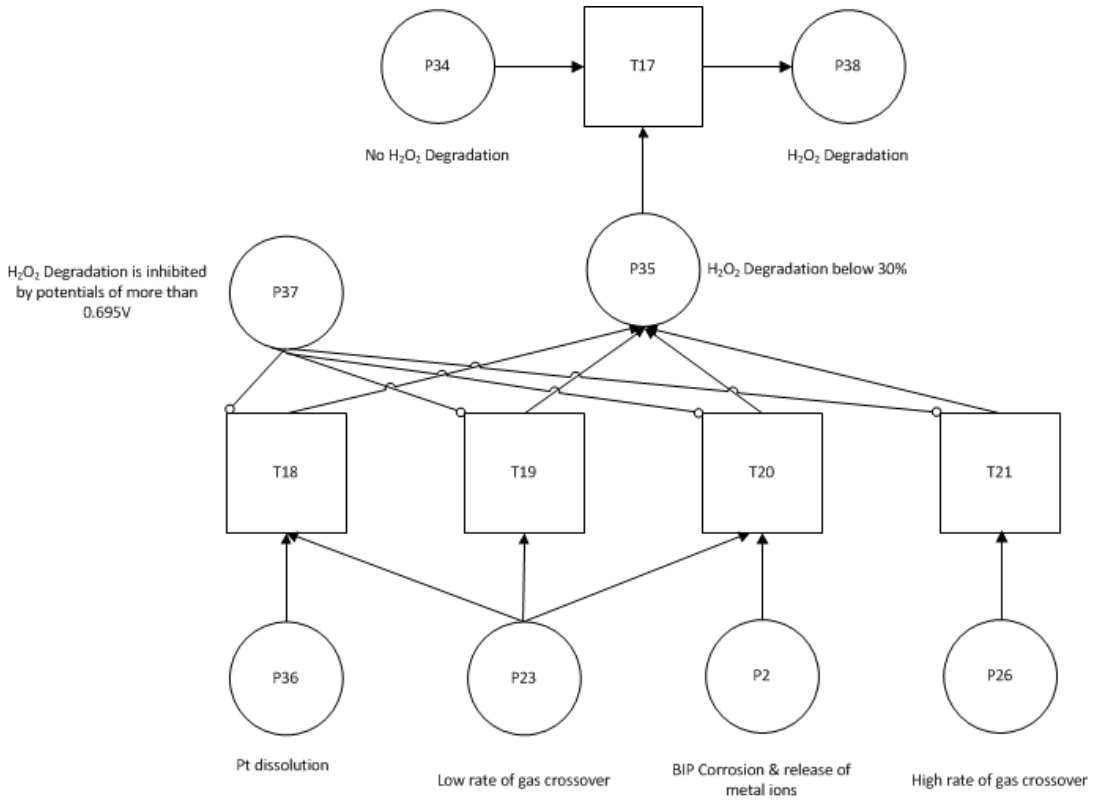


Figure 5.5: Example Petri-Net for H₂O₂ Degradation

$P34$ is the initial place, and is enabled with a token on the first running of the model. It is indicative of a healthy PEMFC and is enabled from the first running of the model, with no H₂O₂ degradation. $T17$ can only fire when there is a token in $P35$ and $P34$ at the same time. $P35$ is used to indicate a state of H₂O₂ degradation, agglomerating the lower level transitions. This is for the integrity of the transition logic. The firing of this transition would enable $P38$, indicating a state of H₂O₂ degradation, and would have an output affecting the performance of the PEMFC and potentially linking into another Petri-Net module. There are a number of contributors to $P35$, stemming from places $P36$ ‘Pt dissolution’, $P23$ ‘Low rate of gas crossover’, $P2$ ‘BIP corrosion & release of metal ions’ and $P26$ ‘High rate of gas crossover’. $P23$ is enabled by an interaction from a separate Petri-Net module, and indicates the presence of Pt which acts as a catalyst for H₂O₂ formation (LaConti, et al. [45]) shown in Equations 5.8-5.10.



Therefore for *T18* to fire, *P36* and *P23* need to be enabled. This would show that there is gas crossover and a free Pt presence to cause a rate of formation of H_2O_2 .

All transitions for this example are instant transitions, and therefore rely on the combinations of previous token movements for its output degradation place marking.

As has been previously mentioned in Equations 3.6-3.11, H_2O_2 can form from the crossover of the reactant gasses through the membrane. Thus, for a high rate of gas crossover, a corresponding rate of H_2O_2 formation is attributed, however if a low rate of gas crossover is observed a separate value is used. This enables the Petri-Net modelling of *T19* and *T21* firing and a corresponding degradation of PEMFC overall performance. Consequently if *P26* is enabled, *T21* will fire, placing a token in *P35*, and if *P23* is enabled, *T19* will fire a token into *P35*.

Pozio, et al.[46] also showed that the presence of Fe_2^+ and Cu_2^+ (Iron and Copper ions) released from BIP corrosion greatly accelerate the degradation due to H_2O_2 formation when there is gas crossover.

'P37' is an inhibitor and serves to prevent the transition of 'T18', 'T19', 'T20' & 'T21'. Borup, et al.[16] state that the potential for H_2O_2 formation ($E^\circ \text{H}_2\text{O}_2$) is equal to 0.695 V, and that any potential greater than this would inhibit the formation of H_2O_2 in the PEMFC.

5.3 Simulation of the Petri-Net

5.3.1 Petri-Net Firing

The firing of the Petri-Net uses the following equation:

$$M_n = M_0 + A^T \sum \quad (5.11)$$

Where M_n is the final marking, M_0 is the initial marking, A^T is the incidence matrix for the module, and \sum is the transition firing count vector.

For each individual Petri-Net module contained within the 'Degradation' transition of the global Petri-Net, there is a corresponding incidence matrix as in Equation 5.12 for H_2O_2 degradation.

$$A^T = \begin{matrix} P_1 \\ P_2 \\ P_3 \\ P_4 \\ P_5 \\ P_6 \\ P_7 \\ P_8 \end{matrix} \begin{pmatrix} T_1 & T_2 & T_3 & T_4 & T_5 \\ -1 & 0 & 0 & 0 & 0 \\ -1 & 1 & 1 & 1 & 1 \\ 0 & -1 & -1 & 0 & 0 \\ 0 & -1 & -1 & -1 & 0 \\ 0 & 0 & -1 & -1 & 0 \\ 0 & 0 & 0 & 0 & -1 \\ 0 & 0 & 0 & 0 & 0 \\ 1 & 0 & 0 & 0 & 0 \end{pmatrix} \quad (5.12)$$

The logic behind each transition from place to place is noted in each A^T matrix for each module. A '-1' indicates the taking of a token from a place, and a '1' indicates the placing of a token into that place.

5.3.2 Petri-Net Simulation Logic

The Petri-Net logic is presented in Figure 5.6, and shows the progression of the process during running of the Petri-Net simulation. The global script is the overall code that runs the Petri-Net system model. It sets all current loss variables to '0' as the model is due to run numerous times and repetition of results per simulation is not desired. Any starting variables are then set, such as the amount of Start-up/Shut-down cycles for the simulation that are not inherent within the model. The incident matrix for the global net is then generated and the loop is started that runs the degradation parameters per time-step. For every time-step, each module of degradation phenomena have their incident matrices generated first, then each step the logic is fired to ascertain degradation. Throughout this process, the degradation level is checked against a pre-determined failure level, and if this threshold is exceeded, the simulation is stopped and results recorded.

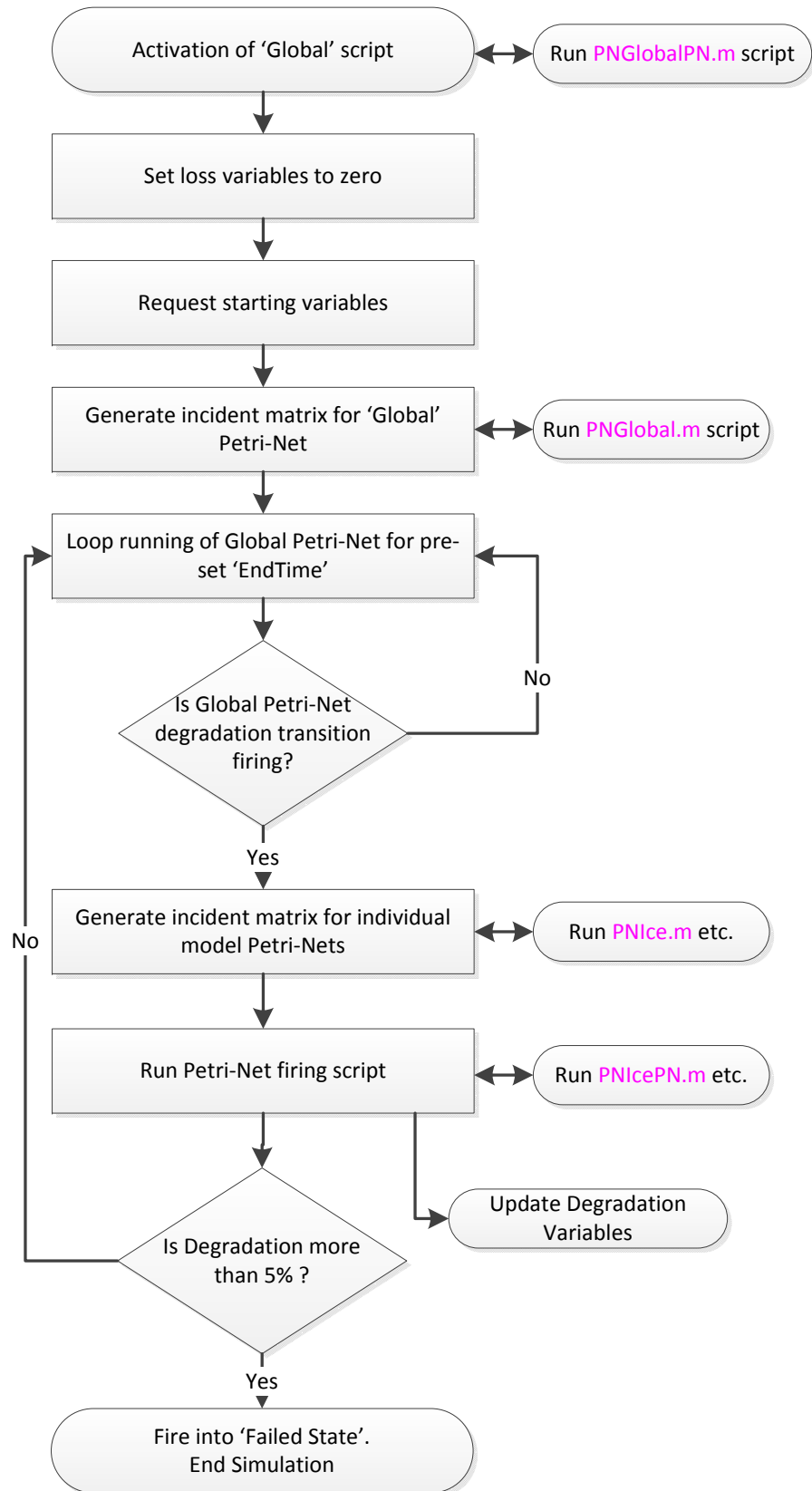


Figure 5.6: Petri-Net Logic Flow Chart

5.3.3 Token movement

The firing of transitions and the movement of tokens can depend on various parameters. Some depend on an operating condition of the degradation model, some depend on previous token movements, and some on specific time related conditions. An example of the movement of a token through a specific starting module in the Petri-Net model is presented in Figure 5.7.

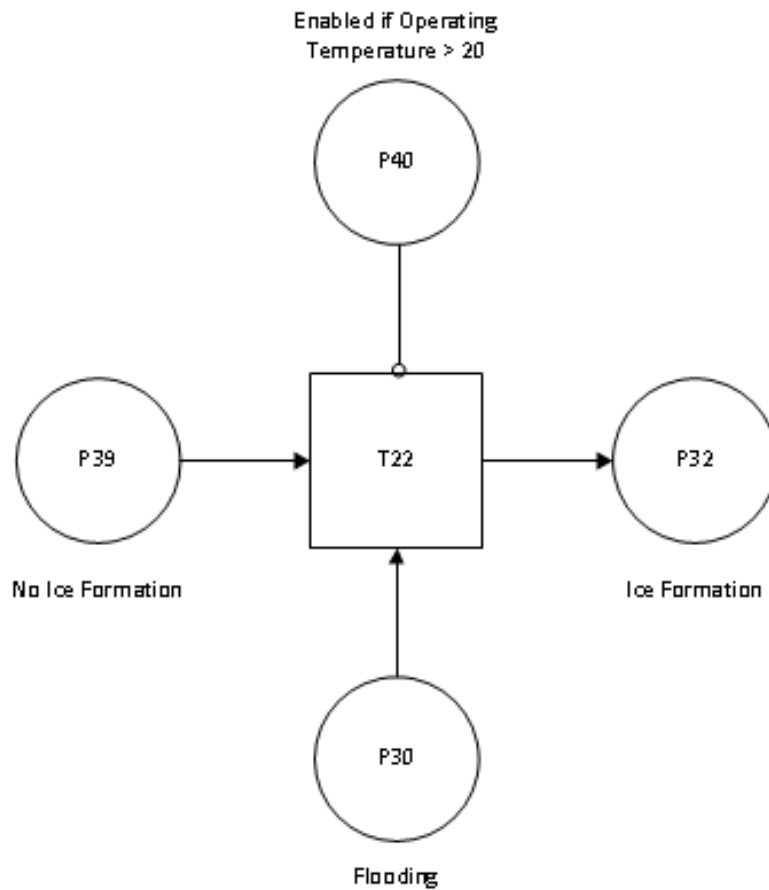


Figure 5.7: Petri-Net module for Ice formation

Figure 5.7 shows the module for ice formation, and would have the token placed in *P39* when the degradation model is first run. The transition can only fire if there is excess water present, placing a token in *P30*. Additionally if *P40* has a token in (which depends on the cell/stack temperature operating parameter from the performance model) then the transition can't fire. The movement of the token from *P39* to *P32* of this module would require two operating parameters from the 1D model to be in certain bounds. This example requires the cell/stack temperature to be below 0, and the RH of the cell to be above 100%. Once these conditions are met, the token will be moved from *P39* to *P32*.

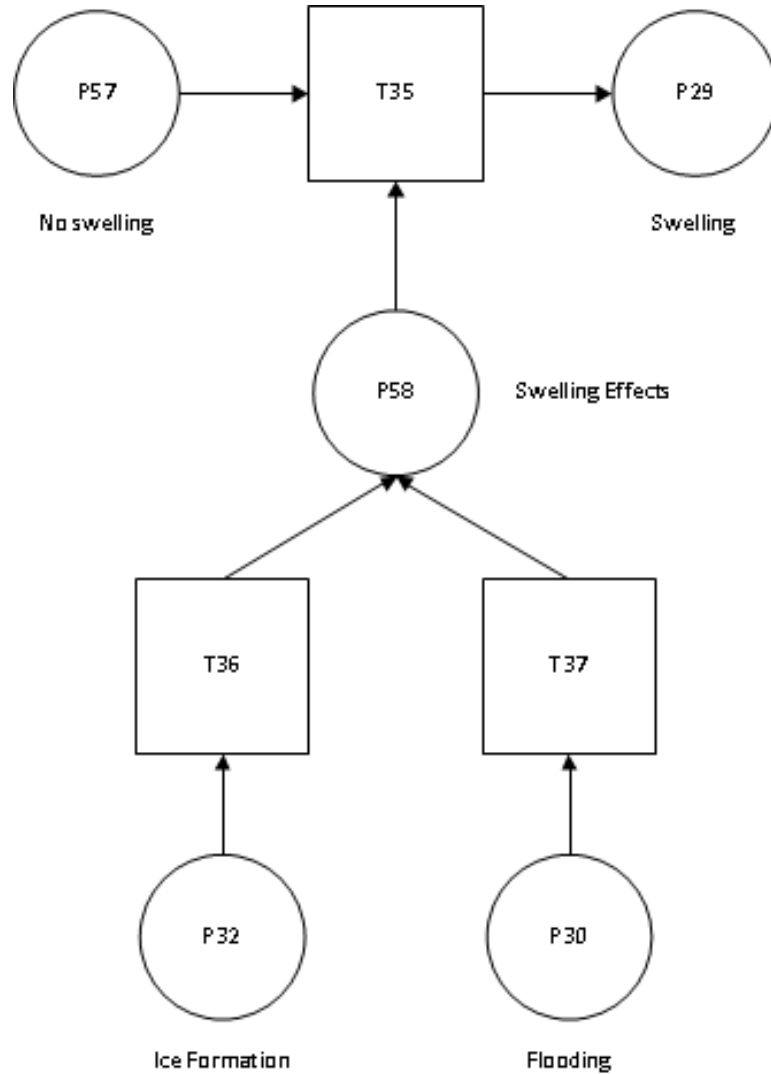


Figure 5.8: Petri-Net module for Swelling

The token placement resulting from the firing of the transition in Figure 5.7 then transfers tokens to other areas of the Petri-Net model. Figure 5.8 shows the module for swelling, and would have *P32* and *P30* harbouring tokens after the interactions were true. If *P32* has a token in Figure 5.7, then *P32* will contain a token for the next interaction of the degradation model. *T36* in Figure 5.8 will fire if there is a token placed in *P32* being an instantaneous firing. This would place a token into *P58* which again triggers an instantaneous transition in *T35*, as long as there is currently no swelling (a token placed into *P57*).

A token placed into *P29* of the swelling module triggers a degradation relationship that is derived from a combination of experimental results and data from the literature, and is covered in more detail in Chapter 7.

In addition to triggering a key hydration related degradation phenomena (covered in more detail in section 6.4.1), a token placed in *P29* of the swelling net influences degradation due to GDL degradation in the such named net (as detailed in Figure 5.9).

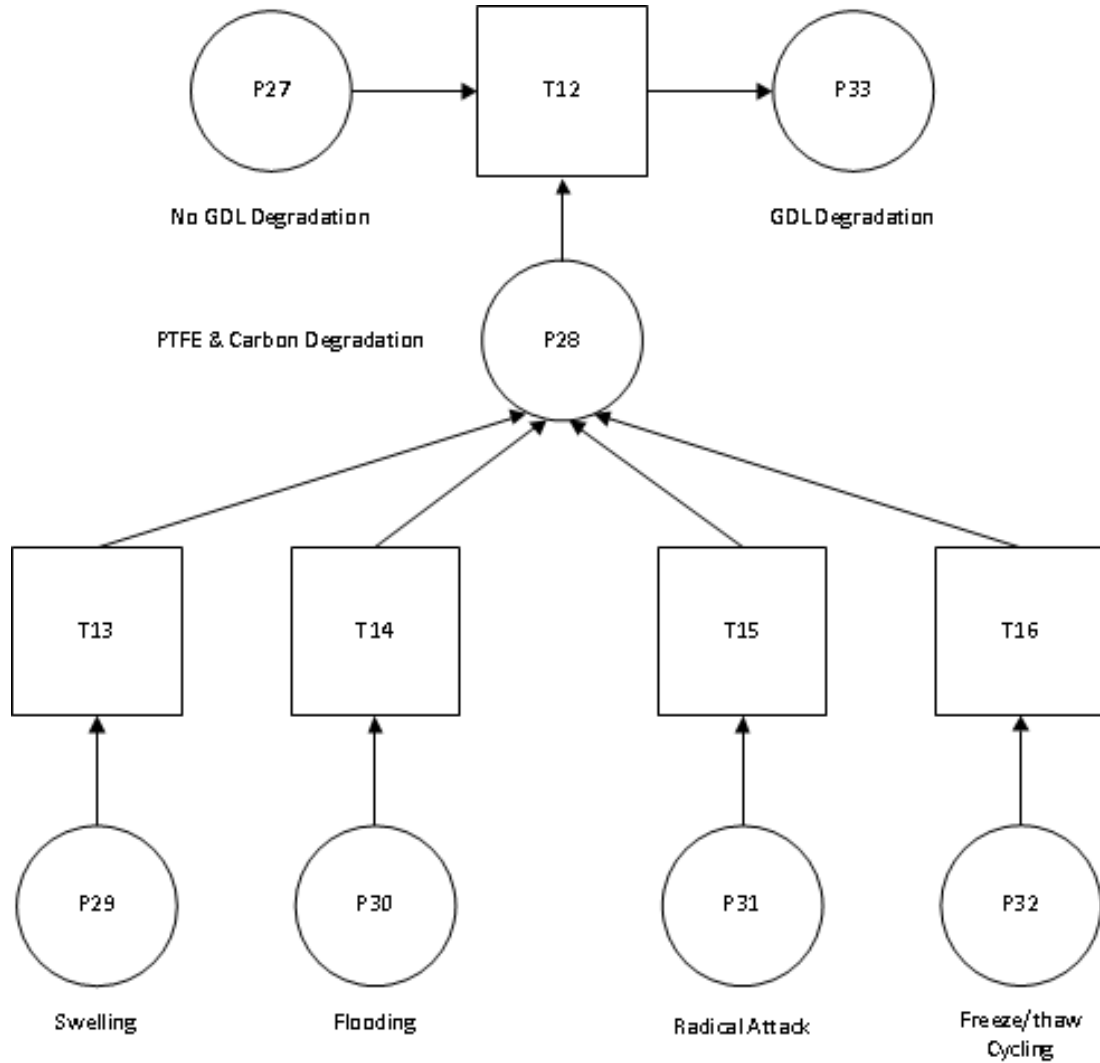


Figure 5.9: Petri-Net module for GDL Degradation

As can be seen in Figure 5.9, both $P29$ and $P30$ enter this module from previous modules. The token that was in $P29$ from the last time-step is now not only directly affecting performance, but is also influencing logic in the GDL Degradation module by becoming an input into $T12$.

The movements of tokens through all of the other Petri-Net modules occur in a similar fashion.

5.4 Derived Rates

There are two aspects of PEMFC operational failure mode analysis that need to be considered: Firstly, the operational condition that causes an initial effect on the system voltage. Secondly, how this operational condition can lead onto the failure modes.

This section presents examples of where the degradation rates are determined from in the literature.

5.4.1 Platinum Agglomeration

As stated in Chapter 3, the catalyst used in FCs is comprised of a Pt ink. During normal operation of a FC, the materials within are subject to strong acidic environments, oxidising conditions, high current loadings and large potential gradients. These difficult conditions mean that degradation to the catalyst itself can occur, specifically in the form of Platinum Agglomeration. The full explanation of the mechanics of Platinum Agglomeration are discussed in Chapter 3.

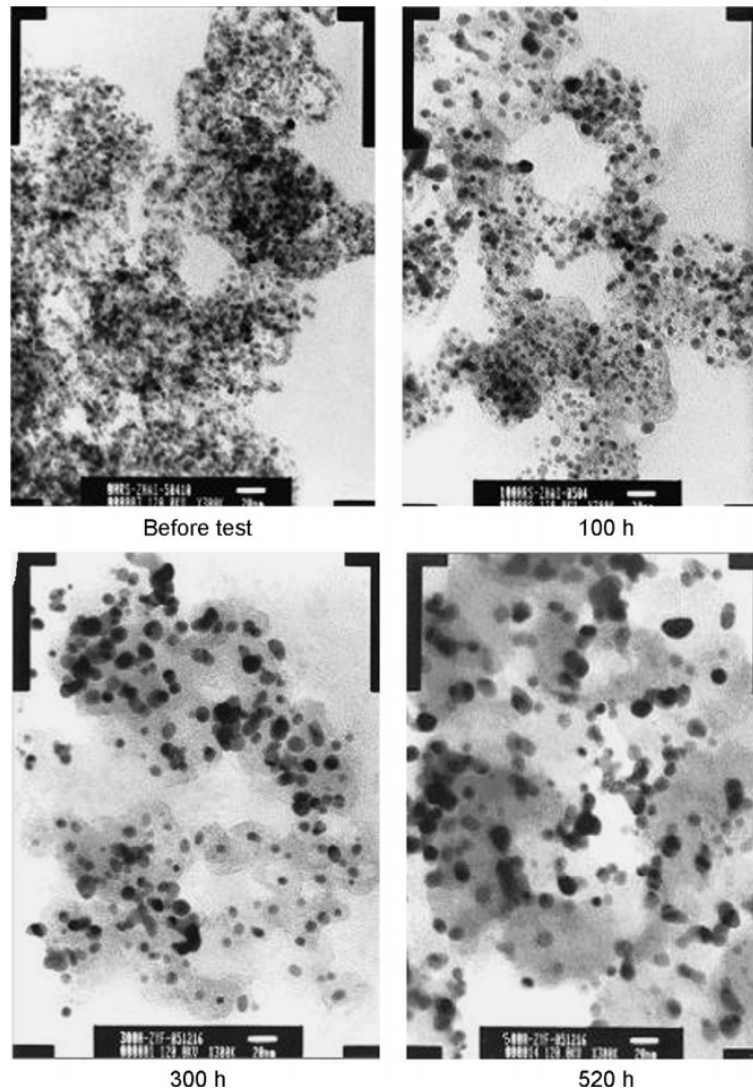
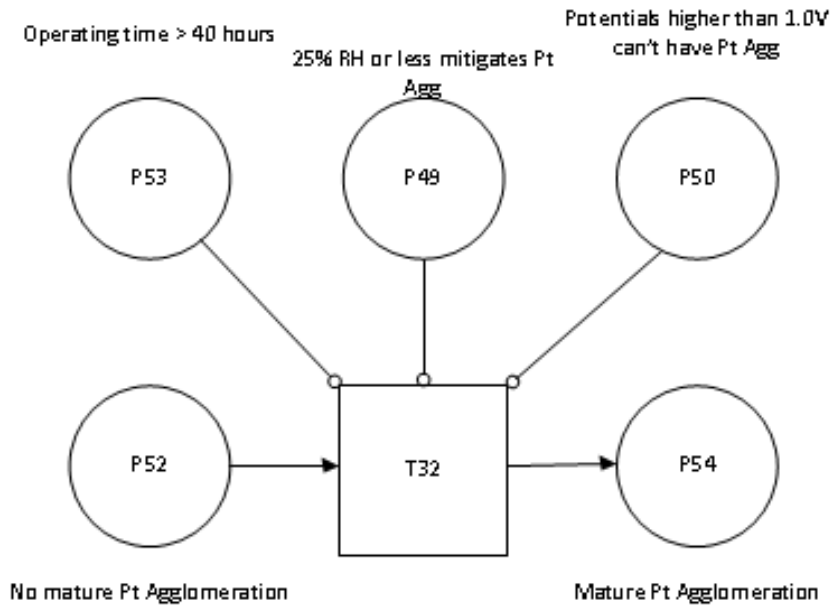


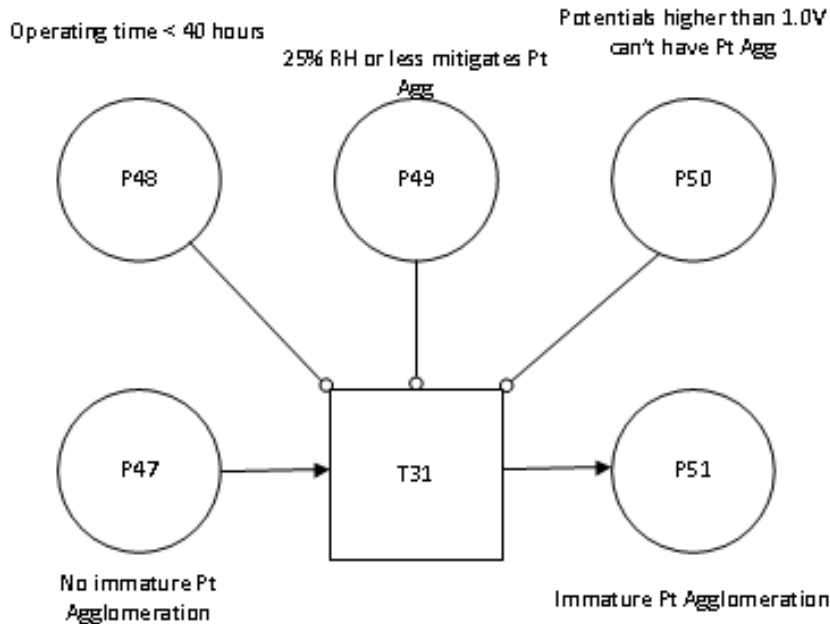
Figure 5.10: Platinum Agglomeration [47]

As can be seen in Figure 5.10, Platinum Agglomeration results in the increase in particle size of the (initial) nano particles, therefore reducing the surface area, and thus reducing the catalytic activity and reaction sites.

The failure logic for the petri-net module for immature and mature platinum agglomeration is presented in Figures 5.11a & 5.11b.



(a) Petri-net for mature platinum agglomeration



(b) Petri-net for immature platinum agglomeration

Figure 5.11: Petri-net modules for immature and mature platinum agglomeration

The inhibitors work by stopping the transition's ability to fire if predetermined conditions are met. *P49* in Figure 5.11 for example, is in an inhibitor related to the RH of the feed gasses going into the FC. If at any point during the running of the model the RH drops below the 25% threshold, Transitions *T32* and *T31* can't fire the token from *P52* and *P47* to *P51* and *P54* respectively. Therefore if a varying RH is experienced as in Figure 5.12, then the degradation will depend on the level of RH.

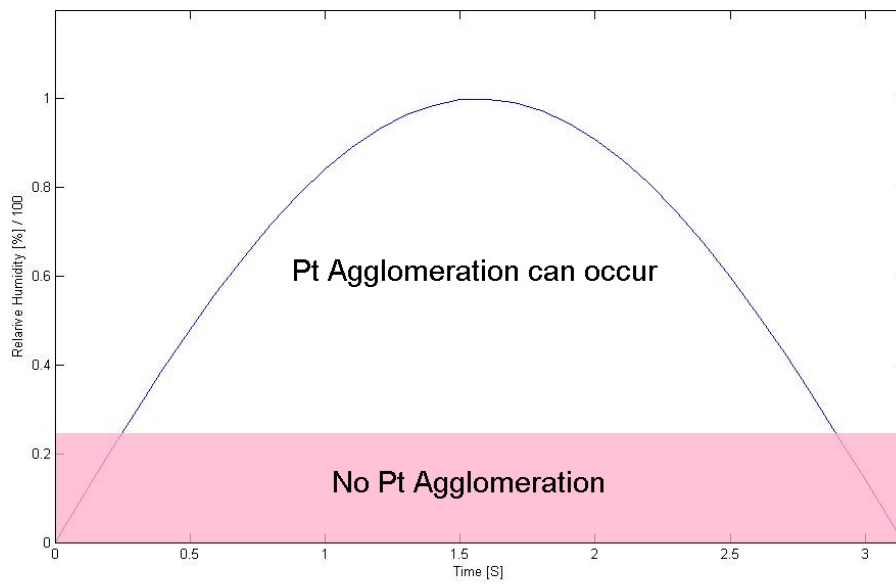


Figure 5.12: Threshold for Pt Agglomeration degradation in relation to RH

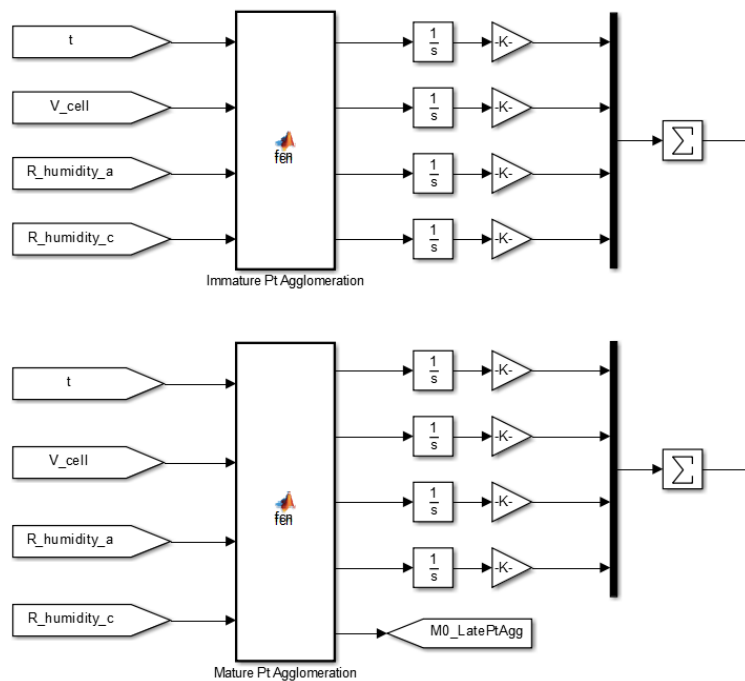


Figure 5.13: Simulink model of Platinum Agglomeration

Experimental work by [60] showed the degradation of FC performance in relation to immature and mature Platinum agglomeration. They found that the rates of particle growth differed when measured from 0-40 hours, and thereafter. The initial 40 hours of operation saw an increase in Pt nanoparticle size from the initial 1.35 nm, to 3.5 nm. However, from that point until 1,784 hours of operation, the particles only grew to a maximum of 3.52 nm. This leads

to differing degradation rates for the first 40 hours of operation (henceforth known as ‘Immature Platinum Agglomeration’), and the lifetime from 40 hours onwards (henceforth known as ‘Mature Platinum Agglomeration’).

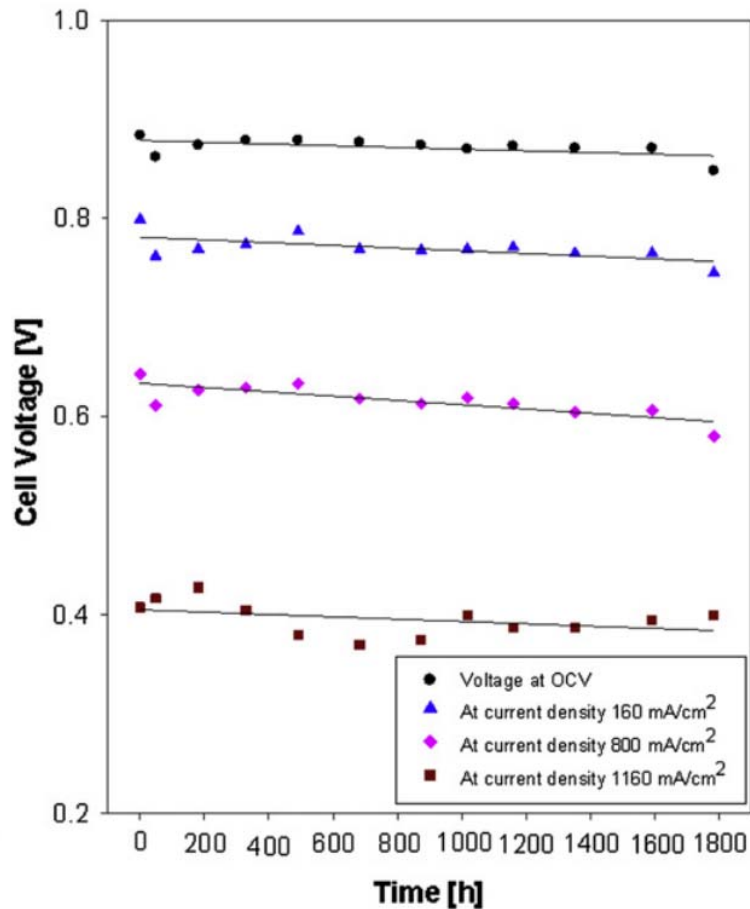


Figure 5.14: Voltage drop data by [60]

The degradation rates were derived from the data presented in Figure 5.14, and applied to the model through a single interaction with overall voltage performance per iteration of the model running. The rate of degradation for the OCV slope was calculated as $2.083 \times 10^{-7} \text{ Vh}^{-1}$, at 160 mA/cm^2 it was 3.472×10^{-7} , at 800 mA/cm^2 it was 2.7×10^{-7} , and at 1160 mA/cm^2 degradation was 6.94×10^{-8} . These degradation rates were then normalised to represent a degradation of voltage per second and in-putted into the four gain blocks of the Simulink simulation in Figure 5.13. The gain blocks are used to multiply a value by a constant, therefore the 1 or 0 exiting the Petri-net module block will either multiply said 1 or 0 by the gain constant which is set as the degradation rate.

5.4.2 Membrane Flooding

The initial drop of voltage due to the operating condition can be derived from data in the current literature regarding PEMFC degradation. Le Canut, et al. [56] performed degradation tests on a Hydrogenics production-type PEMFCs stacks including; membrane drying, membrane flooding and stack poisoning by CO. The data from these studies can be adapted to be used as outputs from the main Petri-Net, to be fed back into the main PEMFC simulation.

To ascertain the degradation in voltage due to flooding, a study by La Canut, et al [56] was analysed.

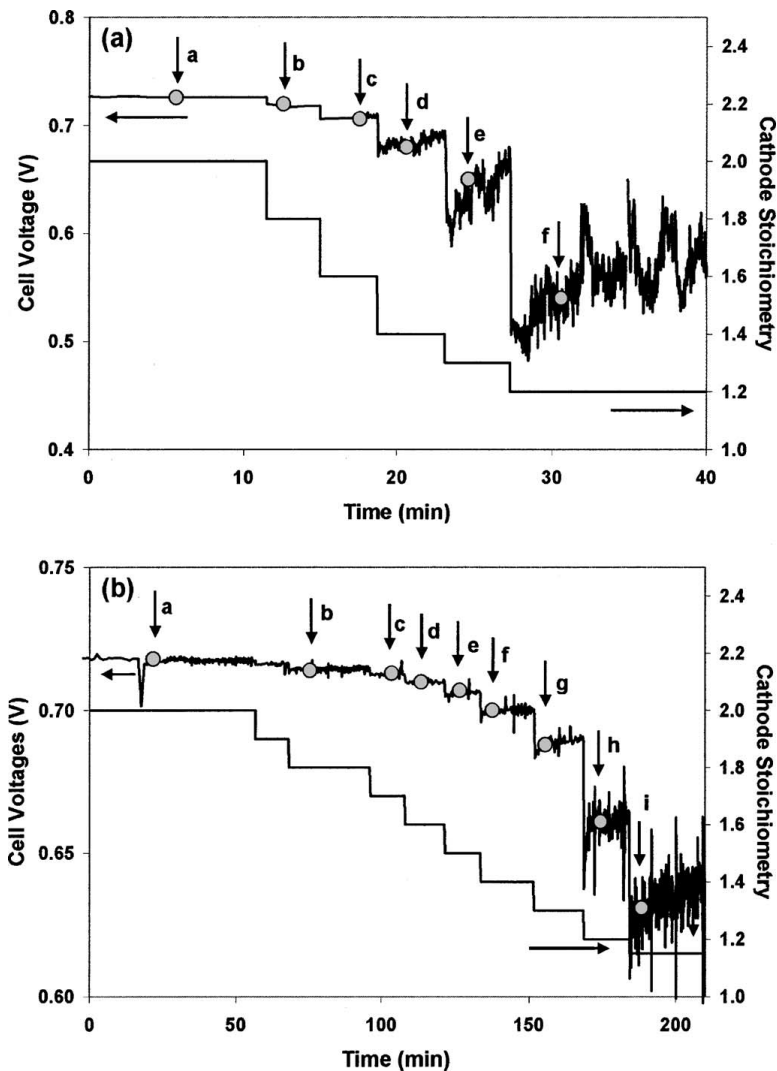


Figure 5.15: PEMFC Membrane flooding degradation test [56]

The flow rate of cathode supply feed was decreased to induce flooding effects in the cell, and produced the results presented in Figure 5.15. Two tests were conducted, and for integrity of results, both test will be considered and averaged for the overall voltage drop due to cell flooding.

In the first test, the initial voltage produced by the cell was 0.72V and dropped to 0.54V, indicating a drop of 0.18V over 27 minutes. This is a rate equal to $6.0 \times 10^{-3} \text{Vmin}^{-1}$, and extrapolated to represent an hourly rate, we observe a voltage degradation rate of 0.4Vh^{-1} .

In the second test, the initial voltage produced by the cell was 0.73V and dropped to 0.63V, indicating a drop of 0.1V over 180 minutes. This is a rate equal to $5.55 \times 10^{-4} \text{Vmin}^{-1}$, and extrapolated to represent an hourly rate, we observe a voltage degradation rate of 0.03Vh^{-1} .

The average of the two rates gives a voltage degradation rate due to flooding, of 0.215Vh^{-1} . Therefore if the output place contains a token it causes a 0.215V decrease in output per time step.

5.4.3 Relative Humidity Variation

RH cycling has been identified as a basic event (See Appendix A) that impacts upon the mechanical strength of the membrane, however there is also a performance drop relative to the RH values in a PEMFC. The model of a PEMFC used in this work uses an empirical relationship of RH in the cell cathode which can show the performance drop due to changes in RH values in the cathode. Figure 5.16 shows the performance model running at 120% RH, and again at 20% RH (dehydrated). There is a noticeable degradation in performance in the lower humidity polarisation curve, and is solely due to the inhibiting effects of low levels of hydration in the membrane. The jump of performance at the higher current range is due to the model not being able to handle less than 0V and errors occurring that wouldn't happen in normal operation of the cell.

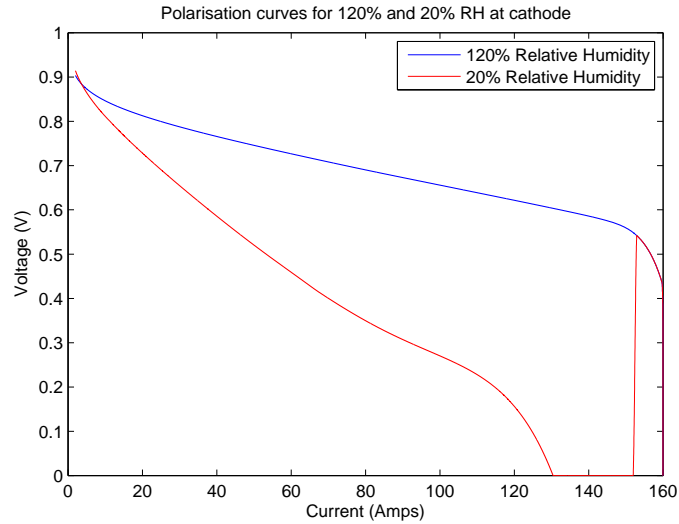


Figure 5.16: Modelled performance drop due to RH drop from 120% to 20%

5.4.4 Hydrogen Peroxide

H_2O_2 degradation is usually studied as far as fluoride release rates are concerned, and the experimental technique is usually the process of boiling a section of the membrane in a H_2O_2 solution to observe fluoride release over time, such as in [44]. This method of testing is valuable to show the effect of H_2O_2 on the membrane itself, however, a degradation rate cannot be attributed to this kind of work. Therefore for an accurate degradation rate to use in the Petri-Net, OCV voltage degradation over time was analysed, where a voltage drop was observed.

Teranishi, et al. [59] observed a drop in voltage over 24 hours of OCV operation. Due to the presence of H_2O_2 and HF in the exhaust gas stream, the authors attributed the drop in performance to the presence of H_2O_2 in the cell, resulting from H_2 gas crossover from the anode.

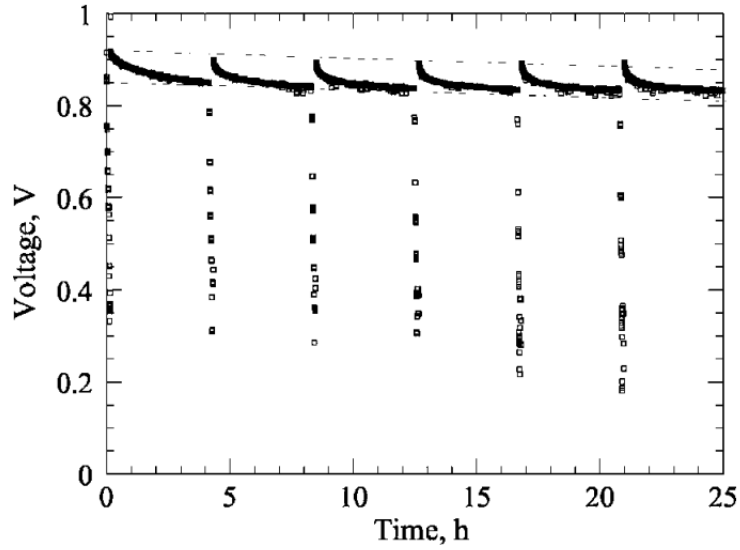


Figure 5.17: Observed voltage drop at OCV due to H_2O_2

The rate observed from the voltage drop in Figure 5.17 is 1.3mVh^{-1} , and is therefore used in the Petri-Net model when the failure mode of H_2O_2 degradation is activated.

5.5 Quantification Data

Not all Petri-Net modules have a degradation rate associated with them as some serve as to input degradation logic into Petri-Nets that do determine degradation. For example, ‘Swelling’ does not have a direct effect on voltage output in this degradation model, however it does feed into other modules that calculate the pressure imparted on the cell, and thus its effect on the voltage drop of the cell.

The Petri-Net modules that do have a direct relationship with voltage drop in the model are listed in Table 5.3, alongside their associated degradation rates and source.

As with the FT work in Section 4, Weibull distributions were used to offer a random variable input into the degradation data. Therefore numerous simulations can be completed to give an estimation of real world degradation levels using flat rate data as the basis.

The Weibull values used for each degradation module are listed in Table 5.4.

Table 5.3: List of Degradation Parameters Used

ID	Failure Mode Parameter	Value (Vs⁻¹)	Ref
FM01	Immature Pt Agglomeration	-	[60]
a	Cell V >0.8	2.083 x 10 ⁻⁷	-
b	Cell V between 0.8 & 0.65	3.472 x 10 ⁻⁷	-
c	Cell V between 0.65 & 0.41	2.7 x 10 ⁻⁷	-
d	Cell V <0.41	6.94 x 10 ⁻⁸	-
FM02	Mature Pt Agglomeration	-	[67]
a	Cell V >0.9	6.23 x 10 ⁻⁹	-
b	Cell V between 0.9 & 0.8	7.79 x 10 ⁻⁹	-
c	Cell V between 0.8 & 0.65	9.34 x 10 ⁻⁹	-
d	Cell V <0.65	1.56 x 10 ⁻⁹	-
FM03	H ₂ O ₂ Peroxide Attack	-	[59]
a	Normal Rate	3.61 x 10 ⁻⁷	-
b	w/Fe+ presence	5.957 x 10 ⁻⁷	-
c	w/ High Gas Crossover	7.22 x 10 ⁻⁷	-
FM04	Radical Attack	3.61 x 10 ⁻⁷	[59]
FM05	Carbon Catalyst Degradation	2.77 x 10 ⁻⁸	Prop.
FM06	Pinholes	1.6 x 10 ⁻⁵	[68]
FM07	Creep	2.77 x 10 ⁻⁸	Prop.
FM08	High Gas Crossover	2.77 x 10 ⁻⁶	Prop.
FM09	Low Gas Crossover	0	Prop.
FM10	Ice Formation	1.3 x 10 ⁻⁴	Prop.
FM11	GDL Degradation	3.33 x 10 ⁻⁴	[69]
FM12	BIP Corrosion	8.796 x 10 ⁻⁷	[70]
FM13	Flooding	5.972 x 10 ⁻⁵	[56]

Table 5.4: Table of Weibull distribution data used

ID	Deg. Rate	Mu (t)	Scale Parameter	Gamma Function	Shape Characteristic
	$\lambda(t)$	$\mu(t)$	η	$\Gamma(\alpha)$	β
FM01a	2.083×10^{-7}	4.800×10^6	4.248×10^6	1.13	0.8
FM01b	3.472×10^{-7}	2.880×10^6	2.549×10^6	1.13	0.8
FM01c	2.7×10^{-7}	3.704×10^6	3.278×10^6	1.13	0.8
FM01d	6.94×10^{-8}	1.441×10^7	1.275×10^7	1.13	0.8
FM02a	6.23×10^{-9}	1.605×10^8	1.420×10^8	1.13	0.8
FM02b	7.79×10^{-9}	1.284×10^8	1.136×10^8	1.13	0.8
FM02c	9.34×10^{-9}	1.071×10^8	9.475×10^7	1.13	0.8
FM02d	1.56×10^{-9}	6.410×10^8	5.673×10^8	1.13	0.8
FM03a	3.61×10^{-7}	2.770×10^6	3.112×10^6	0.89	2
FM03b	5.957×10^{-7}	1.679×10^6	1.886×10^6	0.89	2
FM03c	7.22×10^{-7}	1.385×10^6	1.556×10^6	0.89	2
FM04	3.61×10^{-7}	2.770×10^6	3.112×10^6	0.89	2
FM05	2.77×10^{-8}	3.600×10^7	4.045×10^7	0.89	2
FM06	1.6×10^{-5}	6.25×10^4	7.022×10^4	0.89	2
FM07	2.77×10^{-8}	3.600×10^7	4.045×10^7	0.89	2
FM08	2.77×10^{-6}	3.600×10^5	3.186×10^5	1.13	0.8
FM09	0	0	0	0	0
FM10	1.3×10^{-4}	7.692×10^3	7.692×10^3	1	1
FM11	3.33×10^{-4}	3.003×10^3	3.374×10^3	0.89	2
FM12	8.796×10^{-7}	1.137×10^6	1.277×10^6	0.89	2
FM13	5.972×10^{-5}	1.674×10^4	1.674×10^4	1	1

The Petri-Net was modelled in Simulink software and integrated with the performance model to gain a higher accuracy than assuming voltage or using very basic FC equations. Matlab blocks were used to code the Petri-Net firing and matrices generation. Figure 5.18 shows the Simulink model front for the Petri-Net module ‘Immature Platinum Agglomeration’.

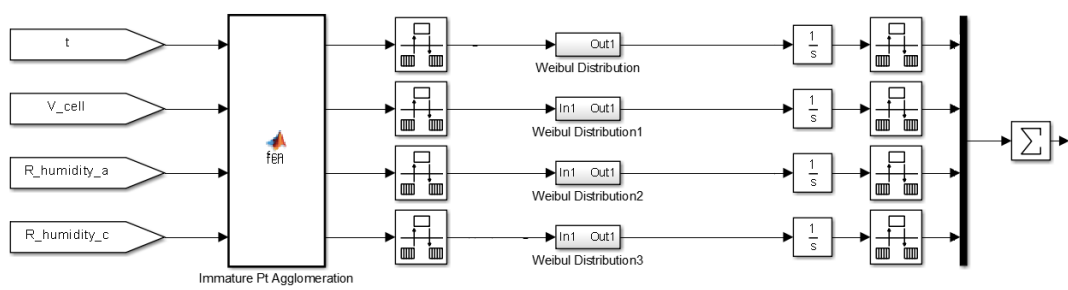


Figure 5.18: Example of Petri-Net in Simulink

Influential data from the performance model is brought in from the left, such as the time ‘ t ’, voltage ‘ V_{cell} ’ and the relative humidities at the anode and cathode ‘ $R_{humidity_a}$ ’ & ‘ $R_{humidity_c}$ ’. The Matlab block contains the Petri-Net coding for the matrices and firing logic, which outputs a ‘1’ or ‘0’ to indicate if there is degradation or not. Therefore if the output place of a module contains a token, a ‘1’ is sent out. This is then smoothed out by a ‘Rate Transition’ block to make sure that either a ‘0’ or ‘1’ is actually being produced. This is because Simulink can sometimes output numbers close to ‘0’ or ‘1’ when indeed you need the full integer. After processing through the rate transition block, the signal is sent to the Weibull distribution block containing the degradation calculations as can be seen in Figure 5.19.

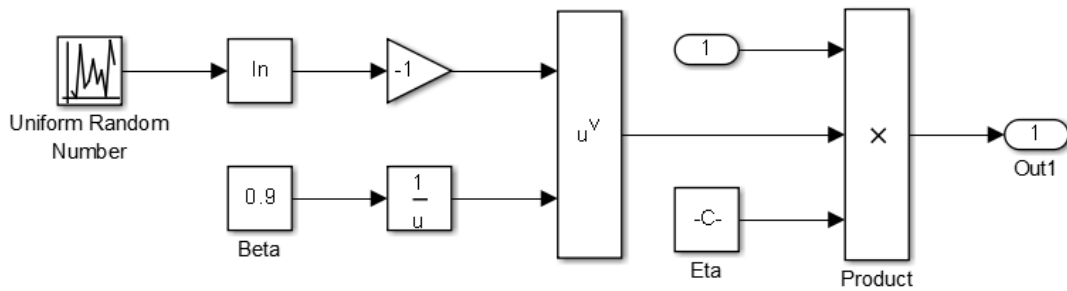


Figure 5.19: Example of Weibull calculation block

Figure 5.19 shows the Simulink block structure for calculating the degradation rate based upon the Weibull distribution. The Weibull equation 4.1 used in Chapter 4.4.2 was modified to give a degradation rate based upon a random variable, rather than a time to failure. The rearranged equation is presented in Equation 5.13.

$$\eta[-\ln(x)]^{\frac{1}{\beta}} \quad (5.13)$$

If a ‘1’ is input, the block processes the Weibull distribution calculation of degradation, if a ‘0’ is input, nothing occurs. Due to the fact that Simulink and Matlab use a predetermined (but very large) data set for their random numbers, the random number generator sets a seed number from that data set that corresponds to the current time in epoch. This ensures that no matter how many times the model is run, a truly random number would be generated. If this method was not used, the random numbers would be the same set of random numbers per simulation run.

The number that leaves the Weibull block is then summed from previous time steps by the ‘Integrator’ block. If this block was not used, the number would reset on every time step and would not represent degradation over time. The number is then restrained from being sent to the overall voltage drop summation by another rate transition block, which makes sure that only one degradation value is sent per time step. The Simulink model can run the FC performance calculation at up to 100 iterations per second, however this block makes sure that only 1 degradation value goes through per second, and not 100. Finally the degradation value is sent to a ‘Mux’ block that sums the entire Petri-Net modules’ values into a voltage drop variable. This can be compared to the degradation threshold value to tell the model when to stop.

Additionally, output data from the degradation modules can feed back into the 1D model to change the performance of the PEMFC being simulated. For example, if a failure mode occurs that would increase the resistance in the membrane in the real world, the output of that failure mode module would output a value of degradation applied to the membrane resistance coefficient value held in the 1D model.

5.6 Integration into Petri-Net Model

The degradation model operates by taking key variables from the 1D model’s output that pertain towards whichever specific failure mode module is being simulated. The data is used to determine the behaviour of the transition firing, effect the rate of degradation, and relay back any changes to the 1D model as an output. Some degradation modules loop back into the 1D model and change operating variables that effect the output voltage.

All of the degradation data ascertained in this section was integrated into the Petri-Net model to form an accurate degradation model. As presented in Figure 5.20, parameters from the performance model that would have an effect on the degradation logic are pulled from the performance Simulink model and fed into the Petri-net degradation blocks (indicated by the ‘Increased Pressure’ MatLab function block). For this example, V_{cell} is the cell voltage, $R_{humidity_a}$ is the relative humidity at the anode, and $R_{humidity_c}$ is the relative humidity at the cathode. Due to the inherent relationship between the humidity in the cell and the pressure in the cell due to swelling (discussed in Section 6.4.1), the variables for that time step from the performance model are drawn upon to get an accurate indication of performance degradation due to swelling.

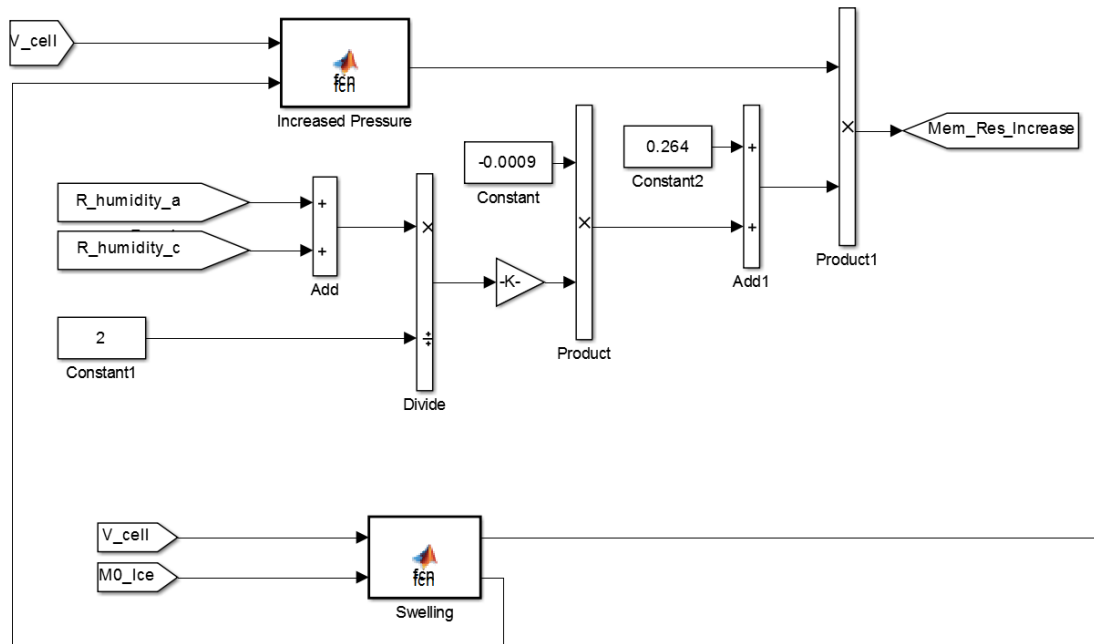


Figure 5.20: Simulink model block of membrane resistance increase due to swelling of the membrane

5.6.1 Informed data generation

Due to the severe lack of data in the field, some degradation rates were proposed from expert opinion and informed prerequisites. For example, there is no available data for how freezing conditions affect cell performance in the literature. As the laboratory facilities could not provide sub-zero operating conditions of our experimental cell/stack, rates had to be proposed from informed backgrounds. During operation of the experimental rig for alternative reasons, a very poor performance was observed when the blockage occurred - peak power reached no more than 5.2W whereas a healthy cell should provide around 52W of power.

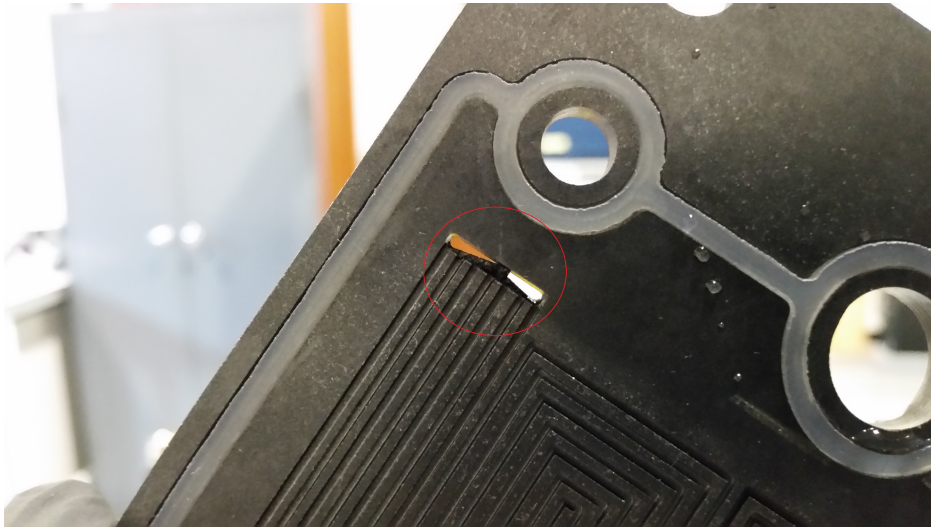
As can be seen in Figure 5.21, a mechanical failure of the graphite BIP material caused the physical blockage of the H_2 from the gas channels on the MEA side of the plate. This blockage was the cause of the drop in performance from 52W peak power, to 5.2W. Under freezing conditions, the gas channels would be subject to blockages given that water was present. Therefore, it was stipulated that a similar drop in performance would be noticed through freezing conditions creating a blockage due to frozen water in the gas channels or distribution manifold. Only under highly humidified conditions would this occur, and only after the cell had been inactive for a period of time. This is because the FC stack would create its own heat during operation, and therefore would struggle to freeze during operation, and would also need water present to freeze. It is therefore assumed that the degradation due to freezing conditions would emulate what was found in Figure 5.21, and is the reason why that drop in performance is used for the freezing degradation failure mode block.

5.7 Petri-Net Conclusions

This section has presented the methodology used in the Petri-Net model, and the logic behind the modules interactions. The total of 20 modules contain the failure logic that has been developed in previous chapters, and created an accurate degradation methodology using Petri-Net modelling techniques. The data used is the most up-to-date available, and is broken down to



(a) Blocked H₂ inlet (plate side)



(b) Blocked H₂ inlet (MEA side)

Figure 5.21: Images showing mechanical failure of BIP material blocking feed gas

the most detailed level possible as such with the varying potential degradation rates of the Platinum Agglomeration modules. Data for the degradation phenomena in each quantifiable module was either taken from in-depth experimental studies, or proposed where not available. The product of the detailed interactions of Petri-Net modules, and highly accurate degradation data, make this model robust.

The model can be run numerous times as to make the most of the Weibull distribution used to ascertain a realistic view of degradation in a FC in the real world. A cumulative average can then be taken of the lifetimes of each simulation run to gain an estimation of FC lifetime when run under specific conditions.

Chapter 6

Experimental Rig & 1D Model Validation

6.1 Introduction

This chapter presents a detailed look at the experimental rig that was built to validate the degradation model described in Chapter 5. Detail regarding the design and capabilities of the rig are discussed, followed by details of MEA characterisation. An MEA was characterised to provide a conditioned MEA, ready to be used in a validation exercise. This MEA was then used under the same operating conditions that were used in a simulation run, as to ascertain whether the 1D model can accurately reproduce the desired outputs that are observed in the real world. Conclusions are then drawn from the experimental work. The validation was required as the 1D model that was used was modified to such a great extent that the existing validation by the authors of the model was redundant.

6.2 Fuel Cell Experimental Rig Development

In order to verify the numerical models (both the 1D FC model and the Petri-net degradation model), a PEMFC experimental rig was built. The experimental rig has the capability to accommodate either a single cell or 7 cell stack as per the schematic in Figure 6.1.

Figure 6.1 from left to right shows the gas panel that serves Air, H₂ and N₂ inlets to the laboratory, and the H₂ and Air outlet valves. Every inlet pipe leading to the test rig has a non-return valve to block any gasses trying to return to the gas panel. To facilitate the choice between H₂ or N₂ going into the mass flow controller on the anode side, two ball valves were installed. The opening of one, and the closing of the other would allow the choice of one of the feed gasses entering the mass flow controller. After the gasses pass through the mass flow controllers, they pass a gas pressure sensor before entering the humidification bottles. Before entering the cell, pressure, temperature and humidity sensors interact with the gas flow. After leaving the cell, the gasses make their way to their associated outlet valves. Individual cell potential voltmeters were used dependent upon the type of test being undertaken.

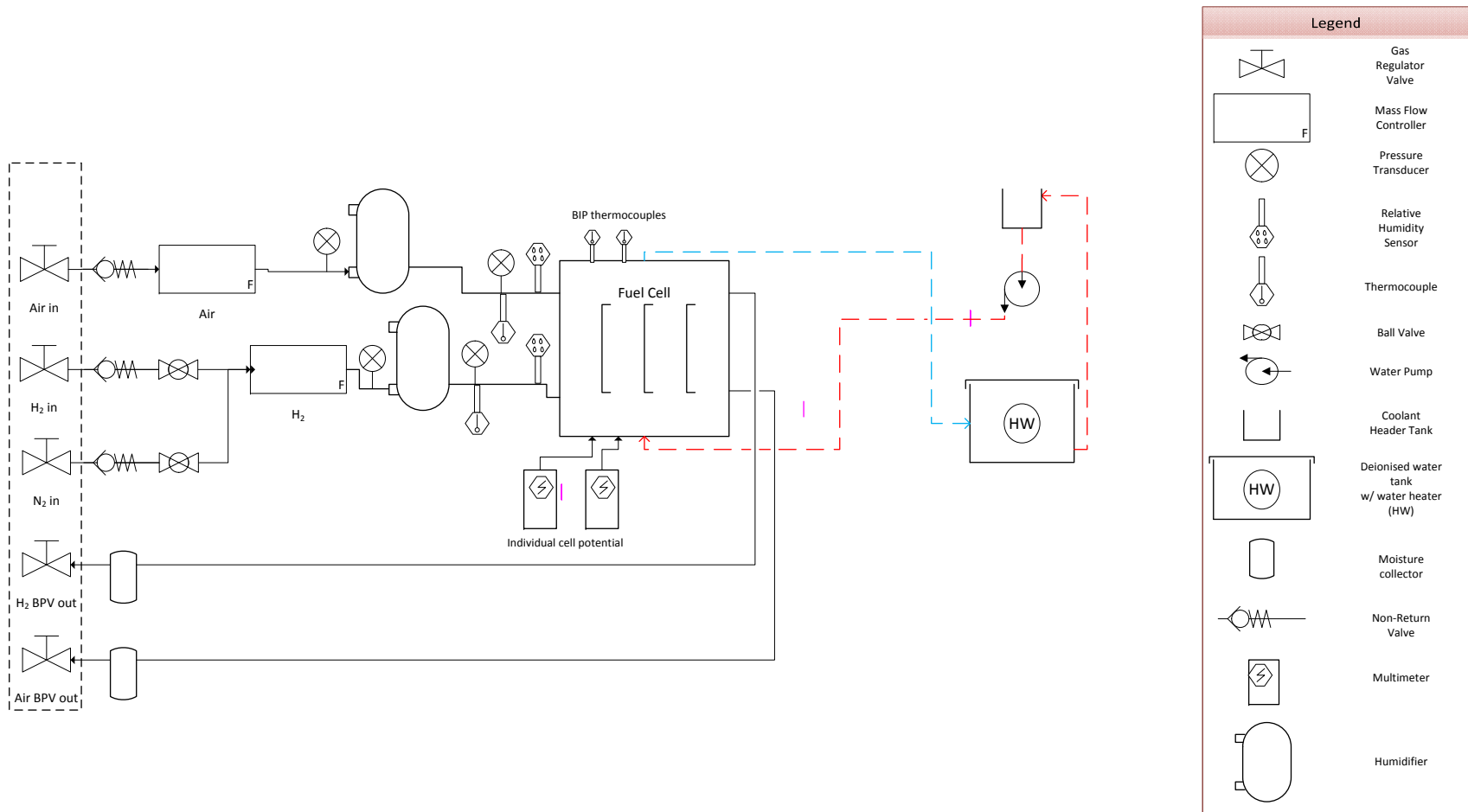


Figure 6.1: Complete test rig schematic

For example, one is used to monitor single cell performance, however two are used for two cells which allows to monitor individual cell potential. For single cell operation, the hot water tank pumps deionised water throughout the cell to bring it to a desired operating temperature.

A PEMFC stack was purchased from Pragma industries (see Figure 6.2), comprising of 7 cells. The cell active area was 100cm^2 providing a nominal power output of 470W.



Figure 6.2: Pragma 7 cell, 470W research development stack

The stack contained pre-made MEAs from the manufacturer of the stack. The membrane was Nafion XL with a thickness of $27.5\mu\text{m}$, sandwiched with a catalyst layer of Platinum ink with a loading of 0.2 mg Pt/cm^2 . Carbon paper type GDL were used to finish the MEA (See Figure 6.3).

The stack is water cooled, or heated, using deionised water sent through a serpentine channel in between each cell in the stack, as in Figure 6.4.

The gas flow field plates were of a square serpentine configuration as shown in Figure 6.5.

H_2 was sourced from a 350 bar gas bottle, and was 99.99999% pure hydrogen as per the international standard [38]. Air was used as the cathode feed gas, sent from an air compressor with filters for oil and water. Both gases were regulated through Hastings mass flow controllers, to accurately control the flow rates of the gas entering the stack at any time.

The gasses were humidified through Nafion tube, bubbler type humidifiers, and were specified to humidify the feed gases at the range of flow rates to be used. Dry gas is passed through the bottle which is filled with grade 1 deionised water. The gas then picks up moisture and is passed through a heated tube section before entering the cell/stack. Temperature was controlled both at the bottle and the heated length of tube. Modifying these two temperatures means that a level relative humidity can be obtained for experimentation.

An electronic load bank was used to 'waste' the energy developed by the stack and log/display the energy use in real time. A TDI Power Systems load bank was used, with a range of 0-150A and 0-800W, as shown in Figure 6.6.

The gas leaving the humidifiers was passed through a custom manufactured humidification sensor T-piece, as seen in Figure 6.7. These sensors measure the humidity levels in the gas stream before entering the stack.

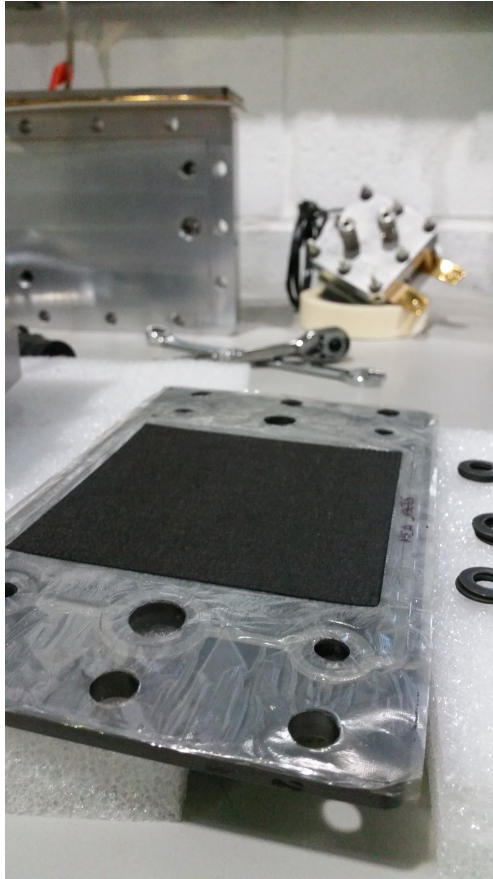


Figure 6.3: MEA assembly

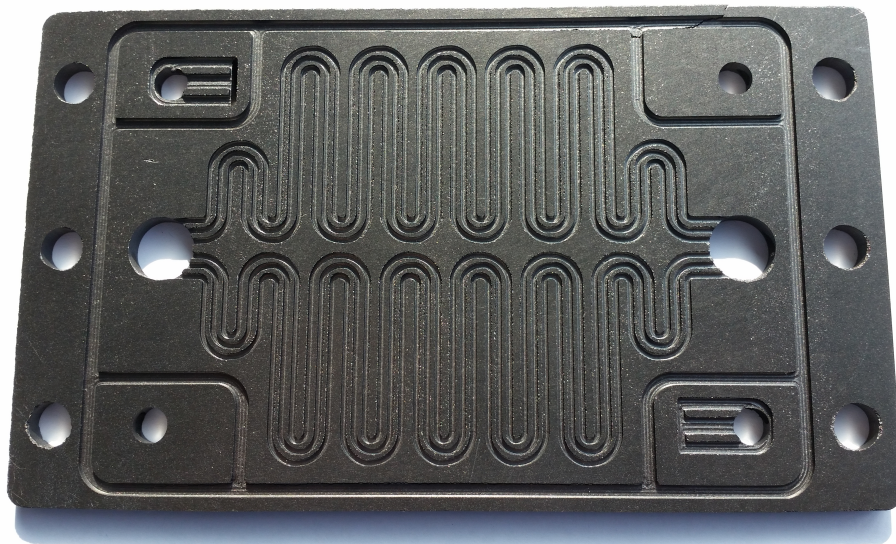


Figure 6.4: Coolant channels in between each cell

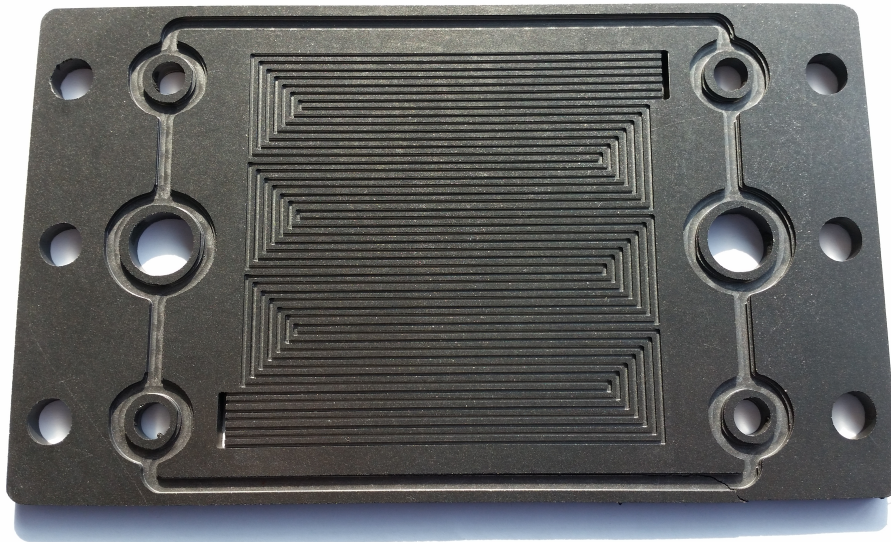


Figure 6.5: Gas channels in between each cell

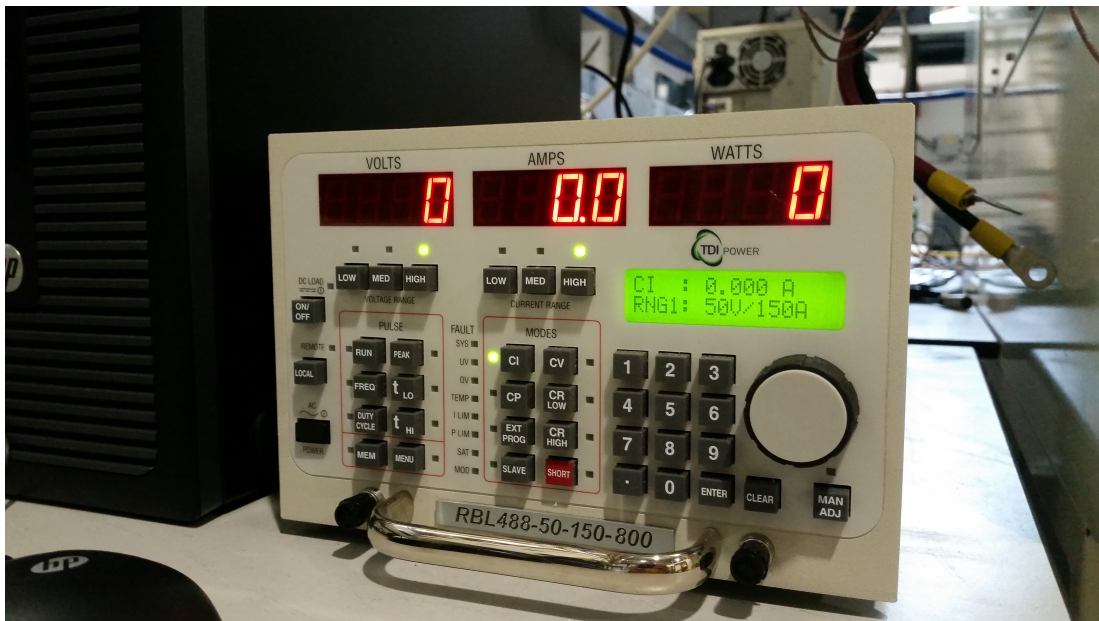


Figure 6.6: TDI Power load bank



Figure 6.7: Humidity sensor T-piece detail



Figure 6.8: Complete test rig

Two set-ups for heating or cooling the stack were built. If the test rig was using a stack, the heat that the stack would produce during operation would require the use of a cooling system. Therefore the water flowing through the stack is passed through an oil cooler type radiator with a funnel cowling exhausting the warm air up into a fume cupboard (see Figure 6.9) with the help of dual 15cm electric fans. A thermocouple is used on the coolant exit from the stack to monitor stack temperature.

If the rig is used for only a single cell, the cell cannot create enough heat to operate at the required temperature, and therefore cell heating is used. A heating element in the header tank

heats the ‘coolant’ water to the desired temperature for the cell, and is pumped through the system, creating heat.

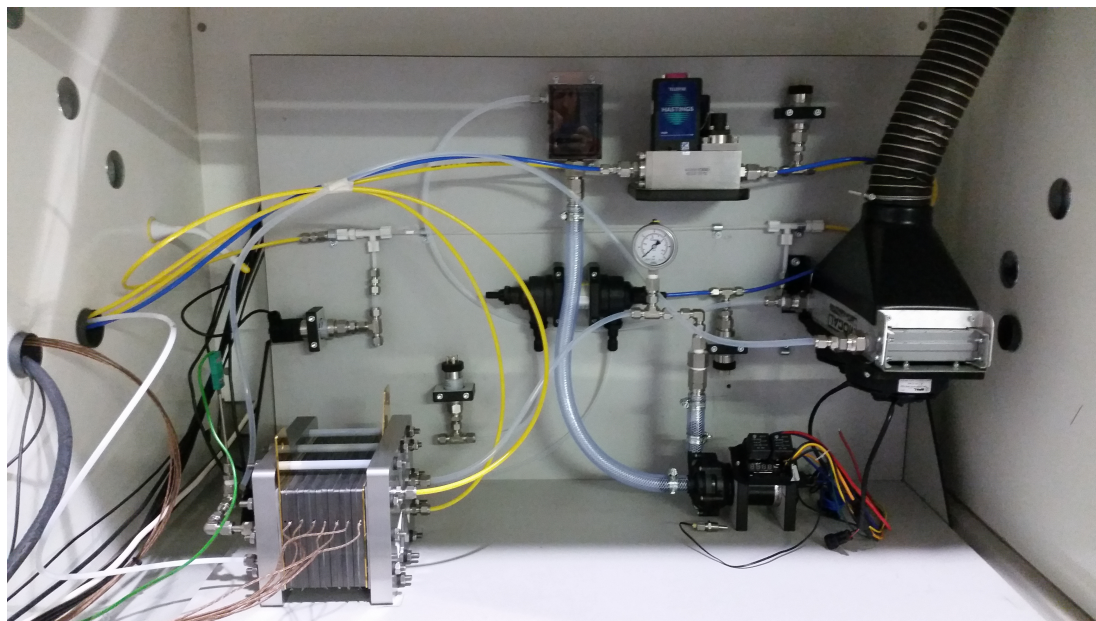


Figure 6.9: Stack cooling system

The finished single cell test rig is presented in Figure 6.8 and shows all contributing components in the fume cupboard, which is used for leak extraction.

A fuel cell monitoring software package was created to monitor fuel cell parameters in real time, and log these variables for data analysis at a later date (see Figure 6.10). The software was built in LabView, and uses data logging equipment supplied by National Instruments. The data logged is shown in Table 6.1.

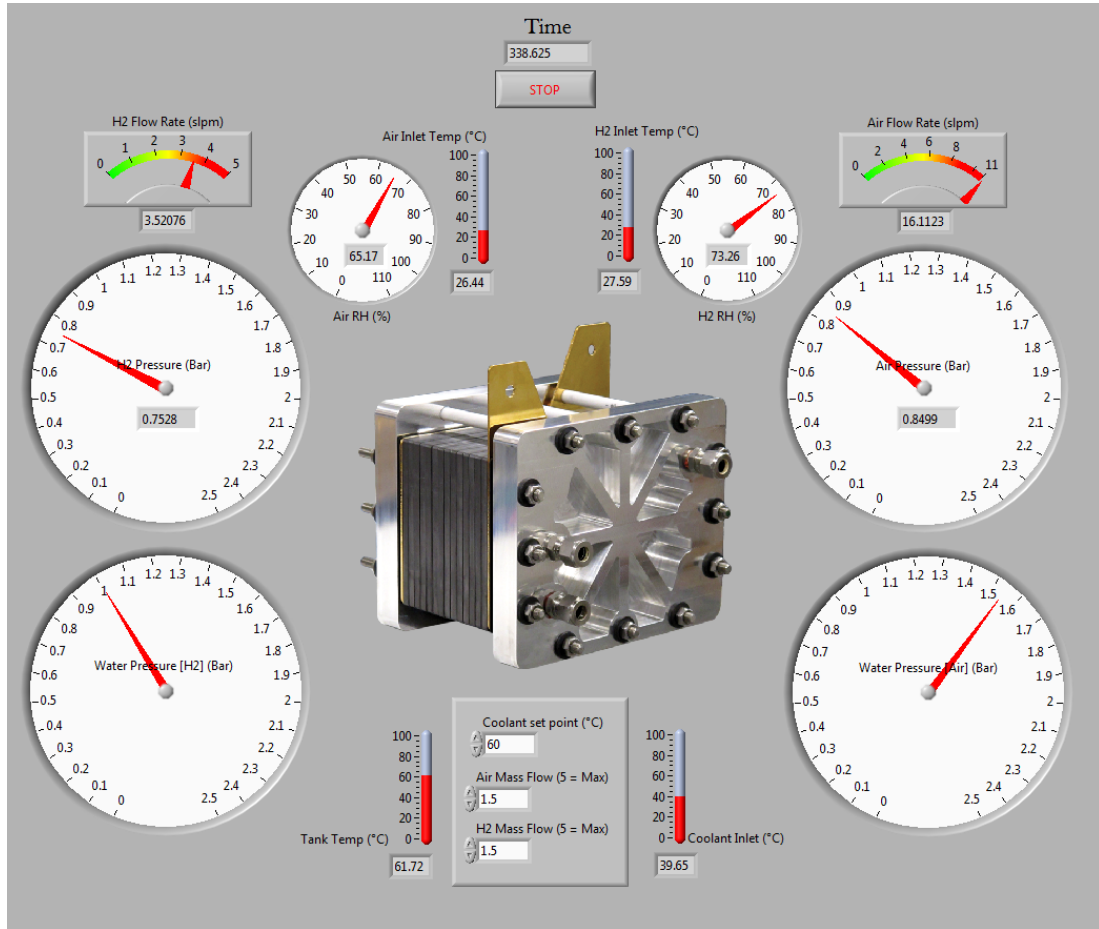


Figure 6.10: Front end of the software developed for the fuel cell test rig

The desired flow rates for the gasses into the cell can be chosen by entering the flow rate into the central control block seen below the fuel cell image in Figure 6.10. This sends a signal of between 0 and 5 Volts to the mass flow controllers to meter gas flow to the rig. The exact value of the flow rate is displayed and logged to file four times per second. The gas pressure is measured before it enters the humidification bubblers as to make sure that the upper limits of the humidifiers are not exceeded during operation. The gas pressure, temperature and humidity is displayed and logged before it enters the cell. The cell temperature is set by the heated water tank and pump system. This is done by entering the value the operator desires into the central control box located under the fuel cell image. This sends a signal to a heating element that uses simple logic to turn off when a target temperature is met. To increase the accuracy of this system, a thermocouple is located at the cell inlet to accurately turn off the heater tank when the temperature set point is achieved.

All gauges and indicators were verified by external calibration of each instrument used.

6.3 Characterisation of MEA

The rig developed was used to characterise a MEA. As is normal with unused MEAs, they must be used in a specific way to bring the MEA up to its optimum performance before use. This process is the initial bedding in of the key layers of the MEA such as the CL. Common practise among the fuel cell community is to run the new MEA at a steady state for around one to two hours (as to let the membrane fully hydrate), then run groups of polarisation curves at

Table 6.1: Table of parameters logged

Parameter	Unit
Time	Seconds
Relative Humidity @ anode inlet	%
Relative Humidity @ cathode inlet	%
Anode pressure before humidifier	bar
Anode pressure before cell	bar
Cathode pressure before humidifier	bar
Cathode pressure before cell	bar
Ambient temperature	$^{\circ}C$
Cell temp 1 - 7	$^{\circ}C$
Anode mass flow rate	slpm
Cathode mass flow rate	slpm
Cathode gas temperature (inlet)	$^{\circ}C$
Anode gas temperature (inlet)	$^{\circ}C$
Coolant temperature	$^{\circ}C$
Heater tank temperature	$^{\circ}C$
Set Point Anode mass flow rate	slpm
Set Point Cathode mass flow rate	slpm
Set Point heater tank temperature	$^{\circ}C$

regular intervals as to cycle the MEA through its full current range. Once the cell has reached an equilibrium at its highest current range, the MEA is considered conditioned.

After a full conditioning run (required before each use), an MEA was characterised using polarisation curve and EIS techniques to form a comparison baseline for degradation testing. EIS is an experimental technique where the different loss mechanisms observed in a fuel cell can be quantified. It is a non-intrusive technique that doesn't degrade the cell whereas techniques such as Cyclic Voltammetry (CV) would. During operation of the cell, AC potential is applied through the fuel cell and the current through the cell is measured. The resulting data is often displayed via a Nyquist plot similar to Figure 6.11.

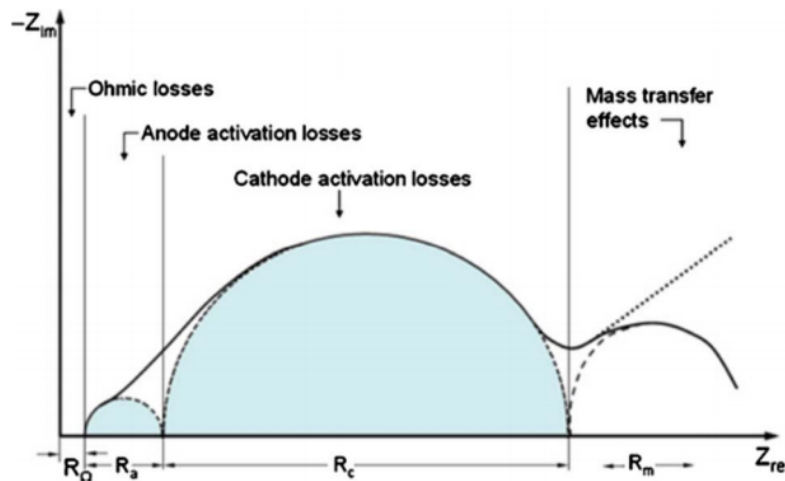


Figure 6.11: EIS Nyquist plot interpretation [71]

As can be seen in Figure 6.11, the three main potential loss areas can be observed through

the use of EIS techniques. This tool was used to increase the confidence in certain failure mode's affects on certain regions of the potential losses. EIS techniques are ran in either galvanostatic or potentiostatic conditions (current held, or voltage/potential held respectively).

For the conditioning runs, the MEA was run for one hour, then at 30 minute intervals after that point, polarisation curves were run in sets of 5 in order to ascertain the health of the cell. Galvanostatic EIS was also undertaken at low, medium and high current densities (0.2, 0.4 and 0.6 A/cm² respectively). This technique was repeated until the MEA showed no more signs of improvement. At this stage, the MEA was considered to be characterised in its highest performance.

The test was run with feed gas pressures of 0.55 bar, the temperatures of the gas feeds at around 30°C, and the cell temperature kept at 39°C as in Figures 6.12 & 6.13. The cell temperature was kept higher than the gas feeds as to avoid the flooding of the cell due to condensation occurring in the cell when a higher temperature gas meets a lower temperature environment.

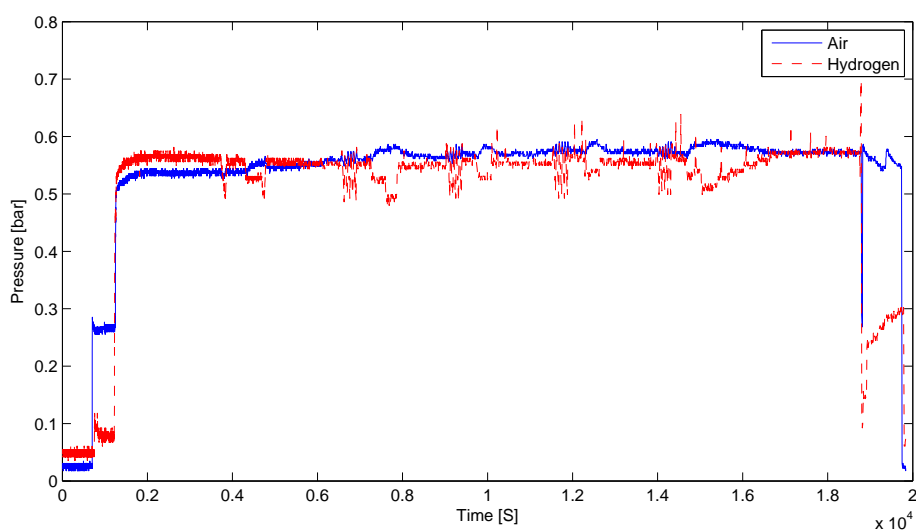


Figure 6.12: Gas feed pressures

The variation in H₂ gas pressure in Figure 6.12 is due to other lab users demanding H₂ from the same bottle being used during the experiment. The variation is negligible at around 0.05 bar, and therefore won't affect the results of the validation. The final variations in pressures are experienced during the shut-down of the rig, and are after the FC was operated.

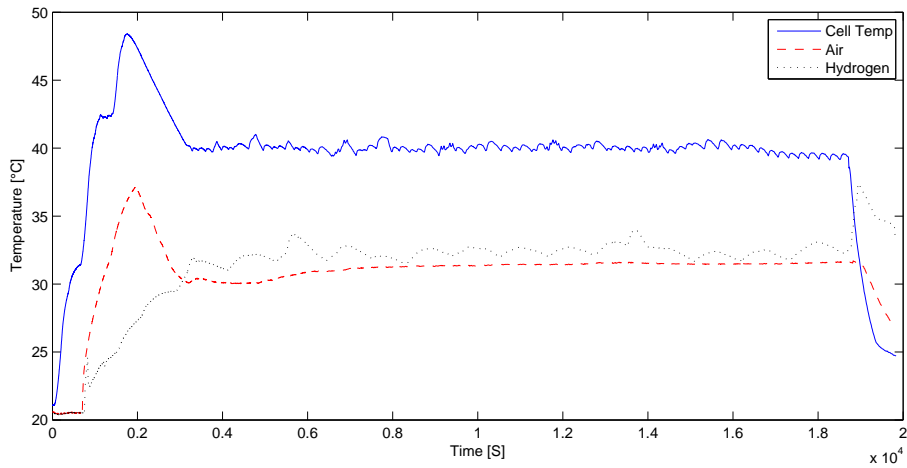


Figure 6.13: Cell and gas feed temperatures

The initial spike in temperature seen in Figure 6.13 is due to the transient response delay of the system control, where the heating element overshoots their target, then returned to the set-point. This will not have an impact upon results as the testing is only commenced when all operating parameters has reached their desired values.

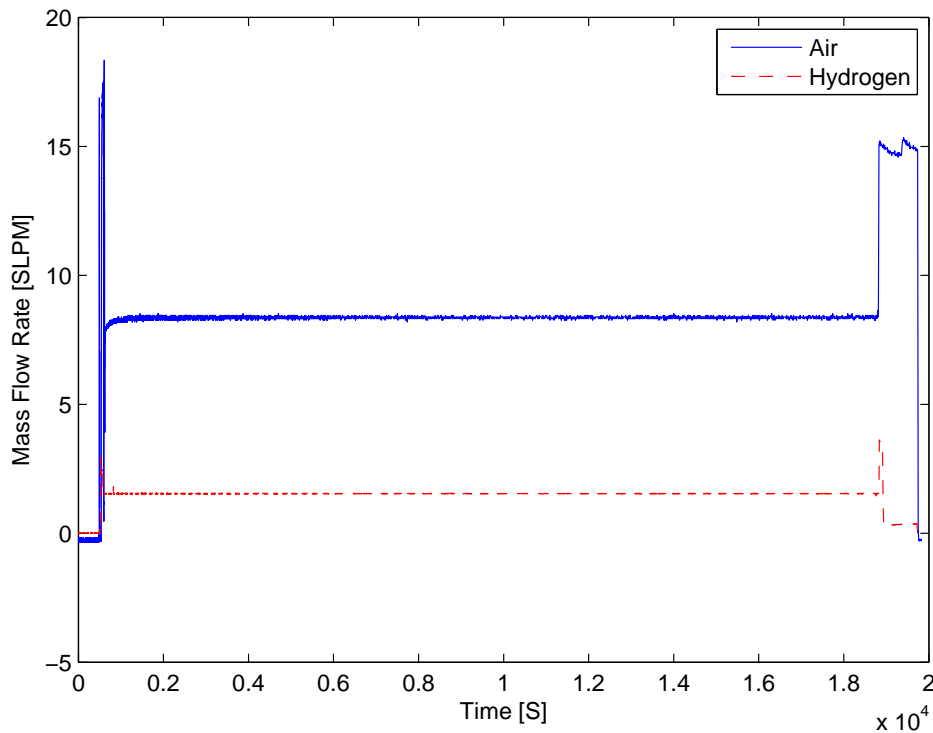


Figure 6.14: Feed gas flow rates

Gas feed flow rates were kept at a hydrogen stoichiometry of 1.2 and air stoichiometry of around 2.5. The flow rates for the experimentation run can be seen in Figure 6.14. The first

spike in flow rate is due to the N_2 purge at the beginning of the cell operation, and the final spike at around 1.9×10^4 seconds is due to the shut-down N_2 purge as is expected.

Relative humidities were set at 70%, however due to the nature of the bubbler type humidifier system, an error of $\pm 5\%$ was found in the air supply, and an error of $\pm 10\%$ was found for the H_2 humidifier during operation. As can be seen at 1.4×10^4 seconds in Figure 6.15, the hydrogen feed RH sensor experienced a flooding event, and became unreliable. However, the values from this point are assumed to be the same as what was experienced previous to the flooding event at around 70%. This assumption can be made when analysing the data from 0.7×10^4 seconds to 1.3×10^4 seconds. Here it can be assumed that (as with the Air feed) the RH measurements were levelling out after the initial fluctuations of transient response delay experienced from 0 seconds to 0.7×10^4 . Therefore, from a visual analysis of the Figure, it is assumed that the RH levels would carry on to repeat what was seen from 0.7×10^4 seconds to 1.3×10^4 seconds.

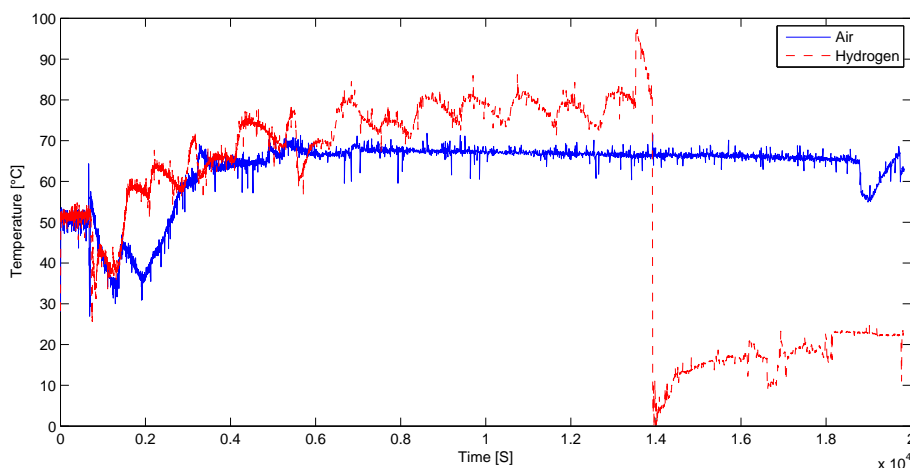


Figure 6.15: Feed gas relative humidities

Once steady state had been reached with the operational variables, the characterisation commenced. Cell potential was maintained at 0.65V in order to avoid degradation as much as was practicable (see Figure 6.16).

Figure 6.16 shows the voltage and current profile over time for the conditioning run of the MEA. Once all of the ancillary equipment was up to pressure and temperature, the H_2 supply was passed through the cell. As soon as the chemical reactions began, the voltage of the cell was set to 0.65V as is common practice with MEA conditioning. After 3600 seconds the cell was temporarily cycled to its maximum current capability to ascertain the performance of the cell. It was assumed at this stage that the cell needed a little longer to hydrate before the full polarisation runs were to be started. At 0.5×10^4 seconds the first set of polarisation runs were started. The green line shows how the voltage of the cell starts at its highest (OCV), then as the current is increased per time-step, it drops to its lowest value. The blue line shows how the current starts at 0, and is increased per time-step to its highest value before the cell voltage gets to its saturation limit. The five peaks in the green line indicates that the polarisation runs were completed five times per polarisation run.

This process was repeated three more times as can be seen by the profiles in Figure 6.16, until equilibrium was reached and the MEA was deemed conditioned. The process of closing down the test rig saw the slow drop off of the current as to not shock the newly conditioned MEA until the cell was no longer producing current, then the rig was purged and shut down.

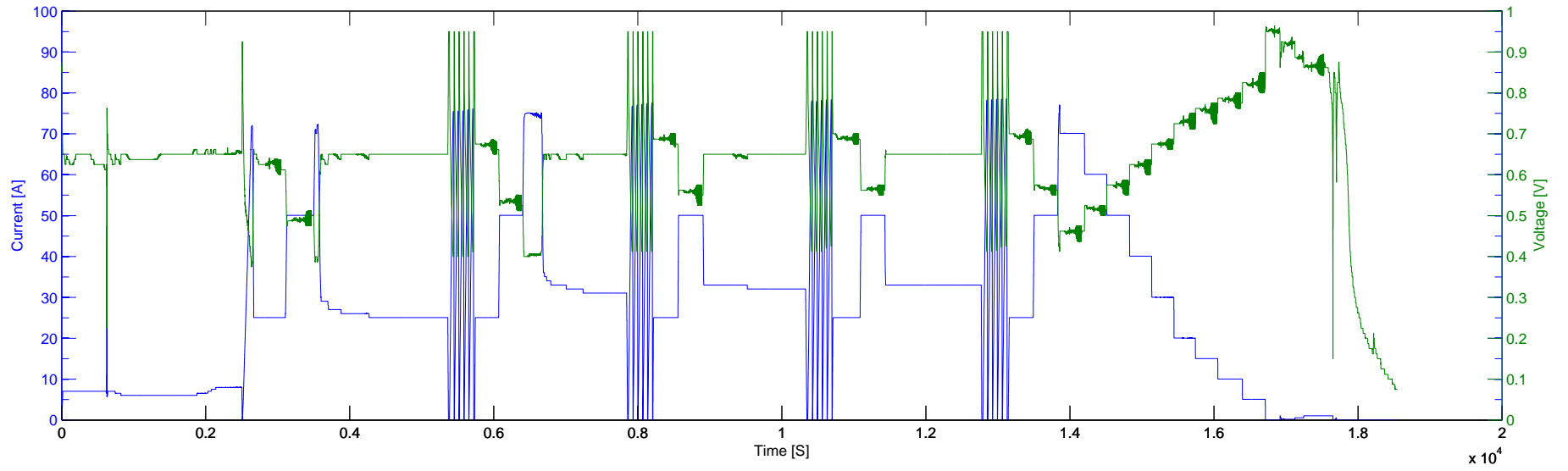


Figure 6.16: Current and Voltage profile throughout test

The tail off of the green voltage profile at the very end of the test is due to the N₂ purge replacing all of the fuel H₂ in the cell during the purge, and therefore the OCV dropping to low levels until the operator is sure that there is no more H₂ in the system.

The overall operating parameters throughout the characterisation are listed in Table 6.2:

Table 6.2: Table of fuel cell operational parameters

Parameter	Value	Unit
Relative Humidity	70 ±5	%
Pressure	0.55	bar
Flow Rate H ₂	1.5	slpm
Flow Rate Air	8.5	slpm
H ₂ Temp	31	Celsius
Air Temp	30.5	Celsius
Cell Temp	39	Celsius

The RH, pressure and flow rates were all desired values that are commonly used in the FC community. However, the temperatures were the maximum values available from the FC rig. All three temperatures would ideally need to be at 70-80 °C.

The averages of each of the sets of five polarisation curves were taken and plotted on the same figure in order to ascertain the health of the cell, see Figure 6.17.

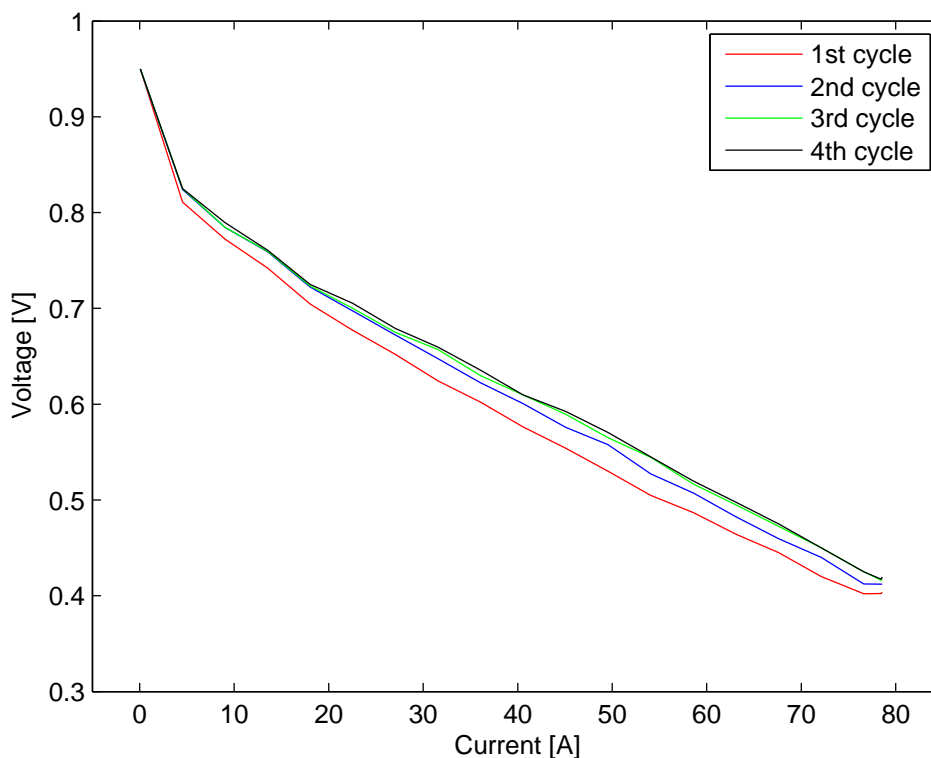


Figure 6.17: Polarisation curve averages for each set of tests

It can be seen that after the 3rd set of polarisation curves, an equilibrium state was achieved, and the health of the cell could be assumed to be optimum. We can see that the polarisation

curves start to correlate quite positively after 3 cycles. A visual indication of an equilibrium of performance is all that is needed to signify an activated MEA.

6.4 Validation of the model

After the MEA was characterised and assumed to be at its peak operating condition, the fuel cell was run for a final polarisation curve. The operating conditions experienced during the experimental polarisation test were input into the performance fuel cell model, and the simulation results were plotted against the experimental (see Figure 6.18). This was done to show how accurate the 1D model replicated what was found during the experimentation on the test rig. If the values correlate on a plot, the 1D model is validated against the test rig.

The fuel cell was run using the previously identified parameters for one polarisation curve. The 1D model with the Petri-net degradation model was then run for one polarisation curve with a broad sweep from low to high current density. The input data for the 1D model was that of the data logged during the polarisation curve on the test rig. The results are presented in Figure 6.18.

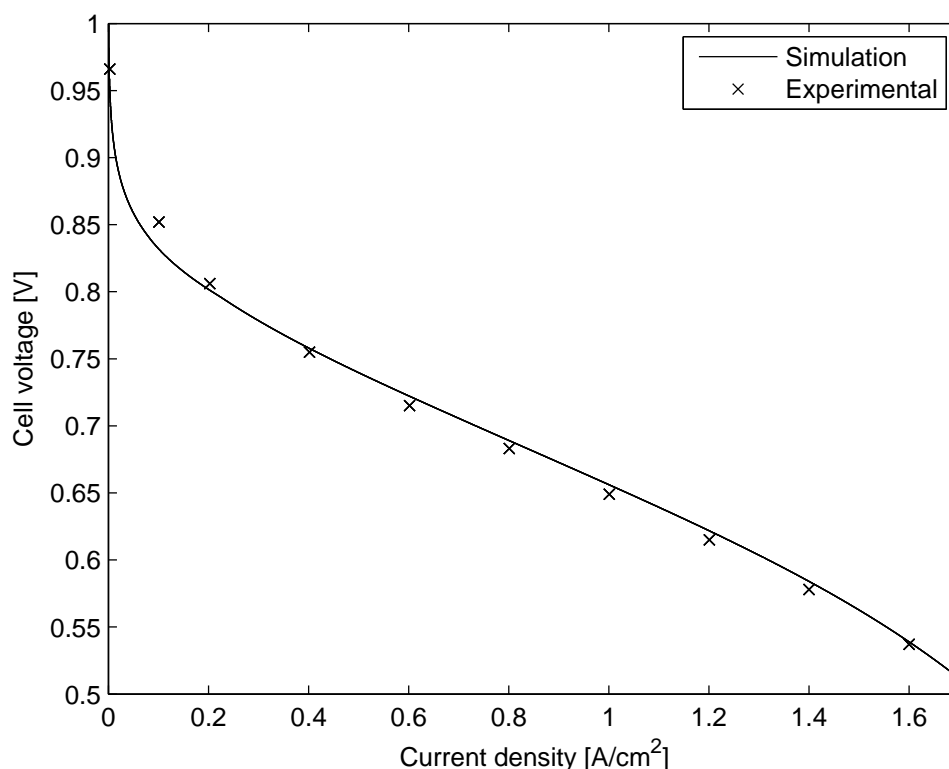


Figure 6.18: Comparison of modelled system performance, and experimental data

As can be seen, the agreement is good and therefore justifies the use of this 1D performance model in the degradation modelling through the Petri-Net analysis. It also shows that one can be confident that any manipulation of operational parameters to the 1D model as a result of degradation modelled by the degradation Petri-Net are robust and justified. This is to say that if the Petri-Net model determines that a certain parameter of the 1D model should be modified to represent degradation (cell resistance for example), one can be sure that this change of variable will have an accurate effect on the performance output of the cell.

6.4.1 Experimental Data

Due to the lack of data currently available for fuel cell degradation and reliability analysis, key failure modes that currently have no data readily available in the literature were studied using the developed experimental set-up.

One of the failure modes that is mentioned numerous times throughout the literature is the issue surrounding BIP torque. However, no data was found in the literature that shows how changes in BIP torque affect the performance of the cell, and as such, is one of the failure modes where experimentation was undertaken.

Experimentation of how BIP Torque affects fuel cell performance

The fuel cell provided by Pragma industries had an associated specification sheet that showed the compression pressure felt in the cell due to a corresponding endplate torque (see Figure 6.19).

Pressure	MPa - N/mm ²	0,1	0,2	0,3	0,4	0,5
	Bar	1	2	3	4	5
	Psi	15	29	44	58	73
Torque	N.m	1,8	2,1	2,3	2,6	2,8

Pressure	MPa - N/mm ²	0,6	0,7	0,8	0,9	1,0
	Bar	6	7	8	9	10
	Psi	87	102	116	131	145
Torque	N.m	3,1	3,3	3,6	3,8	4,1

Pressure	MPa - N/mm ²	1,1	1,2	1,3	1,4	1,5
	Bar	11	12	13	14	15
	Psi	160	174	189	203	218
Torque	N.m	4,3	4,6	4,8	5,1	5,3

Pressure	MPa - N/mm ²	1,6	1,7	1,8	1,9	2,0
	Bar	16	17	18	19	20
	Psi	232	247	261	276	290
Torque	N.m	5,6	5,8	6,1	6,3	6,6

Pressure	MPa - N/mm ²	2,1	2,2	2,3	2,4	2,5
	Bar	21	22	23	24	25
	Psi	305	319	334	348	363
Torque	N.m	6,8	7,1	7,3	7,6	7,8

Pressure	MPa - N/mm ²	2,6	2,7	2,8	2,9	3,0
	Bar	26	27	28	29	30
	Psi	377	392	406	421	435
Torque	N.m	8,1	8,3	8,6	8,8	9,1

Figure 6.19: Look-up table of endplate bolt torques against MEA pressure [72]

However, there was no information available that shows how a change in pressure affects the

performance of the cell in general. Due to this lack of data, a set of experiments was undertaken to fill the knowledge gap, and use the data gained to inform the degradation model.

Polarisation curves were performed in-between tightening the endplate bolts from 2.5 Nm to 6.5 Nm in 1 Nm increments, and are shown in Figure 6.20.

As can be seen in Figure 6.20, from the initial endplate torque of 2.5 Nm, fuel cell performance increased with torque. This corresponds to an initial pressure on the MEA of around 0.4 MPa, and a final MEA compression pressure of around 2.0 MPa.

The MEAs used were unused and unconditioned, and as such, a large increase in performance was seen from initial to final torque levels due to the initial compression of the components of the MEA. When a new MEA is created, there is a large resistance involved due to the lack of interfacial contact between the core components. When the fuel cell is tightened as in this experiment, the contact patch is increased as the GDL material is crushed between the membrane and the BIPs. Interfacial contact resistance is therefore reduced through the increased endplate bolt torque.

After a period of conditioning of the new MEA, the fuel cell was stopped and the endplate bolts torques reduced back to the initial 2.5 Nm. The polarisation curves were then performed using the same torque levels up until 5.5 Nm as 6.5 Nm was at the very upper limit of the BIP's mechanical integrity and as such was avoided. These results are shown in Figure 6.21.

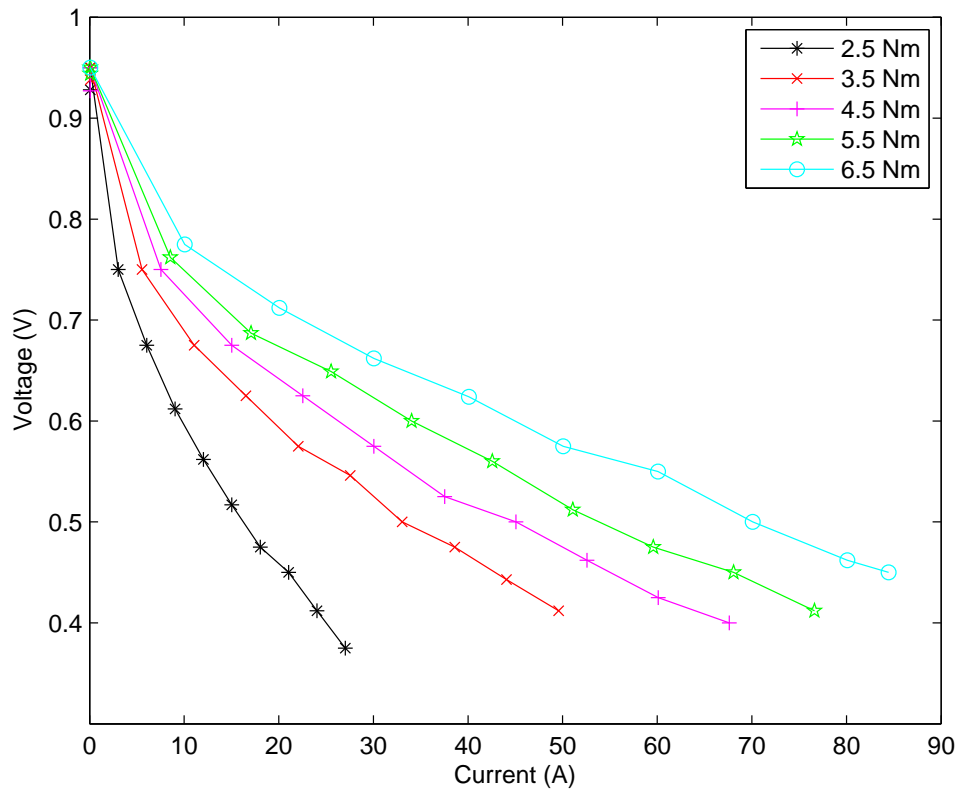


Figure 6.20: Polarisation curves for different endplate torques before conditioning

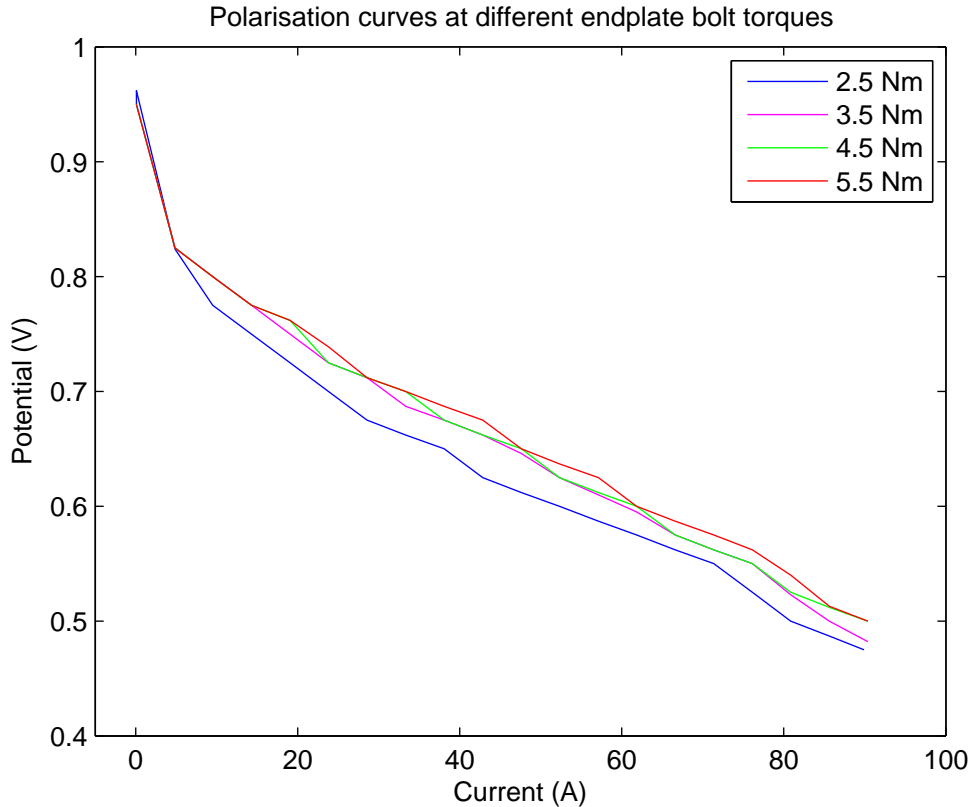


Figure 6.21: Polarisation curves for different endplate torques after conditioning

As can be seen in Figure 6.21, the fuel cell out-performs the pre-conditioning runs by a significant amount. Where the initial runs at 2.5 Nm had a peak current of 27.01 A, the latter run reached a peak current of 89.55 A. This significant gain in performance is partially due to the conditioning period for the MEA, however the newly compressed MEA has irreversible mechanical changes to its structure, and therefore the interfacial contact resistance is still reduced as when compressed to a higher level. It can be seen from Figure 6.21 that the lower torque level still performs badly compared to the higher increments.

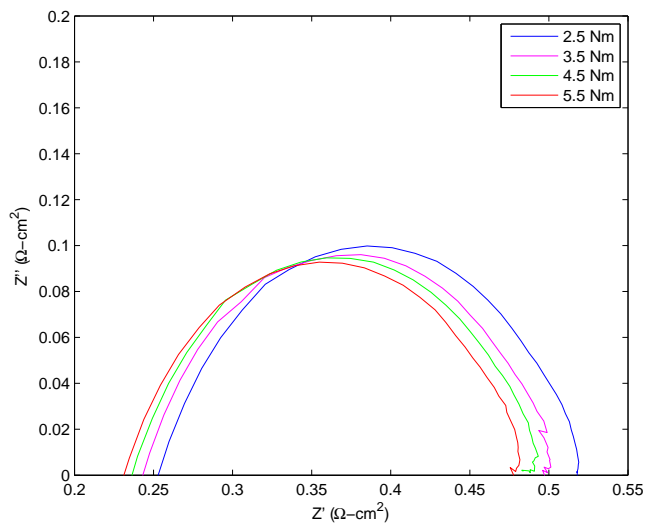
EIS

EIS techniques were used to determine the resistance experienced under different endplate torques at 0.2 A/cm², 0.4 A/cm² and 0.6 A/cm². Galvanostatic EIS sweeps from 500 to 0.1 Hz were undertaken with an amplitude of 20mV. The results were compared and analysed to show resistance in the cell.

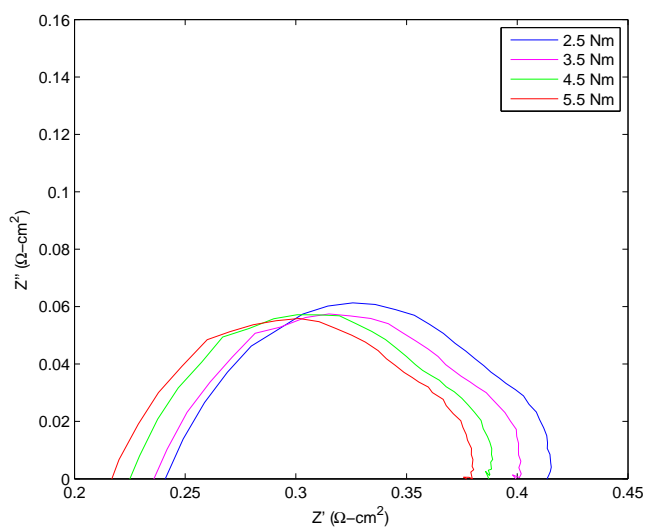
As can be seen in Figure 6.22, the EIS Nyquist plots were very successful, having little to no noise in the signal. A lot of useful information can be determined from Nyquist plots in relation to resistance.

Curve interpretation

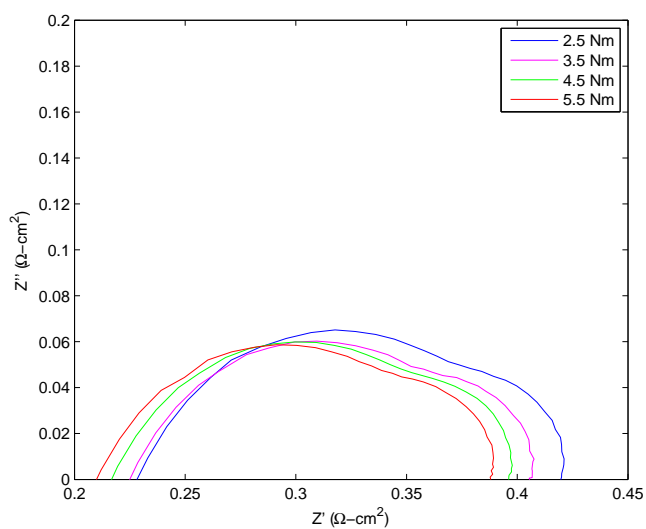
The point at which the curve intersects the X axis at the left of the graph is indicative of the overall resistance experienced in the cell, and therefore the Ohmic losses. Therefore for 5.5 NM at 0.6 A/cm², the resistance of the cell can be considered to be 0.2047 $\Omega - cm^2$. The area of the Nyquist plot from the first intersect to the last is indicative of the anode and cathode activation losses and the mass transfer effects. In a perfect world there would be a small curve



(a) 0.2 A / cm^2



(b) 0.4 A / cm^2



(c) 0.6 A / cm^2

Figure 6.22: Electrochemical Impedance Spectroscopy of different endplate bolt torques at different current densities

for the anode activation losses, a larger curve for the cathode activation losses, and finally a smaller curve for the mass transport losses as in Figure 6.11. However, in practise EIS is more likely to produce either one large curve as in Figure 6.22a which shows the anode, cathode activation and mass transport losses combined, or one large curve and one smaller as in Figure 6.22c which shows the anode and cathode activation combined, and the mass transport region is clearly visible.

Extrapolation of degradation data

Data affecting the performance of the cell was extracted from the above experimentation analysis of BIP torque in fuel cells. The overall resistance was taken from the x axis intercept for each current density and averaged to give the average resistance per torque level over the entire current range of the cell. The average resistance for 2.5 Nm was $0.249\Omega - cm^2$, with average resistances of 0.234 , 0.221 and $0.2145\Omega - cm^2$ for 3.5, 4.5 and 5.5 Nm torque levels respectively. These values were then plotted against the corresponding cell interior pressures with the data from Table 6.19.

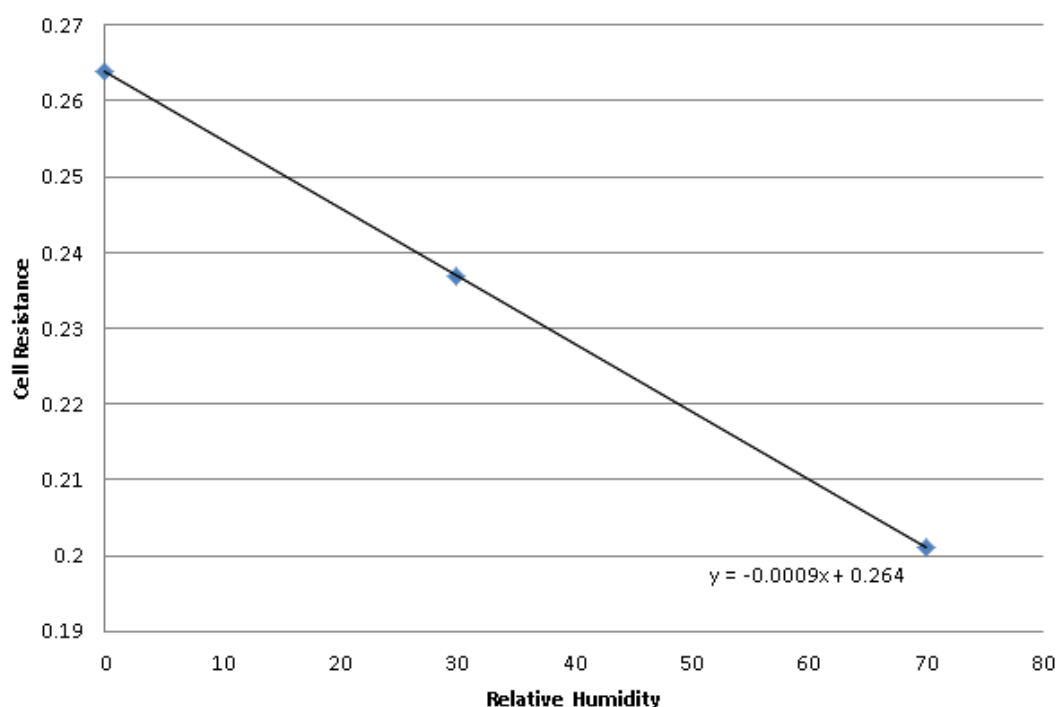


Figure 6.23: RH and resistance equation derivation

Once the resistances for each pressure have been determined, the data can be plotted against data ascertained from the literature regarding operating conditions that would affect pressure; the relationship between water content in the membrane and pressure. A study by Serincan & Pasaogullari [73] detailed the relationship between RH across the cell and the pressure in the cell in their 2011 study. The pressures in the cell for 0%, 30% and 70% RH were taken from this work and plotted against the data obtained from the experimentation (see Figure 6.23) to give the relationship equation; $-0.0009 * RelativeHumidity + 0.264$.

This can be used by the degradation model to show how an increase in cell pressure can increase cell resistance, thus affecting the Ohmic region of the polarisation curve, as in Figure 5.20.

6.5 Conclusions

The 1D model used for this work is an accurate mathematical representation of the chemical interactions of a FC, proved by the validation experimentation. The model was validated against an experimental rig, and the correlation between model and test data was very strong. Advanced techniques such as EIS were used to ascertain improved data over basic polarisation curves to look into resistances in the cell. The EIS data ascertained in this work, combined with numerous data sources from the literature regarding cell pressure and RH, mean that a highly accurate relationship between cell RH and performance can be implemented in the the Petri-net analysis. During operation, failure occurred that could be considered to match failure of other sources, this occurred when a gas inlet channel was damaged, partially blocking the gasses from entering the cell. This could be assumed to emulate the occurrence of an ice blockage in the channel, and as such, is used in the quantification of the Petri-net analysis.

Chapter 7

Degradation Simulation Results

Each of the failure rates, both proposed and taken from literature, were inserted into the Petri-Net model and ran both individually and as part of different operating modes to ascertain fuel cell lifetime. The entirety of the individual Petri-Net modules are omitted for brevity, however key examples are listed below. Additionally, the total results of the interactions of all Petri-Net modules are presented.

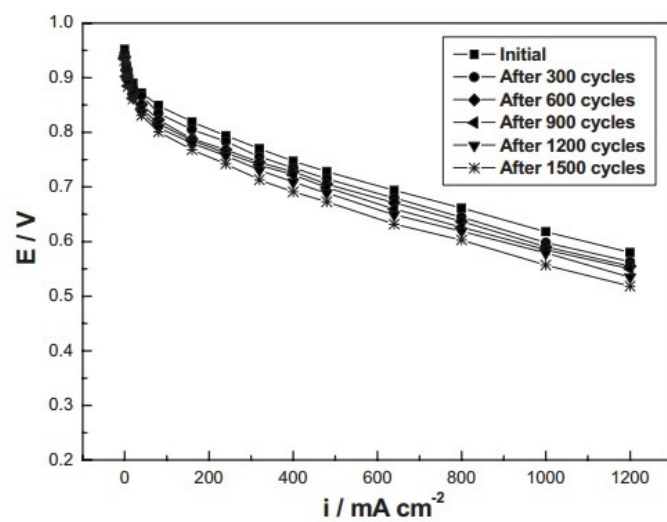
This chapter starts with two examples of what degradation logic occurs on an individual basis for two failure conditions. Startup Shutdown Cycling (SSC) results are presented that show where the degradation data comes from, and what the result is when only SSC is being observed in a FC. The degradation modelled through Petri-Net analysis is then validated by being run under the same conditions as a test undertaken on the FC experimental rig, with results shown. Finally, the Petri-Net model results are shown for the entire interaction of all the Petri-Net modules during operation under an automotive life cycle. Conclusions are then drawn in light of the results.

7.1 Stop/Start Cycling

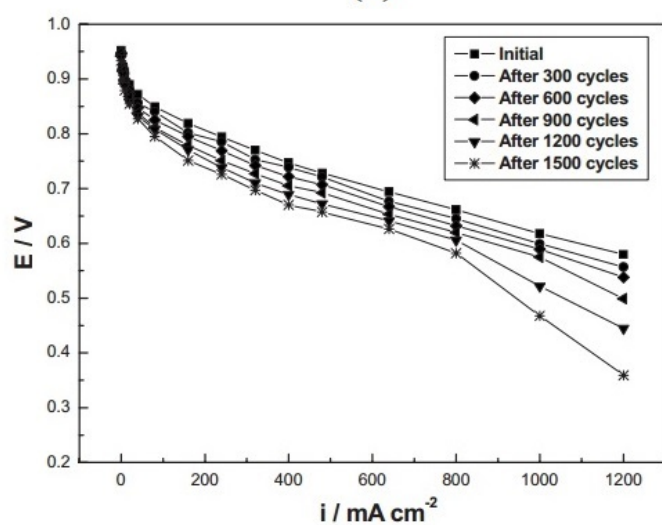
7.1.1 Data extrapolation from literature

A 2010 study [74] showed how the ohmic and mass transport regions of the polarisation curve are affected by SSC in different relative humidity conditions. The in depth study looked into the effects of three humidity levels on the degradation due to SSC for up to 1500 cycles.

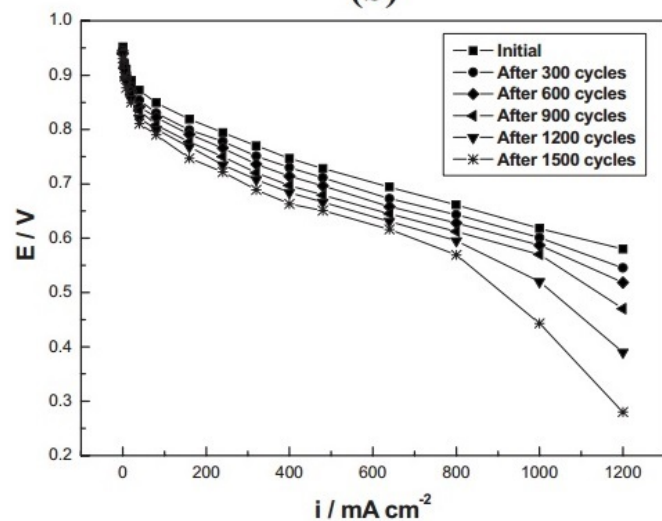
Figure 7.1 shows the experimental results for the three RH conditions from initial operation to 1500 SSCs. The work showed how there was no increase in gas crossover and no increase in membrane resistance, ruling out any membrane degradation. Therefore for the Petri-Net of SSC in this work, the membrane variables relating to gas crossover and resistance were not altered. Instead, the exchange current density and mass transport coefficients were modified in line with what was found in [74], to replicate the results.



(a)



(b)



(c)

Figure 7.1: Experimental results of SSC during (a)0% (b)50% and (c)100% RH [74]

By extrapolating data from Figure 7.1, we find that the degradation drop from initial conditions, to 1500 cycles at 0% humidity is comparable to a drop of exchange current density by an order of magnitude from the healthy 3.2×10^{-8} to 3.2×10^{-9} . The mass transport changes are observable through modifying the mass transport coefficient from a healthy cell value of 3, to 5.5 for 50% RH, and to 5.75 for 100% RH. These values are back calculated from measuring the performance drop from the experimentation, and implemented to emulate the same drop in performance in the model results. The change in model parameter over 1500 cycles is simply divided by the number of cycles to give the degradation due to SSC per cycle.

As the FC model could run anywhere between 0 and 100% RH, an assumption had to be made to make the degradation data span more than just 0, 50 and 100% regions. Therefore it is assumed that the degradation rate experienced under 0% RH in [74] would span the first third of the RH at the cathode. The degradation rate experienced under 50% RH is assumed to be true for the second third of the RH range, and finally the 100% RH degradation rate is assumed to be true for the final third of the RH range at the cathode.

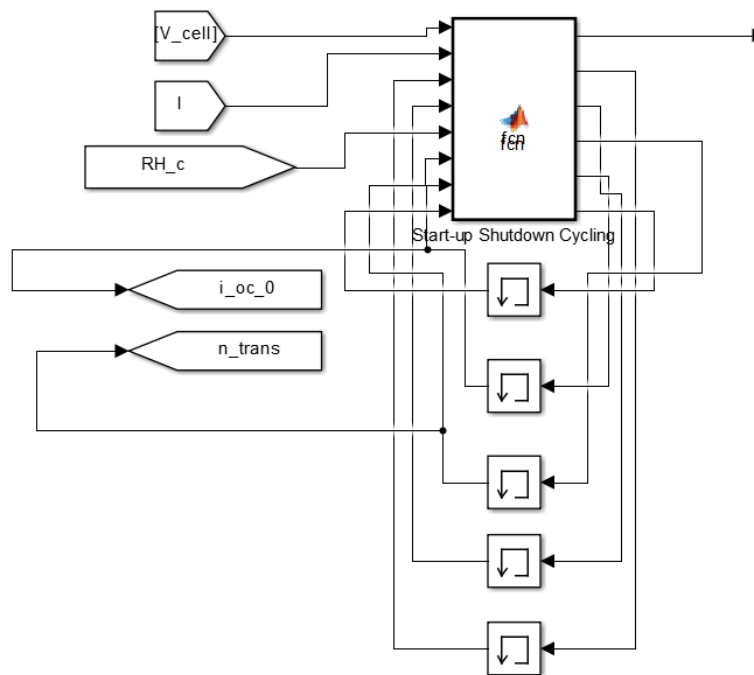


Figure 7.2: SSC module in SimuLink model

As shown in Figure 7.2 the degradation calculation takes data from the voltage of the cell (V_{cell}), the current (I) and the RH at the cathode (RH_c). Inputs are also taken from the outputs of memory loops, and are used to change the values of the exchange current density ($I_{oc,0}$) and the mass transport coefficient (n_{trans}). The vertically aligned boxes below the Matlab function block are used to give the Petri-net logic memory, where an output is then fed back into the input on the next iteration.

The logic for calculating SSC degradation is presented in Figures 7.3 & 7.4.

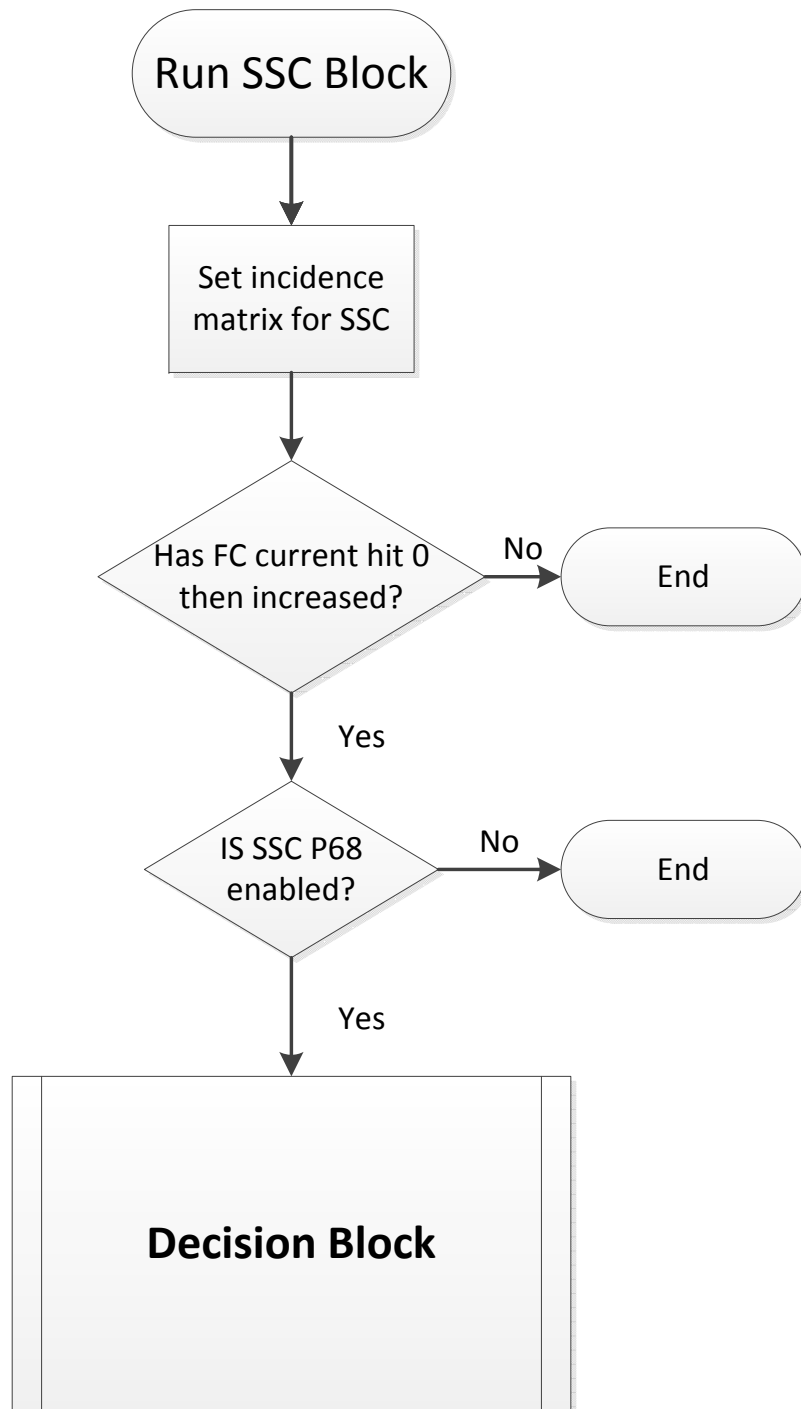


Figure 7.3: SSC logic flow diagram

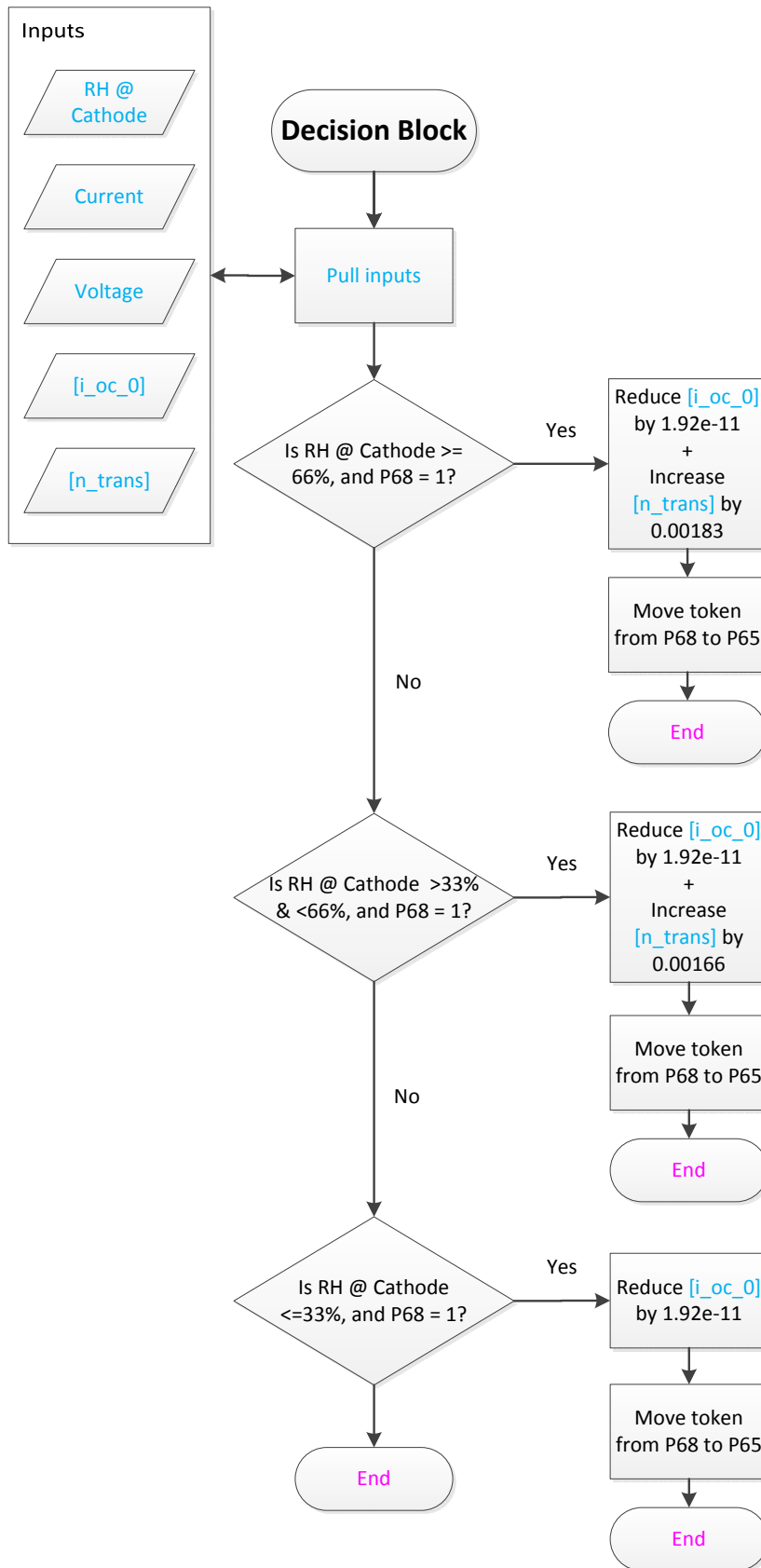


Figure 7.4: SSC logic flow diagram continued

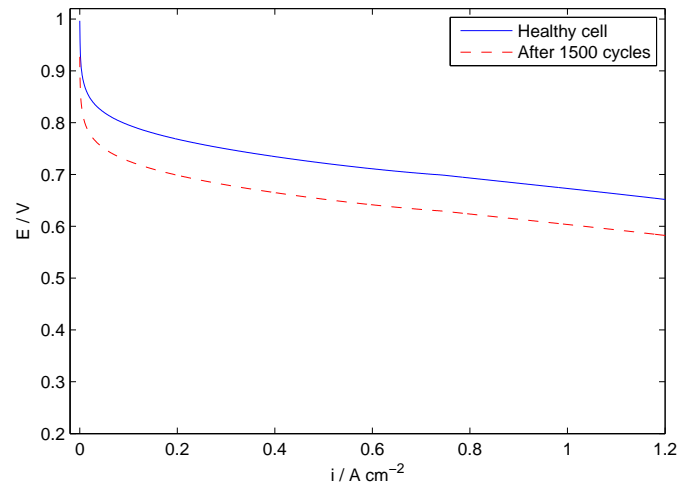
Figure 7.3 shows that the first step is for the Petri-net module to set the incidence matrix for that particular module. The code then checks to see if an instance of SSC has occurred. To do so, the model checks the operational current to see if the current hits 0, then increases above this value. If this is not occurring, the module is skipped. If this is occurring, the model then checks to see if P68 in the net is enabled, signifying that there is currently no SSC happening, see table 5.2. If this is satisfied, the main decision logic is run.

Figure 7.4 shows how the Petri-net module for SSC is dependent upon key input variables. The 1D model output for that time step is tapped into to ascertain the RH at the cathode, current, voltage the exchange current density ($i_{oc.0}$) and the mass transport coefficient (n_{trans}). These values are needed for the Petri-net module to calculate when to fire, and what values to alter in the 1D model.

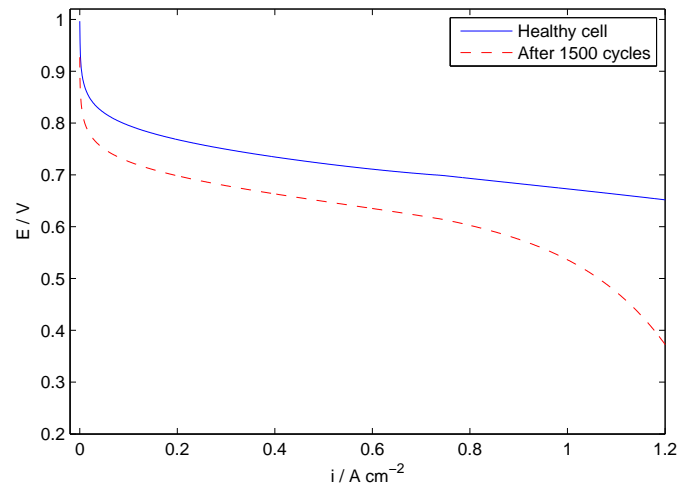
The module code then determines which RH threshold the 1D model is operating in, which determines the extent of the degradation due to SSC. If there is a token in P65 ‘No SSC’ and the RH at the cathode is more than or equal to 66%, the exchange current density is reduced by 1.92×10^{-11} . The mass transport coefficient is increased by 0.00183 per SSC at these operating conditions.

If any of the thresholds are experienced, the variables from the 1D model are altered so that the next time step of the model incurs degradation due to the alterations. The token is also taken from P68 and placed into P65. However due to this being a reversible degradation pathway, the tokens are reset for the next time step.

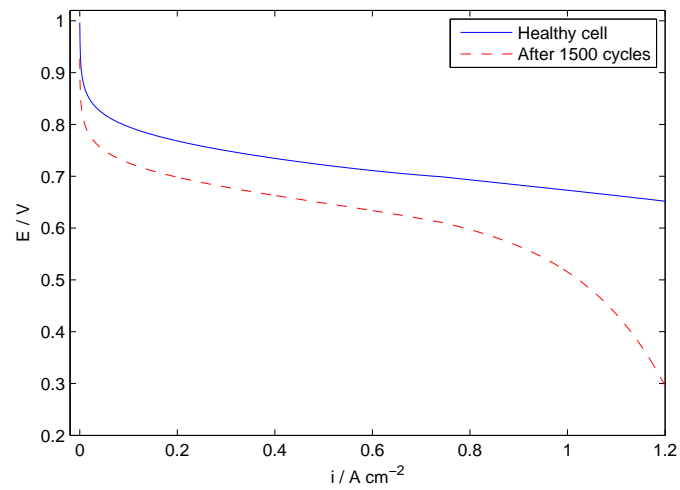
As can be seen in Figure 7.5, the modelled degradation correlates with the experimental results obtained in [74].



(a)



(b)



(c)

Figure 7.5: Modelled SSC degradation for (a)0% (b)50% and (c)100% RH

7.2 Degradation Validation Test

As to ascertain the accuracy of the degradation model, experimentation was undertaken to operate a FC in the same conditions as the model, and degradation over that time was compared between the two.

The FC was operated as if the FC was the sole power source in a road car with the requirements shown in Table 7.1:

Table 7.1: Table of vehicle parameters

Parameter	Value	Description	Unit
m	1200	Vehicle mass	kg
a_tyre	0.01	Mass related tyre friction coefficient	-
b_tyre	0.01	Velocity related tyre friction coefficient	-
rr	0.325	Tyre rolling radius	m
Cd	0.26	Drag coefficient	-
A_f	2	Frontal area	m ²

The vehicle model uses proposed values for an average consumer vehicle. This is required for the model to accurately calculate how much power is needed from a FC stack or single cell to propel the car.

The vehicle was run through the NEDC five times, before being shut-down. Five repetitions are proposed as these five cycles take just over 1.5 hours to complete, which is a feasible amount of time to run the experimental rig for validation of results. This process was repeated for five cycles by programming the current profile for one cell out of the vehicle's stack on the NEDC, into the loadbank, repeated 5 times (see Figure 7.6). One cell was modelled that would be a contributing cell in the stack of this theoretical vehicle. As the current is the same throughout the stack, modelling one cell is justified.

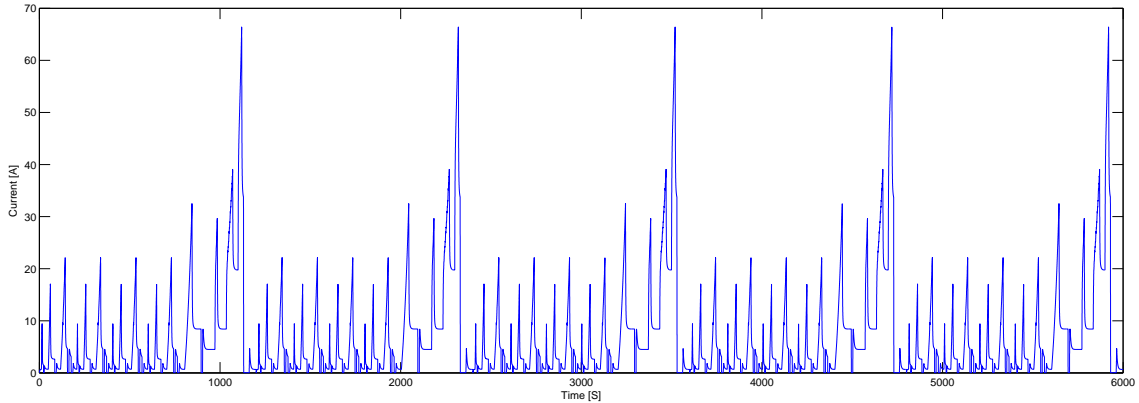


Figure 7.6: Current profile of the FC vehicle for 5 NEDCs

The FC operating conditions were kept as per the characterisation run (see Table 7.2):

After running the load profile of five NEDCs, six polarisation curves were undertaken with EIS curves at low, medium and high current densities. After the sixth polarisation curve, the performance of the cell had reached equilibrium, however the entire run of curves were averaged

Table 7.2: Table of FC operational parameters

Parameter	Value	Unit
Relative Humidity	65 ±5	%
Pressure	0.5	bar
Flow Rate H ₂	1.5	slpm
Flow Rate Air	8.5	slpm
H ₂ Temp	31	Celsius
Air Temp	30.5	Celsius
Cell Temp	39	Celsius

to ascertain the performance of the cell after the load profiles. Figure 7.7 shows the averaged polarisation curves for five cycles of the five NEDCs.

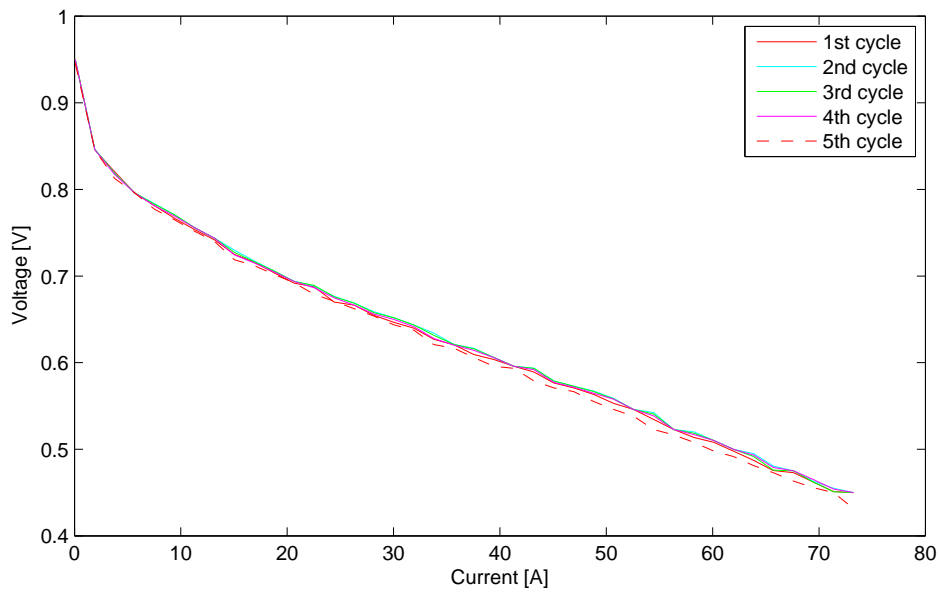


Figure 7.7: Experimental polarisation curves

As can be seen in Figure 7.7, due to the resolution of data points, the curves are difficult to interpret. Therefore the curves were fitted using a fifth order polynomial trend-line as in Figure 7.8. The fifth order polynomial trend-line was chosen for its ability to closely link data points to give a good graphical representation of the results.

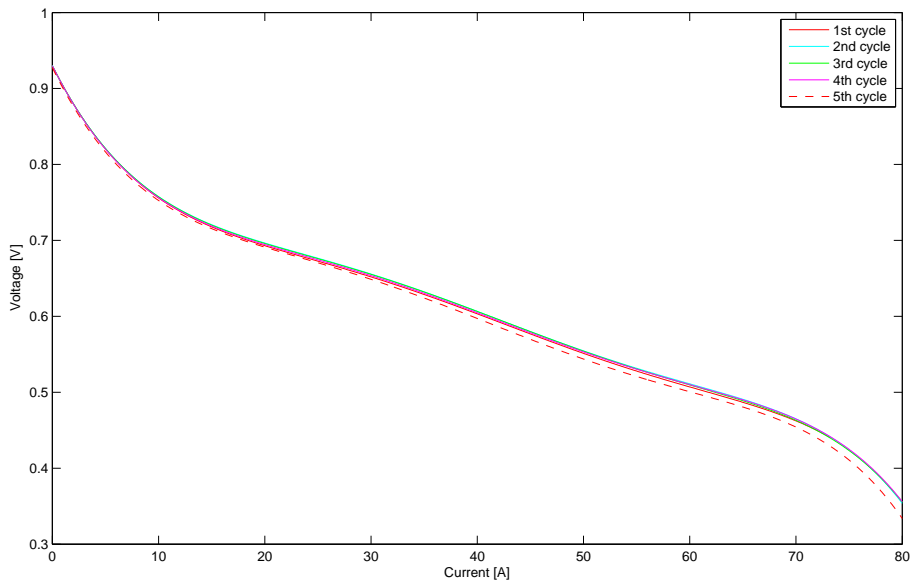


Figure 7.8: Fitted experimental polarisation curves

The fitting of the trend-line smooths out the polarisation curve, making it easier to analyse, however the initial activation drop region is changed from what is expected with the raw data (see Figure 7.9).

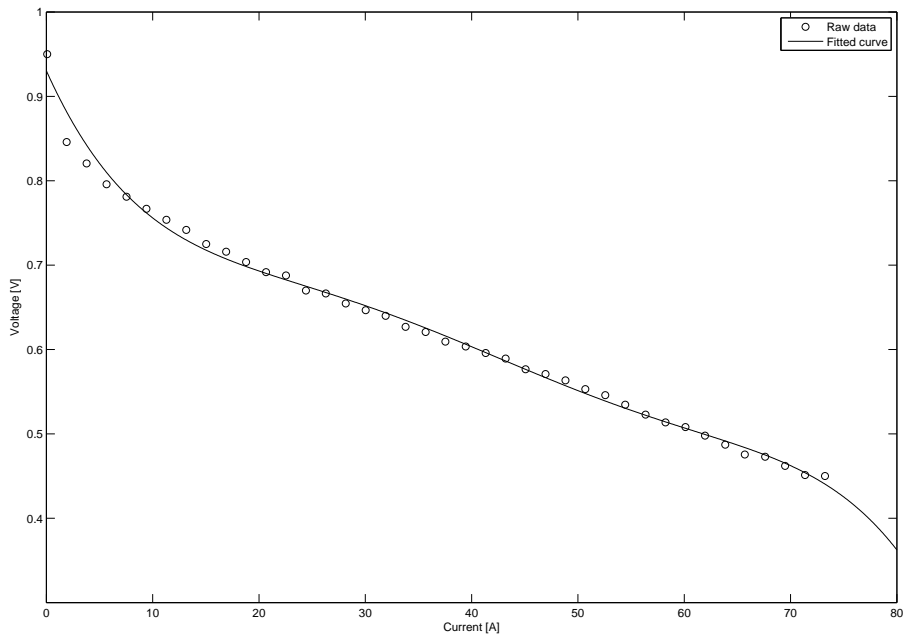


Figure 7.9: Comparison of raw data vs fitted for cycle one

This is due to the relatively low resolution of the raw data. The polarisation curves were

set to run for 15 minutes, and had to equalise at each current density to take a reading. The initial activation loss region changes voltage quite dramatically under low current changes, and as such there is a large gap between data points in this region. Further down the polarisation curve shows how the gap between data points is smaller, as the change in voltage is lower in the ohmic and mass transport regions. What must be taken into account when considering the following analysis, is that the polarisation curve for the fitted experimental data will be higher than usual in the region of 1A to 5A, and lower in the region of 5A to 20A. In an ideal world, the curves would be run for a longer time period, as to get a higher resolution in the initial activation loss region.

The experimental data was then plotted against the 1D & Petri-Net degradation model's results, running under the same operating conditions, and under the same load profile. The results of which are shown in Figure 7.10. The model was run simply to perform one polarisation curve, and therefore no degradation is expected for the one curve. The point of this exercise is to see how accurately the experimental results of a polarisation curve, match that of the model's.

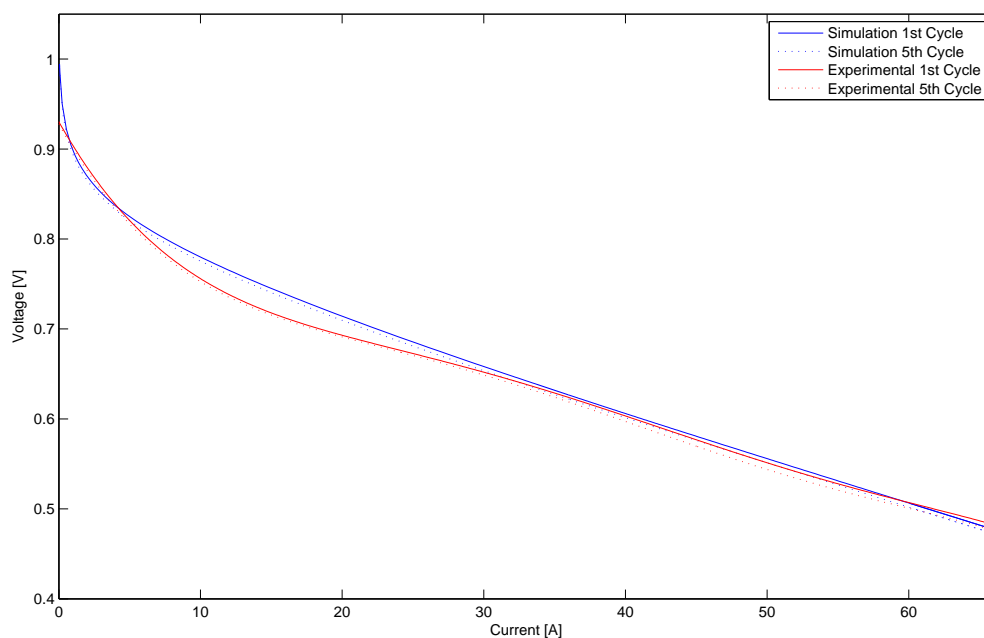


Figure 7.10: Modelled degradation vs experimental degradation

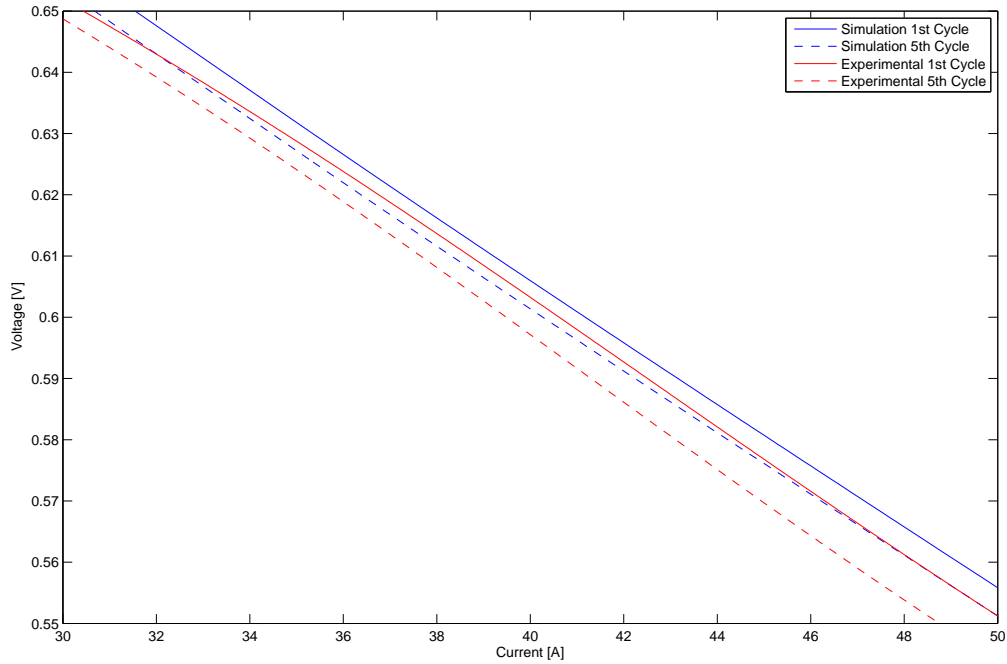


Figure 7.11: Modelled degradation vs experimental degradation zoomed

The solid blue line represents the simulation's first polarisation cycle, whereas the blue dashed line is indicative of the performance of the cell after five cycles. The solid red line represents the measured performance of the cell in the experimental rig on its first cycle. The dashed red line shows the drop in performance that was measured after five cycles in the test rig.

As can be seen in Figure 7.10 & 7.11, the degradation observed in the experimentation matches closely with the degradation that is a product of the Petri-Net modelling for this case. The drop in performance of the experimental data from 5A to 20A is a result of the polynomial fit applied to smooth the raw data, as explained above. The zoomed section shows more clearly the visual agreement of the drop in performance over five cycles in the experimentation, and the same operating data used to run the degradation model.

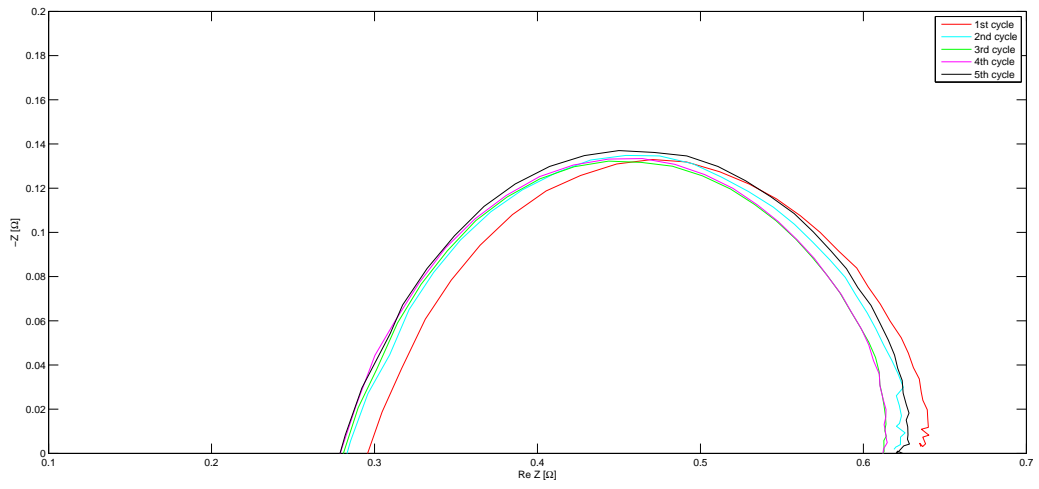
7.2.1 Analysis

The most significant contributors to degradation for this simulation was Pt agglomeration, more specifically the immature Pt agglomeration that occurs in the first 40 hours of operation. This type of degradation is unavoidable and expected during the initial stages of operation. Other contributors to the overall degradation come in the form of H_2O_2 degradation. This failure mode was triggered when operating conditions met the criteria of the inhibitor related to potential of the cell. This is observable through a visual inspection of the cumulative voltage drop variables that can be seen when running the model.

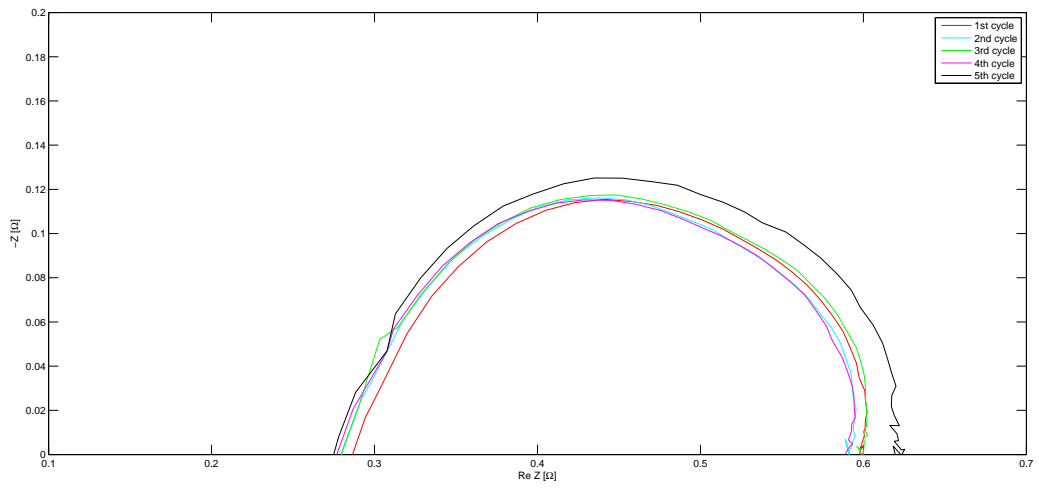
7.2.2 EIS data

To further ascertain if the FC had degraded during its operation, EIS plots were undertaken at low, medium and high current densities (0.2, 0.4 and 0.6A/cm² respectively) after each cycle. Figure 7.12 shows the three plots corresponding to each current density.

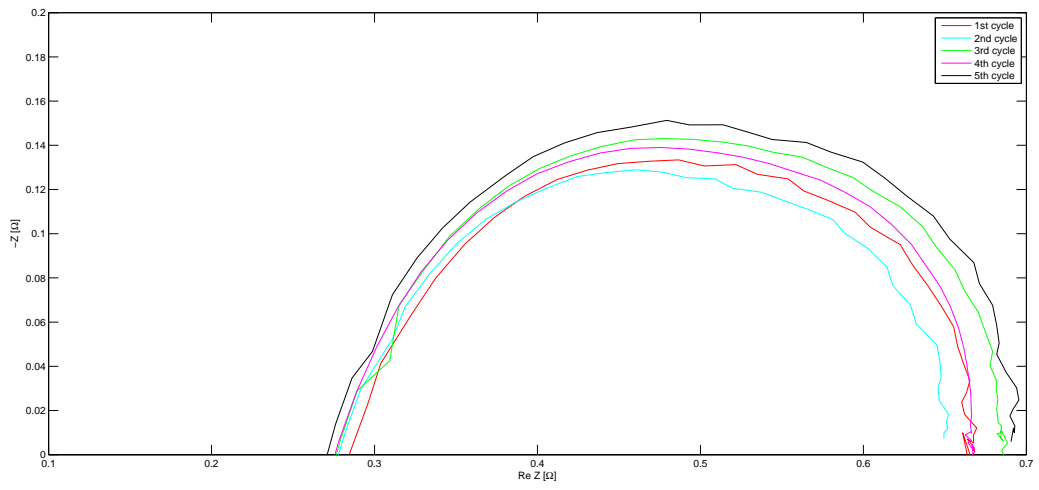
The EIS curves show that for each cycle, the total area of the curve is reduced. This is indicative of a reduction in the activation area of the FC. The EIS data strengthens the claims that immature platinum agglomeration is a major influencer of FC lifetime, showing that the activation area of the EIS plot decreases with each cycle.



(a) $0.2\text{A}/\text{cm}^2$



(b) $0.4\text{A}/\text{cm}^2$



(c) $0.6\text{A}/\text{cm}^2$

143
Figure 7.12: EIS plots for each current density after each cycle

7.3 Weibull Degradation

The Weibull distribution was used to vary the degradation of each failure mode per time step. This was done to integrate a random number into the degradation calculations and offer a more realistic view of what would happen in a real world system.

Weibull was chosen as the type of distribution to use due to its ability to modulate the degradation rate based upon a shape parameter. Some failure modes that can be experienced in a FC are more severe in the early ‘bedding in’ period, some failure modes have a more linear ‘useful life’ affect, whereas others are more prominent only in the ‘wear out’ period towards the end of life. The Weibull distribution is a good tool to make use of these characteristics by having differing shape parameters as described in section 5.5.

Figure 7.13 shows a comparison between a flat rate of degradation vs a single run of a Weibull integrated degradation under the same operating conditions. Flat rate refers to the constant rate of degradation that, whereas the Weibull degradation line shows how the degradation rate varies based upon the Weibull data input.

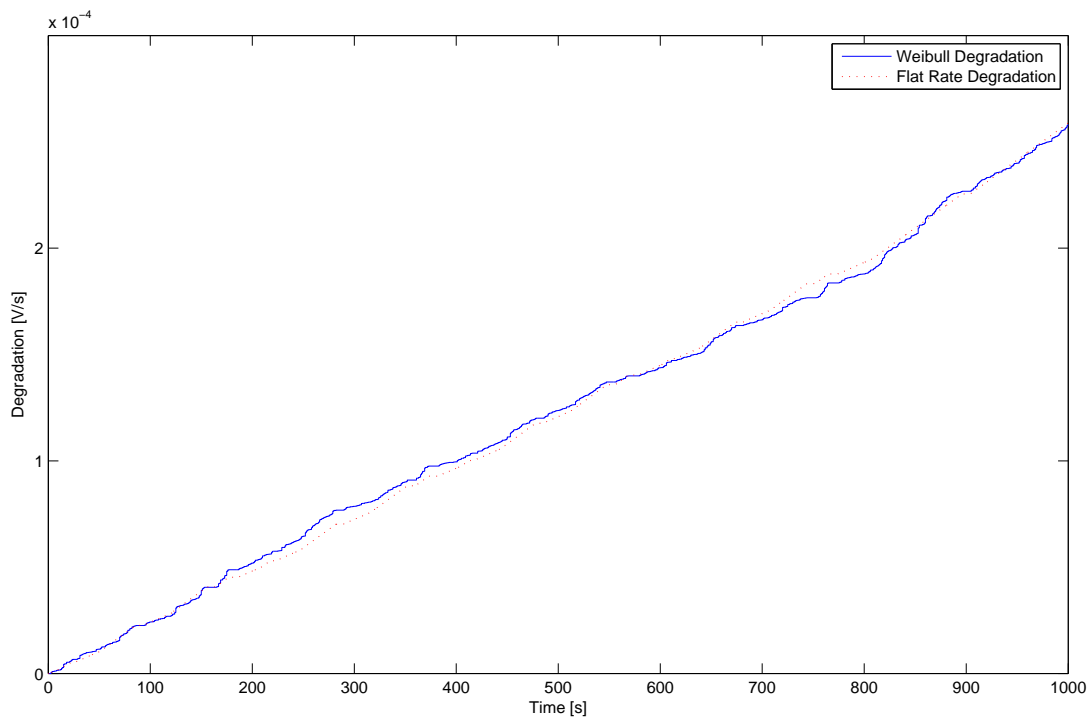


Figure 7.13: Flat rate degradation vs Weibull distribution degradation

As can be seen in Figure 7.13 the Weibull degradation rate is within the range that is expected if using the flat rate of degradation, however it varies dependent upon the random number that was introduced.

Using the Weibull distribution means that one must repeat simulations a number of times to gain an accurate understanding of the total lifetime of the FC. The simulations were run numerous times until confidence was achieved with the cumulative average lifetime for each simulation run.

The overall running of the combined 1D and Petri-net degradation model is shown in Figure 7.14. For the models to run, the initialisation data detailed in section 5.1.1 are input so that the 1D model knows the specification of the MEA. The time and current profiles are needed

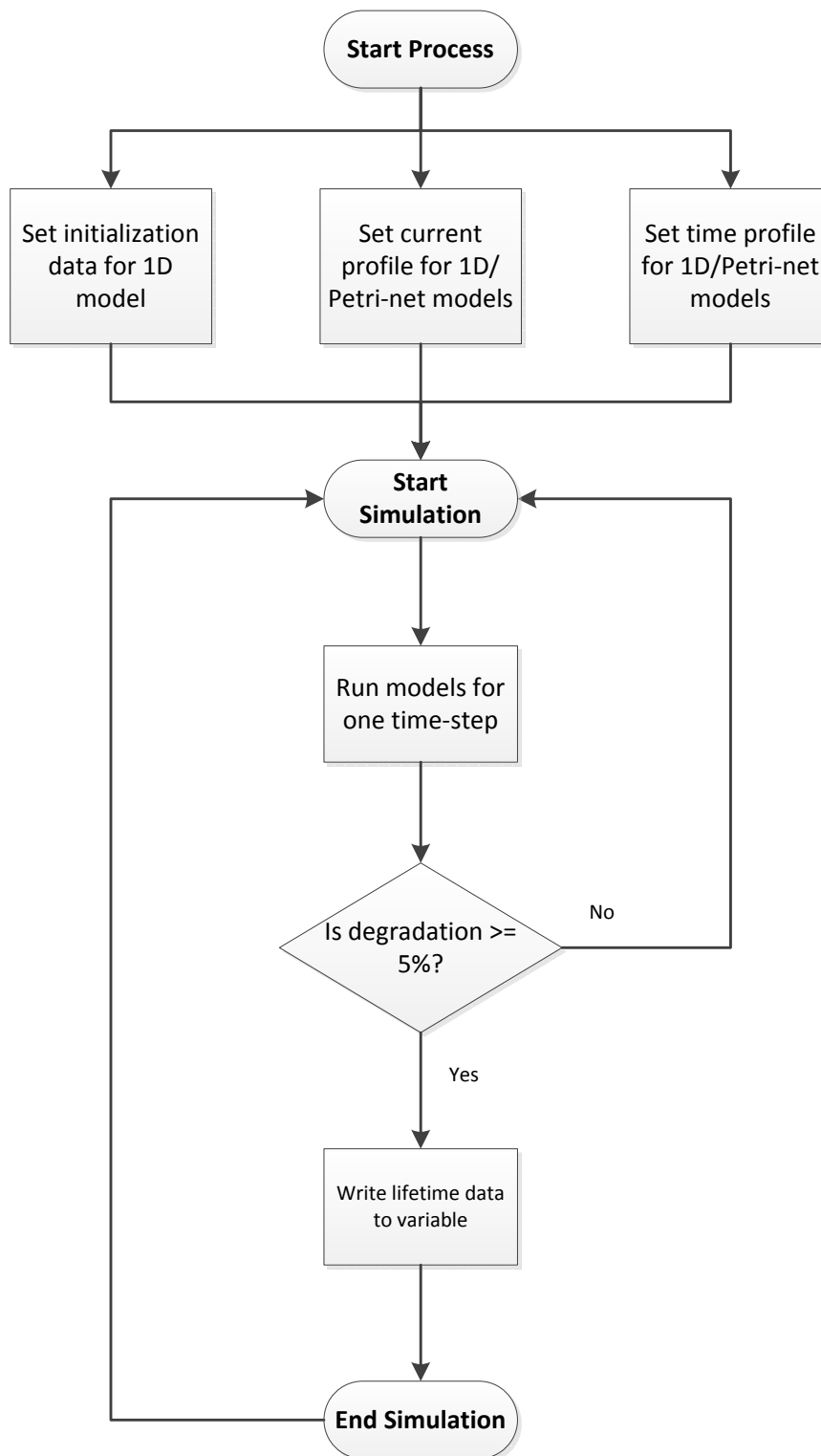


Figure 7.14: Flow diagram of overall degradation model running

for the models to know what cycle the FC is running. After this data is input, the simulation process can start.

The degradation model was run until confidence was sought with the cumulative average lifetime. As can be seen in Figure 7.15, the average lifetime varies significantly during the first 40 simulations, then starts to level out, with a minor fluctuation between 60 and 120 simulations. Confidence in the average lifetime is assumed at 151 iterations of the simulation at a lifetime of 1.224×10^5 which is equal to 34 hours of operation. The most significant contributors to the degradation in this time period were immature platinum agglomeration and H_2O_2 degradation. This was determined by evaluating the contribution of that module versus the others via the real-time value output block of a scope during operation.

The final value ascertained from the degradation simulation performed in this work sits well between the bounds given by the experimental data collected by Borup, et al. [16] in Table 9 of their paper. Their values of 24 hours lifetime due to H_2O_2 degradation and a lifetime of 50 hours due to H_2O_2 degradation and pinhole production agree well with the simulated lifetime of 34 hours with H_2O_2 degradation being a significant contributor to the degradation.

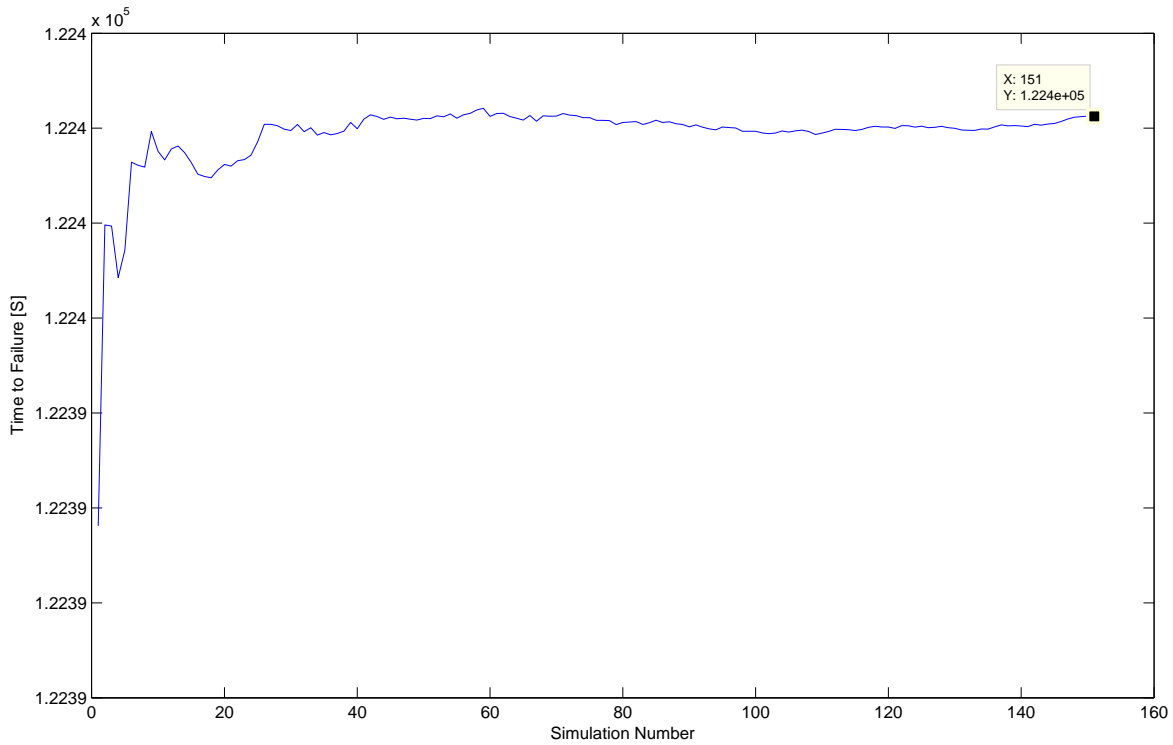


Figure 7.15: Cumulative average lifetime of the cell over 151 simulations

7.4 Conclusions

This chapter has presented the quantitative results of the Petri-Net degradation modelling. The individual results of SSC were presented and showed a strong correlation with experimental results from the literature. It is therefore assumed that degradation due to SSC in the overall Petri-Net model is justified. When the entire Petri-Net model's modules are run with their interactions, the overall lifetime of a cell under the NEDC based drive cycles was ascertained. Due to using Weibull distributions of the degradation data that included the input of a random

number, numerous iteration of the simulation were run until confidence in an average lifetime was gained. This was assumed to be after 151 cycles and was 1.224×10^5 seconds, which is equal to 34 hours of operation. This falls within the boundaries of the experimentation in the literature, and therefore is considered accurate.

Chapter 8

Conclusions and Future Work

8.1 Introduction

The research carried out has achieved the aims and objectives discussed in section 1.7 of chapter 1:

1. An understanding of current PEMFC degradation phenomena and modelling methods was gained through the use of a literature review and FMEA/FTA.
2. A greater understanding of PEMFC reliability studies was ascertained through an in-depth literature review and analysis of previous work in this area.
3. Based upon the literature review;
 - i A comprehensive FMEA including 21 failure modes was developed from knowledge gained from the literature review, and is presented as the most comprehensive and up-to-date FMEA currently published. The membrane had 8 main failure modes, the catalyst layer contained 7 failure modes, the GDL had 4 and the BIP had 2 failure modes associated with it.
 - ii A new FT was developed based upon the failure modes identified in the FMEA, and is also presented as the most up-to-date and specific FT currently in the literature. The quantification of this model used Weibull distributions of degradation data taken from the literature.
4. Interactions and dependencies in a PEMFC were analysed and conclusions presented regarding their effect on reliability analysis.
5. A quantitative degradation model was developed using Petri-net analysis techniques, which predicts fuel cell lifetime under certain operating conditions. 20 failure modes were developed which represented all of the failure modes previously ascertained through the FMEA and FTA research. The product of the work was an estimated lifetime of a cell operating in a certain cycle using Weibull distribution degradation data.
6. The degradation model is validated using an experimental rig that was purpose built, from the ground up. The rig strengthened the confidence in the results of the degradation model by accurately matching the data from previous simulation runs. The rig also offered degradation data to be used in the Petri-net model and filled gaps in the data for degradation of PEMFCs.

The aim of this work was to develop an effective model to predict the lifetime and degradation of a FC in an automotive environment. This has been achieved through the development and presentation of three reliability techniques used to analyse the degradation in a FC system, and the main conclusions are given in 8.2.

8.2 Major contributions in the area of reliability

This research has produced the following enhancements to the area of FC reliability research:

- A fully comprehensive FMEA has been produced that is the most up-to-date tabular analysis of the differing failure modes that could be experienced in a FC environment used in automotive load cycles [75]. This work improved some existing work in the area by Rama, et al. [30].
- A FT has been developed that uses the knowledge built during the completion of the FMEA, to show a top-down approach to reliability analysis. Quantification of the FT was completed using Weibull distributions of data ascertained from the literature for the key failure modes that were identified [49]. The work also demonstrated that FTA is not an accurate method to quantify FC performance due to dependencies and restrictions in logic.
- Petri-Net analysis was used to overcome some key pitfalls of the FT approach, and was used to accurately quantify FC degradation during an automotive drive cycle.
- The Petri-Net modelling was integrated with a 1D fuel cell model that vastly increases the accuracy of the results due to having a link to key operational variables that affect degradation such as RH and cell voltage.

8.3 Experimentation

To help validate and strengthen confidence in the results of the degradation model in terms of real world application, an experimental test rig was built.

- A FC test rig was built and commissioned to verify the degradation data ascertained from the Petri-Net model.
- Experimentation was undertaken to record real world degradation levels of a FC under automotive drive cycles. The drive cycle was created from the NEDC and repeated for duration.
- The time-stamp and corresponding current for the load was logged and was used to feed into the Petri-Net simulation to make sure that the simulation was exactly replicating the experimentation.

8.4 Future Work

This work offers a novel application of Petri-Net modelling to FC degradation and lifetime analysis, and fills a large gap in the literature regarding FC reliability modelling. However, the model is as reliable as the input degradation data, and as such could be slightly improved upon. Due to the lack of data in this field a range of data from a range of different tests was entered into the simulation. As the majority of data used was from accelerated stress tests, it could be assumed that the overall lifetimes ascertained from the simulation may be lower than real world conditions.

Although the verification appears successful when compared to a study presented in [16], other studies in the same paper show a longer lifetime, with fuel cells operating between 18 and 2500 hours. These could be due to differing operational parameters and load profiles, and as such other load profiles should be analysed. It is assumed that a FC will degrade less at potentials in the 0.6V region, and therefore if kept there, the lifetime may increase.

To make the degradation model 100% reliable, all input data would need to be ascertained through experimentation with the exact core materials and operating conditions, singling out

each individual failure mode. This would require an infeasible amount of time and fuel for one organisation, however if testing procedures were standardised, a conglomerate of research groups could create a data set of reliable data.

Expansion of this modelling could also include degradation analysis due to the balance of plant for a FC system. A degraded humidifier for example would cause leached impurities and contaminants entering the FC which are not modelled fully in this work. However, this would require the accurate modelling of humidifier degradation. The integration of any such works would be easy to facilitate due to the nature of Petri-Nets.

Another possibility is to use this degradation model to diagnose real-time degradation in fuel cells to lengthen the life of a unit. If operational states are seen to be degrading the FC, reverse engineering through this model will show what part of the FC is being degraded using information from the FMEA and Petri-net model.

Stack level modelling can currently be replicated through this research, however it does not take into account the effects of degradation in one cell affecting the adjacent cells. Future work could include the ability of this model to take into account effects of stack level degradation by looking into gas consumption along the stack when pinholes or other gas related failure modes are occurring, and temperature differentials along the stack.

Bibliography

- [1] S. Solomon, M. D. Qin, Z. Manning, M. Chen, K. B. Marquis, M. Averyt, Tignor, and H. Miller, “Summary for policymakers. in: Climate change 2007: The physical science basis. contribution of working group i to the fourth assessment report of the intergovernmental panel on climate change,” tech. rep., Cambridge University Press, 2007.
- [2] BERR, “Dti energy price scenarios in the oxford models,” tech. rep., BERR, 2006.
- [3] E. F. for Transport and Environment, “Co2 emissions from new cars,” tech. rep., T&E, 2008.
- [4] DECC, “Decc fossil fuel price projections: summary,” tech. rep., DECC, 2012.
- [5] B. G. Pollet, I. Staffell, and J. L. Shang, “Current status of hybrid, battery and fuel cell electric vehicles: From electrochemistry to market prospects,” *Electrochimica Acta*, no. 0.
- [6] S. Sorrell, J. Speirs, R. Bentley, A. Brandt, and R. Miller, “An assessment of the evidence for a near-term peak in global oil production,” *A report produced by the Technology and Policy Assessment function of the UK Energy Research Centre*, 2009.
- [7] DECC, “2012 uk greenhouse gas emissions, provisional figures and 2011 uk greenhouse gas emissions, final figures by fuel type and end-user,” tech. rep., DECC, 2013.
- [8] D. for Transport, “Factsheets: Uk transport greenhouse gas emissions,” tech. rep., DfT, 2013.
- [9] U. Gov, “Climate change act 2008,” 2008.
- [10] D. M. Bernardi and M. W. Verbrugge, “Mathematical model of the solid-polymer-electrolyte fuel cell,” *Journal of the Electrochemical Society*, vol. 139, no. 9, pp. 2477–2491, 1992. Cited By (since 1996): 842.
- [11] C. E. Thomas, “Fuel cell and battery electric vehicles compared,” *International Journal of Hydrogen Energy*, vol. 34, no. 15, pp. 6005–6020, 2009. Cited By (since 1996): 57.
- [12] B. Cook, “An introduction to fuel cells and hydrogen technology,” 2001.
- [13] E. T. Services, *Fuel Cell Handbook*. 7 ed., 2004.
- [14] N. Yousfi-Steiner, P. Mootguy, D. Candusso, D. Hissel, A. Hernandez, and A. Aslanides, “A review on pem voltage degradation associated with water management: Impacts, influent factors and characterization,” *Journal of Power Sources*, vol. 183, no. 1, pp. 260–274, 2008. Cited By (since 1996): 60.
- [15] C. He, S. Desai, G. Brown, and S. Bollepalli, “Pem fuel cell catalysts: Cost, performance, and durability,” *Electrochemical Society Interface*, vol. 14, no. 3, pp. 41–44, 2005. Cited By (since 1996):29.

- [16] R. Borup, J. Meyers, B. Pivovar, Y. S. Kim, R. Mukundan, N. Garland, D. Myers, M. Wilson, F. Garzon, D. Wood, P. Zelenay, K. More, K. Stroh, T. Zawodzinski, J. Boncella, J. E. McGrath, M. Inaba, K. Miyatake, M. Hori, K. Ota, Z. Ogumi, S. Miyata, A. Nishikata, Z. Siroma, Y. Uchimoto, K. Yasuda, K. I. Kimijima, and N. Iwashita, “Scientific aspects of polymer electrolyte fuel cell durability and degradation,” *Chemical reviews*, vol. 107, no. 10, pp. 3904–3951, 2007. Cited By (since 1996):920.
- [17] A. Beicha, “Modeling and simulation of proton exchange membrane fuel cell systems,” *Journal of Power Sources*, vol. 205, pp. 335–339, 2012.
- [18] T. E. Springer, T. A. Zawodzinski, and S. Gottesfeld, “Polymer electrolyte fuel cell model,” *Journal of the Electrochemical Society*, vol. 138, no. 8, pp. 2334–2342, 1991. Cited By (since 1996): 1487.
- [19] K. Z. Yao, K. Koran, K. B. McAuley, P. Oosthuizen, B. Peppley, and T. Xie, “A review of mathematical models for hydrogen and direct methanol polymer electrolyte membrane fuel cells,” *Fuel Cells*, vol. 4, no. 1-2, pp. 3–29, 2004. Cited By (since 1996): 45.
- [20] D. Cheddie and N. Munroe, “Review and comparison of approaches to proton exchange membrane fuel cell modeling,” *Journal of Power Sources*, vol. 147, no. 1-2, pp. 72–84, 2005. Cited By (since 1996): 104.
- [21] R. F. Mann, J. C. Amphlett, M. A. I. Hooper, H. M. Jensen, B. A. Peppley, and P. R. Roberge, “Development and application of a generalized steady-state electrochemical model for a pem fuel cell,” *Journal of Power Sources*, vol. 86, no. 1, pp. 173–180, 2000. Cited By (since 1996): 288.
- [22] J. Larminie and A. Dicks, *Fuel Cell Systems Explained*. West Sussex: Wiley, 2 ed., 2003.
- [23] J. Wu, X. Z. Yuan, J. J. Martin, H. Wang, J. Zhang, J. Shen, S. Wu, and W. Merida, “A review of pem fuel cell durability: Degradation mechanisms and mitigation strategies,” *Journal of Power Sources*, vol. 184, no. 1, pp. 104–119, 2008. Cited By (since 1996): 127.
- [24] P. T. Yu, W. Gu, R. Makharia, F. T. Wagner, and H. A. Gasteiger, “The impact of carbon stability on pem fuel cell startup and shutdown voltage degradation,” in *ECS Transactions*, vol. 3, pp. 797–809, 2006. Cited By (since 1996):60.
- [25] S. Y. Ahn, S. J. Shin, H. Y. Ha, S. A. Hong, Y. C. Lee, T. W. Lim, and I. H. Oh, “Performance and lifetime analysis of the kw-class pemfc stack,” *Journal of Power Sources*, vol. 106, no. 1-2, pp. 295–303, 2002. Cited By (since 1996): 54.
- [26] M. Villacourt, “Failure mode and effects analysis (fmea): A guide for continuous improvement for the semiconductor equipment industry,” tech. rep., SEMATECH, 1992.
- [27] J. D. Andrews and T. R. Moss, *Reliability and Risk Assessment*. London, England: Professional Engineering Publishing Limited, 2nd ed., 2002.
- [28] P. Rama, R. Chen, and J. Andrews, “A review of performance degradation and failure modes for hydrogen-fuelled polymer electrolyte fuel cells,” *Proceedings of the Institution of Mechanical Engineers, Part A: Journal of Power and Energy*, vol. 222, no. 5, pp. 4214–441, 2008. Cited By (since 1996): 4.
- [29] M. Stamatelatos, W. Vesely, J. Dugan, J. Fragola, J. Minarick, and J. Railsback, “Fault tree handbook with aerospace applications,” tech. rep., NASA, 2002.
- [30] L. Placca and R. Kouta, “Fault tree analysis for pem fuel cell degradation process modelling,” *International Journal of Hydrogen Energy*, vol. 36, no. 19, pp. 12393–12405, 2011. Cited By (since 1996): 2.

- [31] J. Andr, L. Antoni, and J. P. Petit, “Corrosion resistance of stainless steel bipolar plates in a pefc environment: A comprehensive study,” *International Journal of Hydrogen Energy*, vol. 35, no. 8, pp. 3684–3697, 2010. Cited By (since 1996): 11.
- [32] S.-T. Hong and K. S. Weil, “Niobium-clad 304l stainless steel pemfc bipolar plate material: Tensile and bend properties,” *Journal of Power Sources*, vol. 168, pp. 408–417, 6/1 2007.
- [33] T. R. Ralph, G. A. Hards, J. E. Keating, S. A. Campbell, D. P. Wilkinson, M. Davis, J. St-Pierre, and M. C. Johnson, “Low cost electrodes for proton exchange membrane fuel cells: Performance in single cells and ballard stacks,” *Journal of the Electrochemical Society*, vol. 144, no. 11, pp. 3845–3857, 1997. Cited By (since 1996):225.
- [34] N. Yousfi-Steiner, P. Mootguy, D. Candusso, and D. Hissel, “A review on polymer electrolyte membrane fuel cell catalyst degradation and starvation issues: Causes, consequences and diagnostic for mitigation,” *Journal of Power Sources*, vol. 194, no. 1, pp. 130–145, 2009. Cited By (since 1996): 53.
- [35] C. Wieland, O. Schmid, M. Meiler, A. Wachtel, and D. Linsler, “Reliability computing of polymer-electrolyte-membrane fuel cell stacks through petri nets,” *Journal of Power Sources*, vol. 190, no. 1, pp. 34–39, 2009. Cited By (since 1996): 2.
- [36] M. Tanrioven and M. S. Alam, “Reliability modeling and analysis of stand-alone pem fuel cell power plants,” *Renewable Energy*, vol. 31, no. 7, pp. 915–933, 2006. Cited By (since 1996): 12.
- [37] S. G. Kandlikar and Z. Lu, “Thermal management issues in a pemfc stack - a brief review of current status,” *Applied Thermal Engineering*, vol. 29, no. 7, pp. 1276–1280, 2009. Cited By (since 1996):53.
- [38] ISO, “Hydrogen fuel – product specification – part 2: Proton exchange membrane (pem) fuel cell applications for road vehicles,” 2012.
- [39] T. Barlow, S. Latham, I. McCrae, and P. Boulter, “A reference book of driving cycles for use in the measurement of road vehicle emissions,” tech. rep., DfT, 2009.
- [40] F. A. D. Bruijn, V. A. T. Dam, and G. J. M. Janssen, “Review: Durability and degradation issues of pem fuel cell components,” *Fuel Cells*, vol. 8, no. 1, pp. 3–22, 2008. Cited By (since 1996): 168.
- [41] M. B. Satterfield, P. W. Majsztrik, H. Ota, J. B. Benziger, and A. B. Bocarsly, “Mechanical properties of nafion and titania/nafion composite membranes for polymer electrolyte membrane fuel cells,” *Journal of Polymer Science, Part B: Polymer Physics*, vol. 44, no. 16, pp. 2327–2345, 2006. Cited By (since 1996):88.
- [42] H. Wang, H. Li, and X. Yuan, eds., *PEM Fuel Cell Durability Handbook - Fuel Cell Failure Mode Analysis*, vol. 1. Boca Raton: CRC Press, 2012.
- [43] M. Inaba, T. Kinumoto, M. Kiriake, R. Umebayashi, A. Tasaka, and Z. Ogumi, “Gas crossover and membrane degradation in polymer electrolyte fuel cells,” *Electrochimica Acta*, vol. 51, no. 26, pp. 5746–5753, 2006. Cited By (since 1996):205.
- [44] T. Kinumoto, M. Inaba, Y. Nakayama, K. Ogata, R. Umebayashi, A. Tasaka, Y. Iriyama, T. Abe, and Z. Ogumi, “Durability of perfluorinated ionomer membrane against hydrogen peroxide,” *Journal of Power Sources*, vol. 158, no. 2 SPEC. ISS., pp. 1222–1228, 2006. Cited By (since 1996):142.
- [45] A. LaConti, M. Hamdan, R. McDonald, W. Vielstich, A. Lamm, and H. Gasteiger, eds., *Handbook of Fuel Cells: Fundamental, Technology, and Applications.*, vol. 3. 2003.

- [46] A. Pozio, R. F. Silva, M. D. Francesco, and L. Giorgi, "Nafion degradation in pefcs from end plate iron contamination," *Electrochimica Acta*, vol. 48, pp. 1543–1549, 5/15 2003.
- [47] Y. Zhai, H. Zhang, D. Xing, and Z.-G. Shao, "The stability of pt/c catalyst in h3po4/pbi pemfc during high temperature life test," *Journal of Power Sources*, vol. 164, pp. 126–133, 1/10 2007.
- [48] W. Li, Q. Xin, and Y. Yan, "Nanostructured ptfe/c cathode catalysts for direct methanol fuel cell: The effect of catalyst composition," *International Journal of Hydrogen Energy*, vol. 35, pp. 2530–2538, 3 2010.
- [49] M. Whiteley, A. Fly, J. Leigh, S. Dunnett, and L. Jackson, "Advanced reliability analysis of polymer electrolyte membrane fuel cells using petri-net analysis and fuel cell modelling techniques," *International Journal of Hydrogen Energy*, 2015. Article in Press.
- [50] J. Andr, L. Antoni, and J.-P. Petit, "Corrosion resistance of stainless steel bipolar plates in a pefc environment: A comprehensive study," *International Journal of Hydrogen Energy*, vol. 35, pp. 3684–3697, 4 2010.
- [51] K. Eom, E. Cho, S. W. Nam, T. H. Lim, J. H. Jang, H. J. Kim, B. K. Hong, and Y. C. Yang, "Degradation behavior of a polymer electrolyte membrane fuel cell employing metallic bipolar plates under reverse current condition," *Electrochimica Acta*, vol. 78, pp. 324–330, 2012.
- [52] Y. C. Chen, K. H. Hou, C. H. Lin, C. Y. Bai, N. W. Pu, and M. D. Ger, "A synchronous investigation of the degradation of metallic bipolar plates in real and simulated environments of polymer electrolyte membrane fuel cells," *Journal of Power Sources*, vol. 197, pp. 161–167, 2012. Cited By (since 1996): 1.
- [53] M. Whiteley, L. Jackson, and S. Dunnett, "Enhanced fault tree analysis and modelling considerations of a polymer electrolyte membrane fuel cell," in *Proceedings of the European Safety and Reliability Conference, ESREL*, p. 603, CRC Press, 29/09/2013 2013.
- [54] M. Whiteley, L. Jackson, and S. Dunnett, "Fault tree analysis of polymer electrolyte fuel cells to predict degradation phenomenon," in *Proceedings of the 20th Advances in Risk and Reliability Technology Symposium*, pp. 75–89, Loughborough University, 21/05/2013 2013.
- [55] E. A. Cho, U. S. Jeon, S. A. Hong, I. H. Oh, and S. G. Kang, "Performance of a 1 kw-class pemfc stack using tin-coated 316 stainless steel bipolar plates," *Journal of Power Sources*, vol. 142, pp. 177–183, 3/24 2005.
- [56] J. M. L. Canut, R. M. Abouatallah, and D. A. Harrington, "Detection of membrane drying, fuel cell flooding, and anode catalyst poisoning on pemfc stacks by electrochemical impedance spectroscopy," *Journal of the Electrochemical Society*, vol. 153, no. 5, pp. A857–A864, 2006. Cited By (since 1996):85.
- [57] M. Fowler, J. C. Amphlett, R. F. Mann, B. A. Peppley, and P. R. Roberge, "Issues associated with voltage degradation in a pemfc," *Journal of New Materials for Electrochemical Systems*, vol. 5, no. 4, pp. 255–262, 2002. Cited By (since 1996): 20.
- [58] N. Y. Steiner, D. Candusso, D. Hissel, and P. MooteGuy, "Model-based diagnosis for proton exchange membrane fuel cells," *Mathematics and Computers in Simulation*, vol. 81, no. 2, pp. 158–170, 2010. Cited By (since 1996): 1.
- [59] K. Teranishi, K. Kawata, S. Tsushima, and S. Hirai, "Degradation mechanism of pemfc under open circuit operation," *Electrochemical and Solid-State Letters*, vol. 9, no. 10, pp. A475–A477, 2006. Cited By (since 1996):89.

- [60] C. G. Chung, L. Kim, Y. W. Sung, J. Lee, and J. S. Chung, "Degradation mechanism of electrocatalyst during long-term operation of pemfc," *International Journal of Hydrogen Energy*, vol. 34, no. 21, pp. 8974–8981, 2009.
- [61] M. A. Freitas, M. L. G. de Toledo, E. A. Colosimo, and M. C. Pires, "Using degradation data to assess reliability: a case study on train wheel degradation," *Quality and Reliability Engineering International*, vol. 25, no. 5, pp. 607–629, 2009.
- [62] X. Huang, R. Solasi, Y. Zou, M. Feshler, K. Reifsnider, D. Condit, S. Burlatsky, and T. Madden, "Mechanical endurance of polymer electrolyte membrane and pem fuel cell durability," *Journal of Polymer Science, Part B: Polymer Physics*, vol. 44, no. 16, pp. 2346–2357, 2006. Cited By (since 1996): 89.
- [63] A. Fly and R. H. Thring., "Temperature regulation in an evaporatively cooled proton exchange membrane fuel cell stack," *International Journal of Hydrogen Energy*, vol. 40, no. 35, pp. 11976–11982, 2015.
- [64] A. Fly and R. H. Thring, "System thermal and water balance in an evaporatively cooled pem fuel cell vehicle," in *Institution of Mechanical Engineers - VTMS 2011, Vehicle Thermal Management Systems Conference Proceedings*, pp. 267–277, 2013.
- [65] A. Fly, "Thermal and water management of evaporatively cooled fuel cell vehicles, Published Phd, Loughborough University" 2015.
- [66] T. J. Mason, J. Millichamp, T. P. Neville, A. El-kharouf, B. G. Pollet, and D. J. L. Brett, "Effect of clamping pressure on ohmic resistance and compression of gas diffusion layers for polymer electrolyte fuel cells," *Journal of Power Sources*, vol. 219, pp. 52–59, 12/1 2012.
- [67] X. Wang, R. Kumar, and D. J. Myers, "Effect of voltage on platinum dissolution relevance to polymer electrolyte fuel cells," *Electrochemical and Solid-State Letters*, vol. 9, no. 5, pp. A225–A227, 2006.
- [68] M. Hu and G. Cao, "Research on the long-term stability of a pemfc stack: Analysis of pinhole evolution," *International Journal of Hydrogen Energy*, vol. 39, no. 15, pp. 7940–7954, 2014.
- [69] A. Taniguchi, T. Akita, K. Yasuda, and Y. Miyazaki, "Analysis of electrocatalyst degradation in pemfc caused by cell reversal during fuel starvation," *Journal of Power Sources*, vol. 130, pp. 42–49, 5/3 2004.
- [70] J. Wind, R. Sph, W. Kaiser, and G. Bhm, "Metallic bipolar plates for pem fuel cells," *Journal of Power Sources*, vol. 105, pp. 256–260, 3/20 2002.
- [71] S. J. Lee, K. T. Yang, Y. M. Lee, and C. Y. Lee, "The resistive properties of proton exchange membrane fuel cells with stainless steel bipolar plates," *Journal of Fuel Cell Science and Technology*, vol. 7, no. 4, pp. 0410041–0410045, 2010.
- [72] Pragma, "Development stack technical guide," 2014.
- [73] M. F. Serincan and U. Pasaogullari, "Mechanical behavior of the membrane during the polymer electrolyte fuel cell operation," *Journal of Power Sources*, vol. 196, no. 3, pp. 1303–1313, 2011.
- [74] J. H. Kim, E. A. Cho, J. H. Jang, H. J. Kim, T. H. Lim, I. H. Oh, J. J. Ko, and S. C. Oh, "Effects of cathode inlet relative humidity on pemfc durability during startup/shutdown cycling i. electrochemical study," *Journal of the Electrochemical Society*, vol. 157, no. 1, pp. B104–B112, 2010.

- [75] M. Whiteley, S. Dunnett, and L. Jackson, "Failure mode and effect analysis, and fault tree analysis of polymer electrolyte membrane fuel cells," *International Journal of Hydrogen Energy*.

Appendix A

FMEA

Identification	Function	Failure Mode	Local Effect	System Effect	Failure detection method	Mitigation Strategy	Remarks	Relationship	Source
1.0 Polymer Electrolyte Membrane	The 'heart' of the PEMFC. Forms the electrolyte at the centre of the cell. Blocks passage of gasses and electrons, but facilitates passage of hydrogen protons from anode to cathode side.	1.0/1.1 Incorrect BIP torque	Local mechanical stress due to increased pressure. Increase of membrane resistance, consistent with the viscoelastic compression of the membrane.	Reduced passage of H+ protons. Reduction in voltage output	Polarisation Curve, Linear sweep Voltammetry, Electrochemical Impedance Spectroscopy	Check bipolar plate compression torque is suitable for the application		Oxide Film Formation (BIP), Flooding, Ice Formation, Creep.	Satterfield, et al. (2006) Mechanical properties of Nafion and titania/Nafion composite membranes for polymer electrolyte membrane fuel cells. & Wang, H, et al. (2012) PEM fuel cell failure mode analysis. New York, CRC Press. (pp87) & Borup, R, et al. (2007) Scientific aspects of polymer electrolyte fuel cell durability and degradation. Chemical Review, vol. 107, pp3927.
		1.0/1.2 Polymer membrane 'creep'	Causing membrane thinning and pinhole formation	Reduction in voltage output, leading to ultimate catastrophic degradation	Polarisation Curve, Linear sweep Voltammetry	Check bipolar plate compression torque is suitable for the application	Can take 1000's of hours to cause catastrophic failure when at normal operating conditions (hydrated and below 80oC)	Membrane relative humidity, mechanical damage,	Wang, H, et al. (2012) PEM fuel cell failure mode analysis. New York, CRC Press. (pp87)

		1.0/2.1 OH and OOH radicals \& H2O2 contamination to PTFE	End group unzipping. The Polytetrafluoroethylene (PTFE) core material is modified with side chains of Perfluoro-sulfonic acid Ionomers. These can be lost through OH and OOH radical attack. (PFSI) membrane	Weaker membrane, and therefore increase in risk of mechanical damage. Reduction in voltage output. Additional effect from poisoning of active sites	Electron Spin Resonance (ESR) spectroscopy, Polarisation Curve, Linear Sweep Voltammetry, Gas Mass Spectrometry	Modifying polytetrafluoroethylene with in situ sol-gel polymerization of titanium isopropoxide to generate titania quasinetworks in the polar domains of a polymer electrolyte membrane fuel cell, can mitigate against the risk of H2 and O2 gas crossover.	Low humidity and OCV can exacerbate the attack and degradation	Protonic resistance of membrane, H2O2 formation, Mechanical Damage	Wang, H, et al. (2012) PEM fuel cell failure mode analysis. New York, CRC Press. (pp87)
		1.0/3 Presence of foreign cationic ions: Dissolution of metal ions from BIP corrosion / Contaminant from humidifier/air pipe/gas impurity	Adsorption onto membrane or catalyst. Foreign ions have stronger affinity with H+ ions in membrane. Attenuated water flux and proton conductivity, extensive and fast dehydration of membrane	Reduction in voltage output	Polarisation Curve, Cyclic Voltammetry, Gas Mass Spectrometry		Source could be BIP corrosion, humidifier or inlet piping ion leach	Metal ion release from Bipolar plate can catalyse the OH & OOH radical formation	J. Wu et al, (2008) 'A review of PEM fuel cell durability: Degradation mechanisms and mitigation strategies' pp110-111

		1.0/3.1 Ice Formation	Severly impaired mechanical strength due to water molecules not bonded to membrane can freeze below 0deg. Freeze cycling rearranges ionomer at molecular level	Reduction in membrane strength, decreases voltage output	Polarisation Curve, Thermocouple	Purge gas and solution to remove excess water for start-up shutdown cycles, and avoid operation in sub-zero environments	Improves through-the-plane conductivity, however reduces the mechanical strength of the membrane material	Swelling of membrane, reactant maldistribution	McDonald, et al. (2004) Fuel Cells 4
			Severly impaired gas impermeability	Reduction in membrane strength, increases voltage output	Polarisation Curve, Thermocouple	Purge gas and solution to remove excess water for start-up shutdown cycles, and avoid operation in sub-zero environments			McDonald, et al. (2004) Fuel Cells 4
			Severly impaired ionic conductivity	Reduction in membrane strength, increases voltage output	Polarisation Curve, Thermocouple	Purge gas and solution to remove excess water for start-up shutdown cycles, and avoid operation in sub-zero environments			McDonald, et al. (2004) Fuel Cells 4
			Swelling of membrane, increased pressure on membrane and reduced protonic conductivity	Reduction in membrane strength, increases voltage output	Polarisation Curve, Thermocouple	Purge gas and solution to remove excess water for start-up shutdown cycles, and avoid operation in sub-zero environments			McDonald, et al. (2004) Fuel Cells 4

		1.0/3.2 Fatigue from Relative Humidity and Temperature cycling	Weakness in mechanical strength of membrane	Increased probability of pin-hole formation	Polarisation Curve, Electrochemical Impedance Spectroscopy, Linear Sweep Voltammetry	Control strategy to maintain linear level of RH and temperature		Dehydration causes weakening of membrane.	
		1.0/3.3 Excessive Heat Degradation	Sulphur Dioxide OH radical formation	Reduction in voltage output	Polarisation Curve	Don't allow operating temperature to exceed expected range		Relative humidity	Placca, L \& Kouta, R. (2011) Fault tree analysis for PEM fuel cell degradation process modelling. Vol. 36. pp12393-12405
			Glass transition of PSFA polymers	Reduction in voltage output	Polarisation Curve	Don't allow operating temperature to exceed expected range		Relative humidity	Placca, L \& Kouta, R. (2011) Fault tree analysis for PEM fuel cell degradation process modelling. Vol. 36. pp12393-12405
			Drop in protonic conductivity due to lack of membrane hydration	Reduction in voltage output	Polarisation Curve	Don't allow operating temperature to exceed expected range		Relative humidity	Schmittinger, W \& Vahidi, A. (2008) A review of the main parameters influencing long-term performance and durability of PEM fuel cells. Journal of Power Sources 180 (2008) 1-14

		1.0/4 Flooding	Swelling of membrane, increased pressure on membrane and reduced protonic conductivity	Reduced protonic conductivity. Reduction in voltage output	Polarisation Curve, Electrochemical Impedance Spectroscopy, Cyclic Voltammetry	Purge gas and solution to remove excess water for start-up shutdown cycles		Swelling of membrane, relative humidity	
2.0 Catalyst Layer	Layer sandwiched between PEM and GDL. Facilitates electrochemical reaction kinetics of the HOR and ORR.	2.0/1 Pt agglomeration and particle growth	Pt nanoparticles have inherent tendency to combine to reduce their high surface energy. This agglomeration reduces the electrochemically active surface area. Reducing voltage output	Reduction in voltage output	Ex situ transmission electron microscopy (TEM), X-ray diffraction (XRD) using Averbach Fourier transform method for determination of weighted crystallite sizes. Polarisation Curve. Cyclic Voltammetry		Borup et al (2006) showed that Pt particle growth increases with temperature. Critically when increasing temp from 60 - 80°C. Ref (p12 in Wang book)		Wang, H, et al. (2012) PEM fuel cell failure mode analysis. New York, CRC Press. (pp87) & Borup, R, et al. (2007) Scientific aspects of polymer electrolyte fuel cell durability and degradation. Chemical Review, vol. 107, pp3927.
		2.0/2 Pt Elemental loss	Pt nanoparticles detaching from carbon support and dissolving into PEM without redistribution	Reduction in voltage output	Atomic Adsorption Spectroscopy (AAS) & Inductively Coupled Plasma with Mass Spectroscopy (ICP-MS). Cyclic Voltammetry				Wang, H, et al. (2012) PEM fuel cell failure mode analysis. New York, CRC Press. (pp87)

		2.0/3 Pt Migration	Pt nanoparticles move from original position to other areas of the cell, such as the membrane or other areas of the catalyst layer.	Reduction in voltage output	Atomic Adsorption Spectroscopy (AAS) \& Inductively Coupled Plasma with Mass Spectroscopy (ICP-MS) Cyclic Voltammetry				Wang, H, et al. (2012) PEM fuel cell failure mode analysis. New York, CRC Press. (pp87)
		2.0/4 Pt Contamination	Gas contaminants from the fuel, air or system-born contaminants such as silicone or metals, can poison the catalyst layer.	Reduction in reaction kinetics (poisoned reaction sites), Drop in output voltage	Atomic Adsorption Spectroscopy (AAS) \& Inductively Coupled Plasma with Mass Spectroscopy (ICP-MS) Cyclic Voltammetry				Wang, H, et al. (2012) PEM fuel cell failure mode analysis. New York, CRC Press. (pp87)
				Reduced ionic conductivity of PEM, Drop in output voltage					Wang, H, et al. (2012) PEM fuel cell failure mode analysis. New York, CRC Press. (pp87)
				Mass transportation problems due to change in structure of GDL and catalyst layer, Drop in output voltage					Wang, H, et al. (2012) PEM fuel cell failure mode analysis. New York, CRC Press. (pp87)

		2.0/4.1 CO Contamination	CO takes up active sites on the Pt catalyst, thus blocking active sites and reducing the ECSA	Reduction in reaction kinetics (poisoned reaction sites), Drop in output voltage	Polarisation Curve, Electrochemical Impedance Spectroscopy, Cyclic Voltammetry, Gas Mass Spectrometry		Can be reversed with purge of H ₂ gas feed at periodic intervals		
		2.0/4.2 Anion Contamination	Cl ⁻ from feed stream or catalyst preparation promotes dissolution of Pt and produces Pt ions in the inlet side of cathode. Crossover of H ₂ reduces the Pt ions to metal Pt causing Pt band in PEM.	Reduction in reaction kinetics (poisoned reaction sites), Drop in output voltage	Polarisation Curve, Cyclic Voltammetry, Gas Mass Spectrometry				
		2.0/4.3 Other Contaminants	NH ₃ , SO _x and NO ₂ in the airstream cause catalyst degradation.		Polarisation Curve, Cyclic Voltammetry, Gas Mass Spectrometry				
		2.0/4.3.1 NH ₃	NH ₃ degrades the ionomer in the CL	Reduction in reaction kinetics (poisoned reaction sites), Drop in output voltage	Polarisation Curve, Cyclic Voltammetry, Gas Mass Spectrometry				

		2.0/4.3.2 SOx	S-containing species adsorbs on the active sites of a c catalyst surface, occupying the polyatomic sites.	Reduction in reaction kinetics (poisoned reaction sites), Drop in output voltage	Polarisation Curve, Cyclic Voltammetry, Gas Mass Spectrometry				
		2.0/5 Presence of foreign cationic ions: Dissolution of metal ions from BIP corrosion / Contaminant from humidifier/air pipe/gas impurity	Adsorption onto membrane or catalyst. Foreign ions have stronger affinity with H+ ions in membrane. Attenuated water flux and proton conductivity, extensive and fast dehydration of membrane	Reduction in voltage output	Polarisation Curve, Gas Mass Spectrometry		Leads on to reactant maldistribution. Which can either cause: Electron pathway cut-off, delamination of membrane, or Pt agglomeration/dissolution. All classed under Carbon support degradation	Metal ion release from Bipolar plate can catalyse the OH & OOH radical formation	J. Wu et al, (2008) 'A review of PEM fuel cell durability: Degradation mechanisms and mitigation strategies' pp110-111
		2.0/6 Startup/Shutdown Cycling	Reactant maldistribution / non-uniform reactant distribution, leading to either carbon black corrosion mechanism	Reduction in Voltage output			Leads on to reactant maldistribution. Which can either cause: Electron pathway cut-off, delamination of membrane, or Pt agglomeration/dissolution. All classed under Carbon support degradation		J. Wu et al, (2008) 'A review of PEM fuel cell durability: Degradation mechanisms and mitigation strategies' pp110-111

		2.0/7 Flooding	Blockage of porous pathways, leading to reactant mal-distribution	Reduction in Voltage output	Polarization curve	Purge gas and solution to remove excess water for start-up shutdown cycles.	Leads on to reactant mal-distribution. Which can either cause: Electron pathway cut-off, delamination of membrane, or Pt agglomeration/dissolution. All classed under Carbon support degradation		J. Wu et al, (2008) 'A review of PEM fuel cell durability: Degradation mechanisms and mitigation strategies' pp110-111
		2.0/8 Ice Formation	Blockage of porous pathways, leading to reactant mal-distribution	Reduction in Voltage output	Polarization curve/ Thermocouple measurements	Purge gas and solution to remove excess water for start-up shutdown cycles, and avoid operation in sub-zero environments	Leads on to reactant mal-distribution. Which can either cause: Electron pathway cut-off, delamination of membrane, or Pt agglomeration/dissolution. All classed under Carbon support degradation		J. Wu et al, (2008) 'A review of PEM fuel cell durability: Degradation mechanisms and mitigation strategies' pp110-111

3.0 Gas Diffusion Layer	Provides electrical conductivity from reaction site to external circuit. Also known as 'electrode'. GDL is porous carbon with PTFE coatings, the porosity diffuses the reaction gasses and disperses them to the reaction sites on the catalyst layer.	3.0/1.0 OH Radicals contamination to PTFE	OH radicals attack the carbon material in the PTFE and Carbon support, decreasing GDL conductivity and hydrophobicity	Reduction in voltage output	Polarisation Curve, Cyclic Voltammetry, Gas Mass Spectrometry	Using graphitized fibers during GDL preparation to improve GDL oxidative and electrooxidative stability.			J. Wu et al, (2008) 'A review of PEM fuel cell durability: Degradation mechanisms and mitigation strategies' pp110-111
		3.0/1.1 OH Radicals contamination to Carbon	OH radicals attack the carbon material in the PTFE and Carbon support, decreasing GDL conductivity and hydrophobicity	Reduction in voltage output	Polarisation Curve, Cyclic Voltammetry, Gas Mass Spectrometry	Using graphitized fibers during GDL preparation to improve GDL oxidative and electrooxidative stability.			J. Wu et al, (2008) 'A review of PEM fuel cell durability: Degradation mechanisms and mitigation strategies' pp110-111
		3.0/2 Flooding of GDL	Water molecules blocking the passage of gas through the pores of the GDL material	Loss of reaction kinetics, resulting in drop in voltage output until failure of cell	Polarisation Curve, Electrochemical Impedance Spectroscopy	Purge gas and solution to remove excess water for start-up shutdown cycles.			Wang, H, et al. (2012) PEM fuel cell failure mode analysis. New York, CRC Press. (pp87)

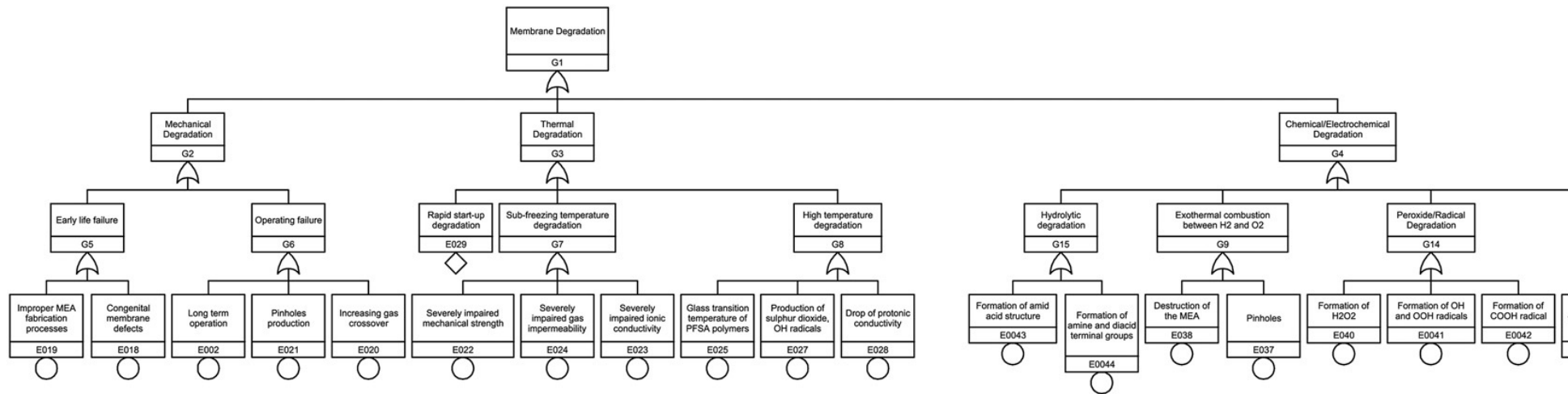
		3.0/3 Water freezing in GDL	Frozen water molecules blocking the passage of gas through the pores of the GDL material	Loss of reaction kinetics, resulting in drop in voltage output until failure of cell	Polarisation Curve, Electrochemical Impedance Spectroscopy	Purge gas and solution to remove excess water for start-up shutdown cycles, and avoid operation in sub-zero environments			Wang, H, et al. (2012) PEM fuel cell failure mode analysis. New York, CRC Press. (pp87)
			Inerfacial delamination due to freeze/thaw cycling. Caused by expansion and contraction of pores during freeze thaw cycling.	Drop in output voltage	Polarisation Curve, Electrochemical Impedance Spectroscopy	Purge gas and solution to remove excess water for start-up shutdown cycles, and avoid operation in sub-zero environments			Wang, H, et al. (2012) PEM fuel cell failure mode analysis. New York, CRC Press. (pp87)
4.0 Bipolar Plate	The BIP is a multifunctional component of a PEMFC. It separates fuel, oxidant gas and coolant; homogeneously distributing reactant gasses to the GDL. It also collects the current from the FC reaction, delivering it to the external circuit.	4.0/1 Oxide film formation	An oxide film layer can form at the junction between GDL and BIP. This can increase in size and increase internal resistance to current flow.	Drop in output voltage due to resistance increase	Polarisation Curve, Gas Mass Spectrometry, Electrochemical Impedance Spectroscopy			Swelling	J. Wu et al, (2008) 'A review of PEM fuel cell durability: Degradation mechanisms and mitigation strategies' pp110-111

		4.0/2 Corrosion leading to release of multivalent cations	The chemical corrosion of alloys can release Fe, Ni and Cr atoms.	Reduction in output voltage	Polarisation Curve, Gas Mass Spectrometry			Catalyses H ₂ O ₂ formation	J. Wu et al, (2008) 'A review of PEM fuel cell durability: Degradation mechanisms and mitigation strategies' pp110-111
--	--	---	---	-----------------------------	---	--	--	---	--

Table A.1: Failure Mode and Effect Analysis

Appendix B

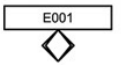
Placca & Kouta FTA [30]



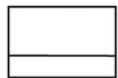
Legend



Basic Event named « E001 »



Event difficult to develop named « E001 »

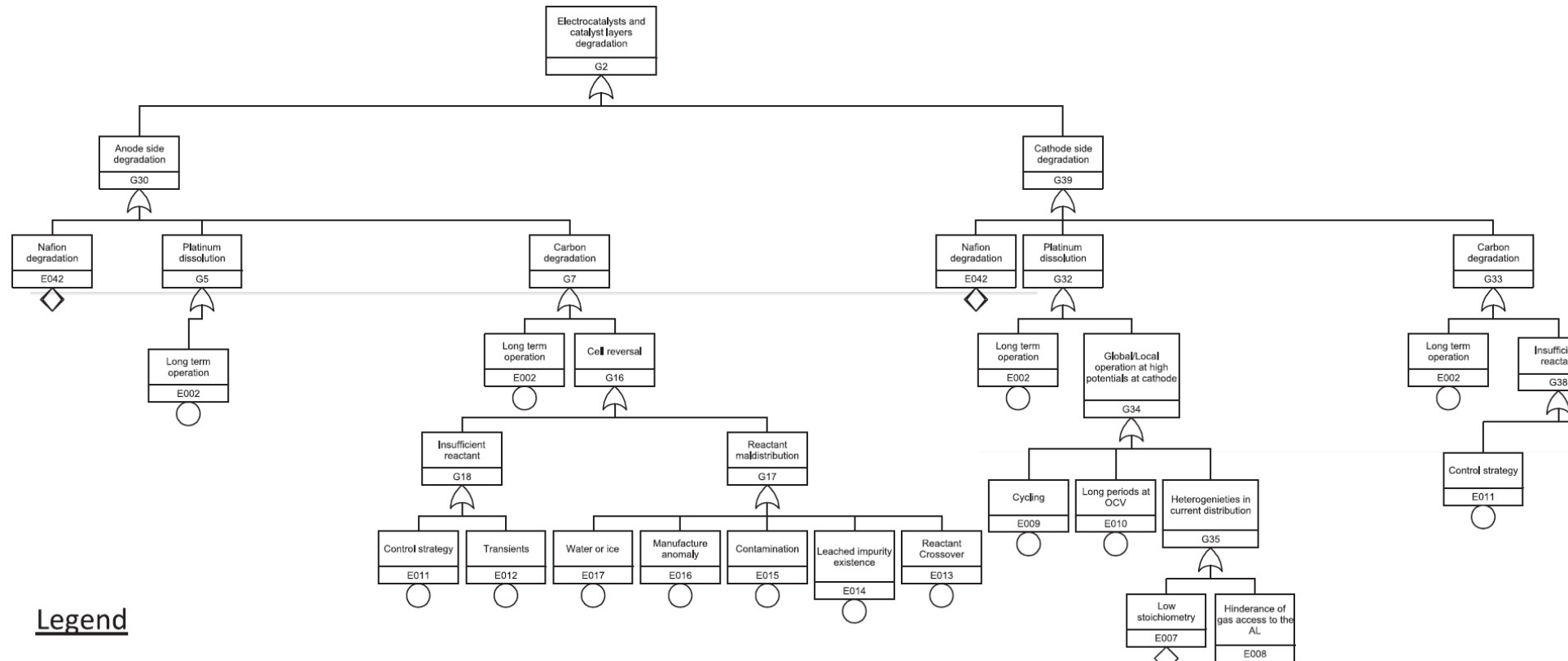


Intermediate Event: a fault event that occurs because one or more antecedent causes acting through logical gates

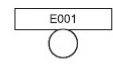
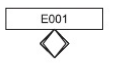
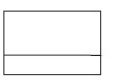



« OR » gate : the causes that can independently bring about the undesired event are arrayed horizontally below the « OR » symbol

Figure B.1: Membrane Layer



Legend

- 
Basic Event named « E001 »
- 
Event difficult to develop named « E001 »
- 
Intermediate Event: a fault event that occurs because one or more antecedent causes acting through logical gates
- 
« OR » gate : the causes that can independently bring about the undesired event are arrayed horizontally below the « OR » symbol

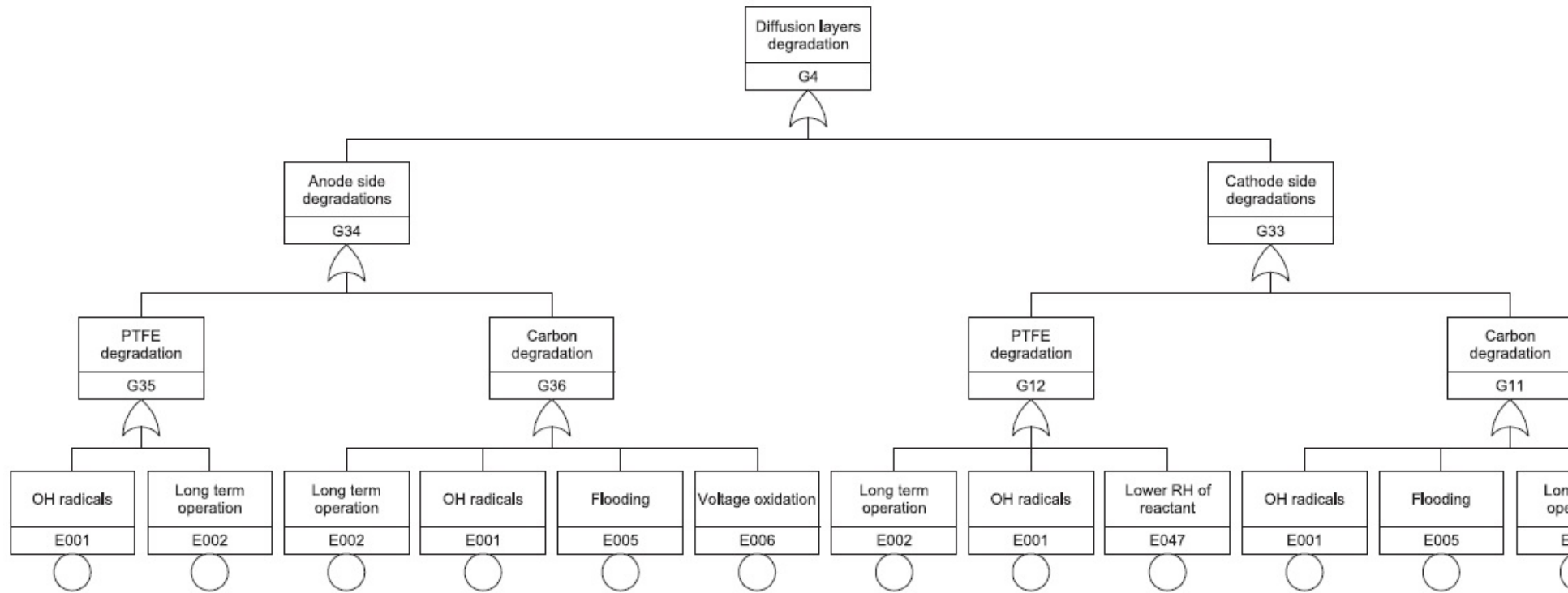


Figure B.3: Gas Diffusion Layer

Appendix C

Rama FMEA & FTA [30]

Degradation / Failure Mode	Fuel Cell Component	Fault	Cause	References	
D1. Increase of Activation Losses	Platinum catalyst	(1) Platinum agglomeration causing loss of EASA	(1) Repetitive on/off load cycling (2) High voltage induce at cathode equivalent to OCV due to residual hydrogen (3) Loss of carbon support	[7] [7] [8] [9]	
		(2) Platinum migration causing loss of catalyst material	(4) Solubility of platinum when cell is operated through hydrogen-air open circuit to air-air open circuit (5) Air impurities such as NO ₂ , SO ₂ and H ₂ S	[10] [11] [12]	
		(3) Adsorption of atmospheric contaminants on platinum causing loss of EASA	(6) Fuel impurities such as CO and CO ₂	[13] [14] [15] [16]	
		(4) Adsorption of fuel impurities on platinum causing loss of EASA	(7) Chemical degradation of silicone sealant	[17]	
		(5) Loss of catalyst due to chemical attack and formation of silicone/oxygen/platinum particles	(8) Residual water in catalyst layers	[18]	
D2. Increase of Mass Transportation Losses	Geometric structure of the catalyst layer	(6) Deformation of catalyst structure by freezing and melting water, resulting in increased pore size and reduced EASA	(9) Fuel starvation (10) Partial coverage of hydrogen on catalyst sites (11) Localised flooding	[19] [20] [19] [20] [19] [20]	
	Carbon support in catalyst layer	(7) Corrosion of carbon to support the current above that provided by the fuel when the cell is supplied with insufficient fuel to support the current drawn	(12) Low flow rate of channel gases (13) Low pressure in gas flow channels (14) Flow-field geometry (15) Degradation of polymer electrolyte in catalyst layer due to impurity ions	[21] [22] [23] [24] [25] [26] [27]	
	Porous and void regions of the cell; catalyst layers, GDLs, BPP flow fields	(8) Flooding caused by the accumulation and condensation of water vapour to induce two-phase flow	(16) Gradual loss of material due to repeated thermal cycling (17) Delamination caused by repeated thermal cycling (18) Damage to material caused by exposure to sub-zero conditions (19) Cell over-compression, impacting the GDL	[28] [29] [28] [29] [30]	
	Geometric structure of catalyst layer	(9) Loss of hydrophobicity in porous regions of the cell treated with hydrophobic material	(20) Ionomer expansion on water uptake causing pores to collapse (21) Excessive ionomer loading (22) Formation of ionomer skins on catalyst layers during the standard decal/hot-press-transfer method	[31] [32] [33]	
		(10) Impedance to transport attributable to presence of ionomer	(23) Presence of residual water from previous shut-down (24) Operation at sub-zero temperatures	[34] [35]	
	GDL	(11) Impedance to transport attributable to ice formation	(25) Over-compression and inhomogeneous compression, induced during cell assembly or by warping of injection-moulded BPPs	[36] [37] [38]	
		(12) Loss of porosity, increased flooding and reduced gas permeability	(26) Impedance to electron transfer due to passivating layer on SS surface	[39]	
	D3. Increase of Ohmic Losses (D3)	Stainless-steel BPP	(13) Loss of surface electrical conductivity	(27) Coating defects such as pinholes and micro-cracks when coated with TiN (28) Degradation of conductive coating (29) Degradation of conductive polymer coating	[40] [41]
		Coated stainless-steel BPP	(-) Loss of surface electrical conductivity	(30) Formation of polymer-rich boundary during injection-moulding process	[42]
		Injection-moulded BPP	(14) Low electrical conductivity	(31) Loss of membrane hydration (32) Replacement of protons by impurity ions causing decrease in the water diffusion coefficient and increase in water transfer coefficient (33) Anisotropic swelling of membrane causing the water diffusion coefficient to decrease	[43] [44]
	Polymer Electrolyte Membrane	(15) Loss of proton conductivity			

Degradation / Failure Mode	Fuel Cell Component	Fault	Cause
D4. Increase of Efficiency Loss, potentially leading to Catastrophic Cell Failure	Polymer electrolyte membrane	(16) Formation of cracks and pinholes	(34) Increased roughness of electrolyte membrane surface, inducing by sub-zero operating conditions (35) Mechanical stresses induced by thermal hotspots in regions of strong electrical contact (i.e., GDL and BPP shoulder), high compression, and high reaction rates (36) Defects during the manufacturing process (37) Peroxide and peroxide radical attack of polymer end groups (38) Repetitive swelling/contraction due to excursion of membrane to states of deep hydration and deep dehydration (39) Excessive pressure differential between anode and cathode gas supply
Catastrophic Cell Failure	GDL/catalyst layer/membrane	(17) Delamination of layers	(40) Thermal cycling including exposure to sub-zero conditions
	Catalyst layer	(18) Excessive adsorption of atmospheric and fuel impurities	(41) Loss of contaminant tolerance
	BPP	(19) Cracking	(42) Inhomogeneous compression (43) Mechanical shock/vibration (44) Irregularities in cell/stack construction
	Seal	(20) Warping (21) Gas leakage	(45) Low initial rigidity of polymer matrix (46) Oxidation of seals
	Polymer electrolyte membrane	(22) Short circuit	(47) Formation of electrical network due to mal-distribution of platinum within (self-humidifying) membrane

Figure C.2: FMEA Part 2

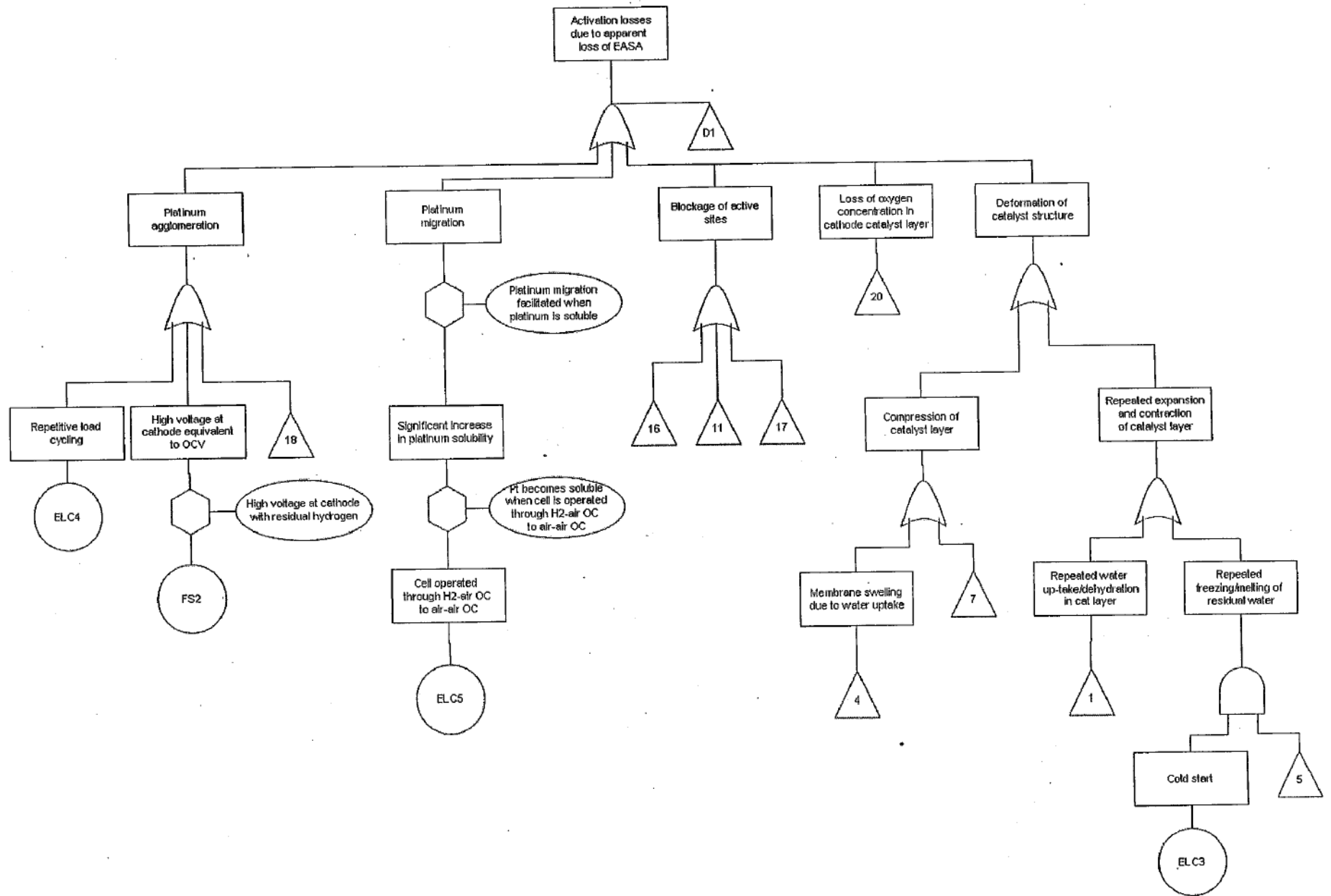


Figure C.3: FTA for Activation losses

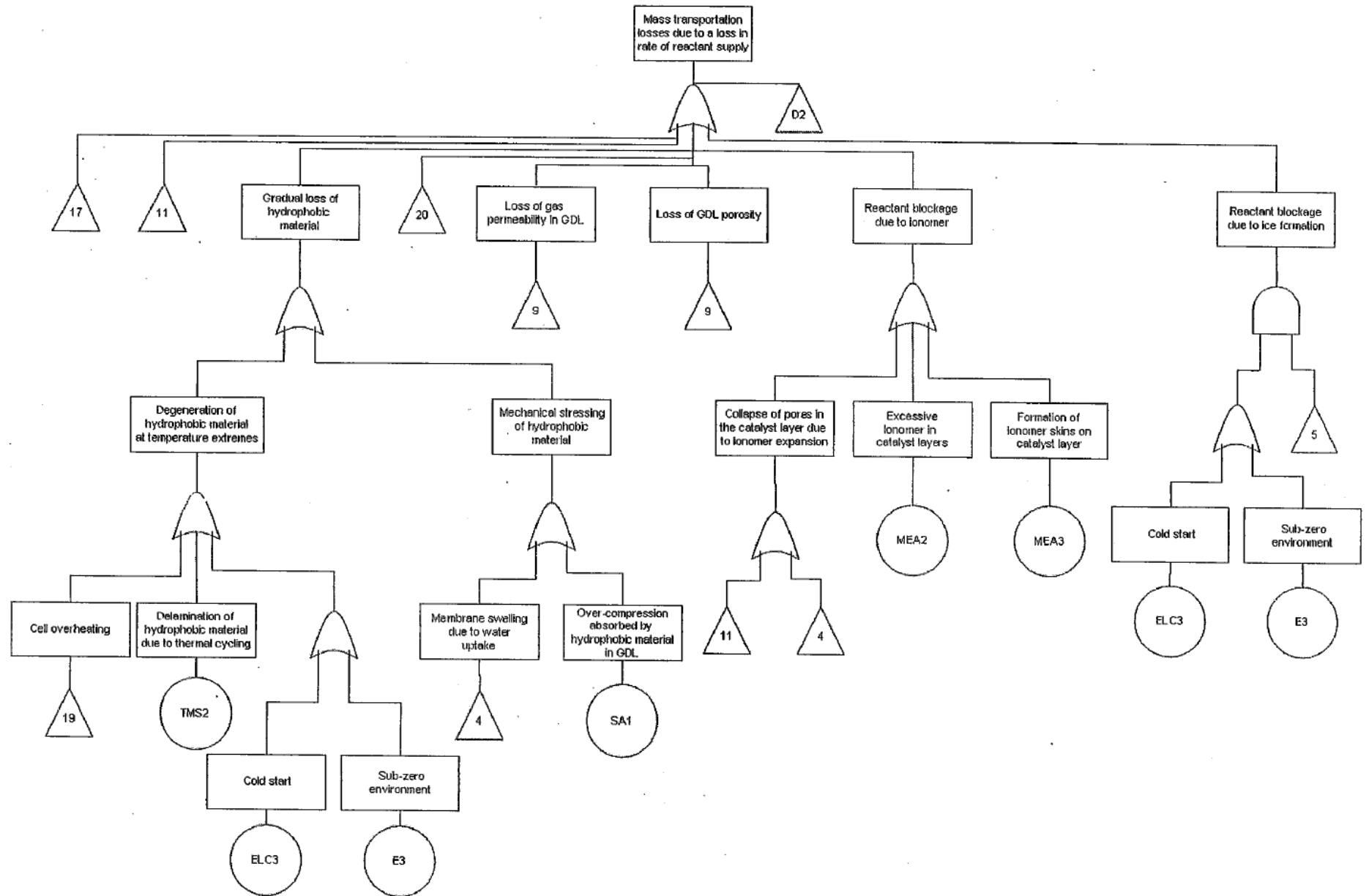


Figure C.4: FTA for Mass Transport Losses

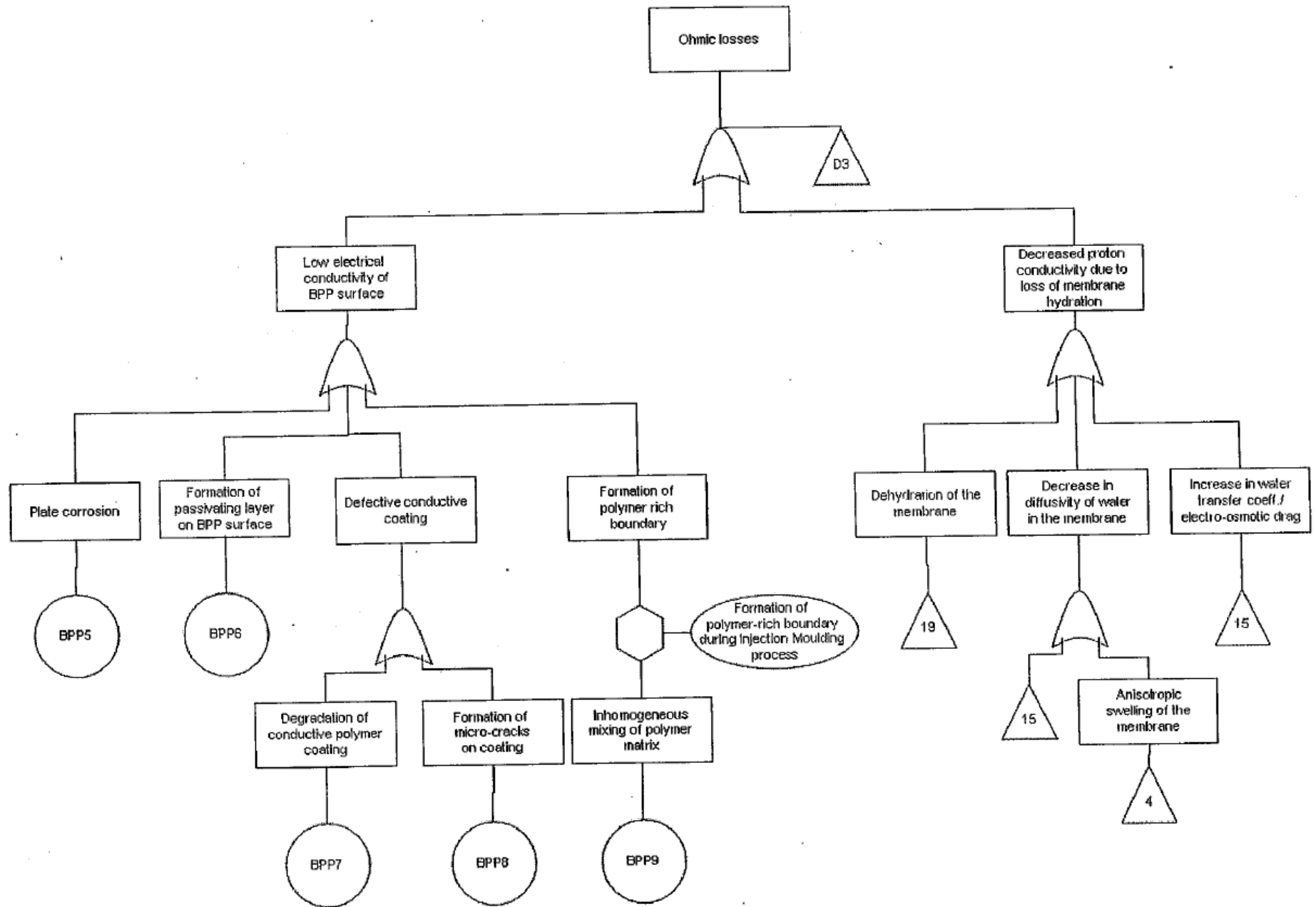


Figure C.5: FTA for Ohmic losses

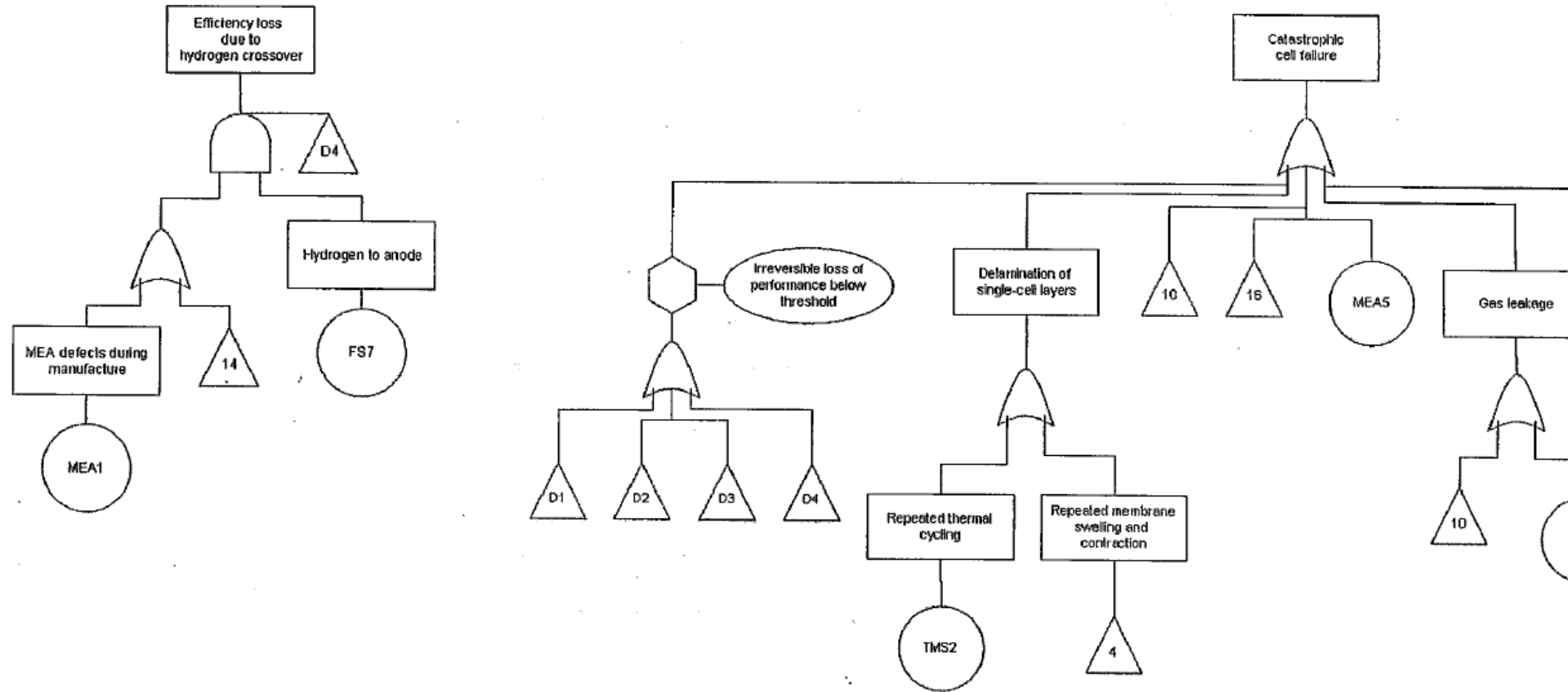


Figure C.6: FTA for Gas Crossover and Catastrophic losses

Appendix D

Petri-Net Degradation Modules

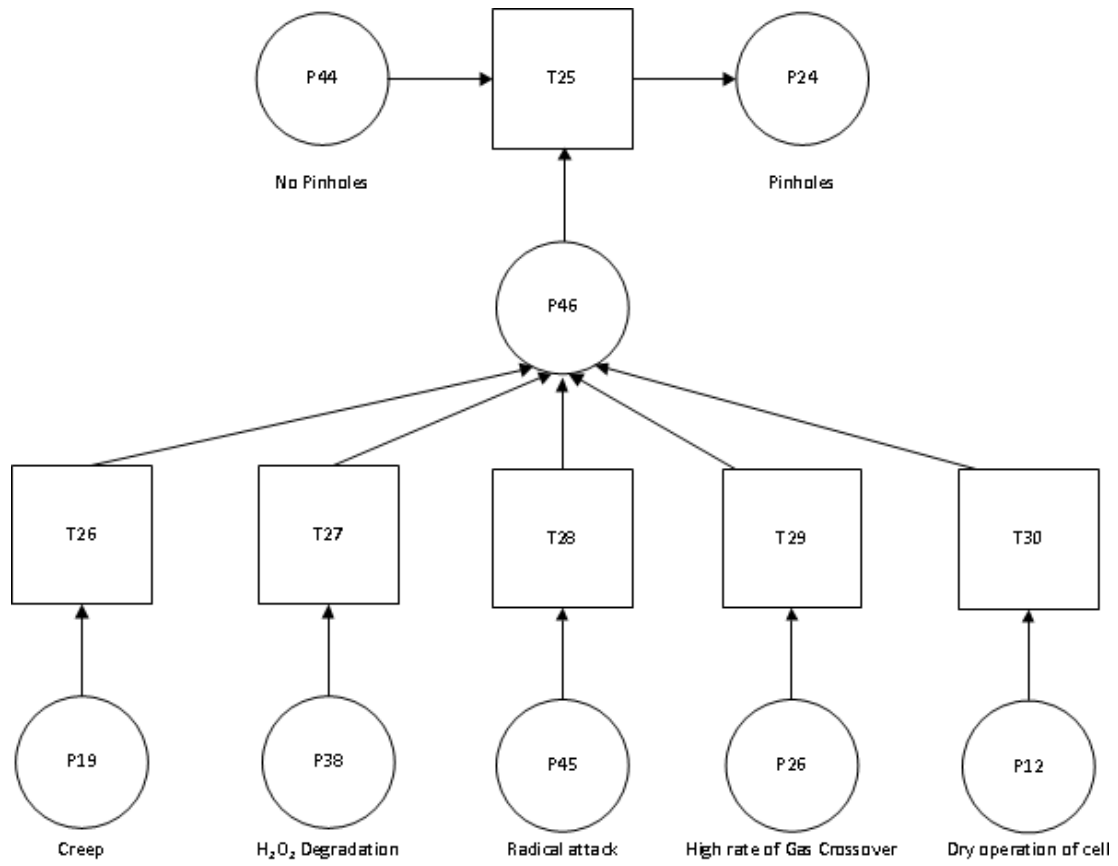


Figure D.1: Pinholes

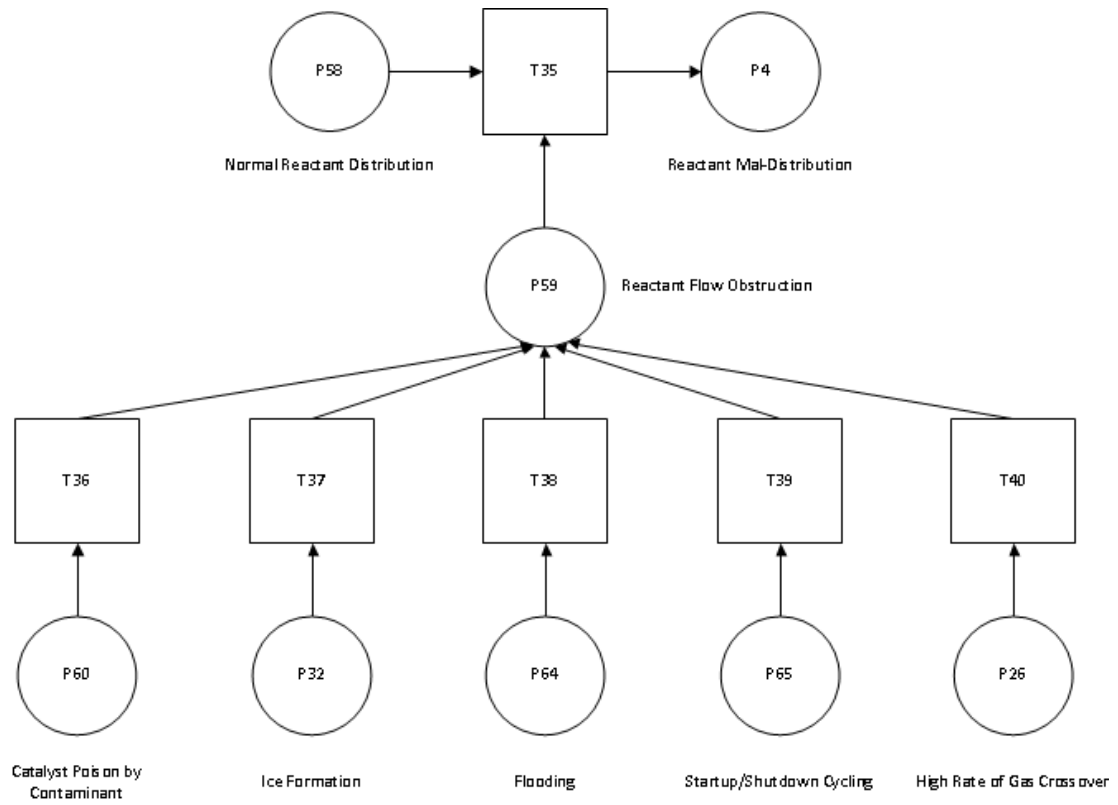


Figure D.2: Reactant MAI-Distribution

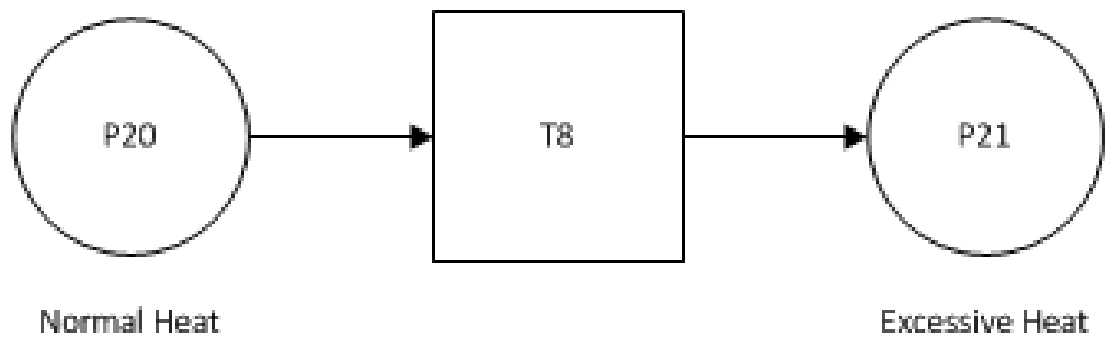


Figure D.3: Excess Heat

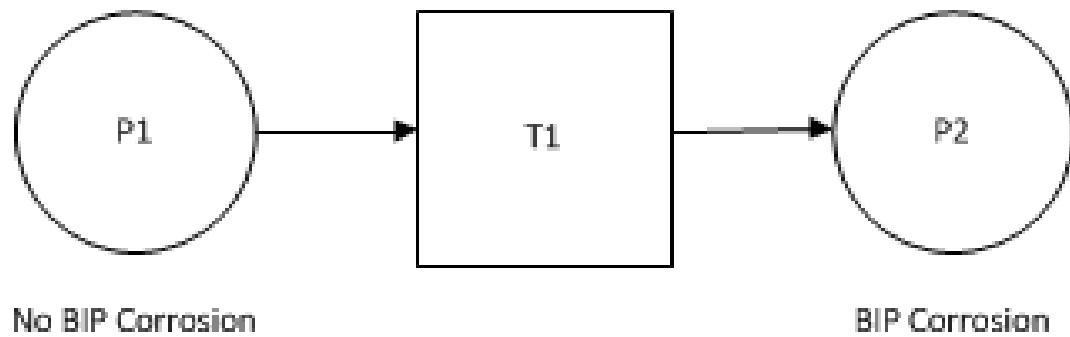
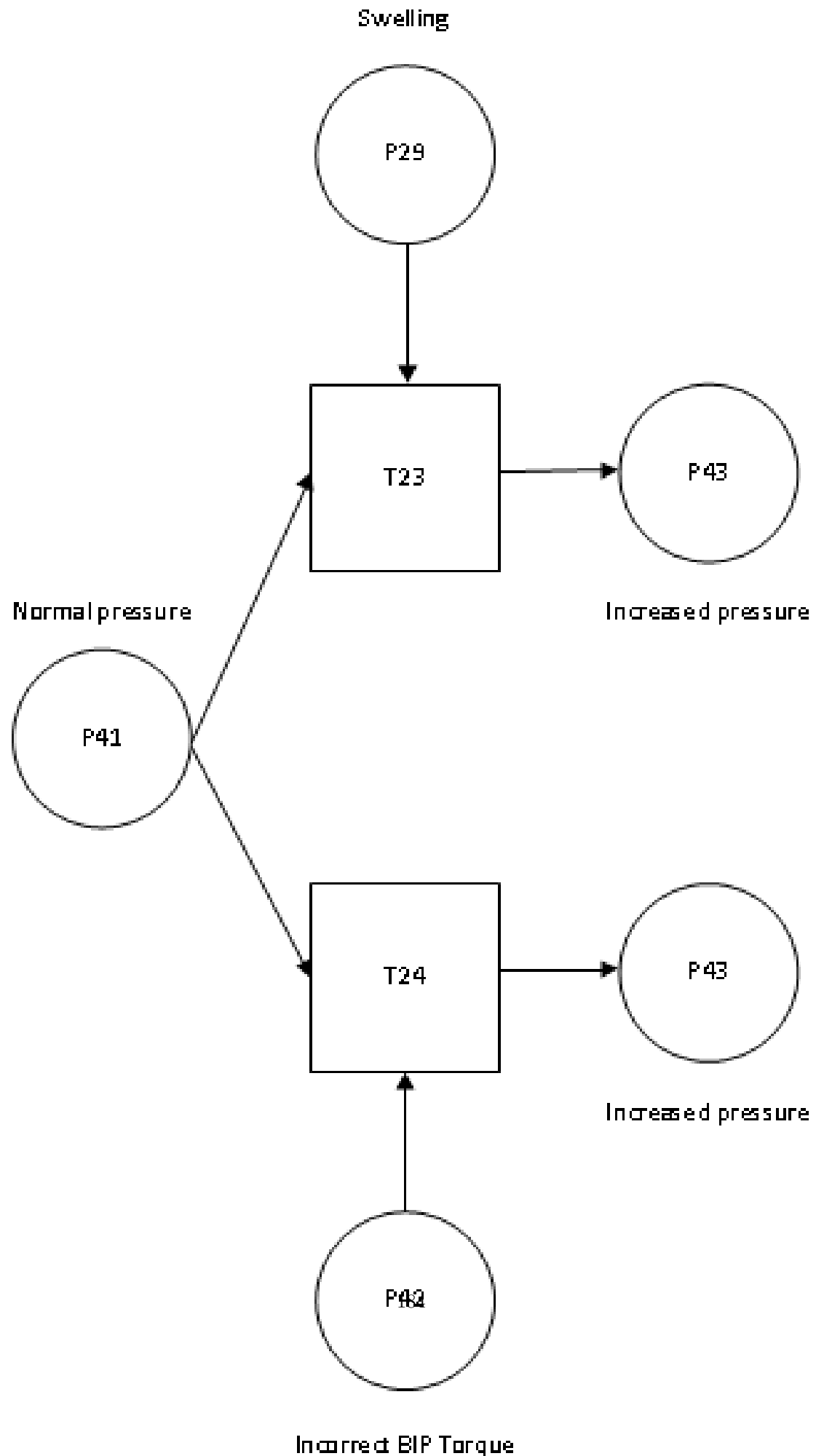


Figure D.4: Bipolar Plate Degradation



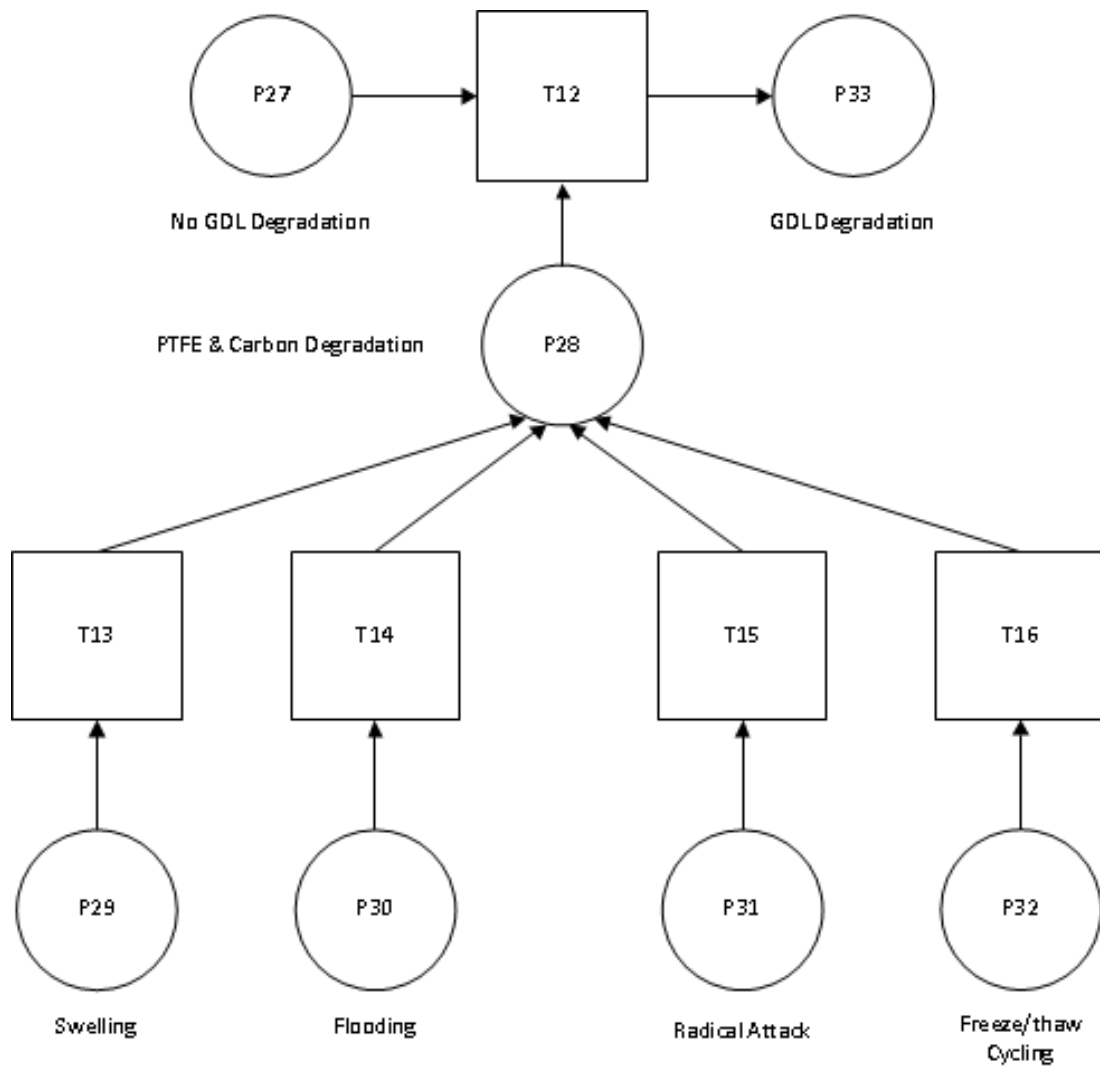


Figure D.6: Gas Diffusion Layer Degradation

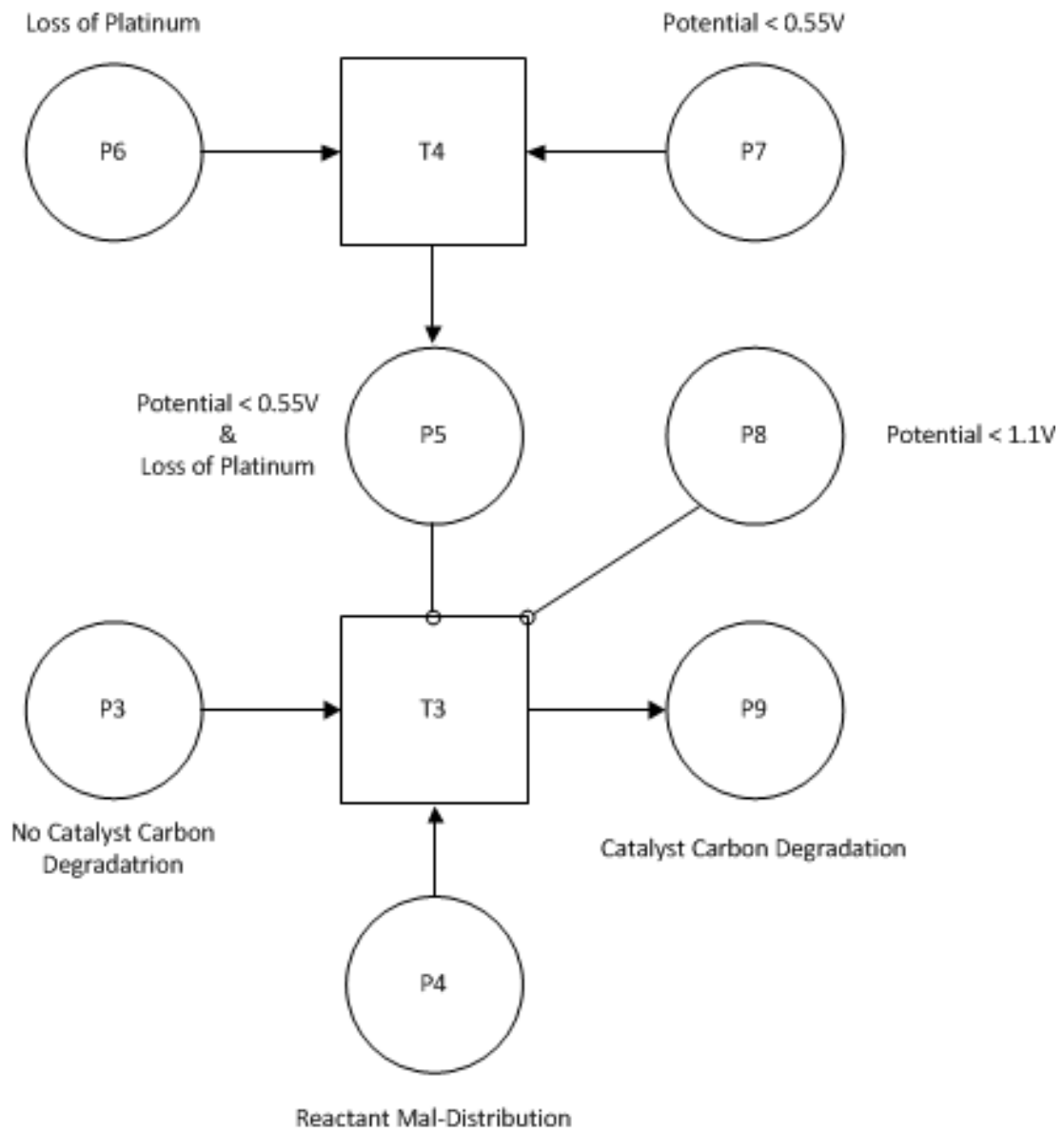


Figure D.7: Catalyst Carbon Degradation

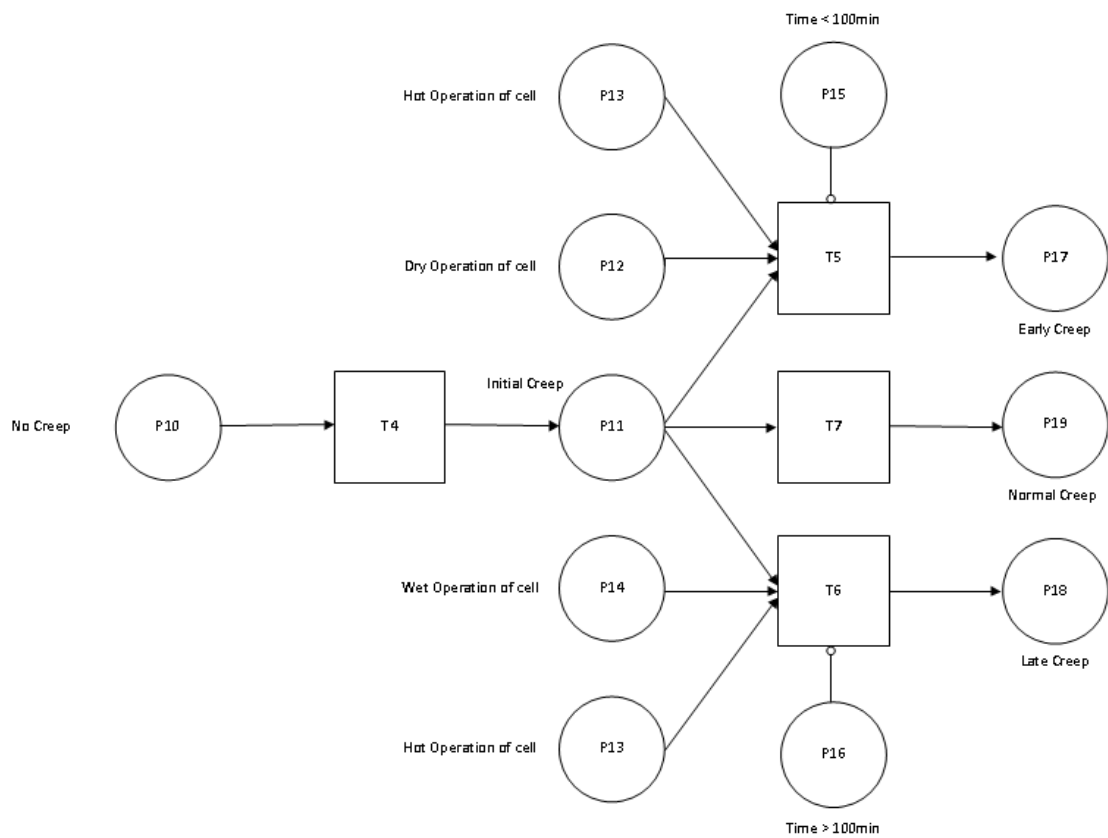


Figure D.8: Polymer Membrane Creep

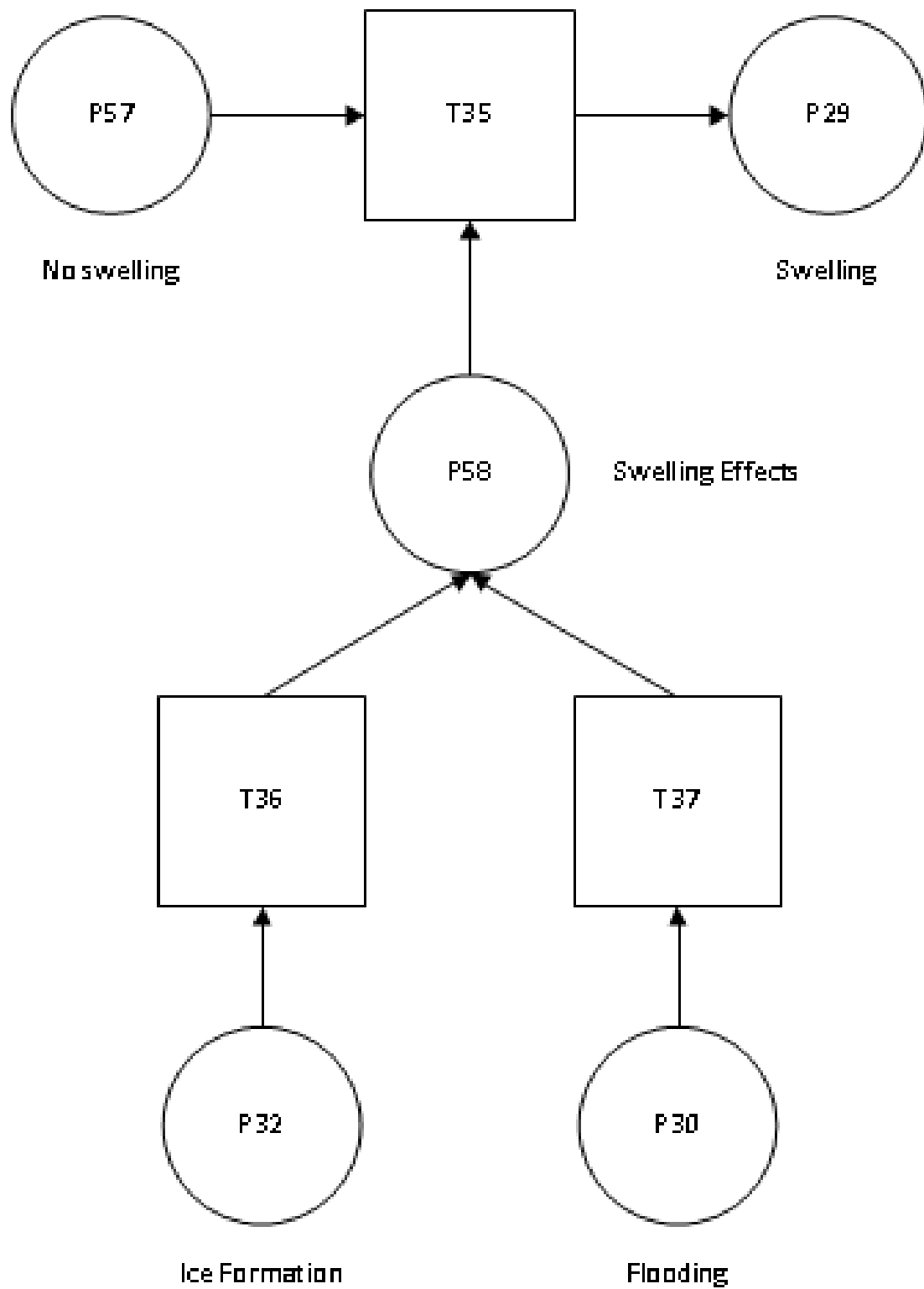


Figure D.9: Swelling of the Membrane

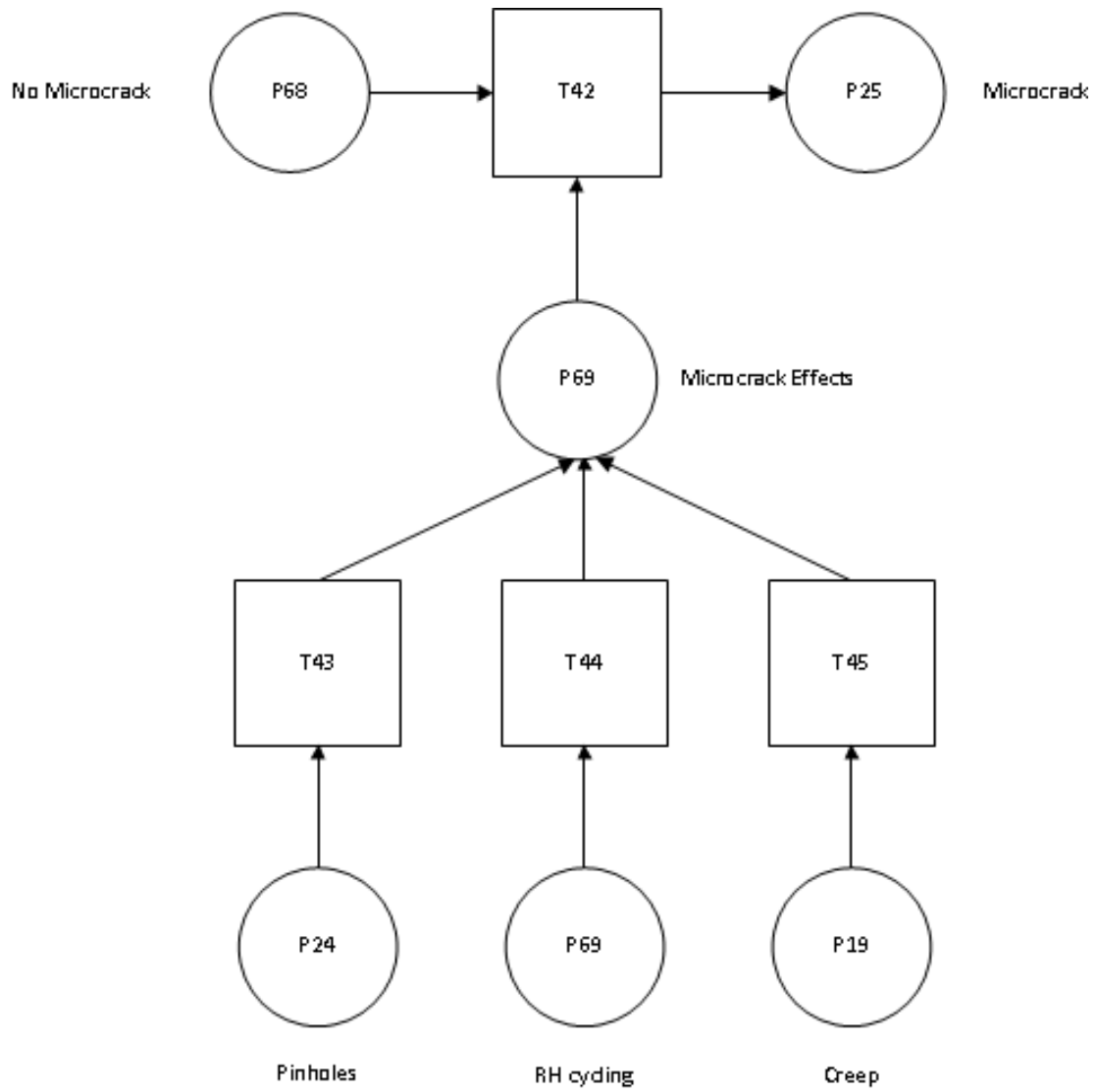


Figure D.10: Micro-Crack Fracture to Membrane

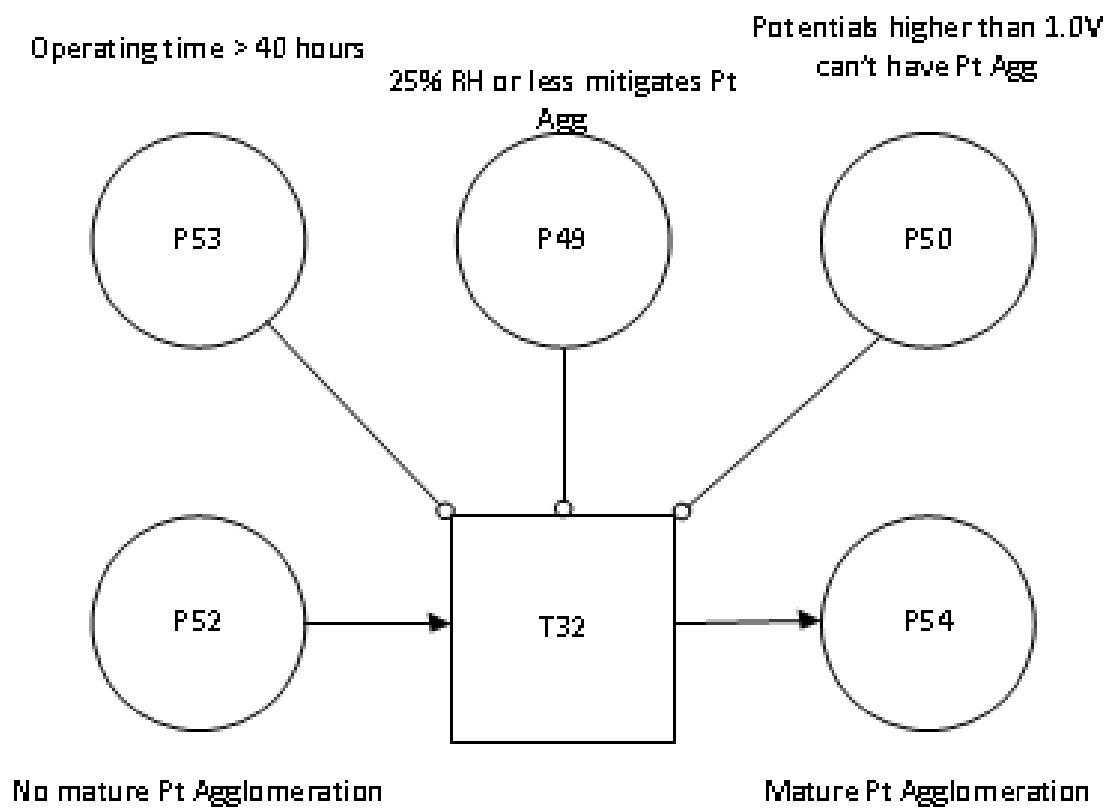


Figure D.11: Mature Pt Agglomeration

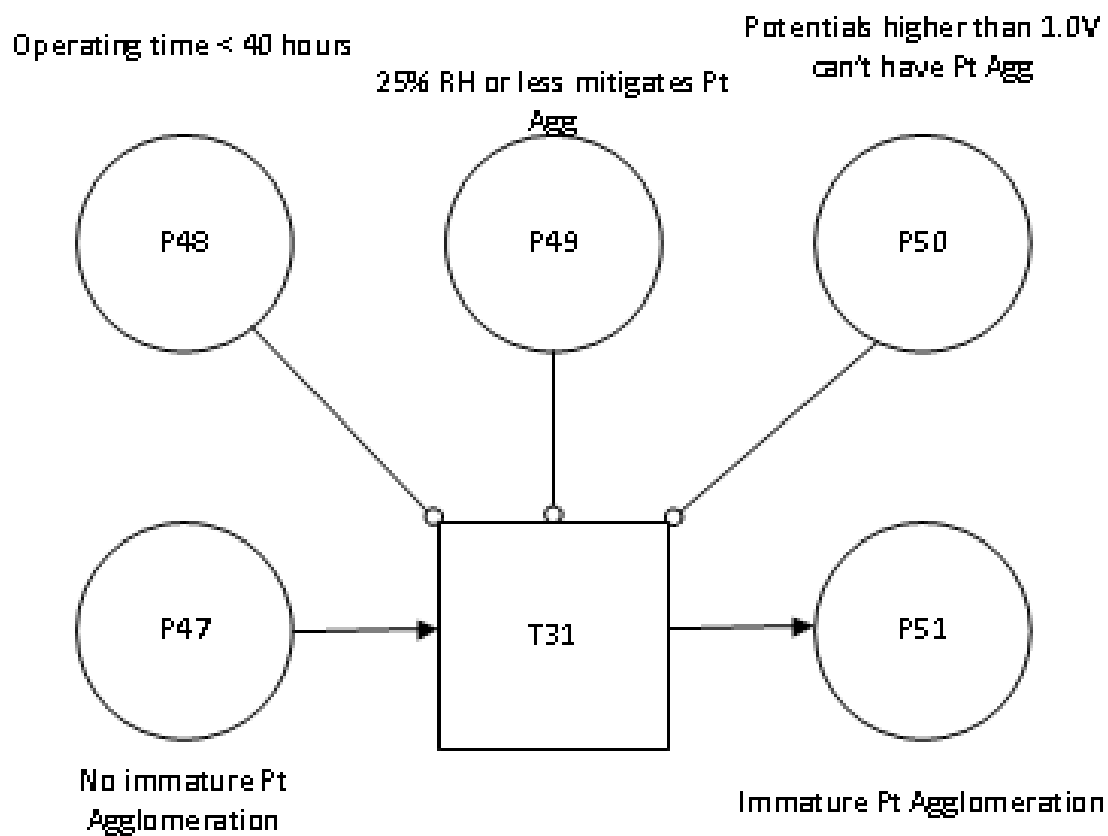


Figure D.12: Immature Pt Agglomeration

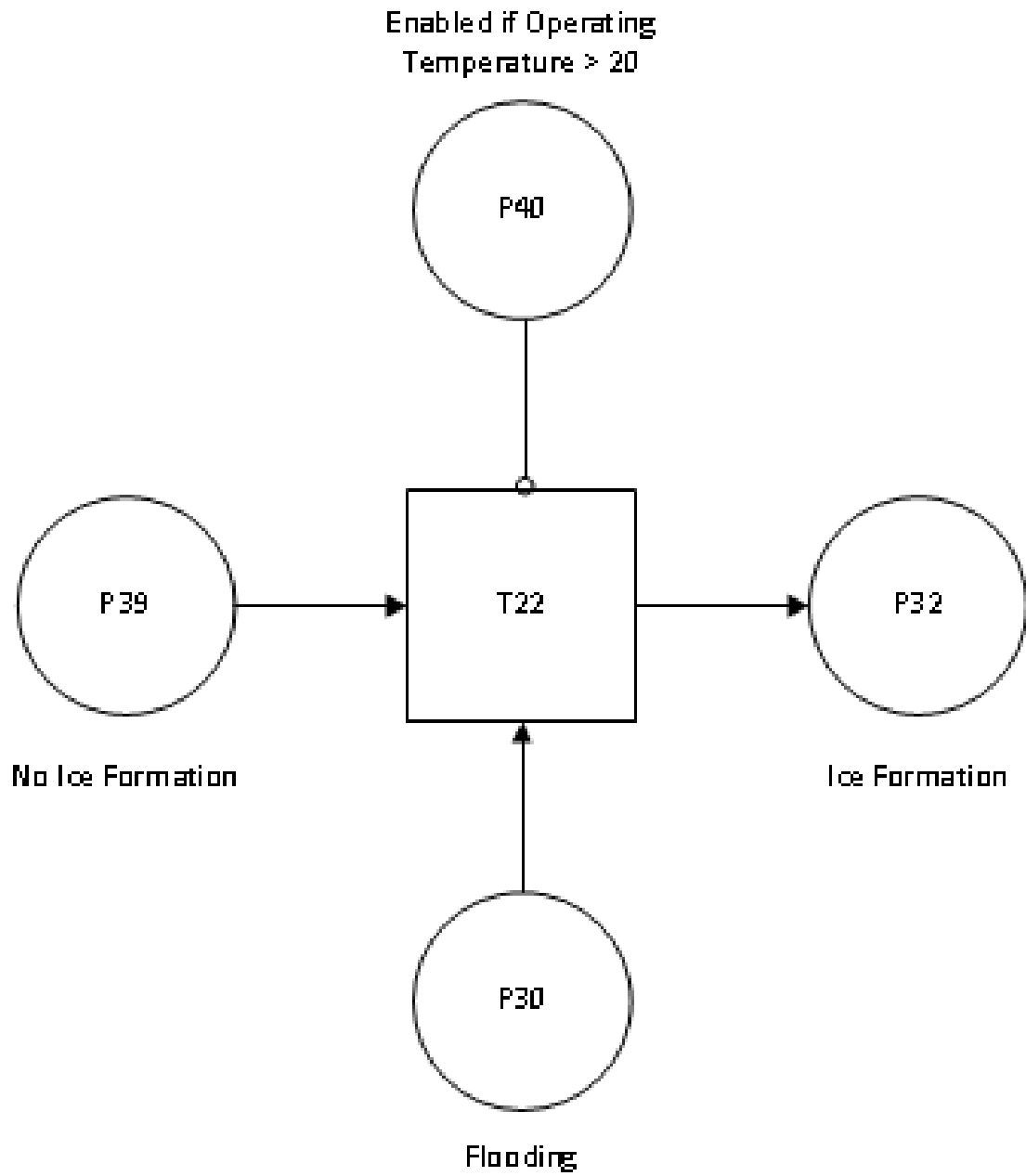


Figure D.13: Ice Formation

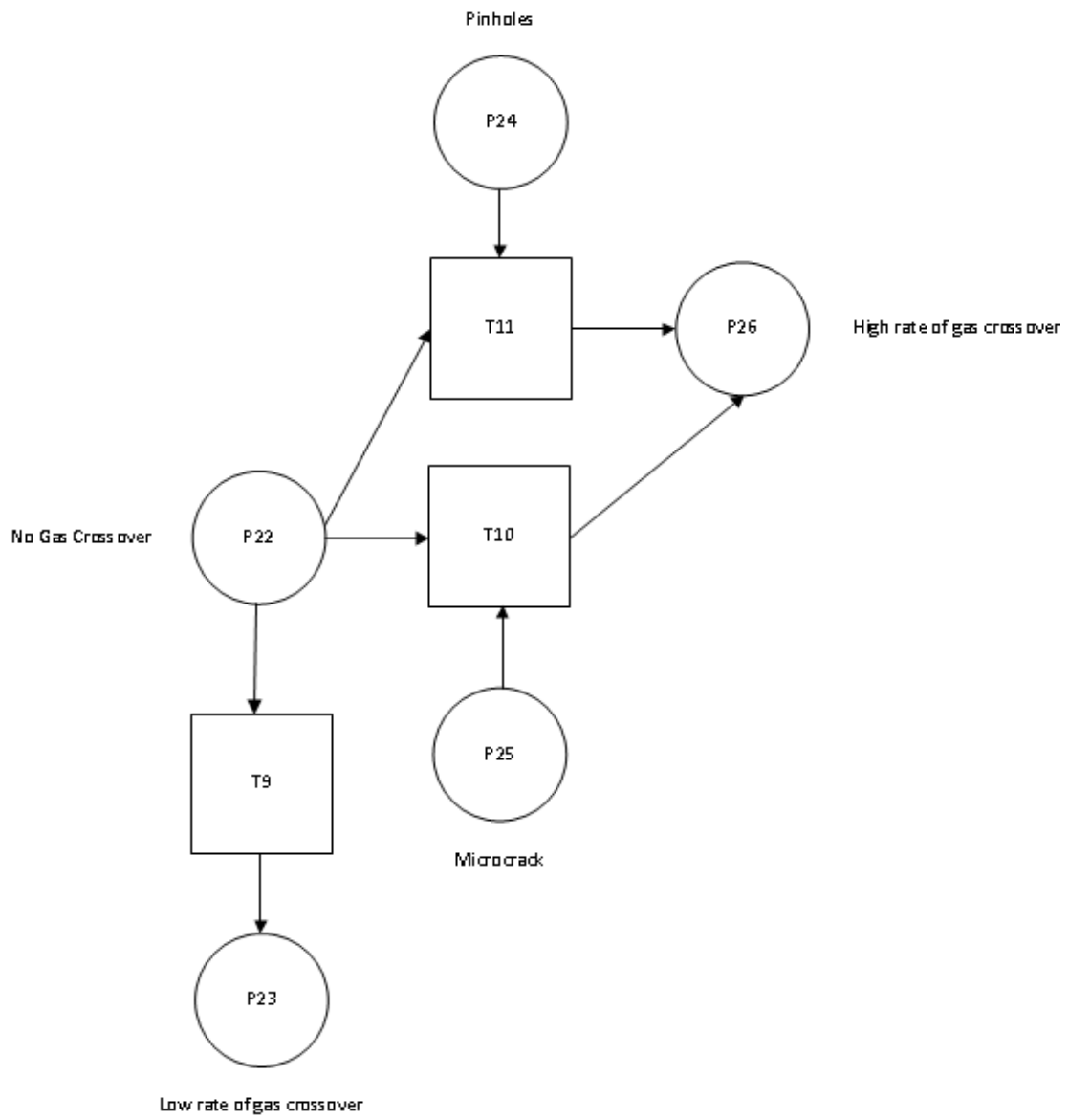


Figure D.14: Gas Crossover

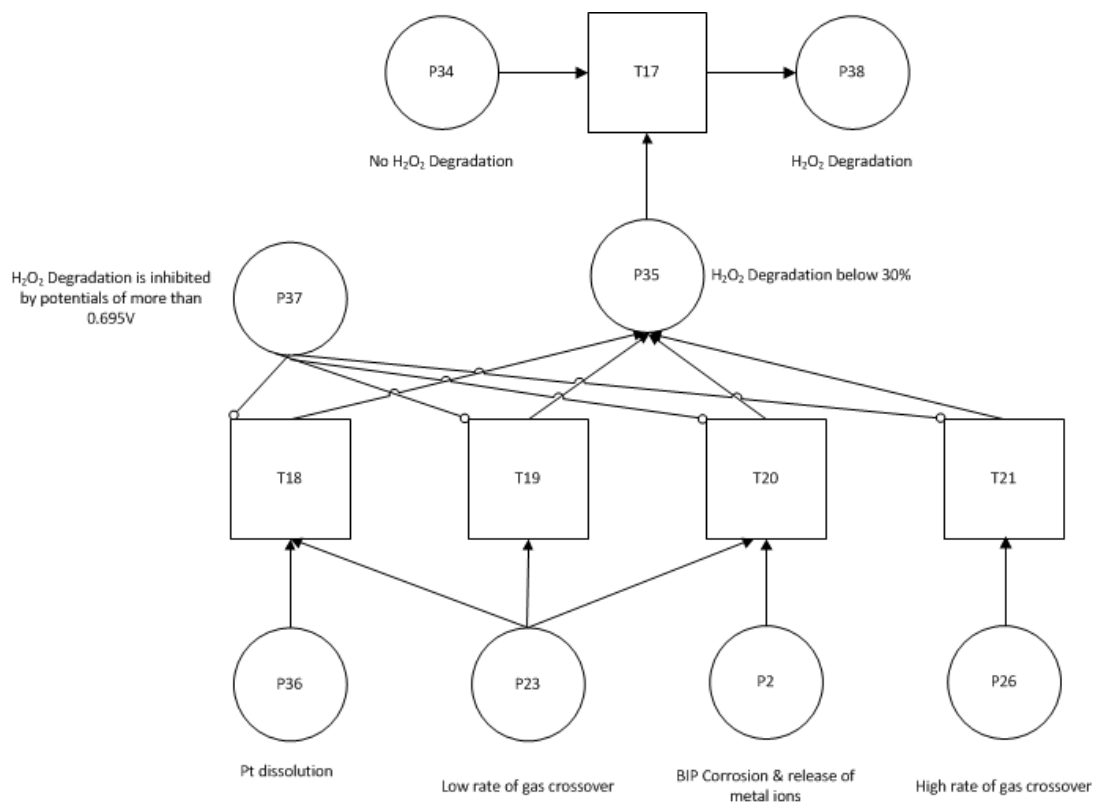


Figure D.15: H₂O₂ degradation

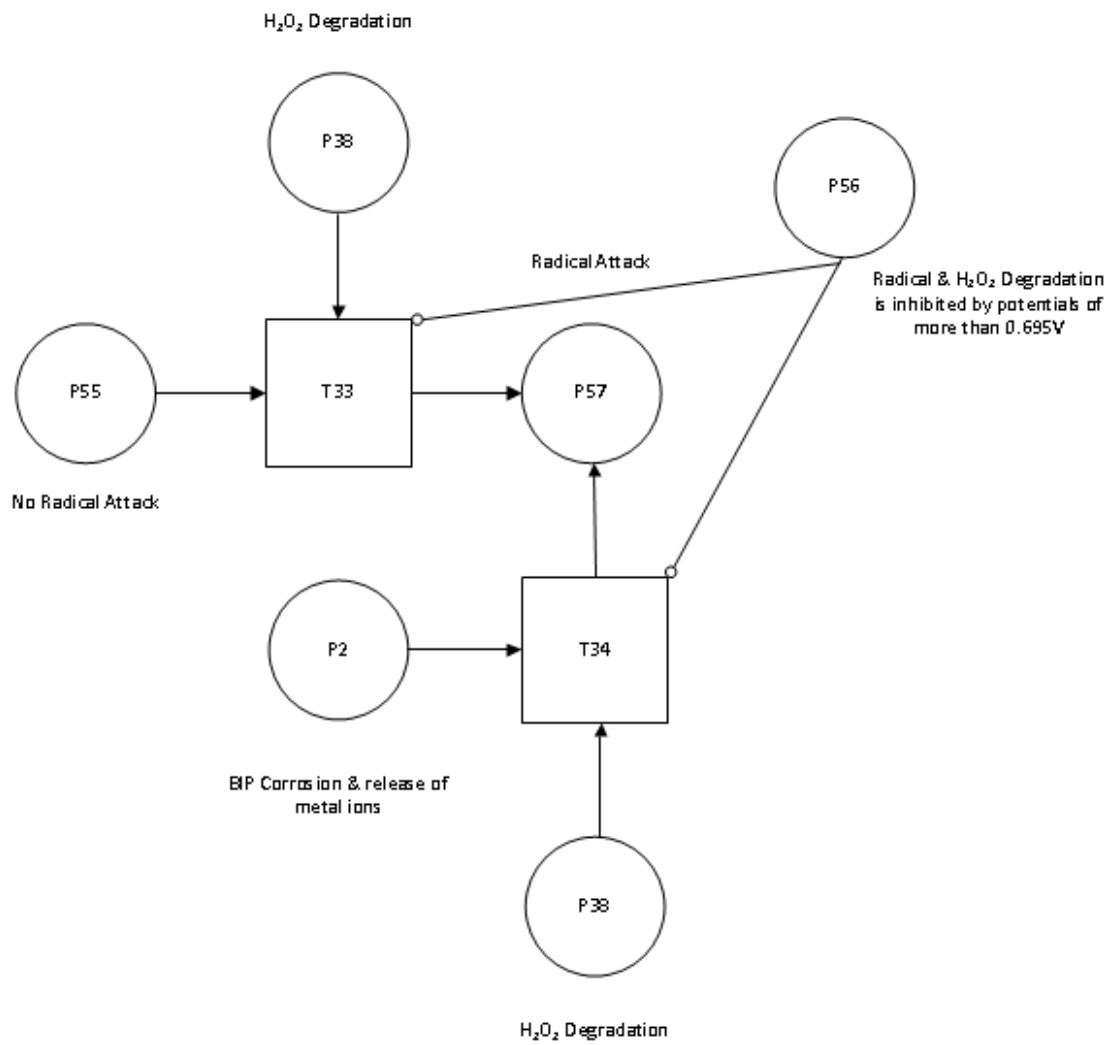


Figure D.16: Radical attack

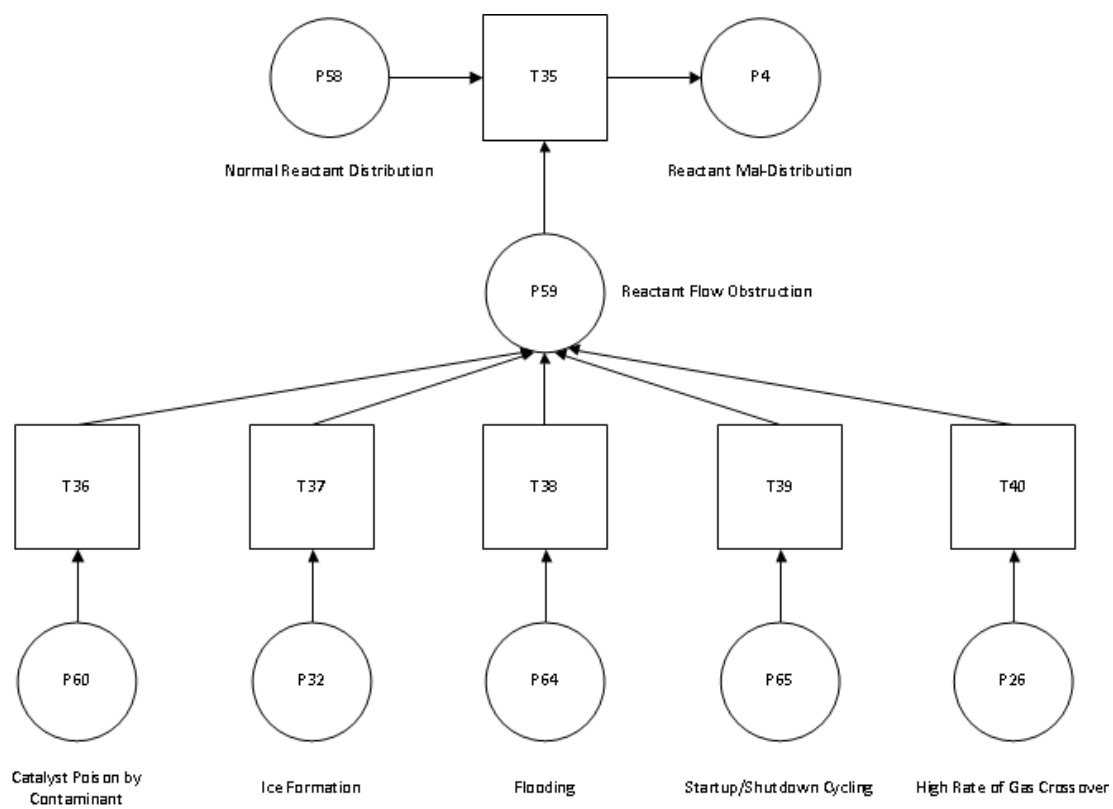


Figure D.17: Reactant Mal-Distribution

Appendix E

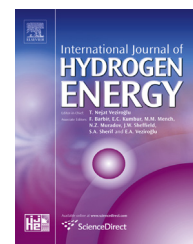
International Journal of Hydrogen Energy Paper



ELSEVIER

Available online at www.sciencedirect.com

ScienceDirect

journal homepage: www.elsevier.com/locate/ijhe

Advanced reliability analysis of Polymer Electrolyte Membrane Fuel Cells using Petri-Net analysis and fuel cell modelling techniques

Michael Whiteley*, Ashley Fly, Johanna Leigh, Sarah Dunnett, Lisa Jackson

Aeronautical & Automotive Engineering Department, Loughborough University, Loughborough, Leicestershire LE11 3TU, United Kingdom

ARTICLE INFO

Article history:

Received 19 November 2014

Received in revised form

15 January 2015

Accepted 26 January 2015

Available online xxx

Keywords:

PEMFC

Reliability

Degradation

Petri-Net

Analysis

ABSTRACT

Reliability issues with fuel cells have held back the commercialisation of this new technology, and as such are required to be studied further. Current reliability standards for automotive applications require an operational lifetime of 150,000 miles or 5000 h. These standards are hard to achieve; therefore in depth reliability analysis and degradation studies can help allude towards the key areas of improvement in fuel cell technology to meet these standards.

Previous Failure Mode and Effect Analysis (FMEA) work has shown that the multi-component system of a Polymer Electrolyte Membrane Fuel Cell (PEMFC) is inherently complex. Dependencies exist between multiple failure modes which discounts Fault Tree Analysis (FTA) as a feasible reliability modelling technique. Therefore, in this study, Petri-Net simulation and fuel cell modelling techniques have been adopted to develop an accurate degradation model. Operational parameters such as water content, temperature and current density and their effects on the occurrence of failure modes can be modelled through this technique. The work will improve previous fuel cell reliability studies by taking into consideration; operating parameters (water content, temperature), fuel cell voltage based on demand (drive cycles) and dependencies between failure modes.

Copyright © 2015, Hydrogen Energy Publications, LLC. Published by Elsevier Ltd. All rights reserved.

Introduction

Why hydrogen fuel cells?

In recent years, climate change and sustainability issues have become more poignant and further discussed. This is due to the evidence that points towards an anthropogenic source of

climate change (Soloman et al. [1]). Man-made activities contribute towards climate change through Greenhouse Gas (GHG) emissions, which include; carbon dioxide (CO₂), methane (CH₄) and nitrous oxide (N₂O) among others.

The UK emitted 549.3 Million tonnes of Carbon Dioxide equivalent (MtCO₂e) in 2011 (Dept. for Transport [2]) and 122.2 MtCO₂e was due to the transport industry, with 74% of this

* Corresponding author. Tel.: +44 07896 009 227.

E-mail address: m.whiteley@lboro.ac.uk (M. Whiteley).
<http://dx.doi.org/10.1016/j.ijhydene.2015.01.154>

0360-3199/Copyright © 2015, Hydrogen Energy Publications, LLC. Published by Elsevier Ltd. All rights reserved.

figure due to cars, taxis and buses (DECC [3]). Other countries have also pledged to tackle climate change, with the US president stating that the US will reduce CO₂ emissions 17% from 2005 levels by 2020, 42% by 2030 and finally 83% by 2050.

Not only are GHG negatively affecting the atmosphere, energy prices are set to continue to rise at alarming rates (BERR. [4]), which could dramatically affect the UK's energy system and energy security concerns. Due to the aforementioned negative environmental impacts of emissions from fossil fuel energy sources and concerns with energy prices and security, this figure needs to be dramatically reduced not only to meet government targets, but for the health of the biosphere.

Hydrogen fuel cells are a zero-emission energy conversion and power generation device. They combine Hydrogen (H₂) and Oxygen (O₂) gases to form water (H₂O), heat and electrical energy. If the H₂ is sourced from renewable means, such as electrolysis of H₂O from wind turbine electricity, the whole process is zero emissions in use. With this in mind, hydrogen fuel cells have the potential to mitigate climate change and energy security concerns.

The Polymer Electrolyte Membrane Fuel Cell

Out of the five main types of fuel cell, the PEMFC has been singled out as the most applicable to automotive applications. This is due to its low operating temperature and rapid startup times.

There are three main hurdles to the commercialisation of PEMFCs; Cost, Infrastructure and Reliability. Currently PEMFCs in automotive applications need to meet the United States (US) Department of Energy (DoE) standards of 5000 h lifetime with a performance drop of no more than 5% over that time, with the Japanese and European standards being similar (Borup et al. [5]). However, modern day PEMFC systems struggle to reach these targets due to unforeseen degradation of the membrane, Catalytic Layer (CL), Gas Diffusion Layer (GDL) and Bipolar Plate (BIP) components, contributing towards a reduction in performance.

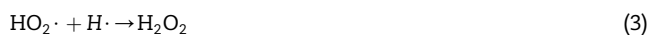
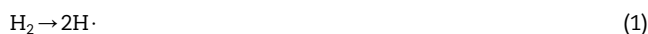
PEMFC

PEMFCs can suffer three main types of degradation during the operating lifetime; chemical, thermal and mechanical degradation. These failure mechanism classes can stem from numerous individual failure modes that the PEMFC can experience. An example of a failure mode linked to chemical degradation is illustrated in [Chemical degradation](#) section.

Chemical degradation

An example of chemical degradation is hydroxyl (OH) and hydroperoxy (OOH) radical attack. OH and OOH radicals are caused by the chemical changes brought around due to H₂O₂ (peroxide) presence. As such, H₂O₂ formation from its two main pathways (diffusion of gasses through membrane and electron reduction) can lead on to a chemical attack of the Polytetrafluoroethylene (PTFE) based membrane and areas of the CL and GDL.

To further explain the pathways, LaConti et al. [6] proposed a method of production of radicals which occurs due to the diffusion of gasses through the membrane.



Equations 1–5 show the stages of how radicals are a product of H₂O₂ production which occurs under normal operating conditions and membrane health. Therefore H₂O₂ needs to be included as the basic event leading to radical formation.

Peroxide can form in another way, by a two electron reduction of O₂ pathway (Pozio et al. [7]) explained in Equation (6);



The way in which radical and peroxide attack affects the degradation of the cell is through the thinning of the membrane over time. This is achieved by end-group unzipping and chain scission processes, actively eating away at the chemical bonds of the PTFE based membrane.

Reliability analysis of PEMFCs

Reliability analysis of PEMFCs is still in its infancy and needs to be further developed to advance the understanding of degradation mechanisms and lifetime of PEMFCs. Previous work includes a failure mode identification and FTA of a general PEMFC by Rama et al. [8]. Additionally, a more recent FTA work was presented by Placca & Kouta [9], looking at the failure modes that could cause PEMFC degradation.

The existing reliability work has proven to be a good start with understanding PEMFC degradation and failure. However, the latest work by Whiteley et al. [10,11] has identified that there were areas that could be improved and developed to further the reliability and degradation field of PEMFC research. These enhancements, including FMEA & FTA are summarised in [FMEA and FTA](#) section respectively.

FMEA

A FMEA was performed to systematically evaluate the potential failures that can occur in a PEMFC system, and their effects on the operation of the system. This work extended the previous work by Rama et al. [8], fully outlining all of the failure modes and their effects in a PEMFC assembly.

The FMEA table consists of the identification of the physical component of the PEMFC being analysed, followed by a brief description of its function. The failure modes that can be experienced in this area are then listed, detailing the effects that this failure mode has. The local effect is the contained

effect of the failure mode, whereas the system effect is how the failure mode will affect the overall operation of the entire system. Failure detection methods are listed for more details on how to distinguish these failures, whether it be in-situ or ex-situ. Mitigation strategies are listed where previous work has identified a way to reduce or mitigate against these failure modes. Any poignant remarks are listed that may help further the understanding of any of the previously highlighted points, followed by any key relationships between the listed failure mode, and any other failure mode in the system that is being analysed. Finally the source of the failure mode information is listed for integrity.

This work filled a gap in current PEMFC degradation literature by providing a comprehensive list of component and system level failure modes that a PEMFC can experience. The outcome was identification of 21 components failure modes, resulting in 39 different potential system failure effects.

FTA

The existing work in FTA for PEMFCs by Placca & Kouta [9] showed 37 individual basic events that could lead to the top-level intermediate events of Membrane Degradation, Catalyst Layers Degradation and Gas Diffusion Layers Degradation. These three intermediate events lead on to the overall top event of Degradation of the Cell. The work harboured key areas that were flagged for improvement, to increase the accuracy of the FTA model. A new state-of-the-art FTA was undertaken by Whiteley et al. [10,11] to rectify the issues arisen in the existing work, which saw a complete re-draw of the failure logic for a PEMFC. Areas that needed attention were; Top Event Ambiguity, BIP Omission, Ambiguity of Intermediate Events, Lack of Standardised Data, Errors in Proposed Degradation Rates and an overall re-think of the failure logic (see Fig. 1).

The failure modes identified and developed to advance the FTA PEMFC work are presented in Table 1, where failure modes listed in bold font are carried over from the existing work by Placca & Kouta [9]:

The FTA work has provided a clear failure logic structure for a PEMFC, identifying the key basic events that contribute to the overall degradation of PEMFC performance. However, one of the main weaknesses of the FTA approach is that it assumes independent failure event occurrence. Hence Petri-Net simulation has been adopted to address this issue.

Petri-Net simulation

Petri-Net simulation is based upon a graphical process of representing component relationships, conditions and events. It can be used to model and analyse dynamic behaviours of systems taking into account relationships and dependencies which FTA cannot.

Petri-Nets are comprised of two main symbols; 'places' (P) and 'transitions' (T). These two nodes are connected by arrows known as 'Arcs' (A), which show the direction of flow of 'tokens'. Tokens are used to describe the state of the system, and are used to mark/enable a place as in Fig. 2.

Fig. 2 shows a simple Petri-Net that has place one enabled (P_1 containing a token). The transition (T_1) will fire based on criteria that could range from time intervals to probability. Once the criteria are met, the transition will take the one token from P_1 and place it into P_2 , denoting a new state.

P , T and A can be defined as by Liu & Chiou [12]:

$$P = \{P_i | P_i \text{ is a place, } 1 \leq i \leq I\},$$

where I is a positive integer

$$T = \{T_i | T_i \text{ is a transition, } 1 \leq i \leq I\}$$

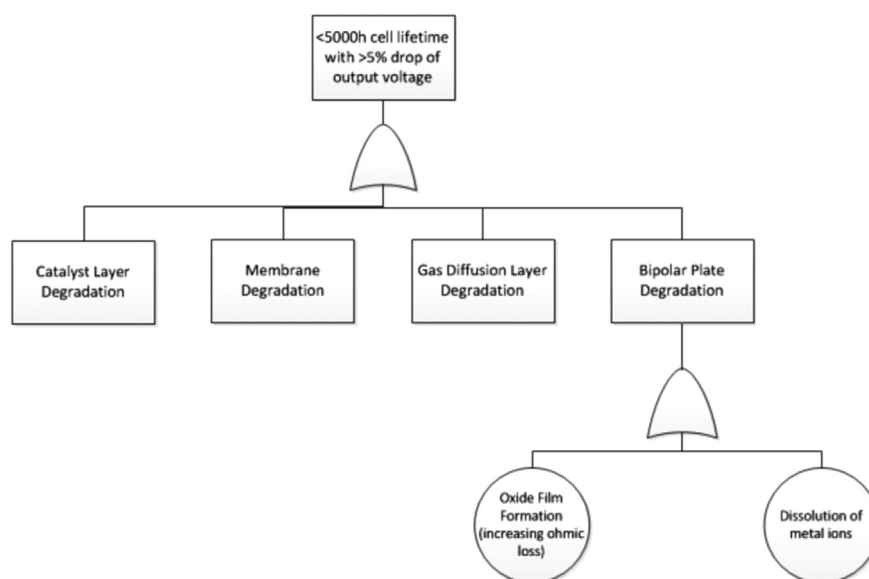


Fig. 1 – Proposed change to 'global' tree.

Table 1 – List of basic events.

Basic events – membrane

Incorrect BIP torque
 Polymer membrane ‘creep’
 Microcrack fracture
 OH and OOH radicals & H₂O₂ contamination to PTFE
 Presence of foreign cationic ions: dissolution of metal ions from BIP – corrosion/contaminant from humidifier/air pipe/gas impurity
 Ice formation
 Fatigue from relative humidity and temperature cycling
 Excessive heat degradation
Flooding

Basic events – catalyst

Pt agglomeration and particle growth
 Pt elemental loss
Pt Migration
Pt Contamination
 Startup/shutdown cycling
Flooding
Ice Formation

Basic events – gas diffusion layer

OH Radicals
Flooding
 Ice formation

Basic events – bipolar plate

Oxide film formation
 Corrosion leading to release of multivalent cations

$$A \subseteq (P \times T) \cup (T \times P)$$

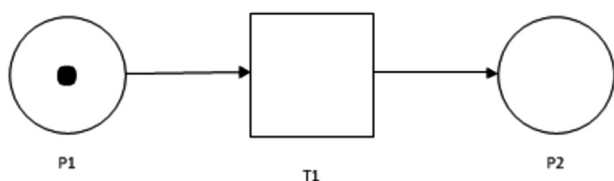
Benefits of Petri-Net simulation

Petri-Net simulation offers significant advantages over FMEA and FTA. FMEA is more geared towards the analysis of individual failure modes, and doesn't look at the interactions between a group of failure modes. FTA can look at the relationships between failure modes in a graphical manor, however the technique cannot take into account dependencies between failure modes.

Petri-Net simulation can take into account dependencies, and has been chosen to analyse the failure characteristics of a PEMFC.

Existing work in the literature

Although Petri-Nets have been used numerous times to assess system degradation and reliability concerns (Volovoi [13] & Malhotra, Trivedi [14]), There is currently only one example of Petri-Net use for reliability analysis of PEMFCs from Wieland

**Fig. 2 – Example, simple Petri-Net.**

et al. [15] and is a good start to develop reliability analysis in this field. However, the model could be further developed to accurately represent all of the previously identified failure modes from FMEA and FTA work presented by Whiteley et al. [10,11].

The existing work in the literature has an initial place which denotes the operational state of a PEMFC. The model can fire through five main transitions; Degradation, Spontaneous event, Reversible event, Repair and Breakdown. All transitions are based upon degradation rates taken from the literature or the authors own assumptions. These rates are selected using the normal distribution based upon mean, lower limit and upper limits, again assumed by the authors.

Limitations with failure rates/probabilities used

Using the normal distribution is a limitation when analysing PEMFCs. Components don't share characteristics with normal distribution probability theory, rather components ageing in a system share more characteristics with the Weibull distribution, owing to the 'bathtub curve' (Fig. 3).

The Weibull shape parameter ' β ' is reflective of what stage the component is in due to the lifetime of the component. This shape parameter can be changed dependent upon the failure mode in question. That is to say that an early life failure mode such as early life Platinum (Pt) agglomeration would have a shape parameter of less than one. Whereas failure due to creep under normal conditions (that can take upwards of 5000 h to cause a failure) would use a shape parameter of more than one.

Limitations with parameters used

The failure parameters used can be considered to be vague and limited in number for an accurate degradation model of a PEMFC. In the work by Wieland et al. [15], degradation transition severity is calculated from a normal distribution using the Natural Aging parameter from 1 to 70 $\mu\text{V h}^{-1}$ (micro-volts per hour). This assumes that degradation is a simple process and can be derived from lifetime test degradation rates. However due to the inherently complex system of a PEMFC, degradation relationships can interact and harbour dependencies that can alter the overall lifetime, based upon their interaction and operating conditions (Whiteley et al. [10]). Spontaneous and reversible parameter use could also be optimised. Wieland et al. [15] suggest that random variables are used to select if one of the spontaneous events or reversible events are occurring. However 'High temperature operation and Start below 0 °C (SBZ)' could never occur together.

The authors themselves acknowledged the limitations of their model:

'There is a lot of simplification done to get this first model. For example, spontaneous events occur independently of the stack state and degradation is steady, instead of increasing at certain times such as summer or winter'.

Wieland et al. [15] pp38.

Proposed model

The proposed work in this paper seeks to enhance the capabilities of the Petri-Net approach for PEMFC degradation modelling. The overall 'Global' Petri-Net is presented in Fig. 4.

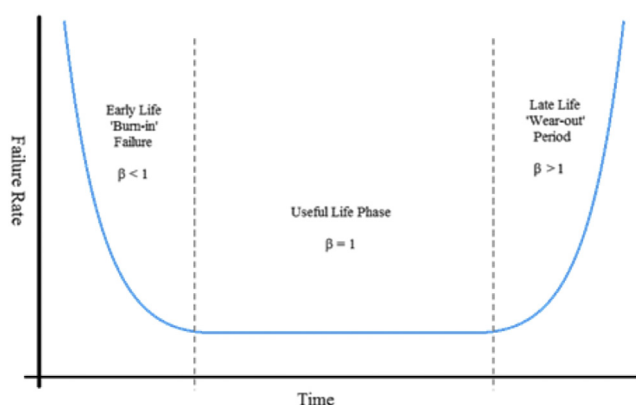


Fig. 3 – Component 'bathtub curve'.

There are two global states 'Operating State' and 'Failed State', The 'Operating State' is initially set at 100% health of the PEMFC and fires through the 'Degradation' transition on every time-step. Contained within the degradation transition, are separate Petri-Nets based upon the knowledge gained through FMEA and FTA as discussed in 4.1. Each failure mode has a relationship Petri-Net to explain its logic, and how it might interact with other failure modes in the system.

The 'Failure' transition will fire based upon the criteria of unacceptable system performance. This is set at a lifetime of less than 5000 h with more than a 5% drop in cell performance over that time as per the US DoE target. If this target threshold is exceeded, the transition will fire into the 'Failed' state.

Degradation modules

Each failure mode previously identified in the FMEA and FTA has a Petri-Net attributed to it, which shows the logic contributing towards its activation. A total of 21 Petri-Net modules have been created however only one is discussed here for brevity. Fig. 5 shows an example of a Petri-Net module for a given failure mode: 'H₂O₂ Degradation'.

P1 is the initial place, and is enabled with a token on the first running of the model. It is indicative of a healthy PEMFC and is enabled from the first running of the model, with no H₂O₂ degradation. T1 can only fire when there is a token in P2 and P1 at the same time. P2 is used to indicate a state of H₂O₂ degradation, agglomerating the lower level transitions. This is for the integrity of the transition logic. The firing of this transition would enable P8, indicating a state of H₂O₂ degradation, and would have an output affecting the performance of the PEMFC and potentially linking into another Petri-Net module. There are a number of contributors to P2, stemming from places P3 'Pt dissolution/redistribution 'Pt Band'', P4 'Low

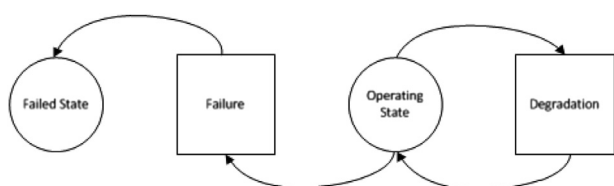
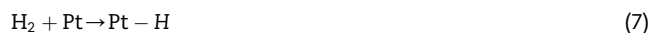


Fig. 4 – Global Petri-Net.

rate of gas crossover', P5 'BIP corrosion & release of metal ions' and P6 'High rate of gas crossover'. P3 is enabled by an interaction from a separate Petri-Net module, and indicates the presence of Pt which acts as a catalyst for H₂O₂ formation (LaConti et al. [6]) shown in Equations 7–9.



Therefore for 'T2' to fire, 'P3' and 'P4' need to be enabled. This would show that there is gas crossover and a free Pt presence to cause a rate of formation of H₂O₂.

As has been previously mentioned in Equation (1)–(6), H₂O₂ can form from the crossover of the reactant gasses through the membrane. Thus for a given rate of gas crossover, a corresponding rate of H₂O₂ formation is attributed. This enables the Petri-Net modelling of 'T3' and 'T5' firing and a corresponding degradation of PEMFC overall performance. Consequently if 'P6' is enabled, 'T5' will fire, placing a token in 'P2', and if 'P4' is enabled, 'T3' will fire a token into 'P2'.

Pozio et al. [7] also showed that the presence of Fe₂⁺ and Cu₂⁺ (Iron and Copper ions) released from BIP corrosion greatly accelerate the degradation due to H₂O₂ formation when there is gas crossover. Therefore a separate rate is associated with 'T4'.

'P7' is an inhibitor and serves to prevent the transition of 'T2', 'T3', 'T4' & 'T5'. Borup et al.[5] state that the potential for H₂O₂ formation (E° H₂O₂) is equal to 0.695 V, and that any potential greater than this would inhibit the formation of H₂O₂ in the PEMFC.

Petri-Net firing

The firing of the Petri-Net uses the following equation:

$$M_n = M_0 + A^T \sum \quad (10)$$

where M_n is the final marking, M₀ is the initial marking, A^T is the incidence matrix for the module, and \sum is the transition firing count vector. The relationship between A^T and \sum is summarised in Equation (11):

$$A^T \sum = \Delta M = M_n - M_0 \quad (11)$$

For each individual Petri-Net module contained within the 'Degradation' transition of the global Petri-Net, there is a corresponding incidence matrix as in Equation (12) for H₂O₂ degradation.

$$A^T = \begin{matrix} P_1 \\ P_2 \\ P_3 \\ P_4 \\ P_5 \\ P_6 \\ P_7 \\ P_8 \end{matrix} \begin{pmatrix} T_1 & T_2 & T_3 & T_4 & T_5 \\ -1 & 0 & 0 & 0 & 0 \\ -1 & 1 & 1 & 1 & 1 \\ 0 & -1 & -1 & 0 & 0 \\ 0 & -1 & -1 & -1 & 0 \\ 0 & 0 & -1 & -1 & 0 \\ 0 & 0 & 0 & 0 & -1 \\ 0 & 0 & 0 & 0 & 0 \\ 1 & 0 & 0 & 0 & 0 \end{pmatrix} \quad (12)$$

The logic behind each transition from place to place is noted in each A^T matrix for each module. A '-1' indicates the

taking of a token from a place, and a '1' indicates the placing of a token into that place.

Fuel cell model

A lumped parameter PEMFC model developed by Fly & Thring [16] is used to validate voltage degradation predictions against observed degradation from the literature. Additionally it can be used to integrate the degradation model and therefore have a more accurate relationship between degradation and operational performance. The fuel cell model is initially run to ascertain the operating conditions of the cell. These data are then used by the Petri-Net to model the degradation based upon the fuel cell's conditions.

Summary of the Petri-Net model

The Petri-Net degradation model developed in this work is a comprehensive model of the interactions between the previously identified failure modes in a PEMFC of standard construction (PTFE based membrane, Carbon/Pt catalyst, steel BIP, carbon GDL). The individual modules range from relatively simple relationships with 2–3 places and a low number of transitions, to larger modules with 8 places and 8 transitions. It contains 21 separate modules that interact to both, deliver a voltage degradation value, and further interact with other failure modes. However, if further interactions or modules are discovered that need to be added, the Petri-Net

model can easily facilitate this occurrence, with a simple addition to the script files. The model parameters and degradation rates for failure modes are listed in Tables 2 and 3.

Using the parameters listed in Table 2, the polarisation curve in Fig. 6 can be achieved using the fuel cell model developed. Data from Ref. [17] is also plotted, and the model shows a good correlation with experimental results.

The parameters listed in Table 3 show the degradation rates used for the Petri-Net model. There is little data in the literature to ascertain all failure mode's interaction upon the voltage of a PEMFC, therefore proposed values are used, based upon the review of experimental data and expert opinion.

The initial setup of the model requires the user to input some starting variables such as; operating temperature (to consider ice formation and excessive heat) and number of startup/shutdown cycles. This data is implicit in placing tokens in the relevant initial places, and inhibitor gates. A dynamic range of inputs can be added to have a varying input (such as temperature) over time. Transition timings for the example in Fig. 5 are instant, but for others could be timed or based upon enabling criteria.

Results

The Petri-Net model was programmed in MATLAB on a desktop PC running a dual core 3.10 GHz processor. For all of the individual Petri-Net models, an A^T matrix was constructed with a corresponding transition 'firing' script to use the A^T

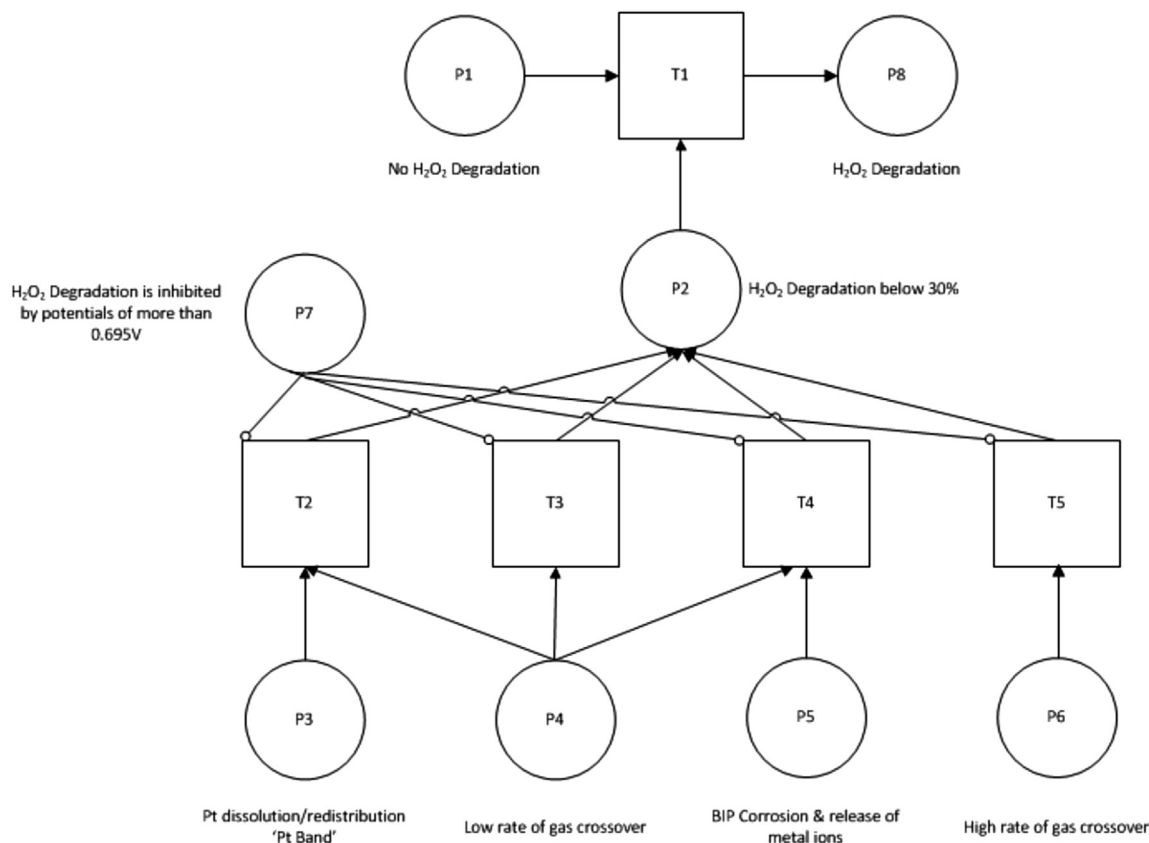


Fig. 5 – Example Petri-Net for H₂O₂ degradation.

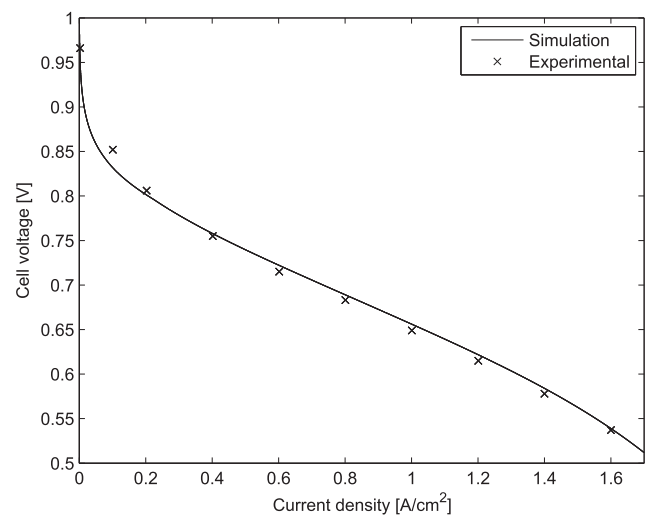
Table 2 – List of fuel cell parameters used.

Cell performance Model Parameter	Value & Unit
Fuel cell rated power	50 kW
Maximum system efficiency	56%
System efficiency @ 50% load	50%
Number of cells	360
Cell active area	200 cm ²
Cathode stoichiometry	2.5
Anode stoichiometry	1.03
Stack mass	30 kg
Stack specific heat	3.5kJ/kg K
Stack cathode volume	0.01 m ³
Stack dimensions	20 × 20 × 60 cm
Ambient humidity	70%
Membrane thickness	100 μm
Internal current density	1.5 × 10 ⁻⁴ A/cm ²
Mass transport coefficient	3 × 10 ⁻⁴
Exchange current density	3.2 × 10 ⁻⁸ A/cm ²
Stack surface heat transfer coefficient	5 W/m ² K
Water entrainment constant	2.0
Molar mass membrane	1.1 kg/mol
Dry density membrane	1.98 g/cm ³
Cathode activation energy	66 kJ/mol

matrix information. For each Petri-Net that has an output for which a reduction in performance is noted, a voltage drop count variable is used to store the total amount of degradation in performance due to the failure relationships. Therefore for each output place in a degradation module Petri-Net, a voltage drop figure is added to the overall voltage drop count. Model initialization is commenced via the input of key operating parameters such as operating temperature and potential amongst others. This will place tokens in specific module initial states ready for simulation runs. The in-putted parameters also decide whether key inhibitor places are enabled or not. The model is run either until 5000 h is reached or a performance drop of >5% is experienced.

Table 3 – List of degradation parameters used.

Failure mode parameter	Value (V h ⁻¹)	Ref
Incorrect BIP torque	10 ⁻³	Proposed
Polymer membrane 'creep'	10 ⁻⁵	Proposed
Microcrack fracture	10 ⁻²	Proposed
OH and OOH radicals & H ₂ O ₂ degradation	1.3 × 10 ⁻³	[18]
Presence of foreign cationic ions	10	Proposed
Ice formation	0.5	Proposed
Fatigue from relative humidity cycling	1.2 × 10 ⁻⁴	[19]
Excessive heat degradation	0.25	[20]
Flooding	0.39	[20]
Pt agglomeration and particle growth	10 ⁻⁵	Proposed
Pt elemental loss	10 ⁻⁵	Proposed
Pt migration	10 ⁻⁴	Proposed
Pt contamination	4.37 × 10 ⁻³	[21]
Startup/Shutdown cycling	5.333 × 10 ⁻⁵ per cycle	[22]
OH Radicals	1.3 × 10 ⁻³	[18]
Oxide film formation	10 ⁻⁶	Proposed
Corrosion leading to release	3.125 × 10 ⁻⁵	[23]

**Fig. 6 – Polarisation curve ascertained from the developed model.**

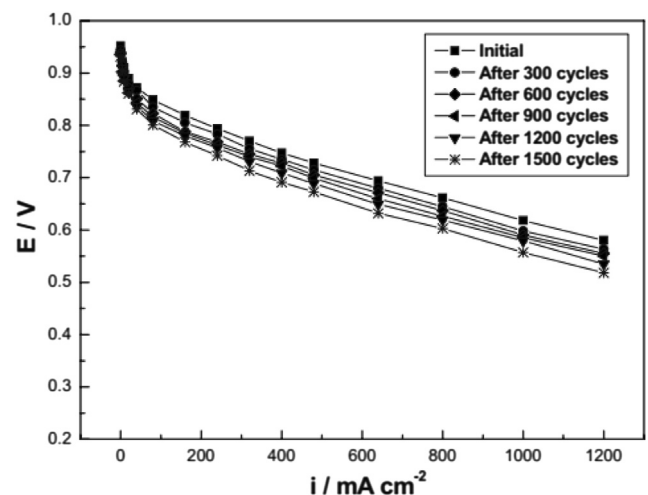
Verification of model

Startup Shutdown Cycling (SSC) degradation was considered through a review of the literature in this area. Kim et al. [22] conducted extensive experimentation to reveal the relationship between SSC and degradation of fuel cell performance. Their results show that after 1500 instances of SSC, a drop in performance of 0.08 V was observed (Fig. 7). Therefore per cycle it can be considered that SSC causes a drop in performance of 5.333×10^{-5} V.

The degradation rate was programmed to take affect per SSC, through the transition T_1 in Fig. 8.

Therefore, for each time there is an instance of SSC, a degradation rate of 5.333×10^{-5} V is applied to a voltage drop count variable.

The results of the Petri-Net model using an SSC degradation module was tested using a polarisation curve model as in Fig. 9.

**Fig. 7 – Startup/shutdown cycling tests [22].**

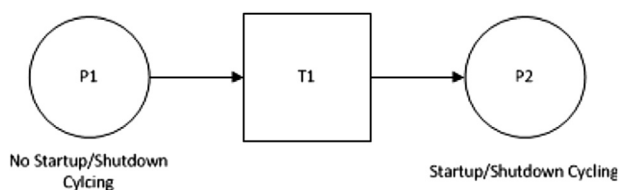


Fig. 8 – Startup/shutdown cycling Petri-Net.

The model shows a good replication of the polarisation curve drop observed by Kim et al. [22] in Fig. 7, with the same logic being carried through the entirety of the Petri-Net model. Each failure mode interaction has a voltage degradation value assigned to it, with some acting reversibly dependent upon the state of the system, and some acting as a counter (irreversible).

Conclusions & future work

The presented work is a step forward in degradation and reliability modelling of PEMFCs. The previous work by the authors leading to this has ensured that the Petri-Net model proposed, is reliably constructed based upon an in-depth, and up-to-date review of PEMFC failure phenomena.

As can be seen in Figs. 7 and 9, the initial activation range of the polarisation curve does not match up correctly. Due to the fuel cell model developed, this area can be modified due to SSC and take into account degradation in different regions of the polarization curve in future work.

Future work will include an integration of this degradation model into a PEMFC performance model, capable of plotting polarisation data from key operational inputs. Currently the degradation model needs operating data in the form of initial inputs from the user. That is to say that operating voltage is

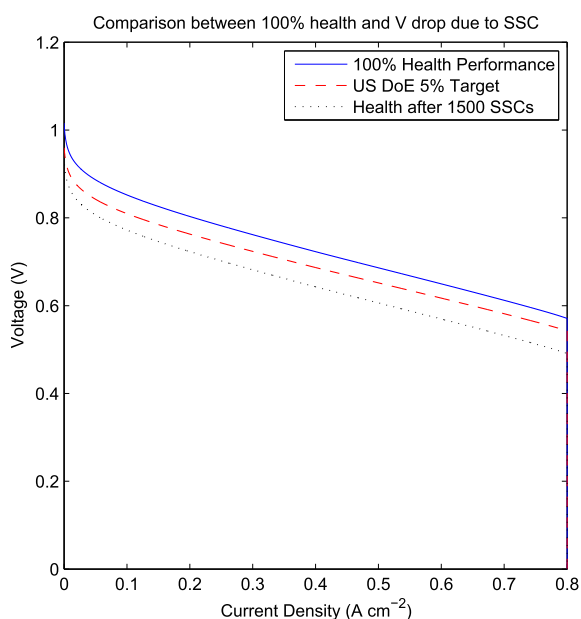


Fig. 9 – Startup/shutdown cycling Petri-Net.

set from the outset, alongside operating temperature, number of SSCs and other variables. Integration into a PEMFC performance model will allow the performance model to output operational data into the degradation Petri-Net model for its inputs. Then after running the Petri-Net model, the outputs would feed back into the performance model. As the process continues, degradation, and its effect on the performance of the cell can be accurately ascertained. Not only does integration with a PEMFC performance model mean more accurate degradation modelling, it also means that PEMFC operational load levels (such as drive cycles) can be preset, and the degradation due to the fluctuation in load (and therefore temperature etc.) can be considered.

Acknowledgements

This was supported by the Engineering and Physical Sciences Research Council (EPSRC) (EP/G037116/1) and the Doctoral Training Centre in Hydrogen Fuel Cells and Their Applications.

REFERENCES

- [1] Solomon S, Qin MD, Manning Z, Chen M, Marquis KB, Averyt M, et al. Summary for policymakers. In: *Climate change 2007: the physical science basis. Contribution of working group I to the fourth assessment report of the intergovernmental panel on climate change*. Cambridge University Press, Tech. Rep.; 2007.
- [2] Department for Transport. Factsheets: UK transport greenhouse gas emissions. DfT, Tech. Rep.; 2010.
- [3] Department for Energy and Climate Change (DECC). 2012 UK greenhouse gas emissions, provisional figures and 2011 UK greenhouse gas emissions, final figures by fuel type and end-user. DECC, Tech. Rep.; 2011.
- [4] Business Enterprise and Regulatory Reform (BERR). Dti energy price scenarios in the oxford models. BERR, Tech.Rep.; 2006.
- [5] Borup R, Meyers J, Pivovar B, Kim YS, Mukundan R, Garland N, et al. Scientific aspects of polymer electrolyte fuel cell durability and degradation. *Chem Rev* 2007;107(10):3904–51.
- [6] LaConti A, Hamdan M, McDonald R, Vielstich W, Lamm A, Gasteiger H, editors. *Handbook of fuel cells: fundamental, technology, and applications*, vol. 3; 2003.
- [7] Pozio A, Silva RF, Francesco MD, Giorgi L. Nafion degradation in pefcs from end plate iron contamination. *Electrochim Acta* 2003;48(11). pp. 15431549, 5/15.
- [8] Rama P, Chen R, Andrews J. A review of performance degradation and failure modes for hydrogen fuelled polymer electrolyte fuel cells. *Proc Institution Mech Eng Part A: J Power Energy* 2008;222(5):4214–441.
- [9] Placca L, Kouta R. Fault tree analysis for pem fuel cell degradation process modelling. *Int J Hydrogen Energy* 2011;36(19). pp. 12 39312 405.
- [10] Whiteley M, Jackson L, Dunnett S. Enhanced fault tree analysis and modelling considerations of a polymer electrolyte membrane fuel cell. In: *Proceedings of the European Safety and Reliability Conference, ESREL*. CRC Press; 29/09/2013. p. 603.

- [11] Whiteley M, Jackson L, Dunnett S. Fault tree analysis of polymer electrolyte fuel cells to predict degradation phenomenon. In: Proceedings of the 20th advances in risk and reliability technology symposium. Loughborough University; 21/05/2013. p. 75–89.
- [12] T.S. Liu, & S. B. Chiou. “The application of Petri nets to failure analysis” *J Reliab Eng Syst Saf*, vol. 57, no. 2, pp. 129–142
- [13] V. Volovoi. “Modeling of system reliability Petri nets with aging tokens” *J Reliab Eng Syst Saf*, vol. 84, no. 2, p149–161
- [14] Malhotra M, Trivedi KS. Dependability modeling using petri-net based models. *IEEE Trans Reliab* 1995;44(3):428–40.
- [15] Wieland C, Schmid O, Meiler M, . Wachtel A, Linsler D. Reliability computing of polymer electrolyte membrane fuel cell stacks through petri nets. *J Power Sources* 2009;190(1):34–9.
- [16] Fly A, Thring RH. System thermal and water balance in an evaporatively cooled PEM fuel cell vehicle. In: Proceedings of institution of mechanical engineers – VTMS; 2011. p. 267–77. Vehicle Thermal Management Systems Conference Proceedings.
- [17] J. P. Meyers, & R. M. Darling, C. Evans, R. Balliet, M.L. Perry. “Evaporatively-cooled PEM fuel-cell stack and system” In *Proc ECS Trans*, volume 3, pp. 1207–1214.
- [18] Teranishi K, Kawata K, Tsushima S, Hirai S. Degradation mechanism of PEMFC under open circuit operation. *Electrochem Solid-State Lett* 2006;9:A475–7.
- [19] Folwer M, Amphlett JC, Mann RF, Peppley BA, Roberge PR. Issues associated with voltage degradation in a PEMFC. *J New Mater Electrochem Syst* 2002;5(4):255–62.
- [20] Kim JH, Cho EA, Jang Jong Hyun, Kim Hyoung Juhn, Lim Tae Hoon, Oh In Hwan, et al. Effects of cathode inlet relative humidity on pemfc durability during startup shutdown cycling in electrochemical study. *J Electrochem Soc* 2010;57(1):B104–12.
- [21] Ahn SY, Shin SJ, Ha HY, Hong SA, Lee YC, Lim TW, et al. Performance and lifetime analysis of the kw-class pemfc stack. *J Power Sources* 2002;106(1–2):295–303.
- [22] Canut JML, Abouatallah RM, Harrington David A. Detection of membrane drying, fuel cell flooding, and anode catalyst poisoning on pemfc stacks by electrochemical impedance spectroscopy. *J Electrochem Soc* 2006;153(5):A857–64.
- [23] Steiner NY, Candusso D, Hissel D, Mooteguy P. Model-based diagnosis for proton exchange membrane fuel cells. *Math Comput Simul* 2010;81(2):158–70.

Appendix F

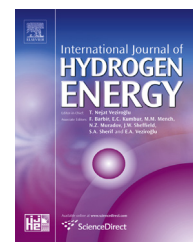
International Journal of Hydrogen Energy Paper (2)



ELSEVIER

Available online at www.sciencedirect.com

ScienceDirect

journal homepage: www.elsevier.com/locate/he

Failure Mode and Effect Analysis, and Fault Tree Analysis of Polymer Electrolyte Membrane Fuel Cells

Michael Whiteley*, Sarah Dunnett, Lisa Jackson

Aeronautical & Automotive Engineering Department, Loughborough University, Loughborough, Leicestershire, LE11 3TU, UK

ARTICLE INFO

Article history:

Received 27 July 2015

Received in revised form

26 October 2015

Accepted 1 November 2015

Available online xxx

Keywords:

PEMFC

Reliability

Fuel cell

Fault Tree

ABSTRACT

Hydrogen fuel cells have the potential to dramatically reduce emissions from the energy sector, particularly when integrated into an automotive application. However there are three main hurdles to the commercialisation of this promising technology; one of which is reliability. Current standards require an automotive fuel cell to last around 5000 h of operation (equivalent to around 150,000 miles), which has proven difficult to achieve to date. This hurdle can be overcome through in-depth reliability analysis including techniques such as Failure Mode and Effect Analysis (FMEA) and Fault Tree Analysis (FTA) amongst others. Research has found that the reliability field regarding hydrogen fuel cells is still in its infancy, and needs development, if the current standards are to be achieved. In this work, a detailed reliability study of a Polymer Electrolyte Membrane Fuel Cell (PEMFC) is undertaken. The results of which are a qualitative and quantitative analysis of a PEMFC. The FMEA and FTA are the most up to date assessments of failure in fuel cells made using a comprehensive literature review and expert opinion.

Copyright © 2015, Hydrogen Energy Publications, LLC. Published by Elsevier Ltd. All rights reserved.

Introduction

With the increase in environmental awareness and climate change concerns in recent years, hydrogen fuel cells have been put forward as a technology that could potentially reduce greenhouse gas emissions. Anthropogenic activities contribute to climate change mainly through Greenhouse Gas (GHG) emissions from fossil fuel based energy sources. These harmful GHGs are comprised of, among others, carbon dioxide (CO₂), methane (CH₄) and nitrous oxide (N₂O) that contribute to the greenhouse effect. Additionally, energy prices are set to

continue to rise by alarming rates [1] which will disrupt the energy system of many countries due to a rise in oil prices. Therefore an alternative energy source would mitigate energy security and pricing concerns to a certain degree.

The United Kingdom (UK) emitted 549.3 Million tones of Carbon Dioxide equivalent (MtCO₂e) in 2011 [2] and 122.2 MtCO₂e was due to the transport industry, with 74% of this figure due to cars, taxis and buses [3]. Due to the aforementioned negative environmental impacts of emissions from fossil fuel energy sources, this figure needs to be dramatically reduced not only to meet government targets, but for the health of the biosphere. The UK government set out targets to

* Corresponding author. Tel.: +44 (0)7896 009 227; fax: +44 (0)1509 227 275.

E-mail address: m.whiteley@lboro.ac.uk (M. Whiteley).

<http://dx.doi.org/10.1016/j.ijhydene.2015.11.007>

0360-3199/Copyright © 2015, Hydrogen Energy Publications, LLC. Published by Elsevier Ltd. All rights reserved.

reduce GHG emissions in the 'Climate Change Act' of 2008. The act presents the targets of an 80% reduction of greenhouse gas levels by 2050, with a closer target of a 34% reduction by 2020. These two targets are based upon the level of GHG emissions in 1990 [4]. The targets are legally bound and therefore must be met, thus many initiatives and research has emerged to aid the UK in reaching these targets. Other countries have also pledged to tackle climate change, with the US president stating that the US will reduce CO₂ emissions 17% from 2005 levels by 2020, 42% by 2030 and finally 83% by 2050.

Hydrogen fuel cells have the potential to mitigate the aforementioned climate change concerns, as they are a zero-emission energy conversion device. They use H₂ and O₂ to form water, releasing heat and electrical energy. Their only emissions are water, meaning that at the point of use, the fuel cell has no carbon emissions associated with it. If the H₂ fuel is sourced from renewable means, the whole process is zero emissions and therefore has the potential to dramatically cut CO₂ emissions in a number of industries.

Fuel cells currently suffer from reliability concerns, and are more likely to contribute to the above issues if the current reliability issues are overcome.

Hence, this paper analyses the reliability of a PEMFC using in-depth techniques in order to understand how their performance can be improved. The layout of the paper is as follows:

In Section **Reliability analysis**, the reasons for studying PEMFCs is given, followed by a brief description of the techniques used in reliability analysis. Section **Reliability analysis** describes the reliability techniques adopted here and previous related studies on the reliability of PEMFCs. Section **Proposed FMEA** describes the FMEA performed and the main conclusions drawn from it. Section **Proposed FT** outlines the Fault Tree (FT) developed and Section **Conclusions** concludes the findings of the study.

Reliability analysis

The US Department of Energy (DoE), Japanese New Energy and Industrial Technology Development Organisation (NEDO) and European Hydrogen and Fuel Cell Technology Platform (HFP) Implementation Panel (IP) have all set reliability targets for PEMFCs in automotive application of a lifetime of more than 5000 h of operation (equivalent to around 150,000 miles operation) [5]. The current state of fuel cell development struggles to meet these targets, and as such, an in-depth reliability analysis of PEMFCs is invaluable to help manufacturers and developers. Such an analysis requires obtaining a detailed understanding of the failure modes of all the different parts of the cell, and the effects the failures have on the cell as a whole.

Currently, the understanding of the reliability of PEMFCs is still in its infancy, and requires further development to help with the commercialisation of this promising technology.

The work presented in this paper uses the techniques of FMEA and FTA to comprehensively ascertain key failure phenomena and analyse their role and effects within in an automotive PEMFC system. Boundaries are set to only consider the PEMFC itself, the balance of plant and supporting ancillaries are omitted as shown in Fig. 1, where the

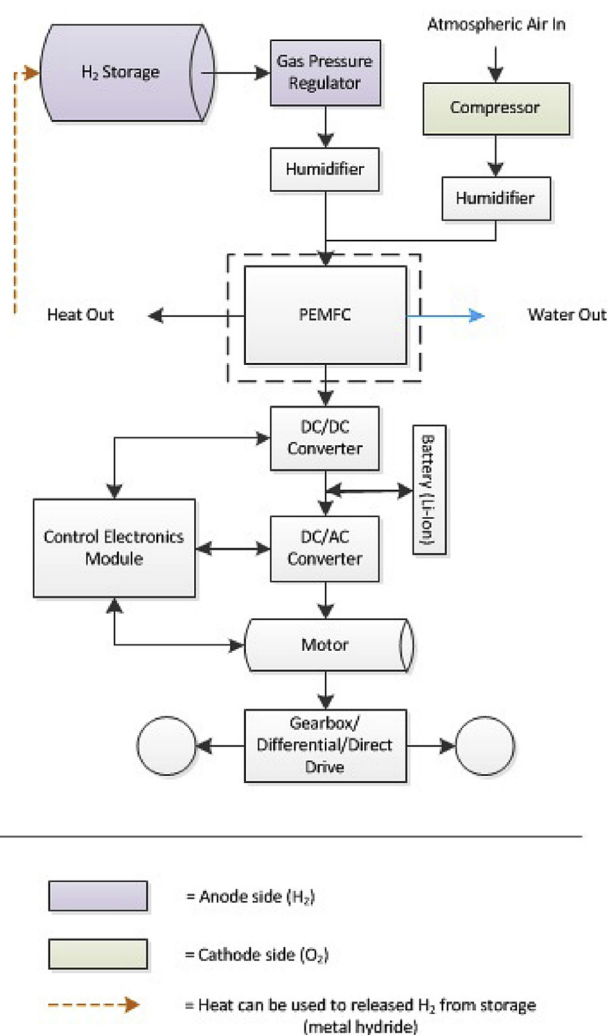


Fig. 1 – Boundaries of presented reliability analysis.

functional block diagram of a simple fuel cell automotive system is shown. The dotted rectangle shows the boundaries of the system considered here.

PEM FMEA

FMEA is a bottom-up approach to analysing equipment, or a system, with relation to its failure events. That is to say that the analysis of the system starts with the individual components that make up the system, rather than looking at the overall system and working top-down. The technique is a systematic scrutiny of all of the individual ways in which a component or piece of equipment can fail, and the effect of that failure on the overall system's operation. Any additional features can be added to a basic FMEA such as mitigation strategies and poignant remarks for the reader. It is ideally used early on in the development cycle in order to ascertain key failure modes that can be designed out as early as possible. It should not, however, be limited to the design stage

of system development, but should be used throughout the development stages as an ongoing process.

FMEA techniques were first used by the US military, and the standard MIL-STD-1629A [6] was developed to help standardise the FMEA process. The process of performing an FMEA includes [7].

- Breaking down the equipment/system into components or sub-assembly blocks.
- Examining each component or block for its modes of failure.
- Listing each mode of failure according to the effect it has locally and on the system.
- Applying failure rates for each failure mode where quantification is required.

Advantages of FMEA

FMEA is a comprehensive way to analyse all of the potential component failure modes in a system. It is widely used in industry as a means to identify, rank and mitigate against the component failure modes.

Disadvantages of FMEA

The main drawback when using only FMEA for reliability analysis, is that the technique is geared towards analysing individual component failure mode occurrences. Because these failure modes are considered one by one, the interaction of multiple failure mode occurrences are often not listed using this method. Additionally, this type of reliability process is not fully quantitative. Severity and risk rankings can be made, however overall reliability levels cannot be deduced using FMEA.

PEM FTA

FTA is a deductive technique that can be used to classify the instrumental relationships leading to a specific failure mode. Whereas FMEA is a bottom-up approach, FTA is a top-down approach and is a graphical representation of the relationships between the failure modes previously identified in the FMEA. In order to describe this approach, Fig. 2 shows an example branch of a FT from a larger FT for a fuel cell system.

'Pinholes' is the top event of the branch of the FT and indicates the overall undesirable event that the FT is modelling. This top event is split by an 'OR' gate into the intermediate event: 'Pinholes due to Mechanical Stress' and the basic event 'Exothermal combustion due to previously formed pinholes'. The 'OR' gate means that either of the two intermediate events could trigger the top event. The intermediate event is then broken down further. 'Pinholes due to Mechanical Stress' is fed by another 'OR' gate. 'Pinholes due to mechanical stress' is fed by an intermediate event 'Swelling & Foreign Particle Presence' and the basic event 'Creep'. 'Swelling & Foreign Particle Presence' is fed by an 'AND' gate that is in-turn fed by an intermediate event ('Local mechanical stress due to increased pressure') and a transfer gate ('Foreign Particle Presence'). A transfer gate takes logic from another part of the overall FT and transfers this logic in without repeating large section of the graph. 'Foreign Particle Presence' itself is fed by an 'OR' gate

resulting from the combinational occurrence of 'Oxide Film Formation', 'Platinum Particle Presence' transferred from another section of the overall tree, 'Dissolution of Metal Ions' and 'Contamination from Humidifier/air pipe/gas impurity'.

The values for 'eta' (η) listed underneath the basic events is the scale parameter for the quantification analysis using Weibull analysis which is discussed in Section [Quantification](#). The values for 'Q' are the unreliability of the basic event, expressed as a number between zero and one. If $Q = 0$, the basic event is 100% live, and if $Q = 1$, the basic event is considered to be 0% live.

Basic events, such as 'Creep' in the above example, are events which cannot be broken down any further and for which basic information, such as failure rate, repair rate etc. is available. All intermediate events can be broken down further until reaching the basic events.

Once a full FT has been created, the Minimal Cut Sets (MCSs) can be obtained from the tree, where a MCS is a minimal combination of basic events that cause the top event. These can then be used to determine the probability or frequency of the top event [7].

Advantages of FTA

Due to being a graphical representation, FTA is structured in such a way that is easy for the reader to comprehend. The interactions between failure modes can be easily determined from the simple representation style. FTA can also be quantitatively analysed to ascertain overall system reliability.

Disadvantages of FTA

The main drawbacks of using FTA is that it cannot take into account dependencies between failure modes. They also don't tend to consider the cause of failure modes, rather just tackling the knock-on effect of the failure's occurrence. Also, a FT must be undertaken individually for each failure mode of interest. The entire range of operating conditions that the system can operate in are not considered in one tree. A tree must be made for each operating condition to be fully accurate.

Existing reliability analysis of PEMFC systems

Fuel cell reliability

The application of reliability techniques to PEMFC systems in the literature is limited. Rama et al. [8] adapted an FMEA approach and presented a tabular format list of failure modes in a PEMFC which was limited to only the area of the failure mode, and a brief description of the failure mode itself. It did not describe the effect of the failure mode on the system. It is a good start to ascertaining the different failure modes attributable to a PEMFC, however it can be further developed to provide additional information and comprehension of failure relationships in a PEMFC.

Other work in the area includes that of Placca & Kouta [9], who present an initial FTA of a PEMFC in no specific application. The work considered failure modes and their effects for a total of 37 individual basic events in a single cell PEMFC. Component failure modes including; 'Creep', 'Fatigue from relative humidity and temperature cycling' and 'Oxide film formation' were considered. The overall FTA top event of 'Degradation of the cell' was split into three of the four

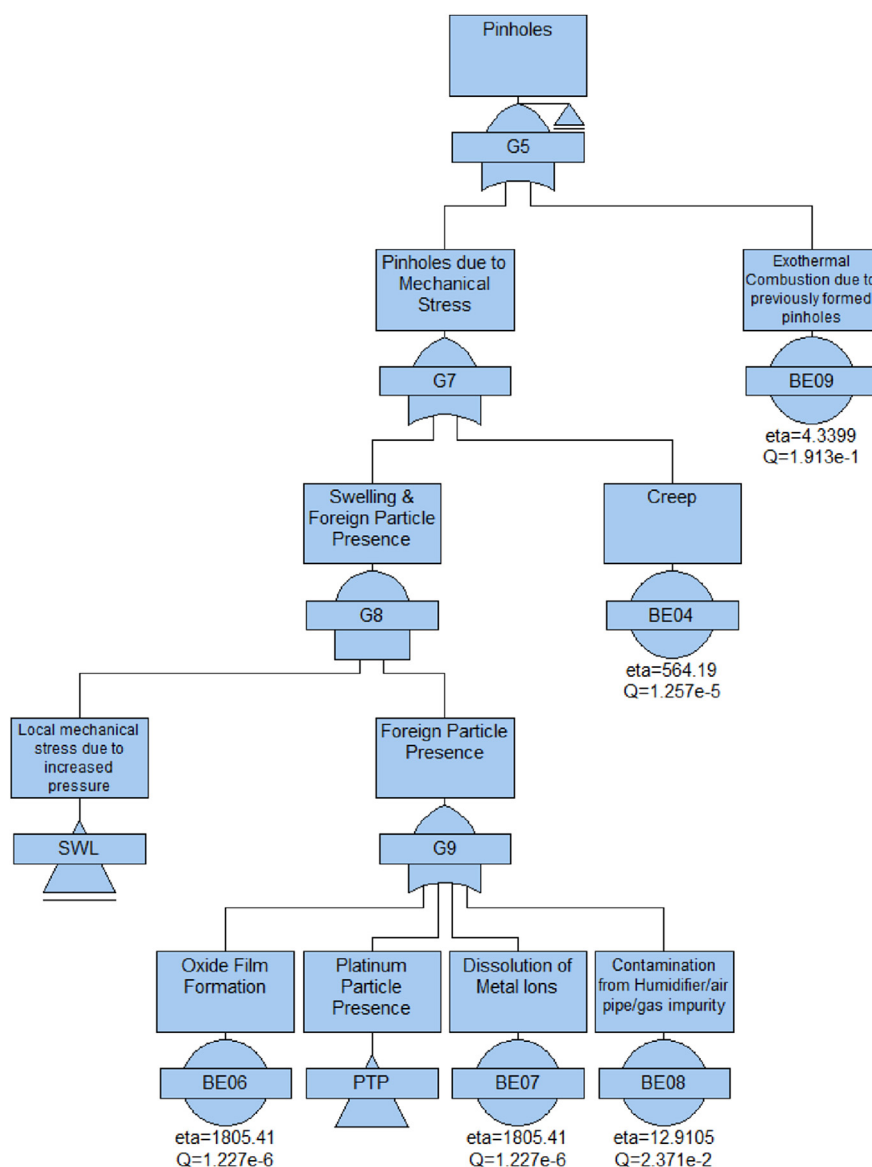


Fig. 2 – Example branch of a Fault Tree.

physical components of the cell; membrane, Catalyst Layer (CL) and Gas Diffusion Layer (GDL). The Bipolar Plate (BIP) was omitted for undisclosed reasons.

FTs have been used in other works regarding water management in PEMFCs [10], however this work was not targeted at PEMFC degradation, and rather singled out the contributing factors towards water management concerns.

FTA was used by Ref. [11] to explain failures in a solid oxide fuel cell. It used fuzzy logic terms for the basic events for failures, such as: ‘Decrease in stack power’ and ‘Increase in stack power’. The authors discuss how FTA is used to: “clear out” complex relationships between failure modes, however one of the main stumbling blocks of FTA is that it cannot take into account dependencies and intricate relationships.

Other reliability techniques such as Markov Modelling (MM) [12] and Petri-Net simulation [13] have been used to study fuel cell systems. In the study by Ref. [12] the reliability of PEMFCs in power plant environments was considered. The

authors used the common fuel cell Nernst equation to model fuel cell performance, then used a simple Markov Model to plot reliability using a Weibull distribution for degradation rates, based upon an assumed overall lifetime of 5000 h. Using MM for fuel cell reliability would require very large models that could show degradation in stages for each component.

Petri-Net simulation has been used by Ref. [13] to model the reliability of PEMFCs using a relatively simple Petri-Net as shown in Fig. 3.

The work uses the Petri-Net in Fig. 3 to calculate a simulated reliability of a single cell, stack or even fleet of fuel cell cars. It uses a set of parameters for six of the conditions that a fuel cell can operate in, and an associated degradation rate when in those operating conditions. The degradation rates are taken from literature and applied throughout the running of the model. The authors acknowledge that the model is simplified as regards steady state degradation instead of changing rates determined by stack age or operational conditions.

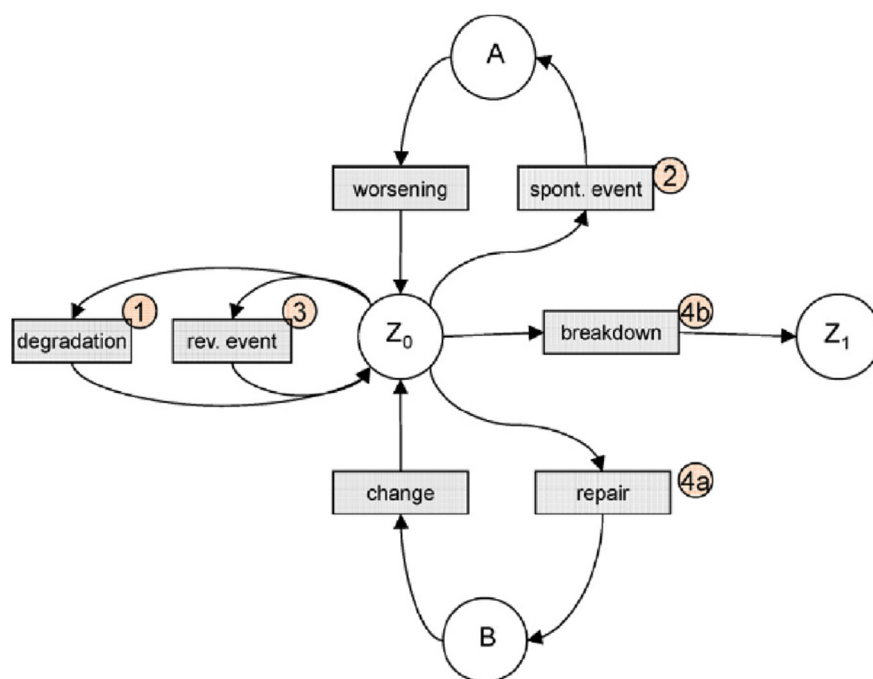


Fig. 3 – Petri-Net Model of fuel cell/stack/fleet of cars.

Fuel cell degradation, prognosis & simulation

Although the area of fuel cell reliability modelling is not well covered in the literature, fuel cell degradation studies are prominent. Countless component level experimentation and analyses are presented in the literature body, with [5] [14], and [15] proving to be very good review papers discussing the range of failure modes analysed in the literature.

The vast majority of works in the literature related to degradation are individual component experiments, or studies of the operating condition's affect on PEMFC performance. An example of which is presented by Ref. [16], and looks at the lifetime prediction of a PEMFC under 'accelerated startup-shutdown' cycling.

Some prognosis work using neural network modelling to determine flooding and drying out of membranes is presented by Ref. [17]. This work uses FTA techniques to qualitatively understand what happens when a membrane dries or floods, then uses said information to inform the neural network model to simulate flooding and drying out.

Additional work by Ref. [18] used polarisation curve and Electrochemical Impedance Spectroscopy (EIS) techniques to characterise real world fuel cell degradation, then predicting ageing time in the future through analysis of key features in the polarisation and EIS data sets.

As the work described in this paper uses FMEA and develops a FT for a PEMFC, the previous studies of [8] & [9] are directly relevant and hence have been described in more detail below.

Rama et al. [8] 'Failure mode identification'

The previous work in Ref. [8] identified 22 failure modes attributable to reduction in performance or catastrophic cell failure. Overall degradation was divided into the electrochemical overpotential pathways; activation, mass transport,

ohmic and fuel efficiency losses, with catastrophic cell failure also noted as a division of overall degradation. A list of faults is presented that shows a cause, however no system effect for each failure mode is given. The comprehensive list of failure modes relating to the loss mechanisms includes all types of PEMFC construction at the time of writing, some of which are no longer used.

Placca & Kouta [9] FTA

FTA was recently presented by Placca & Kouta [9] in an attempt to model the reliability of a single cell PEMFC. From various literary sources, they came to the conclusion that there are 37 individual basic events to be considered when analysing the degradation of a PEMFC. The FT presented is a physical analysis of a single cell PEMFC, splitting the top-event of the 'Degradation of the Cell' down through an OR gate into three physical components of a PEMFC; Membrane (G2), Gas Diffusion Layer (G4) and Catalyst Layer (G3) as shown in Fig. 4. These are three of the four main physical components of a PEMFC with only the bipolar plate being omitted.

G2, G3 and G4 each had 12, 12 and 6 intermediate events respectively, which further branched down through OR gates to the basic events. As all of the gates in the presented FT were of the OR variety, the minimum cut sets are simply single events, representing the basic events of the tree.

Contribution of this research

The qualitative failure identification table presented by Rama et al. [8] has proved to be a good start in identifying the multitude of failure modes in a PEMFC system.

The aforementioned presented quantitative FTA by Placca & Kouta [9] has proven to be a good first step in degradation analysis and failure forecasting. Some areas that need to be

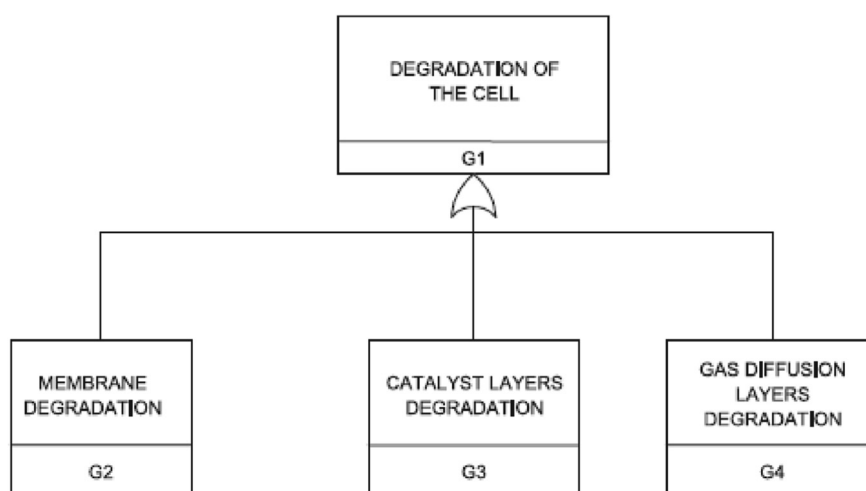


Fig. 4 – ‘Global’ Fault Tree presented in Ref. [9].

addressed have been identified in Ref. [19] & [20], in particular critical component omission, basic event logic & structure, ambiguity of events and lack of standardised data sets. It is envisaged that if these issues can be addressed, the overall degradation analysis of PEMFCs will become increasingly more accurate.

The research contained within this paper contributes to the reliability area by providing the *first, fully comprehensive FMEA* which details the *most up-to-date failure modes* in a tabular format. The FTA contains the *most current and advanced logic of failure* in a PEMFC.

Proposed FMEA

PEMFC construction

Due to the range of materials and components that can be used to create a PEMFC, the following analysis is based upon the key assumptions of material and construction (Fig. 5);

- Standard PEMFC construction
 - (PTFE) based membrane
 - Carbon GDL
 - Pt/C catalyst layer
 - Stainless-Steel BIP
- Using H_2 fuel feed with a purity of 99.97% as required by the ISO standard 14687-2:2012 [21].

In the FMEA & FT the PEMFC has been considered to be composed of the following components: membrane, GDL, catalyst and BIP as described in the following sections.

PTFE membrane

PTFE membranes are perfluorinated polymers, with the most commonly available being Nafion. Perfluorinated polymer membranes are also available from Tokuyama (Neosepta-F[®]), W. L. Gore and Associates, Inc. (Gore-Select[®]), Asahi Glass Company (Flemion[®]), Asahi Chemical Industry (Asiplex[®]) and

Dow. Nafion has a backbone chemical structure very similar to PTFE (Teflon[®]) however, where it differs is that Nafion includes sulfonic acid (SO_3-H^+) functional groups. The PTFE backbone forms the strength of the membrane, and the SO_3-H^+ terminal groups provide charge sites for protonic transport.

Carbon GDL

The GDL is made from a carbon-fibre based material that is either formed into a paper or woven cloth type. Carbon-fibre is used due to its high electrical conductivity and high porosity values. Due to the materials for each method of constructing the GDL being identical, the failure mechanisms that can be experienced by either construction method are the same, therefore in any reliability analysis of the PEMFC it is not necessary to consider the construction methods separately.

Pt/C catalyst

Pt and C are mixed in an ionomer and usually ball milled to mix into an ink. This is then either screen printed or directly painted onto the membrane or GDL surfaces.

Stainless-steel BIP

The endplates, or BIPs are usually made from steel, and are routed to form serpentine channels for the gas to be delivered to the GDL component.

Operating conditions

The operating conditions for the system are considered to be reflective of the power requirements of the New European Drive Cycle (NEDC), used to assess the emissions of car engines and fuel economy in passenger cars. The NEDC is representative of the typical usage of a car in Europe, consisting of an Economic Commission for Europe (ECE)-15 urban drive cycle repeated four times, followed by an extra-urban driving cycle. The product of which is shown in Fig. 6. It is assumed that due to the power demand from the vehicle during this cycle, a range of failure modes can occur.

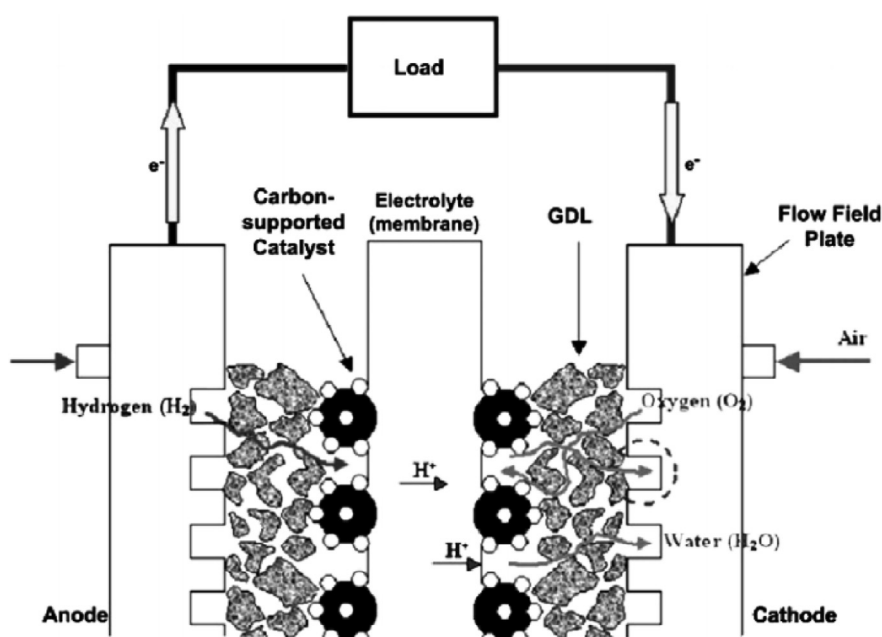


Fig. 5 – Components of a PEMFC [22].

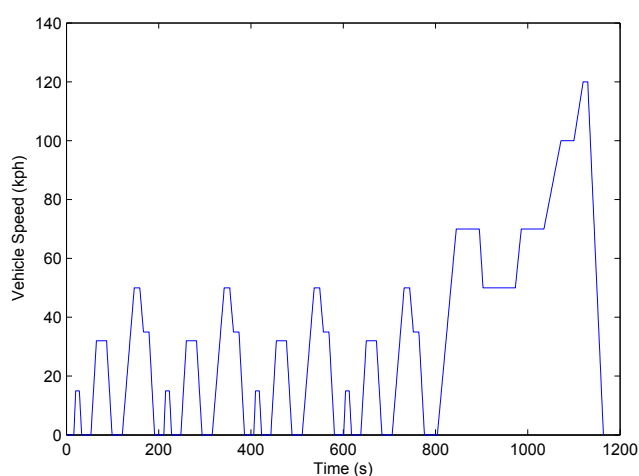


Fig. 6 – New European drive cycle.

The fuel cell is assumed to be of an open anode configuration, and therefore purging strategies need not be considered in the failure analysis. During operation in the above context, the fuel cell can experience a range of operating conditions that can trigger a number of failure modes. The FMEA developed in this work details the entirety of these based upon the current knowledge of PEMFC degradation.

New, comprehensive FMEA

The full FMEA developed contains 15 individual failure modes (Table 1) pertaining to the four main components of a PEMFC; Membrane, CL, GDL and BIP. The failure modes listed in bold

Table 1 – List of events

Basic events – Membrane

Flooding
Ice Formation
Incorrect BIP torque
Creep
Fatigue from Relative Humidity and Temperature cycling
Oxide Film Formation
Dissolution of Metal Ions
Contamination form Humidifier/air pipe/gas impurity
OH or OOH Radical attack
Previously Formed Pinholes
Excess Heat
Exothermal Combustion due to previously formed pinholes

Basic events – Catalyst

Pt Loss and Distribution
Pt Migration
Dissolution of Metal Ions
Contamination form Humidifier/air pipe/gas impurity
Pt Agglomeration/Dissolution
Ice Formation
Flooding
Creep
Exothermal Combustion due to previously formed pinholes

Basic events – Gas diffusion layer

OH or OOH Radical attack
Flooding
Ice Formation

Basic events – Bipolar plate

Oxide Film Formation
Corrosion leading to release of multivalent cations

font are carried over from the work presented by Placca & Kouta [9]. The other failure modes have been obtained from previously published experimental results from numerous sources, however built upon to more accurately represent up-to-date PEMFC reliability analysis. Certain failure modes identified in Ref. [8] were omitted from this work. Namely:

- ‘Gas leak from seals’ – This is not considered as part of this work as seal degradation has been singled out as a negligible failure mode when PEMFC construction is quality controlled, See Ref. [14]. Gasket seals that do suffer from degradation are the liquid applied sealant types used in the past. Modern systems use a solid type gasket that doesn't suffer the same degradation.
- ‘BIP warping of polymer matrix’ – As the boundaries for this work state a steel BIP, a polymer BIP failure is not necessary.
- ‘BIP cracking’ – This has been omitted as the steel plates do not suffer from cracking, only the polymer and graphite BIPs suffer from this.
- ‘Injection-moulded BIP low electrical conductivity’ – Polymer material BIPs are not considered in this work
- ‘Coated stainless-steel BIP loss of surface electrical conductivity’ – As above, only plain stainless steel BIPs are considered in this work.

The four failure modes related to the BIP are all omitted due to the material considerations. The work in Ref. [8] considered multiple construction materials for the BIP, however for the sake of an accurate end result pertaining to a single construction type PEMFC that would be manufactured with only one type of BIP, this work only considers one construction type BIP (stainless-steel).

Aside from the above omissions from previous studies, this work shares some similarities with previous examples, however developments to logic and basic event definitions have been made.

The full FMEA was constructed by considering each of the component failure modes listed in Table 1 in detail. The effects that the failure mode has local to the component and to the cell as a whole were identified. Any methods available to detect the failure were listed. The FMEA also included information on mitigation strategies and relationships between the failure modes resulting in 14 pages. The full FMEA has not been included here for brevity.

Although the majority of the failure modes in Table 1 are re-designated and present the latest understanding of failure logic, the failure modes listed in bold are new for this work.

One of the most important component failure mode identified by the authors is presented in Table 2 and explained below. The importance is derived from the effect that the failure mode has on the system, and its relationship with other failure modes and operating conditions of the fuel cell.

Radical and Hydrogen Peroxide attack in the membrane has a complicated relationship with other components and failure modes within a PEMFC system. The ways in which this failure mode was analysed is through results from chemical degradation studies [5] [23] [24]. It has been discovered that radicals can be formed from oxygen molecules permeating through from the cathode side of the fuel cell, to the anode

side of the fuel cell. This O₂ can reduce at the anode Pt catalyst, forming ·OOH radicals, and then lead on to H₂O₂ formation, and more radical formation [5]. showed that Hydrogen and Platinum can interact, forming radicals and ultimately, hydrogen peroxide.

If there are foreign ions present such as Fe²⁺ and Cu²⁺ released from BIP degradation, the H₂O₂ formed can further develop into ·OH and ·OOH radicals, and at a higher rate. Therefore the metal ions from the BIP catalyse, and severely increased the rate of radical and peroxide degradation to the membrane, as presented in Ref. [5].

Another mechanism for radical and peroxide attack is presented in Ref. [25]. The authors proposed a method of production of radicals, which occurs due to the diffusion of gasses through the membrane, and formation of H₂O₂.

It is also suggested in Ref. [26] that peroxide can form by a 2 electron reduction of O₂ pathway.

Due to the above, OH and OOH radical attack, and H₂O₂ attack were grouped into one basic events; ‘OH and OOH radicals & H₂O₂ contamination to PTFE’, which represents the formation under normal conditions, and H₂O₂ created from 2 electron reduction of O₂ on Pt.

The way in which radicals and peroxide degrade the membrane, is through end-group unzipping, as stated in the local effect column of the FMEA entry (Table 2). The PTFE backbone of the membrane is modified with end-groups or side chains of perfluorosulfonic acid ionomers which help facilitate the fuel cell reaction. These are attacked and ‘unzip’ from the PTFE core, releasing fluorine into the exhaust water. All the entries in Table 2 are explained below.

Column:

1. Identifies the component of the PEMFC where the given failure mode is experienced. In this instance, ‘OH and OOH radicals & H₂O₂ contamination to PTFE’ affects the membrane, and as such the Polymer Electrolyte Membrane component is listed.
2. Gives a brief description of the component and its function within the PEMFC. The Polymer Electrolyte Membrane component of a PEMFC is the central part of the cell which forms the electrolyte, and serves to block the passage of reactant gasses and electrons released during the reaction, however allows the passage of hydrogen protons from the anode side, to cathode.
3. Contains the identification number and description of the failure mode to affect the PEMFC. The number 1.0 is in relation to the Polymer Electrolyte Membrane, listed in column one. The number/2.1 identifies the second failure mode listed of that section, in its own subsection. Therefore failure modes 1.0/2.1 and 1.0/2.2 are both primarily related to mechanical degradation.
4. Contains information pertaining to the local effect of the failure mode, as explained earlier.
5. Lists how this local effect affects the system overall. For this example if the membrane is weakened, there is an increased risk of mechanical damage to the membrane and an overall reduction in the performance of the stack/cell. This can be observed in a polarisation curve from a linear drop in the centre section of the curve.

Table 2 – Failure Mode and Effect Analysis – Radical and Hydrogen Peroxide attack.

Identification	Function	Failure mode	Local effect	System effect	Failure detection method	Mitigation strategy	Remarks	Relationship	Source
1.0 Polymer Electrolyte Membrane	The 'heart' of the PEMFC. Forms the electrolyte at the centre of the cell. Blocks passage of gasses and electrons, but facilitates passage of hydrogen protons from anode to cathode side	1.0/2.1 OH and OOH radicals & H ₂ O ₂ contamination to PTFE	End group unzipping. The Polytetrafluoroethylene (PTFE) core material is modified with side chains of Perfluorosulfonic acid Ionomers. These can be lost through OH and OOH radical attack. (PFSI) membrane	Weaker membrane, and therefore increase in risk of mechanical damage. Reduction in voltage output	Electron Spin Resonance (ESR) spectroscopy, Polarisation Curve, Linear Sweep Voltammetry	Modifying polytetrafluoroethylene with in situ sol-gel polymerization of titanium isopropoxide to generate titania quasiretworks in the polar domains of a Polymer Electrolyte Membrane Fuel Cell, can mitigate against the risk of H ₂ and O ₂ gas crossover.	Low humidity and OCV can exacerbate the attack and degradation	Protonic resistance of membrane, H ₂ O ₂ formation, Mechanical Damage	Wang, H et al. (2012) PEM fuel cell failure mode analysis. New York, CRC Press. (pp87)

- Lists the potential methods to detect this failure mode's affect on the system. For this example, a polarisation curve would show a drop, as the failure mode is affecting the system. Linear sweep voltammetry could potentially identify this failure mode as it is most commonly used to identify gas crossover. The rate of gas crossover would change with mechanical damage of the membrane through radical attack.
- Lists any potential mitigation strategies to reduce the likelihood of occurrence, or the severity of the effect. For this example, preconditioning the membrane with a modified PTFE compositing to include in-situ sol-gel polymerization of titanium isopropoxide to generate titania quasiretworks in the polar domains of the membrane [27].
- Contains any pertinent remarks that would either help the reader to understand the entire row, or any factors to consider regarding the failure mode.
- Lists any relationships that this failure mode may have with other aspects of the FMEA. For this example, The resistance of the membrane relating to proton exchange is affected through membrane thinning. Additionally, H₂O₂ formation is increased through an increase in gas crossover, and of course, mechanical degradation is facilitated.
- Finally, the source of the data is noted for ease of referencing the experimentation that tested the failure mode. The references for this example are from a review book [27].

The FMEA showed that there are many failure modes in a PEMFC that are not completely understood. The work now provides the first fully comprehensive FMEA using the latest information to understand more failure modes than ever before. Relationships are considered which prove to be invaluable in linking failure modes which is of paramount importance in PEMFC science.

Proposed FT

Following investigation into the operation of the PEMFC and the FMEA analysis carried out to understand the effect of the component failure modes described above, a FT was constructed to consider the event '<5000 h cell lifetime with >5% drop of output voltage'. 15 basic events were found relating to this top event, and for which data is available for a quantitative analysis.

The structure of the FT presented by Ref. [9] was modified to more accurately represent an up-to-date analysis of PEMFC degradation. The top event in Fig. 4 was modified to be less ambiguous, BIP degradation was added to the 'global tree' (see Fig. 7), and the interactions between basic event failure logic were vastly modified. The level 2 intermediate events are also presented in Fig. 7, Catalyst Layer Degradation, Membrane Degradation, Gas Diffusion Layer Degradation and Bipolar Plate Degradation. All intermediate events lead to a 5% drop in voltage corresponding with the top event. The Bipolar plate omission by Ref. [9], has been addressed with the addition of a fourth level 2 intermediate

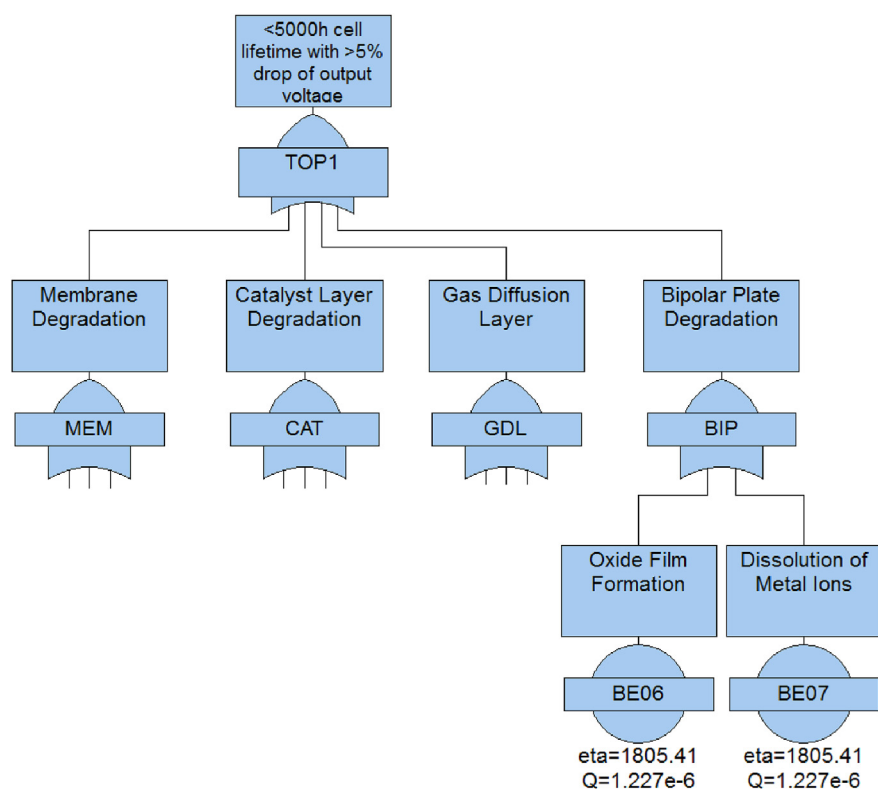


Fig. 7 – Proposed change to 'Global' Tree.

event; 'Bipolar Plate Degradation'. The basic events feeding this intermediate event are; 'Oxide film Formation' and 'Dissolution of metal ions', both of which cause the plate to degrade. Cho et al. [28] showed that the corrosion of the metal bipolar plates for stainless steel releases metallic elements such as Fe, Ni, Cr and Ti. The dissolution of these metals into the Membrane Electrode Assembly (MEA) can increase the ohmic resistance and the charge transfer resistance by taking up space on the active sites of the catalyst. Wu et al. [15] discuss the degradation mechanisms of bipolar plate materials in a PEMFC, paying attention to the formation of an oxide film on the plate. A large concern with bipolar plates, is the contact resistance between the BIP and the GDL, attributed to the resistance caused by the formation of the oxide film. Due to the aforementioned factors observed in Refs. [28] and [15], these two factors are included in the presented FT as shown in Fig. 7.

All of the intermediate events shown in Fig. 7 are expanded out until they only contain basic events. For example; The membrane degradation branch of the global FT is further split down into the three main pathways of degradation in the membrane; 'Mechanical Degradation', 'Chemical Degradation' and 'Thermal Degradation', with the mechanical section being presented in Fig. 8 for brevity.

The intermediate events of the sub-branch shown in Fig. 8 include; 'Local mechanical stress due to increased pressure', 'Microcrack Fracture' and 'Pinholes'. Any localised mechanical stress is caused by swelling inside the cell, and as such the swelling relationships detailed under the event 'Local mechanical stress due to increased pressure' are repeated in the 'Microcrack Fracture' branch as shown by the transfer symbol.

Microcrack fractures can be considered to be anything that results in a physical breach of the membrane, and is segregated from pinholes due to geometry. Microcracks can be considered to be tears, whereas pinholes are circular holes. These are not grouped under one mechanical breach intermediate event due to the varying conditions and events leading to each phenomena. The Pinholes section describes the basic events and combinations of events leading to the formation of pinholes on the membrane material. The two main pathways described are from either mechanical stress (such as punctures from foreign bodies) and a branch transferred in via the transfer gate (denoted by a triangle) labelled 'COMB' in Fig. 8 from the chemical degradation segment of the membrane FT. The branches 'Chemical Degradation' and 'Thermal Degradation' of the membrane were developed in a similar way.

Fault Tree summary

The FT was split into branches representing the physical components of a PEMFC; membrane, CL, GDL and BIP. These were further broken down depending upon the categorisation of the failure phenomena. The FT was drawn based upon information from the FMEA completely previously.

The membrane is a single component which can experience failures from mechanical, thermal or chemical degradation mechanisms. Therefore this section was split into the three degradation mechanisms.

The GDL has a single component construction, however there are two GDL layers in a PEMFC and as such, this segment was split into anode side and cathode side degradation

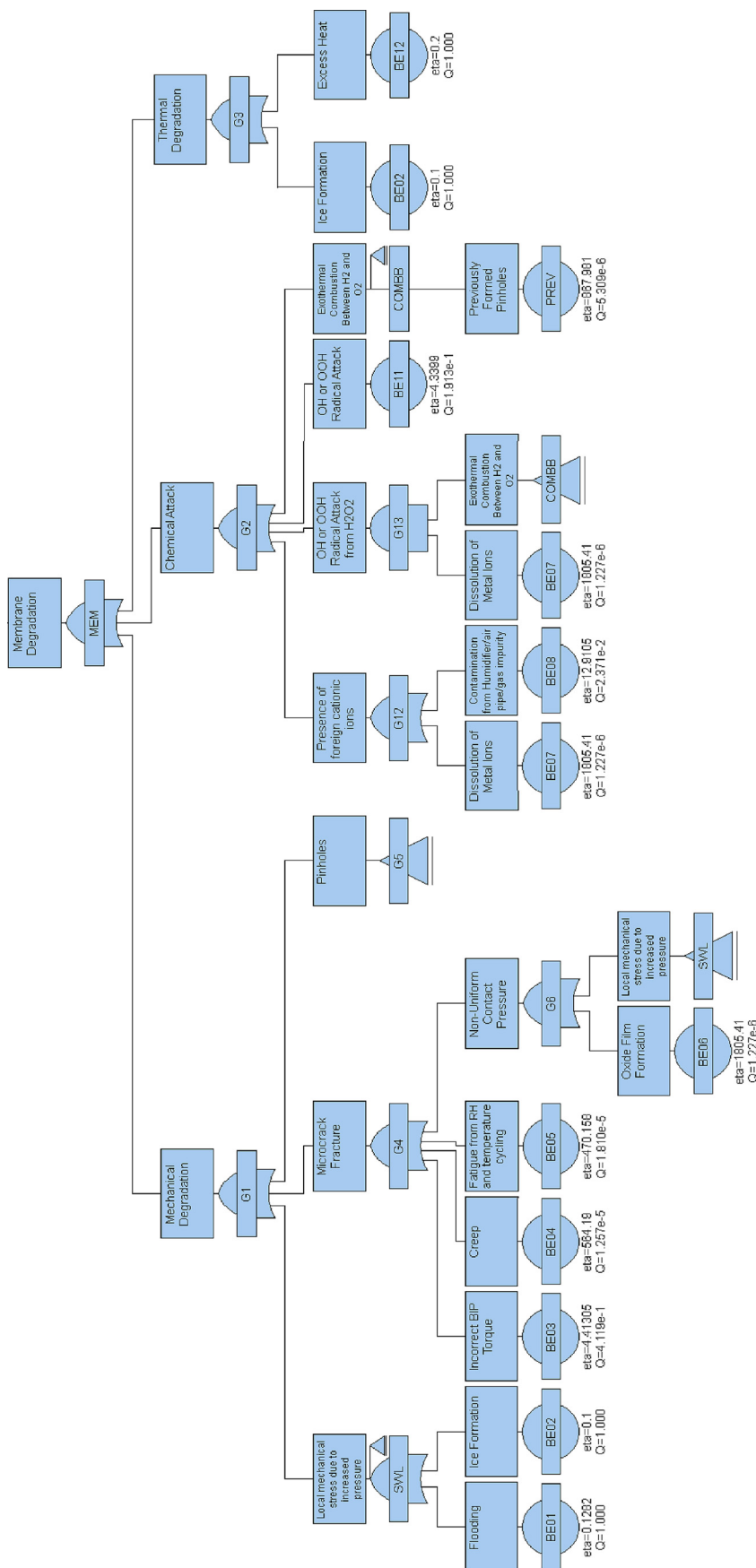


Fig. 8 – Proposed 'Membrane' FT mechanical.

mechanisms. Mechanical compression was also included which would affect both sides of the GDL. The BIP is a very simple segment with only few failure mechanisms that do not need to be further split down into sub-categories. The CL is split into its constituent carbon support, ionomer and Platinum particle construction materials. These three intermediate events then branch down into the basic events and intermediate events leading to the degradation of the component materials for the CL.

In terms of the full tree, there are 37 indistinct intermediate events. The majority of basic events input into OR gates as each basic event can lead to the overall top event individually, leaving only two AND gates in the membrane section. Similarly to the work in Ref. [9], the MCS for the overall FT are just single basic events. Due to the complicated nature of the interactions of basic events, and the gradual degradation of components in a PEMFC, individual component failure modes can cause the top event in the presented FT.

Quantification

Quantification of the FT was undertaken to gain an understanding of the expected failure occurrence during operating life. Degradation rates were sought from the literature where available, with any gaps in the data filled by expert evaluation as in Table 3. For example, where available, previously published experimental studies were analysed and the degradation rate presented due to an adverse operating condition was used in this work as the rate associated with the same basic event occurring. For example [29] found that when flooding occurred, a degradation in voltage equal to 0.39 V h^{-1} was observed. Therefore this rate was used to correspond to the failure mode of “flooding”.

In their experimentation, the flow rate of cathode supply feed was decreased to induce flooding effects in the cell, and produced the results presented in Fig. 9. Two testes were conducted, and for integrity of results, both test were considered and averaged for the overall voltage drop due to cell flooding of 0.39 V h^{-1} .

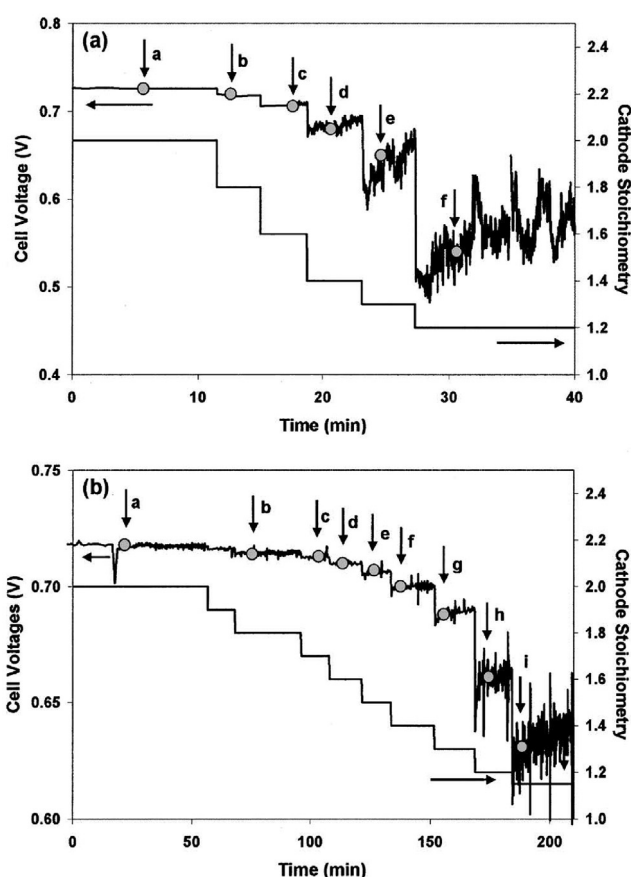


Fig. 9 – PEMFC Membrane flooding degradation test [29].

Table 3 shows the basic event codes for each corresponding basic event description. This code will be used in later tables for brevity and formatting limitations.

As in Ref. [9], for each basic event listed in Table 3, $\mu(t)$ is assumed to follow a Weibull distribution, where $\mu(t) = 1/\lambda(t)$ and $\lambda(t)$ is the degradation rate. The probability density function $F(t)$ is given by Equation (1).

$$F(t) = \frac{\beta}{\eta_d} \left(\frac{t - \gamma}{\eta_d} \right)^{\beta-1} e^{-\left(\frac{t - \gamma}{\eta_d} \right)^{\beta}} \quad (1)$$

Where β is the shape parameter or Weibull slope, η_d is the scale parameter or characteristic lifetime, and γ is the location parameter. The shape parameter is equal to the slope of the line in a probability plot.

The scale parameter can be determined from:

$$\eta_d = \frac{\mu(t)}{\Gamma\left(1 + \frac{1}{\beta}\right)} \quad (2)$$

Where:

$$\Gamma(\eta) = \int_0^{\infty} x^{\eta-1} e^{-x} dx \quad (3)$$

The location parameter, γ , is left at 0 for this study, as it is assumed that all degradation starts at the beginning of life for the cell.

Table 3 – List of degradation parameters used.

ID	Failure mode parameter	Value (Vh^{-1})	Ref
BE01	Flooding	0.39	[29]
BE02	Ice Formation	0.5	Proposed
BE03	Incorrect BIP torque	10^{-3}	Proposed
BE04	Creep	10^{-5}	Proposed
BE05	Fatigue from Relative Humidity Cycling	1.2×10^{-4}	[30]
BE06	Oxide film formation	3.125×10^{-5}	[31]
BE07	Dissolution of metal ions	3.125×10^{-5}	[31]
BE08	Contamination from Humidifier..	4.37×10^{-3}	[32]
BE09	Exothermal Combustion due to..	1.3×10^{-2}	[33]
BE10	Previously Formed Pinholes	1.3×10^{-3}	[33]
BE11	OH or OOH Radical Attack	1.3×10^{-3}	[33]
BE12	Excess Heat	0.25	[29]
BE13	Pt Agglomeration/Dissolution	2.5×10^{-2}	[34]
BE14	Pt Loss & Distribution	2.5×10^{-2}	[34]
BE15	Pt Migration	2.5×10^{-2}	[34]

Table 4 – Table of Weibull distribution data used.

ID	Deg. rate	Mu (t)	Scale parameter for $\mu(t)$	Scale parameter for T	Gamma function	Shape characteristic
	$\lambda(t)$	$\mu(t)$	η_d	η	$\Gamma(\alpha)$	β
BE01	0.39	2.56	2.56	0.13	1	1
BE02	0.5	2	2	0.1	1	1
BE03	10^{-3}	100	88.26	4.41	1.13	0.8
BE04	10^{-5}	10,000	11283.79	564.19	0.89	2
BE05	1.2×10^{-4}	8333.33	9403.16	470.16	0.89	2
BE06	3.125×10^{-5}	32,000	36108.13	1805.41	0.89	2
BE07	3.125×10^{-5}	32,000	36108.13	1805.41	0.89	2
BE08	4.37×10^{-3}	228.83	258.21	12.91	0.89	2
BE09	1.3×10^{-2}	76.92	86.80	4.34	0.89	2
BE10	1.3×10^{-2}	76.92	86.80	4.34	0.89	2
BE11	1.3×10^{-2}	76.92	86.80	4.34	0.89	2
BE12	0.25	4	4	0.2	1	1
BE13	2.5×10^{-2}	40	35.30	1.77	1.13	0.8
BE14	2.5×10^{-2}	40	35.30	1.77	1.13	0.8
BE15	2.5×10^{-2}	40	35.30	1.77	1.13	0.8

It was shown in Ref. [35] that if $\mu(t)$ follows a Weibull distribution with parameters β & η_d then times to failure (T) will also follow a Weibull distribution with parameters β and $\eta = D_f \eta_d$. Where D_f is the degradation level at which failure occurs. In the analysis performed here, failure is assumed to occur when there is a 5% drop in voltage. Therefore $D_f = 0.05V_{in}$ where V_{in} is the initial voltage of the cell. V_{in} is assumed to be 1 V for this work.

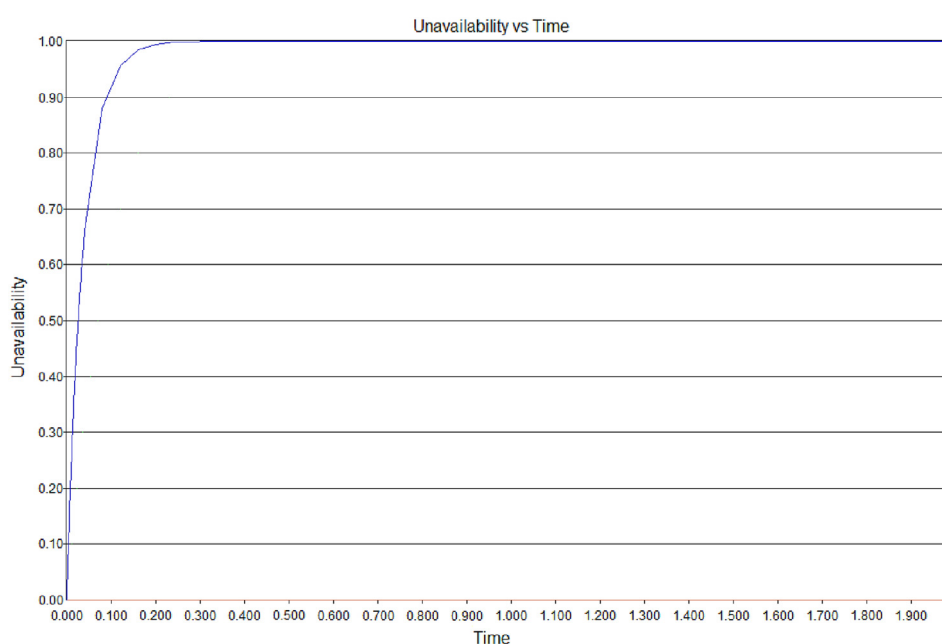
Using the parameters η and β for T in the Fault Tree, enables the probability of the top event to be determined.

Each parameter calculated for each basic event is listed in Table 4, and shows the degradation rate, multiplicative inverse, scale parameter for $\mu(t)$, scale parameter for T, gamma function, and the shape parameter.

Results

The minimal cut sets for the FT developed are in fact the basic events themselves due to the fact that the vast majority of the logic gates are of 'OR' gates. This means that the basic event with the highest likelihood of failure will trigger the top event first under every iteration of the model. A plot of the unavailability of the cell over time is shown in Fig. 10.

As can be seen, the unavailability of the fuel cell – when the cell is considered failed – is after around 30 min hours. This is a very low lifetime for a fuel cell, and is solely due to the highest degradation rate interacting with the logic of the FT. BE02 - Ice Formation, has a degradation rate of 0.5 Vh^{-1} as operating a fuel cell in sub-zero temperatures has severe effects on the materials of the fuel cell and even the blockage of

**Fig. 10 – Unavailability of cell over time.**

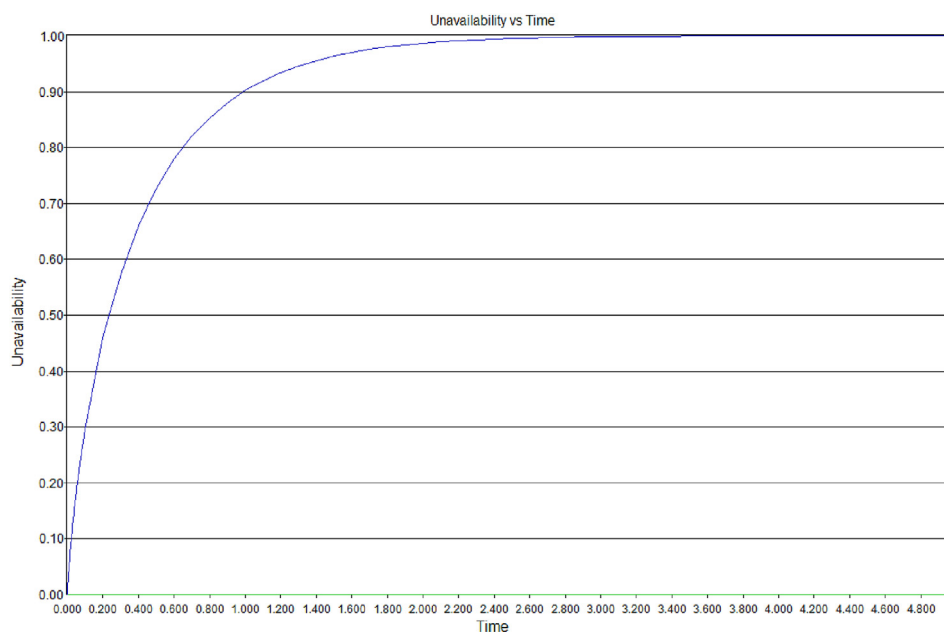


Fig. 11 – Unavailability.

feed gasses to the reactant sites, however the probability of this occurring depends on operating conditions.

If high degradation failure modes such as BE12, BE02 and BE01 are removed, we see the unavailability increase to around 3 h of operation (Fig. 11), which is consistent with a failure due to the next highest degradation rate. This shows that the failure mode with the lowest η and corresponding β will be the failure mode to trigger the top event soonest.

BE01, BE02 and BE12 are failure modes that shouldn't occur under normal operating conditions, however they can be triggered by the occurrence of alternative failure modes. If pinholes occur during normal operation, they can trigger the exothermal combustion of the feed gasses, which leads to excess heat. The FTA approach does not consider these knock on failure occurrences, and is an additional pitfall to using this technique for a highly accurate degradation model.

Also, in order to understand the degradation experienced under all possible operating conditions, a FT would need to be analysed for each condition, which can be considered to be infeasible. Alternative methods to understand degradation in fuel cells is needed to overcome this shortfall.

Conclusions

This work has re-evaluated FT logic determined in the earlier work, including the addition of previously omitted failure modes. The new FT layout developed here is a more logical progression of the failure modes in a PEMFC than shown previously, and as such is a step forward in the reliability analysis of PEMFC. Up to date validity of the causes of degradation in a PEMFC have also been shown, enhancing the understanding of reliability issues in PEMFCs.

The presented FMEA and FTA work provides an understanding of failure logic in a PEMFC which can be used by

developers and manufacturers of PEMFC systems, to identify key areas of improvement in the area. The FMEA provides a detailed, systematic breakdown of each failure mode that a PEMFC can experience, and the failure modes' effect on the system, and other components. To date, this FMEA is the only comprehensive, up-to-date listing of failure modes that a PEMFC can experience, to this level of detail.

The presented FTA goes on from the FMEA to graphically show the logical interactions between failure mode areas. The FTA has highlighted where each failure mode stems from, with reference to each physical component of a PEMFC. Although the FTA presented is a step forward in the qualitative reliability understanding of PEMFCs, the work has uncovered the fact that relationships and dependencies between failure modes exist that make a quantifiable reliability analysis not totally accurate when using FTA methods. Dependencies have been found to exist between failure modes which would discount FTA for a quantitative analysis of a PEMFC. Specifically, any failure due to pinholes was highlighted as an area where loops occur, and basic events are intrinsically linked through dependent relationships. As pinholes can be caused by the crossover of gas, which increases the rate of gas crossover, which in turn increases pinhole production. Additionally, due to the minimal cut sets being each individual failure mode, the failure mode with the shortest η is the failure mode that will inevitably cause the occurrence of the top event first. The presented FTA considers all possible failure modes in a fuel cell, and as such contains failure modes that are not normally observed in ideal operating conditions. A FT would need to be developed for each operating condition for every time-step for it to be completely accurate, which is infeasible due to scale.

Hence, although FTA can be seen as a tool to gain a greater understanding of how failure occurs in a PEMFC, and what basic events lead on to in a cell, it has limited use in reliability

assessment as no useful quantification can be made. If a true understanding of the probability or frequency of failure is required, a different approach must be adopted.

Markov modelling and Petri-Net simulation can take into account dependencies between failure modes and could therefore be exploited in a PEMFC study. However, as discussed in Section [Reliability analysis](#), Markov Modelling is not suitable for detailed component failure modelling due to the sheer amount of states that would be required for each of the many components in the system. As such, future work will entail development of a Petri-Net model that can take into account dependencies between failure modes and deal with the inherent issues with using FTA for quantitative analysis of PEMFCs.

Acknowledgements

This work was supported by the Engineering and Physical Sciences Research Council (EPSRC) (EP/G037116/1) and the Doctoral Training Centre in Hydrogen Fuel Cells and Their Applications.

REFERENCES

- [1] BERR DTI. Energy price scenarios in the Oxford models. Technical Report, BERR. 2006.
- [2] DECC. UK Greenhouse gas emissions, provisional figures and 2011 UK greenhouse gas emissions, final figures by fuel type and end-user. Technical Report, DECC, 2013. 2012.
- [3] Technical Report, DfT D. for transport, factsheets: UK transport greenhouse gas emissions. 2013.
- [4] U. Gov, Climate change act 2008. 2008.
- [5] Borup R, Meyers J, Pivovar B, Kim YS, Mukundan R, Garland N, et al. Scientific aspects of polymer electrolyte fuel cell durability and degradation. *Chem Rev* 2007;107:3904–51. Cited By (since 1996):920.
- [6] MIL-STD-1629A. Procedures for performing a failure mode, effects and criticality analysis. 1980.
- [7] Andrews JD, Moss TR. Reliability and risk assessment, professional Engineering publishing limited. 2nd ed. London: England; 2002.
- [8] Rama P, Chen R, Andrews J. A review of performance degradation and failure modes for hydrogen-fuelled polymer electrolyte fuel cells. *Proc Inst Mech Eng Part A J Power Energy* 2008;222:4214–441. Cited By (since 1996): 4.
- [9] Placca L, Kouta R. Fault tree analysis for PEM fuel cell degradation process modelling. *Int J Hydrogen Energy* 2011;36:12393–405. Cited By (since 1996): 2.
- [10] Yousfi-Steiner N, Mootguy P, Candusso D, Hissel D, Hernandez A, Aslanides A. A review on PEM voltage degradation associated with water management: Impacts, influent factors and characterization. *J Power Sources* 2008;183:260–74. Cited By (since 1996): 60.
- [11] Steiner NY, Hissel D, Mootguy P, Candusso D, Marra D, Pianese C, et al. Application of fault tree analysis to fuel cell diagnosis. *Fuel Cells* 2012;12:302–9.
- [12] Tanrioven M, Alam MS. Reliability modeling and analysis of stand-alone PEM fuel cell power plants. *Renew Energy* 2006;31:915–33. Cited By (since 1996): 12.
- [13] Wieland C, Schmid O, Meiler M, Wachtel A, Linsler D. Reliability computing of polymer-electrolyte-membrane fuel cell stacks through Petri nets. *J Power Sources* 2009;190:34–9. Cited By (since 1996): 2.
- [14] Bruijn FAD, Dam VAT, Janssen GJM. Review: Durability and degradation issues of PEM fuel cell components. *Fuel Cells* 2008;8:3–22. Cited By (since 1996): 168.
- [15] Wu J, Yuan XZ, Martin JJ, Wang H, Zhang J, Shen J, et al. A review of PEM fuel cell durability: degradation mechanisms and mitigation strategies. *J Power Sources* 2008;184:104–19. Cited By (since 1996): 127.
- [16] Bae SJ, Kim S-J, Park JI, Park CW, Lee J-H, Song I, et al. Lifetime prediction of a polymer electrolyte membrane fuel cell via an accelerated startup–shutdown cycle test. *Int J Hydrogen Energy* 2012;37:9775–81.
- [17] Steiner NY, Hissel D, Mootguy P, Candusso D. Diagnosis of polymer electrolyte fuel cells failure modes (flooding & drying out) by neural networks modeling. *Int J Hydrogen Energy* 2011;36:3067–75.
- [18] Onanena R, Oukhellou L, Candusso D, Harel F, Hissel D, Aknin P. Fuel cells static and dynamic characterizations as tools for the estimation of their ageing time. *Int J Hydrogen Energy* 2011;36:1730–9.
- [19] Whiteley M, Jackson L, Dunnett S. Enhanced fault tree analysis and modelling considerations of a polymer electrolyte membrane fuel cell. In: Proceedings of the European safety and reliability Conference, ESREL. CRC Press; 2013. p. 603.
- [20] Whiteley M, Fly A, Leigh J, Dunnett S, Jackson L. Advanced reliability analysis of Polymer Electrolyte Membrane Fuel Cells using Petri-Net analysis and fuel cell modelling techniques. *Int J Hydrogen Energy* 2015. Article in Press.
- [21] ISO, Hydrogen fuel – product specification – part 2: proton exchange membrane (pem) fuel cell applications for road vehicles. 2012.
- [22] Kandlikar SG, Lu Z. Thermal management issues in a PEMFC stack – A brief review of current status. *Appl Therm Eng* 2009;29:1276–80. Cited By (since 1996):53.
- [23] Inaba M, Kinumoto T, Kiriake M, Umebayashi R, Tasaka A, Ogumi Z. Gas crossover and membrane degradation in polymer electrolyte fuel cells. *Electrochimica Acta* 2006;51:5746–53. Cited By (since 1996):205.
- [24] Kinumoto T, Inaba M, Nakayama Y, Ogata K, Umebayashi R, Tasaka A, et al. Durability of perfluorinated ionomer membrane against hydrogen peroxide. *J Power Sources* 2006;158:1222–8. Cited By (since 1996):142.
- [25] LaConti A, Hamdan M, McDonald R, Vielstich W, Lamm A, Gasteiger H, editors. Handbook of fuel cells: fundamental, technology, and applications, vol. 3; 2003.
- [26] Pozio A, Silva RF, Francesco MD, Giorgi L. Nafion degradation in PEFCs from end plate iron contamination. *Electrochimica Acta* 2003;48:1543–9.
- [27] Wang H, Li H, Yuan X, editors. PEM fuel cell durability handbook – fuel cell failure mode analysis, vol. 1. Boca Raton: CRC Press; 2012.
- [28] Cho EA, Jeon US, Hong SA, Oh IH, Kang SG. Performance of a 1 kW-class PEMFC stack using TiN-coated 316 stainless steel bipolar plates. *J Power Sources* 2005;142:177–83.
- [29] Canut JML, Abouatallah RM, Harrington DA. Detection of membrane drying, fuel cell flooding, and anode catalyst poisoning on PEMFC stacks by electrochemical impedance spectroscopy. *J Electrochem Soc* 2006;153:A857–64. Cited By (since 1996):85.
- [30] Fowler M, Amphlett JC, Mann RF, Peppley BA, Roberge PR. Issues associated with Voltage Degradation in a PEMFC. *J New Mater Electrochem Syst* 2002;5:255–62. Cited By (since 1996): 20.

- [31] Steiner NY, Candusso D, Hissel D, Mooteguy P. Model-based diagnosis for proton exchange membrane fuel cells. *Math Comput Simul* 2010;81:158–70. Cited By (since 1996): 1.
- [32] Ahn SY, Shin SJ, Ha HY, Hong SA, Lee YC, Lim TW, et al. Performance and lifetime analysis of the kW-class PEMFC stack. *J Power Sources* 2002;106:295–303. Cited By (since 1996): 54.
- [33] Teranishi K, Kawata K, Tsushima S, Hirai S. Degradation mechanism of PEMFC under open circuit operation. *Electrochem Solid-State Lett* 2006;9:A475–7. Cited By (since 1996):89.
- [34] Chung CG, Kim L, Sung YW, Lee J, Chung JS. Degradation mechanism of electrocatalyst during long-term operation of PEMFC. *Int J Hydrogen Energy* 2009;34:8974–81.
- [35] Freitas MA, de Toledo MLG, Colosimo EA, Pires MC. Using degradation data to assess reliability: a case study on train wheel degradation. *Qual Reliab Eng Int* 2009;25:607–29.

Appendix G

Publications

Whiteley, M. Jackson, L. Dunnett, S. (2013) Fault Tree analysis of polymer electrolyte fuel cells to predict degradation phenomenon ARTS Conference, Loughborough UK. ISBN 978-1-907382 61 1

Whiteley, M. Bartlett, L. Dunnett, S. (2013) Enhanced Fault Tree Analysis and Modelling Considerations of a Polymer Electrolyte Membrane Fuel Cell ESREL Conference, Amsterdam Netherlands, ISBN 9781138001237

Whiteley, M. Leigh, J. Fly, A. Bartlett, L. & Dunnett, S. (2014) Advanced reliability analysis of Polymer Electrolyte Membrane Fuel Cells using Petri-Net analysis and Fuel Cell modelling techniques World Hydrogen Energy Conference 2014, South Korea.

Whiteley, M. Leigh, J. Fly, A. Bartlett, L. & Dunnett, S. (2014) Using Petri-Net Analysis for Advanced Reliability Analysis of Polymer Electrolyte Membrane Fuel Cells ESREL 2014, Poland.

Whiteley, M. Leigh, J. Fly, A. Bartlett, L. & Dunnett, S. (2015) Advanced reliability analysis of Polymer Electrolyte Membrane Fuel Cells using Petri-Net analysis and Fuel Cell modelling techniques International Journal of Hydrogen Energy, InPress

Whiteley, M. Fly, A. Leigh, J. Jackson, L. Dunnett, S. (2015) 'Reliability modelling using Petri-Net Simulation of Polymer Electrolyte Membrane Fuel Cell Degradation in Automotive Applications' RAMS Conference, Florida, USA.

Whiteley, M. Fly, A. Leigh, J. Jackson, L. Dunnett, S. (2015) 'Petri-Net analysis of Polymer Electrolyte Membrane Fuel Cells to ascertain degradation and lifetime prognostication in automotive applications' ARTS conference, Loughborough UK.

Whiteley, M. Fly, A. Leigh, J. Jackson, L. Dunnett, S. (2015) 'Degradation analysis of polymer electrolyte membrane fuel cells using petri-net simulation and experimental validation', World Hydrogen Technologies Convention, Sydney, Australia

Whiteley, M. Jackson, L. Dunnett, S. (2015) 'Failure Mode and Effect Analysis, and Fault Tree Analysis of Polymer Electrolyte Membrane Fuel Cells' International Journal of Hydrogen Energy, InPress